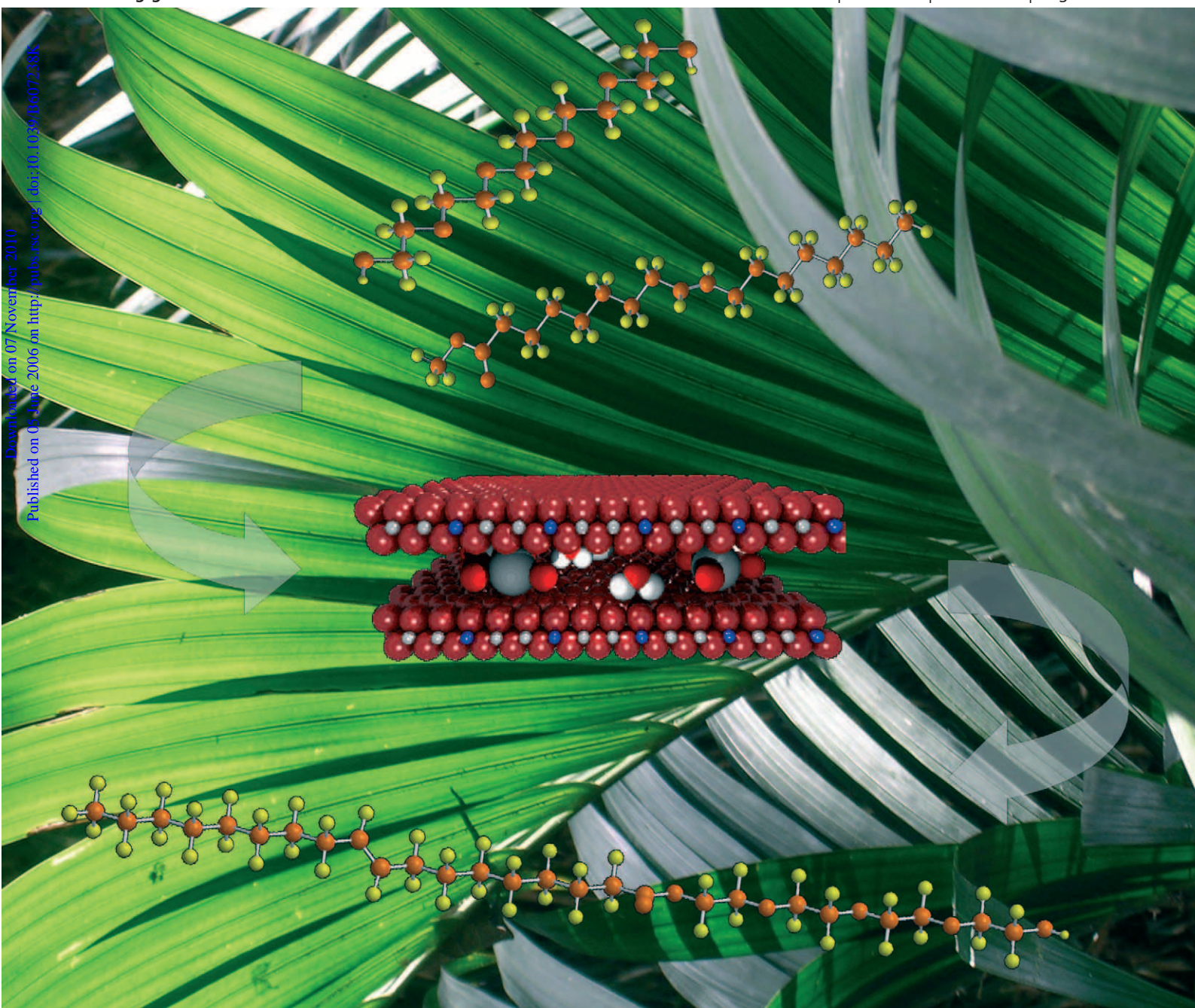


Green Chemistry

Cutting-edge research for a greener sustainable future

www.rsc.org/greenchem

Volume 8 | Number 6 | June 2006 | Pages 497–584



Downloaded on 07 November 2010
Published on 05 June 2006 in <http://pubs.rsc.org>. DOI: 10.1039/B607238K

ISSN 1463-9262

RSC Publishing

Climent *et al.*
Chemicals from biomass derived products

Hooper *et al.*
Synthesis of 9-methylgermacrene B from a renewable resource

Lou *et al.*
Impact of ionic liquids on papain

Nadagouda and Varma
Green synthesis of gold and platinum nanomaterials using vitamin B₂



1463-9262 (2006) 8:6;1-8

NEW ORGANIC CHEMISTRY REACTIONS AND METHODOLOGIES FOR GREEN PRODUCTION

continuation of the
SUMMER SCHOOL ON GREEN CHEMISTRY
 Ninth event

Lecce-Otranto (Italy)
29 October – 10 November 2006

Advanced
 Study
 Institute



INCA
 Interuniversity Consortium
 Chemistry for the Environment

Deadline for applications: 31st July, 2006

Co-Director: Pietro Tundo, tundop@unive.it

Co-Director: Mohamed Tawfic, motawfic@tedata.net.eg

Coordinator: Alvisse Perosa, alvisse@unive.it

Organiser: Vittorio Esposito, incalecce@unive.it

www.unive.it/inca

Comments received from just a few of the thousands of satisfied RSC authors and referees who have used ReSource - the online portal helping you through every step of the publication process.

authors benefit from a user-friendly electronic submission process, manuscript tracking facilities, online proof collection, free pdf reprints, and can review all aspects of their publishing history

referees can download articles, submit reports, monitor the outcome of reviewed manuscripts, and check and update their personal profile

NEW!! We have added a number of enhancements to ReSource, to improve your publishing experience even further.

New features include:

- the facility for authors to save manuscript submissions at key stages in the process (handy for those juggling a hectic research schedule)
- checklists and support notes (with useful hints, tips and reminders)
- and a fresh new look (so that you can more easily see what you have done and need to do next)

Go online today and find out more.

Registered Charity No. 207890

'ReSource is the best online submission system of any publisher.'

'I wish the others were as easy to use.'

Green Chemistry

Cutting-edge research for a greener sustainable future

www.rsc.org/greenchem

RSC Publishing is a not-for-profit publisher and a division of the Royal Society of Chemistry. Any surplus made is used to support charitable activities aimed at advancing the chemical sciences. Full details are available from www.rsc.org

IN THIS ISSUE

ISSN 1463-9262 CODEN GRCHFJ 8(6) 497-584 (2006)



Cover

The palm tree as a source of fatty acid derivatives and their transformation in biodegradable surfactants using double layered hydroxides as catalysts. Image reproduced by permission of Avelino Corma from *Green Chem.*, 2006, 8(6), 524.

CHEMICAL TECHNOLOGY

T21

Chemical Technology highlights the latest applications and technological aspects of research across the chemical sciences.

Chemical Technology

June 2006/Volume 3/Issue 6

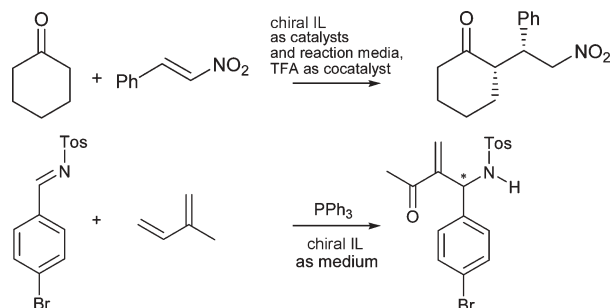
www.rsc.org/chemicaltechnology

HIGHLIGHT

507

Highlights

Markus Hölscher reviews some of the recent literature in green chemistry.



EDITORIAL STAFF

Editor

Sarah Ruthven

News writer

Markus Hölscher

Publishing assistant

Emma Hacking

Team leader, serials production

Stephen Wilkes

Administration coordinator

Sonya Spring

Editorial secretaries

Lynne Braybrook, Jill Segev, Julie Thompson

Publisher

Adrian Kybett

Green Chemistry (print: ISSN 1463-9262; electronic: ISSN 1463-9270) is published 12 times a year by the Royal Society of Chemistry, Thomas Graham House, Science Park, Milton Road, Cambridge, UK CB4 0WF.

All orders, with cheques made payable to the Royal Society of Chemistry, should be sent to RSC Distribution Services, c/o Portland Customer Services, Commerce Way, Colchester, Essex, UK CO2 8HP. Tel +44 (0) 1206 226050; E-mail sales@rscdistribution.org

2006 Annual (print + electronic) subscription price: £859; US\$1571. 2006 Annual (electronic) subscription price: £773; US\$1414. Customers in Canada will be subject to a surcharge to cover GST. Customers in the EU subscribing to the electronic version only will be charged VAT.

If you take an institutional subscription to any RSC journal you are entitled to free, site-wide web access to that journal. You can arrange access via Internet Protocol (IP) address at www.rsc.org/ip. Customers should make payments by cheque in sterling payable on a UK clearing bank or in US dollars payable on a US clearing bank. Periodicals postage paid at Rahway, NJ, USA and at additional mailing offices. Airfreight and mailing in the USA by Mercury Airfreight International Ltd., 365 Blair Road, Avenel, NJ 07001, USA.

US Postmaster: send address changes to Green Chemistry, c/o Mercury Airfreight International Ltd., 365 Blair Road, Avenel, NJ 07001. All despatches outside the UK by Consolidated Airfreight.

PRINTED IN THE UK

Advertisement sales: Tel +44 (0) 1223 432246; Fax +44 (0) 1223 426017; E-mail advertising@rsc.org

Green Chemistry

Cutting-edge research for a greener sustainable future

www.rsc.org/greenchem

Green Chemistry focuses on cutting-edge research that attempts to reduce the environmental impact of the chemical enterprise by developing a technology base that is inherently non-toxic to living things and the environment.

EDITORIAL BOARD

Chair

Professor Colin Raston,
Department of Chemistry
University of Western Australia
Perth, Australia
E-mail clraston@chem.uwa.edu.au

Dr Janet Scott, Centre for Green
Chemistry, Monash University,
Australia

Dr A Michael Warhurst,
University of Massachusetts,
USA
E-mail michael-warhurst@uml.edu

Professor Buxing Han, Chinese
Academy of Sciences
E-mail hanbx@iccas.ac.cn

Scientific editor

Professor Walter Leitner,
RWTH-Aachen, Germany
E-mail leitner@itmc.rwth-aachen.de

Professor Tom Welton,
Imperial College, UK

E-mail t.welton@ic.ac.uk
Professor Roshan Jachuck,
Clarkson University, USA

Associate editors

Professor C. J. Li, McGill
University, Canada
E-mail cj.li@mcgill.ca
Professor Kyoko Nozaki
Kyoto University, Japan
E-mail nozaki@chembio.tu-tokyo.ac.jp

Members

Professor Joan Brennecke,
University of Notre Dame, USA
Professor Steve Howdle, University
of Nottingham, UK

Dr Paul Anastas, Green Chemistry
Institute, USA
E-mail p_anastas@acs.org

INTERNATIONAL ADVISORY EDITORIAL BOARD

James Clark, York, UK
Avelino Corma, Universidad
Politécnica de Valencia, Spain
Mark Harmer, DuPont Central
R&D, USA
Herbert Hugl, Lanxess Fine
Chemicals, Germany
Makato Misono, Kogakuin
University, Japan
Robin D. Rogers, Centre for Green
Manufacturing, USA

Kenneth Seddon, Queen's
University, Belfast, UK
Roger Sheldon, Delft University of
Technology, The Netherlands
Gary Sheldrake, Queen's
University, Belfast, UK
Pietro Tundo, Università ca
Foscari di Venezia, Italy
Tracy Williamson, Environmental
Protection Agency, USA

INFORMATION FOR AUTHORS

Full details of how to submit material for publication in Green Chemistry are given in the Instructions for Authors (available from <http://www.rsc.org/authors>). Submissions should be sent via ReSource: <http://www.rsc.org/resource>.

Authors may reproduce/republish portions of their published contribution without seeking permission from the RSC, provided that any such republication is accompanied by an acknowledgement in the form: (Original citation) – Reproduced by permission of the Royal Society of Chemistry.

© The Royal Society of Chemistry 2006. Apart from fair dealing for the purposes of research or private study for non-commercial purposes, or criticism or review, as permitted under the Copyright, Designs and Patents Act 1988 and the Copyright and Related Rights Regulations 2003, this publication may only be reproduced, stored or transmitted, in any form or by any means, with the prior permission in writing of the Publishers or in the case of reprographic reproduction in accordance with the terms of

licences issued by the Copyright Licensing Agency in the UK. US copyright law is applicable to users in the USA.

The Royal Society of Chemistry takes reasonable care in the preparation of this publication but does not accept liability for the consequences of any errors or omissions.

Ⓢ The paper used in this publication meets the requirements of ANSI/NISO Z39.48-1992 (Permanence of Paper).

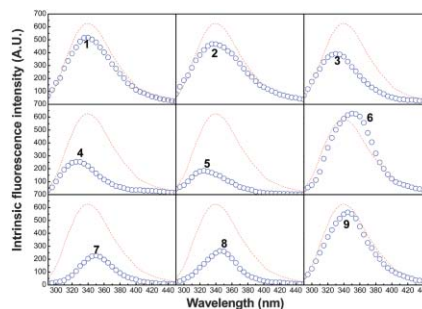
Royal Society of Chemistry: Registered Charity No. 207890

509

Impact of ionic liquids on papain: an investigation of structure–function relationships

Wen-Yong Lou, Min-Hua Zong,* Thomas J. Smith, Hong Wu and Ju-Fang Wang

Ionic liquids (ILs) containing a range of 1-alkyl-3-methylimidazolium cations and various anions affect papain's catalytic performance and thermostability in a manner that correlates closely with the effects of the ILs on the conformation of the enzyme as assessed by using ATR-FTIR and fluorescence techniques.

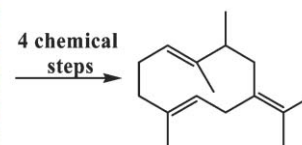


513

Synthesis of 9-methylgermacrene B, racemate of the sex pheromone of *Lutzomyia longipalpis* (Lapinha), from the renewable resource, *Geranium macrorrhizum* essential oil

A. M. Hooper, J.-B. Farcet, N. P. Mulholland and J. A. Pickett*

The sex pheromone of *Lutzomyia longipalpis* (Lapinha), 9-methylgermacrene B, can be prepared from germacrene, the major constituent of the essential oil of the renewable resource *Geranium macrorrhizum*.

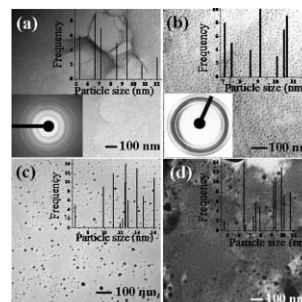


516

Green and controlled synthesis of gold and platinum nanomaterials using vitamin B₂: density-assisted self-assembly of nanospheres, wires and rods

Mallikarjuna N. Nadagouda and Rajender S. Varma*

Density-assisted self-assembly of gold and platinum in various forms such as nanospheres, nanowires and nanorods occurs at room temperature using vitamin B₂ without employing any special capping or dispersing agent.

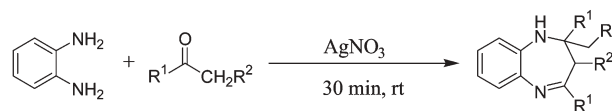


519

An efficient synthesis of 1,5-benzodiazepine derivatives catalyzed by silver nitrate

Rupesh Kumar, Preeti Chaudhary, Surendra Nimesh, Akhilesh K. Verma and Ramesh Chandra*

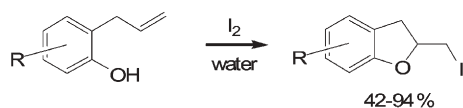
Silver nitrate was found to be an efficient reagent for the preparation of 1,5-benzodiazepine derivatives of *o*-phenylenediamine and ketones under solvent-free conditions.



R¹, R² = H or Alkyl

COMMUNICATIONS

522

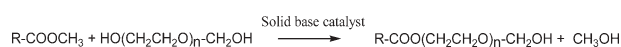
**Water-promoted iodocyclisation of 2-allylphenols**

Manolis Fousteris, Carole Chevrin, Jean Le Bras* and Jacques Muzart*

2-Allylphenols react with iodine in water to produce the corresponding 2-iodomethyl-2,3-dihydrobenzofurans in the absence of any additives or organic solvents.

PAPERS

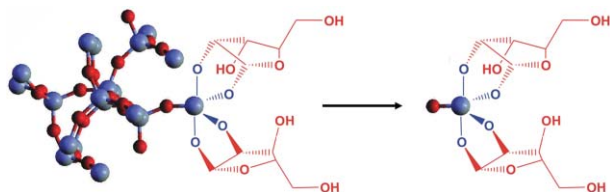
524

**Chemicals from biomass derived products: synthesis of polyoxyethyleneglycol esters from fatty acid methyl esters with solid basic catalysts**

M. José Climent, A. Corma,* Sharifah B. A. Hamid, S. Iborra and M. Mifsud

Polyoxyethyleneglycol esters, widely used as “green” surfactants, have been successfully prepared by transesterification between fatty acid methyl esters and polyethylene glycols using solid base catalysts.

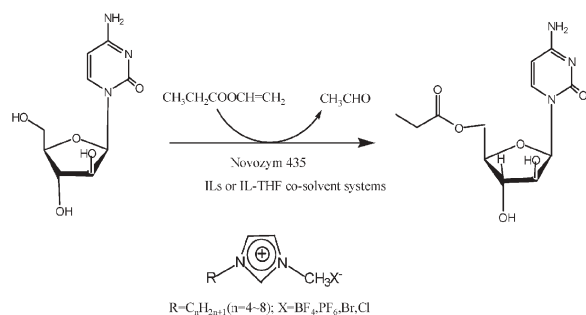
533

**Silicate digestion with fructose under mild conditions**

Gang Lu, Jonathan E. Grossman, Joseph B. Lambert,* Zhijun Xiao and Dan Fu

A novel and simple procedure for digestion of silicate materials utilizes the weak base triethylenetetraamine (TETA), instead of strong bases, in the presence of D-fructose.

538

**Efficient regioselective acylation of 1-β-D-arabinofuranosylcytosine catalyzed by lipase in ionic liquid containing systems**

Xiao-Feng Li, Wen-Yong Lou, Thomas J. Smith, Min-Hua Zong,* Hong Wu and Ju-Fang Wang

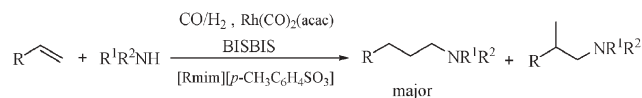
The enzymatic 5'-monoacylation of unmodified ara-C: compared with traditional organic solvents, $\text{C}_4\text{MIm}\cdot\text{PF}_6$ can serve as an excellent co-solvent with tetrahydrofuran with greatly enhanced solubility of the substrate, enzyme stability and similar enzyme activity.

545

Efficient biphasic hydroaminomethylation of long chain olefins in ionic liquids

Ying Yong Wang, Mei Ming Luo,* Qi Lin, Hua Chen and Xian Jun Li

Hydroaminomethylation of long chain olefins was performed efficiently in ionic liquids [Rmim][p-CH₃C₆H₄SO₃] (R = n-butyl, octyl, dedecyl, cetyl) using Rh-BISBIS complex as catalyst.

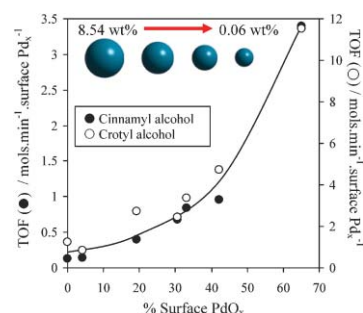


549

On the active site in heterogeneous palladium seleno catalysts

Adam F. Lee,* Simon F. J. Hackett, Justin S. J. Hargreaves and Karen Wilson

The nature of the active site in the Pd-catalysed aerobic selective oxidation of cinnamyl and crotyl alcohols has been directly probed by bulk and surface X-ray techniques. The importance of high metal dispersions and the crucial role of surface palladium oxide have been identified.

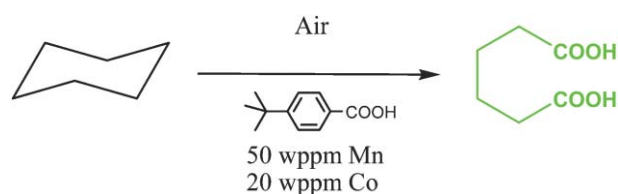


556

Innovative direct synthesis of adipic acid by air oxidation of cyclohexane

Didier Bonnet, Tania Ireland, Eric Fache and Jean-Pierre Simonato*

A single-step air oxidation of cyclohexane, based on a new lipophilic catalytic system, leads to the production of adipic acid with excellent results. The catalytic activity outperforms previous reported catalytic systems for this reaction, and provides an environmentally benign alternative to an important industrial reaction.

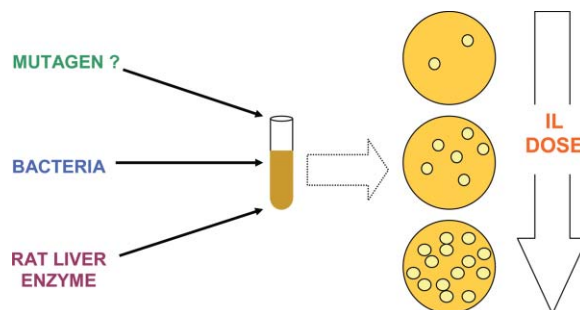


560

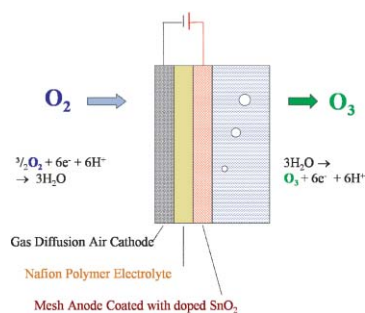
An assessment of ionic liquid mutagenicity using the Ames Test

Kathryn M. Docherty,* Susanne Z. Hebbeler and Charles F. Kulpa, Jr.

The Ames Test for mutagenicity determines that imidazolium, pyridinium and quaternary ammonium ionic liquids are not mutagenic.



568

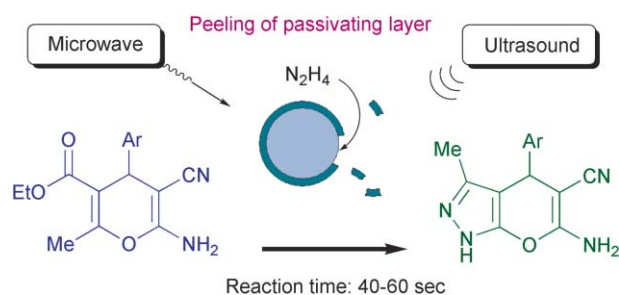


Synthesis of ozone from air *via* a polymer-electrolyte-membrane cell with a doped tin oxide anode

Yun-Hai Wang, Shaoan Cheng and Kwong-Yu Chan*

Oxygen in air is converted to ozone through water in an electrochemical cell fitted with a doped tin oxide anode, a polymer electrolyte, and a gas diffusion air cathode.

573

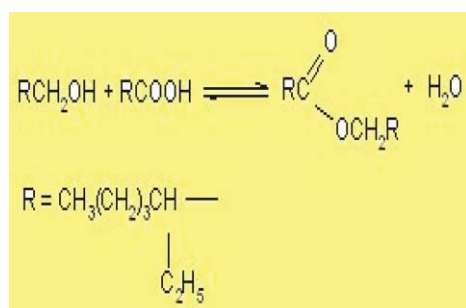


Surface cleaning under combined microwave and ultrasound irradiation: flash synthesis of 4*H*-pyrano[2,3-*c*]pyrazoles in aqueous media

Yanqing Peng, Gonghua Song* and Ruiling Dou

A clean, rapid and energy-efficient approach to solid–aqueous heterogeneous reactions was developed utilizing the synergistic effect of microwave and ultrasound irradiation.

576



Continuous esterification or dehydration in supercritical carbon dioxide

Hassan S. Ghaziaskar,* Ali Daneshfar and Lourdes Calvo

Esterification of 2-ethyl-1-hexanol with 2-ethylhexanoic acid to produce 2-ethylhexyl 2-ethylhexanoate has been investigated in supercritical CO_2 .

AUTHOR INDEX

- | | | | |
|---------------------------|-------------------------------|---------------------------------|----------------------------|
| Bonnet, Didier, 556 | Fousteris, Manolis, 522 | Lee, Adam F., 549 | Simonato, Jean-Pierre, 556 |
| Calvo, Lourdes, 576 | Fu, Dan, 533 | Li, Xian Jun, 545 | Smith, Thomas J., 509, 538 |
| Chan, Kwong-Yu, 568 | Ghaziaskar, Hassan S., 576 | Li, Xiao-Feng, 538 | Song, Gonghua, 573 |
| Chandra, Ramesh, 519 | Grossman, Jonathan E., 533 | Lin, Qi, 545 | Varma, Rajender S., 516 |
| Chaudhary, Preeti, 519 | Hackett, Simon F. J., 549 | Lou, Wen-Yong, 509, 538 | Verma, Akhilesh K., 519 |
| Chen, Hua, 545 | Hamid, Sharifah B. A., 524 | Lu, Gang, 533 | Wang, Ju-Fang, 509, 538 |
| Cheng, Shaoan, 568 | Hargreaves, Justin S. J., 549 | Luo, Mei Ming, 545 | Wang, Ying Yong, 545 |
| Chevrin, Carole, 522 | Hebbeler, Susanne Z., 560 | Mifsud, M., 524 | Wang, Yun-Hai, 568 |
| Climont, M. José, 524 | Hooper, A. M., 513 | Mulholland, N. P., 513 | Wilson, Karen, 549 |
| Corma, A., 524 | Iborra, S., 524 | Muzart, Jacques, 522 | Wu, Hong, 509, 538 |
| Daneshfar, Ali, 576 | Ireland, Tania, 556 | Nadagouda, Mallikarjuna N., 516 | Xiao, Zhijun, 533 |
| Docherty, Kathryn M., 560 | Kulpa, Jr., Charles F., 560 | Nimesh, Surendra, 519 | Zong, Min-Hua, 509, 538 |
| Dou, Ruiling, 573 | Kumar, Rupesh, 519 | Peng, Yanqing, 573 | |
| Fache, Eric, 556 | Lambert, Joseph B., 533 | Pickett, J. A., 513 | |
| Farcet, J.-B., 513 | Le Bras, Jean, 522 | | |

FREE E-MAIL ALERTS AND RSS FEEDS


Contents lists in advance of publication are available on the web *via* www.rsc.org/greenchem - or take advantage of our free e-mail alerting service (www.rsc.org/ej_alert) to receive notification each time a new list becomes available.

RSS Try our RSS feeds for up-to-the-minute news of the latest research. By setting up RSS feeds, preferably using feed reader software, you can be alerted to the latest Advance Articles published on the RSC web site. Visit www.rsc.org/publishing/technology/rss.asp for details.

ADVANCE ARTICLES AND ELECTRONIC JOURNAL

Free site-wide access to Advance Articles and the electronic form of this journal is provided with a full-rate institutional subscription. See www.rsc.org/ejs for more information.

* Indicates the author for correspondence: see article for details.

 Electronic supplementary information (ESI) is available *via* the online article (see <http://www.rsc.org/esi> for general information about ESI).

Chemicals in the Environment

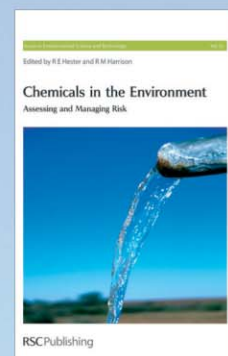
Assessing and Managing Risk

By R M Harrison

Chemicals in the Environment addresses important environmental issues relating to all aspects of risk management and regulation including:

- Current legislation on risk management of chemical products
- Scientific and technical issues
- Evaluating the risk of chemicals to humans and the environment
- Issues on evaluating metals in the environment
- Modelling the behaviour of organic chemicals

Ideal for industry, academia and government organisations - particularly those in environmental chemistry sectors.



Hardcover | 2006 | xvi + 158 pages | £45.00 | RSC member price £29.25 | ISBN-10: 0 85404 206 7 | ISBN-13: 978 0 85404 206 7

Registered Charity No. 207890

RSCPublishing

www.rsc.org/books/2067

Looking for that **special** research paper?

TRY one of these free news services:

Chemical Biology

www.rsc.org/chembiology

Chemical Science

www.rsc.org/chemicalscience

Chemical Technology

www.rsc.org/chemicaltechnology

- highlights of newsworthy and significant advances from across RSC journals
- free online access
- updated daily
- free access to the original research paper from every online article
- also available as free print supplements in selected RSC journals.*

*A separately issued print subscription is also available.

Registered Charity Number: 207890



RSC Publishing

Highlights

DOI: 10.1039/b606232f

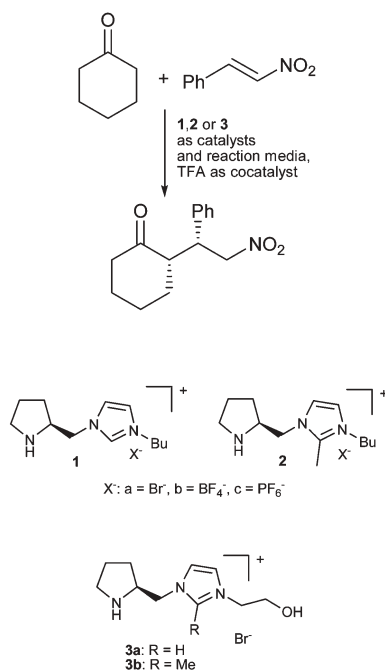
Markus Hölscher reviews some of the recent literature in green chemistry.

Introduction of chiral information into chemical reactions *via* chiral reaction media/catalysts and chiral crystals

The introduction of chiral information into a chemical compound can be accomplished in several ways, *e.g.* by using chiral reactants. Another common alternative is the use of chiral catalysts. Examples in which the chiral information is introduced by a chiral reaction medium have been reported, however enantioselectivities have remained moderate until now. Very recently three different groups have independently reported approaches in which chiral reaction media and chiral crystals were successfully used for chirality transfer. The approaches differ in certain details, but were all highly successful in terms of the enantioselectivities obtained: (1) Luo and Cheng from the Chinese Academy of Sciences, Beijing and Nankai University (Tianjin) focused on chiral ionic liquids, which accomplished the role of both catalyst and reaction medium in Michael additions.¹ (2) Leitner *et al.* from RWTH Aachen successfully proved that for aza-Baylis–Hillman reactions, achiral reactants are transformed to chiral products by achiral catalysts in high enantioselectivities when the reaction is carried out in a chiral ionic liquid.² (3) Soai *et al.* from the Tokyo University of Science used chiral one-component single-crystals of hippuric acid to mediate, highly enantioselectively, the asymmetric autocatalytic addition of diisopropyl zinc to pyrimidine-5-carbaldehyde.³

(1) Ionic liquids (ILs), which have received considerable attention in recent years due to their unique physico-chemical properties, can be functionalized synthetically to yield novel ILs with chiral cations. The functionalization offers the possibility of introducing catalytically competent moieties. Luo and Cheng reasoned that by covalently binding a pyrrolidine substituent to the

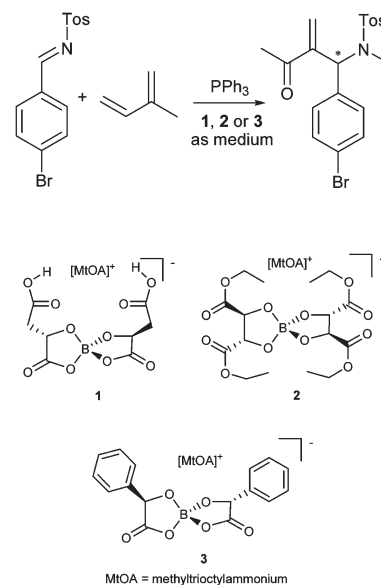
commonly used imidazolium ring, chiral ILs should result which show catalytic activity in Michael additions. To prove the concept the authors synthesized a variety of ILs consisting of the four different cations shown below.



The Michael addition of cyclohexanone and *trans*- β -nitrostyrene was chosen as a test reaction, and interestingly the obtained *syn/anti* ratios varied between 94 : 6 and 99 : 1, while *ee* values ranged between 82 and 99%. Among all ILs investigated the combination of cation **1** with either bromide or tetrafluoroborate as the anion turned out to perform best, while the introduction of methyl groups or alcoholic side chains reduced the *ee* values and the yields substantially, as did the use of PF₆⁻ as the anion. Small amounts of trifluoroacetic acid were needed to obtain high yields, however.

(2) In contrast to the approach outlined above, chirality transfer by a chiral IL is also possible when achiral reactants and achiral catalysts are used. Leitner *et al.* investigated aza-Baylis–Hillman reactions of imines with activated

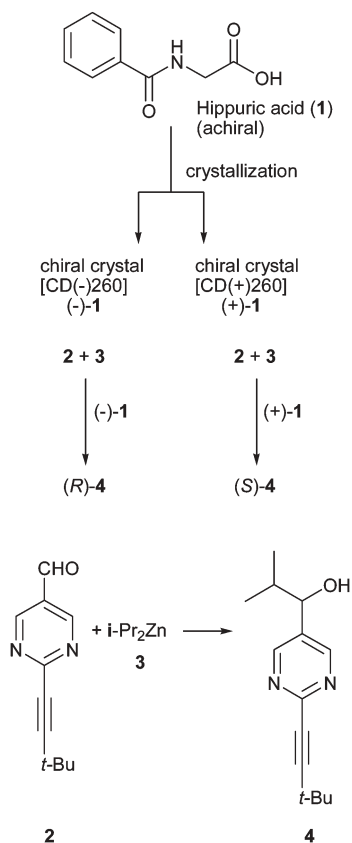
alkenes, as the reaction products are interesting highly functionalized chiral allyl amines. A variety of phosphines catalyze the reaction. From mechanistic considerations this reaction should be influenced strongly by Brønsted acidic sites as well as electrostatic interactions, which makes it a useful test case to investigate if chiral ILs bearing Brønsted acid sites can induce a significant enantiomeric excess in the reaction product. For this purpose three new anionic chiral ILs (**1**, **2**, **3**) were synthesized and tested as reaction media in the aza-Baylis–Hillman reaction.



When the reaction was carried out in IL **1** (4 independently synthesized samples of **1** were tested) the product was obtained with conversions in the 35 to 40% range and *ee* values between 71 and 84%, clearly demonstrating a significant chiral induction. ILs **2** and **3** yielded lower conversion (*ca.* 15%) and racemic product, proving the necessity of a Brønsted acid site for high enantioselectivities. Also, dilution of **1** (and some of its chiral predecessors during synthesis) with conventional solvents, such as THF or CH₂Cl₂, yielded only small amounts of racemic product, which indicates that **1** needs to be employed as

the sole reaction medium for obtaining reasonable conversions and enantiomeric excesses.

(3) Achiral organic compounds can crystallize in chiral space groups generating enantiomorphous crystals, which can be used to introduce chiral information into a chemical reaction. Soai *et al.* reported very recently that hippuric acid, **1**, forms enantiomorphous crystals, which can be used to induce chirality in the addition of diisopropyl zinc to pyrimidine-5-carbaldehyde **2**. The enantiomorphous single crystals can be distinguished by solid state circular dichroism with the two enantiomorphous forms exhibiting positive and negative Cotton effects, respectively.



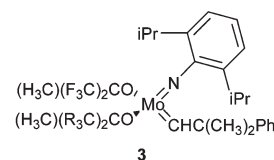
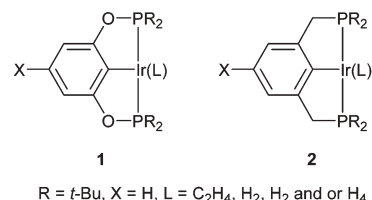
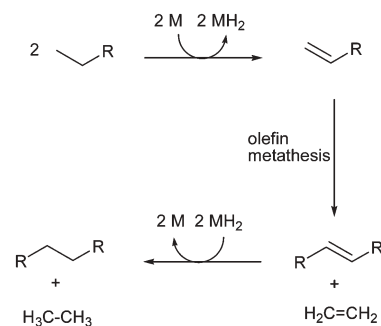
When either one of the enantiomorphous forms was powdered and introduced into reaction mixtures of *i*-Pr₂Zn, **3** and **2**, the corresponding alcohol, **4**, was obtained in 88% yield and 73% ee (*S*)-**4** when crystals with a positive Cotton effect were used, while those with a negative Cotton effect gave (*R*)-**4** with

89% yield and 89% ee. The initial reaction proceeds on the chiral surface of the crystals present and subsequently leads to amplification of chiral excess by asymmetric autocatalysis.

Production of linear *n*-alkanes via catalytic dehydrogenation–metathesis–hydrogenation catalysis

Liquid hydrocarbons can be made from CO/H₂ using Fischer–Tropsch chemistry, which might witness increasing interest in the future as oil reserves decrease. The reason behind this is that alkanes constitute, to a very high degree, classical transportation fuels. However, Fischer–Tropsch syntheses do not yield alkane mixtures with the narrow molecular weight distribution desired for many applications; and as there is presently no elaborated technique for the transformation of low molecular weight alkanes into their counterparts with higher molecular weights, Goldman (Rutgers University) and Brookhart *et al.* (University of North Carolina, Chapel Hill) took up the challenge and investigated two-component homogeneous catalyst systems for the sequential dehydrogenation–metathesis–hydrogenation of alkanes.⁴ The idea is that a suitable dehydrogenation catalyst can transform an alkane to a terminal alkene, which undergoes metathesis in the presence of a second catalyst yielding ethylene and the corresponding internal alkene, both of which are then hydrogenated again by the first catalyst.

Dehydrogenation–hydrogenation catalysts **1** and **2** proved to be successful for this concept when used together with metathesis catalyst **3**. Upon heating an *n*-hexane solution to 125 °C for 24 h the authors found a complex product mixture consisting of C₂ to C₁₅ *n*-alkanes with a concentration in the C₂ to C₅ and C₇ to C₁₀ range. Not only is the catalyst system useful for disproportionation, it also proved efficient in comproportionations, as shown by the reaction of a mixture of *n*-hexane and *n*-eicosane, yielding products in the C₂ to C₃₈ range,



the major product fractions being again in the C₂ to C₅ and in the C₇ to C₁₀ range. However, C₁₁ to C₁₄ and C₁₅ to C₁₉ products also were present in significant amounts. As the authors experienced deactivation issues with the metathesis catalyst **3**, they investigated an alternative catalyst system comprised of the iridium catalyst and heterogeneous catalyst Re₂O₇/Al₂O₃, which also proved effective for the reaction. After nine days at 175 °C the product mixture consisted of C₂ to C₃₀ alkanes with an approximately Gaussian product distribution centred at C₁₀.

References

- S. Luo, X. Mi, L. Zhang, S. Liu, H. Xu and J.-P. Cheng, *Angew. Chem.*, 2006, **118**, 3165–3169.
- R. Gausepohl, P. Buskens, J. Kleinen, A. Bruckmann, Ch. W. Lehmann, J. Klankermayer and W. Leitner, *Angew. Chem.*, 2006, **118**, 3635.
- T. Kawasaki, K. Suzuki, K. Hatase, M. Otsuka, H. Koshima and K. Soai, *Chem. Commun.*, 2006, 1869–1871.
- A. S. Goldman, A. H. Roy, Z. Huang, R. Ahuja, W. Schinski and M. Brookhart, *Science*, 2006, **312**, 257–261.

Impact of ionic liquids on papain: an investigation of structure–function relationships†

Wen-Yong Lou,^{ab} Min-Hua Zong,^{*a} Thomas J. Smith,^c Hong Wu^a and Ju-Fang Wang^a

Received 20th January 2006, Accepted 30th March 2006

First published as an Advance Article on the web 7th April 2006

DOI: 10.1039/b600930a

Ionic liquids (ILs) containing a range of 1-alkyl-3-methylimidazolium cations and various anions affect papain's catalytic performance and thermostability in a manner that correlates closely with the effects of the ILs on the conformation of the enzyme as assessed by using ATR-FTIR and fluorescence techniques.

The use of ILs as novel solvents or co-solvents for organic synthesis or biocatalytic transformations has received considerable interest.¹ Following pioneering work by Erbeldinger *et al.*,² enzymes of widely different types have been demonstrated to be active in systems containing ILs, in some cases showing comparable or higher activity, selectivity and stability than in organic solvents.³ It is therefore surprising that the influence of ILs on enzyme structure has only recently become a focus of study. Spectroscopic techniques (especially fluorescence, circular dichroism and Fourier transform infrared analysis) that can be employed for conformational characterisation of proteins and to study stabilization or denaturation of enzymes⁴ have recently been used to correlate changes in the stability and activity of monellin,⁵ *Candida antarctica* lipase B,⁶ α -chymotrypsin,⁷ cytochrome *c*⁸ and cellulase⁹ with their secondary structure in IL-containing systems. Here, papain from *Papaya latex* (EC 3.4.22.2) was chosen for study because of its well-characterized molecular structure and wide applications.¹⁰ Single pass attenuated total reflection Fourier transform infrared (ATR-FTIR) and fluorescence techniques were applied to monitor its conformation in systems involving various ILs.

Papain (>98% purity) was purchased as lyophilized powder from Sigma (USA) and was further purified by a Sephadex G-100 column (50 cm \times 2.5 cm) to become electrophoretically pure before being used for spectroscopic analysis. Papain-mediated asymmetric hydrolysis of D,L-*p*-hydroxyphenylglycine methyl ester (D,L-HPGME) was selected as the model reaction owing to its potential application for preparing enantiopure *p*-hydroxyphenylglycine,¹¹ a key building block in the manufacture of semisynthetic antibiotics.¹² The nine ILs (1–9, refer to Table 1; >96% purity) used in this study, kindly donated by Dr Xue-Hui Li (Department

of Chemical Engineering, South China University of Technology, China), are based on the 1-alkyl-3-methylimidazolium cation ($C_n\text{MIm}^+$, $n = 2–6$) combined with the anions BF_4^- , HSO_4^- , Cl^- , NO_3^- , or CH_3COO^- . The ILs were further purified according to a published purification procedure¹³ by filtration through silica gel to remove halides and washing with sodium carbonate to remove acidic impurities prior to use. These ILs are miscible with water in all proportions, and were used as co-solvents with phosphate buffer (50 mM, pH 7.0). The apparent pH of the co-solvent system was measured at various concentrations of each IL used. When $C_n\text{MIm}\cdot\text{BF}_4$ ($n = 2–6$) content was above 30% (v/v, by volume), the pH of the mixed solvent was clearly lowered with increasing concentration of the IL. No appreciable variation of the pH, however, was observed in the cases where $C_n\text{MIm}\cdot\text{BF}_4$ ($n = 2–6$) concentration was below 20% (v/v), which is in good accordance with our previous observations.^{11,14} Similarly, when the concentration of $C_4\text{MIm}\cdot\text{HSO}_4$, $C_4\text{MIm}\cdot\text{Cl}$, $C_4\text{MIm}\cdot\text{NO}_3$ or $C_4\text{MIm}\cdot\text{CH}_3\text{COO}$ present in the mixed solvent was $\leq 15\%$ (v/v), the pH was hardly affected by the ILs. Thus, the effect of different ILs on papain was determined in the presence of 15% (v/v) content of each IL examined (unless specified otherwise).

Many reports show that the effects of various ILs on enzymatic reactions vary widely and unpredictably.¹⁵ Our use of systems involving various ILs allowed us to focus on the influence of the cations and anions of the IL on the catalytic performance and conformation of papain in a range of IL systems containing $C_n\text{MIm}^+$ cations. In the case of $C_n\text{MIm}\cdot\text{BF}_4$ ($n = 2–6$), both the hydrophobicity and viscosity of the IL increase with increasing length of the alkyl group (*i.e.* length of C-chain) attached to the cation, while the polarity decreases to some extent.¹⁶ Papain-mediated hydrolysis of D,L-HPGME became slower and more enantioselective {expressed in terms of the enantiomeric ratio (*E*-value)¹⁷ unless specified otherwise} with the length of C-chain attached to the cation in $C_n\text{MIm}\cdot\text{BF}_4$ ($n = 2–6$) (Table 1). In comparison with aqueous phosphate buffer (50 mM, pH 7.0), comparable or higher activity and enantioselectivity exhibited by papain were obtained in the $C_n\text{MIm}\cdot\text{BF}_4$ ($n = 2–6$)-based systems, while activity and enantioselectivity were lower in systems involving $C_4\text{MIm}\cdot\text{HSO}_4$, $C_4\text{MIm}\cdot\text{Cl}$, $C_4\text{MIm}\cdot\text{NO}_3$ or $C_4\text{MIm}\cdot\text{CH}_3\text{COO}$ (Table 1). The results suggest that the IL anion may be more crucial in determining the activity and enantioselectivity of the enzyme than the length of the alkyl chain on the cation. One possible explanation for this is that the enzyme-compatible anions show lower hydrogen bond basicity, which may minimize interference with the internal hydrogen bonds of the enzyme.¹⁸ Consistent with this notion, the enzyme has low activity in $C_4\text{MIm}\cdot\text{Cl}$, $C_4\text{MIm}\cdot\text{NO}_3$, $C_4\text{MIm}\cdot\text{CH}_3\text{COO}$ and $C_4\text{MIm}\cdot\text{HSO}_4$, all of which have high hydrogen-bond basicity. BF_4^- , on the other

^aLaboratory of Applied Biocatalysis, South China University of Technology, Guangzhou, 510640, China. E-mail: wylou@scut.edu.cn; bmhzong@scut.edu.cn; Fax: +86 20-2223-6669; Tel: +86 20-8711-1452

^bThe State Key Laboratory of Bioreactor Engineering, East China University of Science and Technology, Shanghai, 200237, China

^cBiomedical Research Centre, Sheffield Hallam University, Owen Building, Howard Street, Sheffield, UK S1 1WB. E-mail: t.j.smith@shu.ac.uk

† Electronic supplementary information (ESI) available: Experimental section. See DOI: 10.1039/b600930a

Table 1 The catalytic performance exhibited by papain in different media^a

Medium	IL number ^b	Activity/ $\mu\text{mol min}^{-1}$	Selectivity (<i>E</i> -value) ^c	K_m ^d /mM	V_{max} ^d / $\mu\text{mol min}^{-1}$
C ₂ MIm·BF ₄	1	1.4	34	16	1.6
C ₃ MIm·BF ₄	2	1.3	52	17	1.5
C ₄ MIm·BF ₄	3	1.2	99	18	1.4
C ₅ MIm·BF ₄	4	1.0	109	23	1.2
C ₆ MIm·BF ₄	5	0.8	118	36	1.0
C ₄ MIm·HSO ₄	6	0.1	1	18	0.2
C ₄ MIm·Cl	7	0.3	7	19	0.4
C ₄ MIm·NO ₃	8	0.4	11	20	0.5
C ₄ MIm·CH ₃ COO	9	0.6	23	23	0.7
Aqueous buffer		0.8	42	35	1.0

^a The full experimental details are available as ESI†. ^b 1: 1-Ethyl-3-methylimidazolium tetrafluoroborate (C₂MIm·BF₄); 2: 1-propyl-3-methylimidazolium tetrafluoroborate (C₃MIm·BF₄); 3: 1-butyl-3-methylimidazolium tetrafluoroborate (C₄MIm·BF₄); 4: 1-amy-3-methylimidazolium tetrafluoroborate (C₅MIm·BF₄); 5: 1-hexyl-3-methylimidazolium tetrafluoroborate (C₆MIm·BF₄); 6: 1-butyl-3-methylimidazolium bisulfate (C₄MIm·HSO₄); 7: 1-butyl-3-methylimidazolium chloride (C₄MIm·Cl); 8: 1-butyl-3-methylimidazolium nitrate (C₄MIm·NO₃); 9: 1-butyl-3-methylimidazolium acetate (C₄MIm·CH₃COO). ^c Enantiomeric ratio was calculated from the following equation: $E\text{-value} = \ln[(1 - C)(1 - ee_s)] / \ln[(1 - C)(1 + ee_s)]$, *C*: substrate conversion, *ee*_s: enantiomeric excess of remaining substrate.¹⁷ ^d The apparent kinetic parameters (K_m , V_{max}) were estimated as described in the ESI†. Each experiment was conducted at least in duplicate and the average variation in each parameter was less than 0.6%.

hand, spreads its negative charge over four fluorine atoms and thus weakens the hydrogen bond basicity of C_{*n*}MIm·BF₄ (*n* = 2–6), which accordingly afford high enzyme activities (Table 1). Another important factor may be that the enzyme-compatible anion BF₄[−] exhibits lower nucleophilicity than the other anions tested and thus may show a lower tendency to induce conformational changes by interacting with positively charged sites on the enzyme.⁶ It is interesting that there was a negative correlation between activity and selectivity when the C-chain length in C_{*n*}MIm·BF₄ (*n* = 2–6) was varied (Table 1; ILs 1–5), but a positive correlation between activity and selectivity when the anions were changed (Table 1; ILs 6–9). The reasons for this phenomenon are the subject of ongoing investigation in our laboratory.

In the systems containing the above-mentioned ILs, the enzymatic hydrolysis was regarded as a monosubstrate reaction

since water was in great excess, and was found to follow Michaelis–Menten kinetics. The apparent K_m and V_{max} values of the reactions conducted in different media are presented in Table 1. With respect to C_{*n*}MIm·BF₄ (*n* = 2–6), K_m increased and V_{max} decreased with increasing length of C-chain, indicating a positive correlation between the affinity of papain towards the substrate and the polarity of the IL. Low V_{max} and high K_m values with the IL anions other than BF₄[−] were consistent with the overall activity results (Table 1).

Second derivative ATR-FTIR spectra in the amide I region of papain were used as a particularly sensitive probe of protein conformation.^{8,19} In spite of some spectral variations it can be observed that the protein shows similar patterns of bands in the systems containing C_{*n*}MIm·BF₄ (*n* = 2–6) (Fig. 1, curves 1–5) and in the aqueous phosphate buffer (50 mM, pH 7.0) control system,

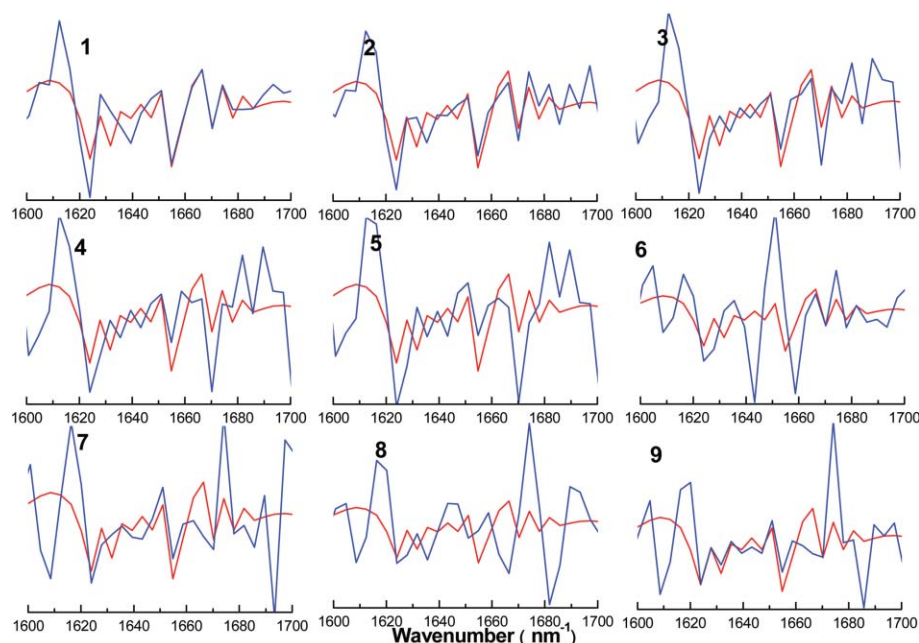


Fig. 1 Comparison of the second derivative ATR-FTIR spectra in the amide I region of papain in the systems involving ILs 1–9 (blue curves) and the aqueous buffer control (red curve)

suggesting that papain is in a near native conformation in all these systems. In particular, the key peaks at around 1624, 1655 and 1672 cm^{-1} (typically assigned to β -turn, α -helix and β -sheet, respectively) are generally retained in the $C_n\text{MIm}\cdot\text{BF}_4$ ($n = 2-6$)-containing systems, in agreement with the fact that papain displays high activity in the systems involving these ILs. Additionally, it is notable that, although the α -helix structure was partially unfolded in the $C_n\text{MIm}\cdot\text{BF}_4$ ($n = 2-6$)-containing systems, both β -turns and β -sheets clearly increased, possibly resulting in a more compact and stable enzyme conformation capable of exhibiting catalytic activity.^{6,7} As predicted, the second derivative spectra in the systems involving $C_4\text{MIm}\cdot\text{Cl}$, $C_4\text{MIm}\cdot\text{NO}_3$, $C_4\text{MIm}\cdot\text{CH}_3\text{COO}$ and especially $C_4\text{MIm}\cdot\text{HSO}_4$ (Fig. 1) were greatly different from the buffer control. The complete absence of α -helix peak at 1655 cm^{-1} and the presence of two strong peaks at 1643 and 1660 cm^{-1} , which could be assigned to random coil structure and non-hydrogen-bonded carbonyls of β -turn, were observed in the system containing $C_4\text{MIm}\cdot\text{HSO}_4$, which gave the most non-native spectrum. In the case of $C_4\text{MIm}\cdot\text{Cl}$, $C_4\text{MIm}\cdot\text{NO}_3$ or $C_4\text{MIm}\cdot\text{CH}_3\text{COO}$, the peaks at around 1692, 1681 or 1686 cm^{-1} , typically assigned to random coil conformations, greatly increased, but α -helix content at 1655 cm^{-1} was clearly reduced. The extent of perturbation of secondary structure was consistent with the losses of the activity observed (Table 1).

For proteins such as papain that contain fluorophore residues (e.g., Trp, Tyr or Phe), structural variations can be reflected by changes in the maximal intensity of fluorescence (I_{max}) and the maximal emission wavelength (λ_{max}), both of which result from altered polarity of the microenvironment of these residues. Upon selective excitation of Trp residues at 285 nm, the intrinsic fluorescence spectrum of the enzyme exhibited a λ_{max} of 339 nm in the aqueous phosphate buffer (50 mM, pH 7.0) control (Fig. 2), which was blueshifted in the systems involving $C_n\text{MIm}\cdot\text{BF}_4$ ($n = 2-6$), whilst I_{max} decreased (Fig. 2, curves 1–5). The blueshift fluorescence in λ_{max} can be attributed to conformational changes in the vicinity of two surface-exposed tryptophans (Trp-33 and Trp-42),²⁰ presumably owing to internalization in a more hydrophobic environment caused by the ILs $C_n\text{MIm}\cdot\text{BF}_4$ ($n = 2-6$). A similar blueshift fluorescence has been previously reported for

glucose isomerase.²¹ Conversely, λ_{max} was redshifted in the IL-containing systems involving the anions HSO_4^- , Cl^- , NO_3^- and CH_3COO^- (Fig. 2, curves 6–9), suggesting substantial unfolding of the protein. This might be explained by the fact that the four ILs contain strong nucleophilic anions that interact readily with positively charged sites on the enzyme, allowing the breakage of internal hydrogen bonds or the formation of new hydrogen bonds that perturb the structure. Furthermore, owing to its relatively strong acidity $C_4\text{MIm}\cdot\text{HSO}_4$ could give rise to the breakage of the disulfide bond between Cys-56 and Cys-95 located in the helical domain of the papain molecule²² and concomitant denaturation of the protein. Consistent with this theory, $C_4\text{MIm}\cdot\text{HSO}_4$ appears to reduce the amount of α -helix in the protein (Fig. 1, curve 6). This unfolding may also impact on Trp-177, which is in close proximity (through space) to the helical domain.^{19,21}

In fluorescence studies, the spectral changes associated with protein unfolding also provide information about enzyme stability. Generally, a red shift of λ_{max} in an aqueous system corresponds to unfolding of the enzyme, which enhances the exposure of Trp residues to the bulk solvent.^{5,7,19,21} Hence, a comparison as a function of temperature (30–95 °C) was made between activity loss profiles and changes in the λ_{max} of papain in the IL-containing systems, in order to further understand the structure–function relationships of the enzyme in each reaction medium. In all cases, the λ_{max} was redshifted with increasing temperature due to the unfolding of the enzyme, which corresponded to the observed decrease in the residual activity (Fig. S1 in ESI†). There was a clear correlation between enzyme stabilization and blueshifting of the λ_{max} temperature profile and between enzyme destabilization and redshifting of the λ_{max} temperature profile. The striking stabilization of papain by $C_n\text{MIm}\cdot\text{BF}_4$ ($n = 2-6$) seems to be directly correlated with the observed evolution of α -helix to β -turn and β -sheet secondary structure of the enzyme (Fig. 1), leading to a more compact and stable enzyme conformation.

Additionally, IL concentration in the mixed solvent showed a substantial effect on the stability of papain. Papain's stability increased with increasing content of the IL in the case of $C_n\text{MIm}\cdot\text{BF}_4$ ($n = 2-6$) and, conversely, decreased with increasing content of $C_4\text{MIm}\cdot\text{HSO}_4$, $C_4\text{MIm}\cdot\text{Cl}$, $C_4\text{MIm}\cdot\text{NO}_3$ or $C_4\text{MIm}\cdot\text{CH}_3\text{COO}$ in the reaction systems within the range (0–50%, v/v) examined (Fig. S2 in ESI†). This clearly demonstrates that $C_n\text{MIm}\cdot\text{BF}_4$ ($n = 2-6$) markedly improves the stability of the enzyme, but the presence of $C_4\text{MIm}\cdot\text{HSO}_4$, $C_4\text{MIm}\cdot\text{Cl}$, $C_4\text{MIm}\cdot\text{NO}_3$ or $C_4\text{MIm}\cdot\text{CH}_3\text{COO}$ makes the enzyme less stable.

In summary, the nature of the cation and especially the anion components of the ILs had a profound impact on the catalytic performance and structure of papain. The enzyme was more native in structure, active, enantioselective and stable in $C_n\text{MIm}\cdot\text{BF}_4$ ($n = 2-6$)-containing systems. Conversely, it was less native in structure and less active, enantioselective and stable in the systems involving $C_4\text{MIm}\cdot\text{HSO}_4$, $C_4\text{MIm}\cdot\text{Cl}$, $C_4\text{MIm}\cdot\text{NO}_3$ or $C_4\text{MIm}\cdot\text{CH}_3\text{COO}$.

Acknowledgements

ILs provided by Dr Xue-Hui Li (Department of Chemical Engineering, South China University of Technology, China) are gratefully acknowledged. The authors wish to thank the National Natural Science Foundation of China (Grant No.20406006), BBSRC China Partnering Award

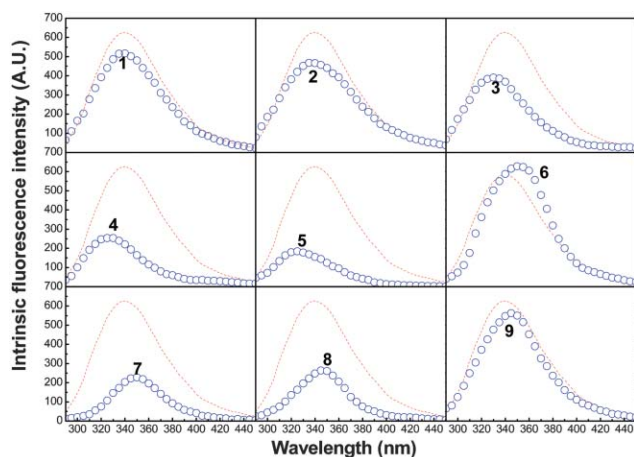


Fig. 2 Comparison of the intrinsic fluorescence spectra of papain in the systems involving ILs 1–9 (blue curves) and the aqueous buffer control (red curve).

(Grant No. PA1519) and the State Key Laboratory of Bioreactor Engineering, East China University of Science and Technology for financial support.

References

- U. Kragl, M. Eckstein and N. Kaftzik, *Curr. Opin. Biotechnol.*, 2002, **13**, 565; F. van Rantwijk, R. M. Lau and R. A. Sheldon, *Trends Biotechnol.*, 2003, **21**, 131; C. E. Song, *Chem. Commun.*, 2004, 1033; Z. Yang and W. B. Pan, *Enzyme Microb. Technol.*, 2005, **37**, 19.
- M. Erbeltinger, A. J. Mesiano and A. J. Russell, *Biotechnol. Prog.*, 2000, **16**, 1129.
- M. Persson and U. T. Bornscheuer, *J. Mol. Catal. B: Enzym.*, 2003, **22**, 21; R. M. Lau, F. van Rantwijk, K. R. Seddon and R. A. Sheldon, *Org. Lett.*, 2000, **26**, 4189; K. W. Kim, B. Song, M. Y. Chio and M. J. Kim, *Org. Lett.*, 2001, **3**, 1507; M. Eckstein, M. V. Filho, A. Liese and U. Kragl, *Chem. Commun.*, 2004, 1084; Y. Y. Liu, W. Y. Lou, M. H. Zong, R. Xu and H. Wu, *Biocatal. Biotransform.*, 2005, **23**, 89; W. Y. Lou, M. H. Zong, H. Wu, R. Xu and W. J. Fang, *Green Chem.*, 2005, **7**, 500; W. Y. Lou, R. Xu and M. H. Zong, *Biotechnol. Lett.*, 2005, **27**, 1387; A. Basso, S. Cantone, P. Linda and C. Ebert, *Green Chem.*, 2005, **7**, 671; P. Lozano, T. de Diego, S. Gmouh, M. Vaultier and J. L. Iborra, *Biotechnol. Prog.*, 2004, **20**, 661.
- P. Lozano, T. de Diego and J. L. Iborra, *Eur. J. Biochem.*, 1997, **248**, 80; F. Secundo and G. Carrea, *J. Mol. Catal. B: Enzym.*, 2002, **19**, 93; Y. Mei, L. Miller, W. Cao and R. A. Gross, *Biomacromolecules*, 2003, **4**, 70.
- S. N. Baker, T. M. McCleskey, S. Pandey and G. A. Baker, *Chem. Commun.*, 2004, 940.
- R. M. Lau, M. J. Sorgedraeger, G. Carrea, F. van Rantwijk, F. Secundo and R. A. Sheldon, *Green Chem.*, 2004, **6**, 483; T. de Diego, P. Lozano, S. Gmouh, M. Vaultier and J. L. Iborra, *Biomacromolecules*, 2005, **6**, 1457.
- T. de Diego, P. Lozano, S. Gmouh, M. Vaultier and J. L. Iborra, *Biotechnol. Bioeng.*, 2004, **88**, 916.
- K. Fujita, D. R. MacFarlane and M. Forsyth, *Chem. Commun.*, 2005, 4804.
- M. B. Turner, S. K. Spear, J. G. Huddleston, J. D. Holbrey and R. D. Rogers, *Green Chem.*, 2003, **5**, 443.
- F. Edwin and M. V. Jagannadham, *Biochem. Biophys. Res. Commun.*, 1998, **252**, 654; L. Panella, J. Broos, J. F. Jin, M. W. Fraaije, D. B. Janssen, M. Jeronimus-Stratingh, B. L. Feringa, A. J. Minnaard and J. G. de Vries, *Chem. Commun.*, 2005, 5656.
- W. Y. Lou, M. H. Zong and H. Wu, *Biotechnol. Appl. Biochem.*, 2005, **41**, 151; W. Y. Lou, M. H. Zong and H. Wu, *Biocatal. Biotransform.*, 2004, **22**, 171.
- B. K. Hubbard, M. G. Thomas and C. T. Walsh, *Chem. Biol.*, 2000, **7**, 931; A. Bruggink, E. C. Roos and E. de Vroom, *Org. Process Res. Dev.*, 1998, **2**, 128.
- S. Park and R. J. Kazlauskas, *J. Org. Chem.*, 2001, **66**, 8395.
- W. Y. Lou, M. H. Zong and T. J. Smith, *Green Chem.*, 2006, **8**, 147.
- R. Irimescu and K. Kato, *J. Mol. Catal. B: Enzym.*, 2004, **30**, 189; F. Stock, J. Hoffmann, J. Ranke, R. Störmann, B. Ondruschka and B. Jastorff, *Green Chem.*, 2004, **6**, 286; R. A. Sheldon, R. M. Lau, M. J. Sorgedraeger and F. van Rantwijk, *Green Chem.*, 2002, **4**, 147.
- S. V. Dzyuba and R. A. Bartsch, *ChemPhysChem*, 2002, **3**, 161; H. Zhao, *Phys. Chem. Liquids*, 2003, **41**, 545; S. Park and R. J. Kazlauskas, *J. Org. Chem.*, 2001, **66**, 8395.
- C. S. Chen, Y. Fujimoto, G. Girdaukas and C. J. Sih, *J. Am. Chem. Soc.*, 1982, **104**, 7294; J. L. L. Rackels, A. J. J. Straathof and J. J. Heijnen, *Enzyme Microb. Technol.*, 1993, **15**, 1051.
- J. L. Kaar, A. M. Jesionowski, J. A. Berberich, R. Moulton and A. J. Russell, *J. Am. Chem. Soc.*, 2003, **125**, 4125; S. Park and R. J. Kazlauskas, *Curr. Opin. Biotechnol.*, 2003, **14**, 432.
- W. K. Surewicz, H. H. Mantsch and D. Chapman, *Biochemistry*, 1993, **32**, 389.
- A. Naeem, K. A. Khan and R. H. Khan, *Arch. Biochem. Biophys.*, 2004, **432**, 79.
- S. A. Pawar and V. V. Deshpande, *Eur. J. Biochem.*, 2000, **267**, 6331.
- F. Edwin and M. V. Jagannadham, *Biochim. Biophys. Acta*, 2000, **1497**, 69.

Synthesis of 9-methylgermacrene B, racemate of the sex pheromone of *Lutzomyia longipalpis* (Lapinha), from the renewable resource, *Geranium macrorrhizum* essential oil

A. M. Hooper, J.-B. Farcet, N. P. Mulholland and J. A. Pickett*

Received 27th February 2006, Accepted 5th April 2006

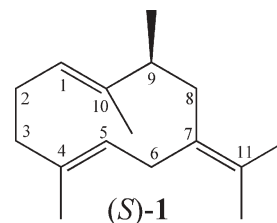
First published as an Advance Article on the web 19th April 2006

DOI: 10.1039/b602875f

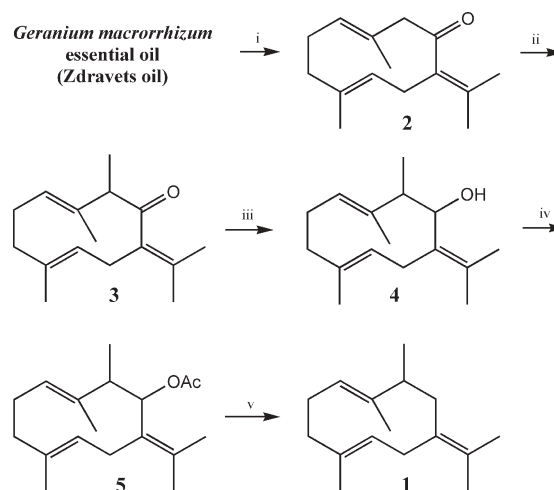
The sex pheromone of *Lutzomyia longipalpis* (Lapinha), comprising the unusual homosesquiterpene, 9-methylgermacrene B, can be prepared by methylation and deoxygenation of germacrene, the major constituent of Zdravets oil, the essential oil of the renewable resource *Geranium macrorrhizum*.

The sandfly *Lutzomyia longipalpis* (Lutz and Neiva) (Diptera: Psychodidae) is the vector of the causative agent of visceral leishmaniasis in the New World.¹ Female *L. longipalpis* are highly attracted to leks of males that release a sex pheromone from glands on the tergites of the abdomen.² It is these females that vector the parasite while biting to obtain a blood meal for development of her eggs. Thus, by attracting females to lures containing the synthetic sex pheromone there is potential to reduce infection rates in humans. *L. longipalpis* is a species complex, and different populations of *L. longipalpis* use separate male-produced sex pheromones.³ In the Jacobina region of Brazil, the sex pheromone has been identified as (1*S*,3*S*,7*R*)-3-methyl- α -himachalene, which has been successfully synthesised by Mori *et al.*^{4,5} In the Lapinha region of Brazil (Minas Gerais State) the sex pheromone has been identified as (*S*)-9-methylgermacrene B [(*S*)-**1**].⁶ Whilst impressive total syntheses of this material have also been achieved racemically⁷ and enantiospecifically⁸ to verify the structure of the pheromone, the large number of chemical transformations (the racemic synthesis comprises 13 steps) make this an unsuitable method to obtain sufficient quantities of the pheromone for field trials, or for the transfer of production technology to the developing world areas where the pheromone can be deployed. Our previous work has relied on renewable resources in order to generate other semiochemicals. Using whole plants in the field, molasses grass *Melinis minutiflora* produces (*E*)-4,8-dimethylnona-1,3,7-triene, which is attractive to the stemborer parasitoid *Cotesia sesamiae*,⁹ while other semiochemicals, the aphid sex pheromones (4*aS*,7*S*,7*aR*)-nepetalactone and its chemically generated derivative (1*R*,4*aS*,7*S*,7*aR*)-nepetalactol, are renewably resourced from the catmint plant *Nepeta cataria*,¹⁰ which is now produced on a commercial scale by Botanix Ltd (Kent).

The 10-membered ring structure of 9-methylgermacrene B (**1**) is a synthetic challenge to construct¹¹ but exists in the natural product germacrene, produced in high concentration in Zdravets oil, the essential oil of the cranesbill *Geranium macrorrhizum* (Geraniaceae).¹² *G. macrorrhizum* was grown by Botanix Ltd

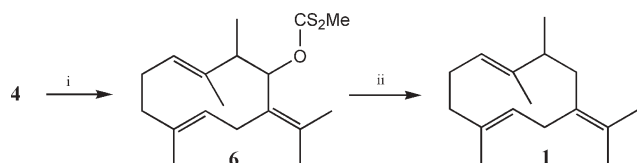


(Kent), and the essential oil obtained by steam distillation. GC analysis showed germacrene comprised 59% of the essential oil, which is a production level high enough to make the plant useful as a chemical factory for generating synthetic starting material. Recrystallisation of the oil (60 g) in ethanol at $-20\text{ }^{\circ}\text{C}$ afforded germacrene **2** [27.2 g, mp $52\text{ }^{\circ}\text{C}$ (from EtOH)]. (*S*)-**1** is a biosynthetically unusual homosesquiterpene pheromone and therefore requires introduction of an extra methyl group. The enolate produced from germacrene is conjugated. However, the conditions needed for highly regioselective α -methylation were found to be HMPA complexation of the LDA-generated enolate (Scheme 1). Removal of the ketone group was achieved by LiAlH_4 reduction, acetylation and dissolving metal reduction. Standard conditions for dissolving metal reduction (Li in NH_3 , $-78\text{ }^{\circ}\text{C}$) gave 9-methylgermacrene B (**1**) in only 4% yield by GC. The products of the dissolving metal reduction of **5** were predominately



Scheme 1 Reagents and conditions: (i) recrystallisation from EtOH; (ii) $-78\text{ }^{\circ}\text{C}$, 1.2 eq. LDA, 1.2 eq. HMPA, 5 eq. MeI, 54%; (iii) LiAlH_4 ; (iv) Ac_2O , pyridine, DMAP, 93% (2 steps); (v) Li, HNEt_2 , $-10\text{ }^{\circ}\text{C}$, 10% on 1 g scale.

Rothamsted Research, Harpenden, Herts, AL5 2JQ, UK.
E-mail: john.pickett@bbsrc.ac.uk; Fax: +44 (0)1582 762595;
Tel: +44 (0)1582 763133



Scheme 2 Reagents and conditions: (i) 1.1 eq. BuLi, 10 eq. CS₂, 10 eq. MeI; (ii) 1.5 eq. Bu₃SnH, 1 eq. BEt₃, O₂, 35% on 1 g scale over 2 steps.

starting material and **4**. Warming the reaction to 0 °C produced more of the desired product but also a large number of byproducts by GC. The best results came from using Li in Et₂NH maintained at -10 °C, producing **1** in 50% yield by GC. However, when the reaction was scaled up from 100 mg of **5** to 0.5 g, the purified yield was only 26%, and on a scale of 1 g or above the reaction proved unreliable, with low purified yields of approximately 10%.[†]

A better method of deoxygenation was achieved by derivatising **4** as the methyl dithiocarbonate (**6**) followed by reduction with tributyltin hydride (Scheme 2). Initiation of the reaction was best performed by triethylborane with addition of dry air through a syringe pump, and gave reproducible yields of over 30% after column chromatography using petroleum ether.¹³ Although this shortened synthesis of the pheromone is facilitated by generation of the starting material from a renewable resource, with

concomitant reduction of chemical and energy input, solvents, waste, and cost, the synthetic route does use some very toxic materials. Reducing toxicity in the deoxygenation step in particular would further benefit this synthesis, and as there is no biotechnological process available, the use of selective catalytic hydrogenolysis instead of radical chemistry could be explored.¹⁴ Chiral GC analysis of **1** resolves the enantiomers, and the biologically active (*S*)-**1** enantiomer co-elutes with the natural material (Fig. 1).¹⁵ Synthetic pheromone can now be prepared from a renewable resource, and with a simple synthetic route of 4 steps compared to the previous 13 steps. *G. macrorrhizum* is a hardy geranium and tolerant of a variety of light, moisture and soil pH conditions, making it a good candidate for technology transfer to areas of Brazil where populations of *L. longipalpis* use 9-methylgermacrene B as the sex pheromone, as previous studies have shown that (*R*)-**1** does not interfere with (*S*)-**1** activity.⁶

Rothamsted Research receives grant-aided support from the Biotechnology and Biological Sciences Research Council. *G. macrorrhizum* essential oil was supplied in collaboration with Dr R. Marriott, Botanix Ltd.

References and notes

[†] Methodology for the synthesis of **1**. In a flame-dried flask, butyllithium (2.5 M, 1.2 eq., 11.0 ml) was added to a solution of diisopropylamine (1.2 eq., 3.86 ml) in dry THF (100 ml). The mixture was cooled to -78 °C and a solution of germacrone (5.0 g, 22.9 mmol) in dry THF (25 ml) was added dropwise. After 30 minutes, HMPA (1.2 eq., 4.78 ml) was added and the reaction stirred for a further 1 h. Iodomethane (5 eq., 7.14 ml) was added and the reaction warmed to room temperature overnight. Standard work up and flash column chromatography (3% Et₂O in petroleum ether) afforded methylgermacrone **3** (2.85 g, 54%). A solution of LiAlH₄ (821 mg, 21.64 mmol) in ether (50 ml) was added to a suspension of LiAlH₄ (821 mg) in dry ether (100 ml) at 0 °C. On completion of the reaction and standard work up, the crude material **4** was dissolved in pyridine (40 ml) and Ac₂O (8 ml) with a small addition of dimethylaminopyridine. The reaction was stirred overnight, worked up and after flash column chromatography (10% Et₂O in petroleum ether) **5** was isolated (5.56 g, 93% over 2 steps). **1** from **5**: A solution of **5** (0.5 g, 1.81 mmol) in ether (6 ml) was added to a blue solution of Li (0.5 g) dissolved in 30 ml NHET₂ at -10 °C under N₂. The reaction was quenched with ammonium chloride and extracted (Et₂O) to afford **1** (101 mg, 26%) after flash column chromatography (petroleum ether). **1** from **6**: To a solution of **4** (1.0 g, 4.24 mmol) at 0 °C was added butyllithium (1.1 eq., 2.5 M, 1.90 ml) and the solution stirred for 10 min. Carbon disulfide (10 eq., 2.6 ml) was added and the solution stirred for 2 h at 40 °C. Iodomethane (10 eq., 2.63 ml) was added and the reaction stirred overnight. The crude product was dissolved in toluene (45 ml) at 0 °C, and BEt₃ (1 eq., 4.44 ml) added. Tributyltin hydride (1.5 eq., 1.8 ml) was added as a toluene solution (30 ml), and 50 ml of dry air injected into the solution through a syringe pump at 40 ml h⁻¹. Work up and flash column chromatography (petroleum ether) afforded **1** (0.33 g, 35%). $\nu_{\max}/\text{cm}^{-1}$ 2925s, 1660w (CC), 1453m, 1372m; δ_{H} (CDCl₃, 400 MHz) 1.02 (3H, d, *J* 7.1 Hz, 9-Me), 1.42 (3H, s, 10-Me), 1.52 (3H, s, 4-Me), 1.67 (3H, s, 11-Me), 1.69 (3H, s, 11-Me), 1.70 (1H, obscured m, H-8a), 1.93 (1H dt, *J* 5.3 12.1 Hz, H-3a), 2.00 (1H, m, H-2a), 2.16 (1H, m, H-3b), 2.18 (1H, m, H-9), 2.25–2.35 (3H, m, H-2b, H-6a, H-8b), 3.05 (1H, d, *J* 13.3 Hz, H-6b), 4.38 (1H, d, *J* 10.8 Hz, H-5), 4.71 (1H, dd, *J* 3.1, 12.0 Hz, H-1); δ_{C} (CDCl₃, 100 MHz) 11.2 (10-Me), 16.4 (4-Me), 20.5, 20.8, 20.9 (11-Me₂, 9-Me), 25.3 (2), 34.4 (6), 38.9 (3), 40.7 (8), 46.3 (9), 125.7 (1), 127.0 (11), 128.7 (5), 130.9 (4), 133.7 (7), 140.2 (10). *m/z* (EI) 218.2025 (M⁺. C₁₆H₂₆ requires 218.2035).

- 1 <http://www.who.int/topics/leishmaniasis/en/>; R. Lainson and J. J. Shaw, *Nature*, 1978, **273**, 595–600.
- 2 R. P. Lane, A. Phillips, D. H. Molyneux, G. Procter and R. D. Ward, *Ann. Trop. Med. Parasitol.*, 1985, **79**, 225–229.
- 3 A. Phillips, R. D. Ward, L. Ryan, D. H. Molyneux, R. Lainson and J. J. Shaw, *Acta Trop.*, 1986, **43**, 271–276.
- 4 J. G. C. Hamilton, A. M. Hooper, K. Mori, J. A. Pickett and S. Sano, *Chem. Commun.*, 1999, 355–356.

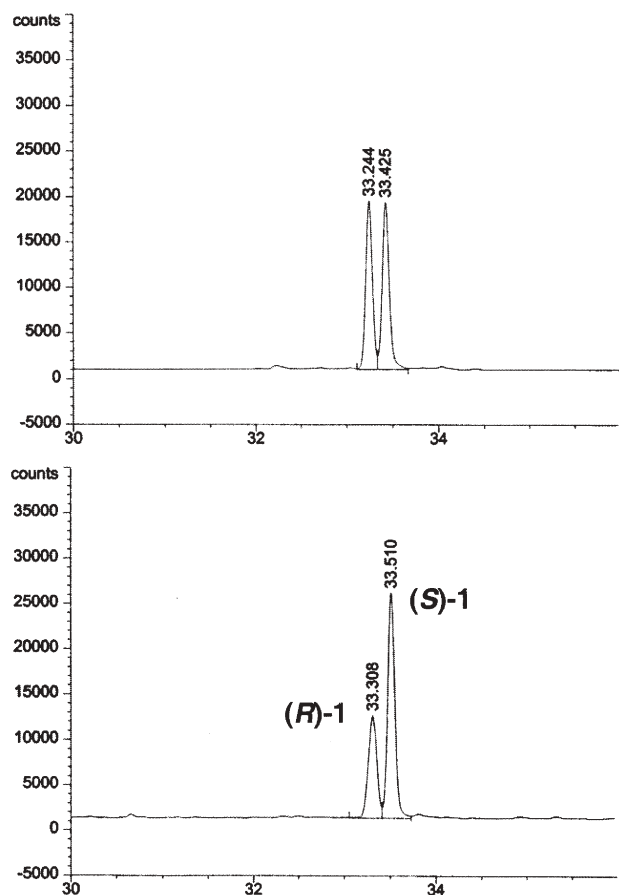


Fig. 1 (Top) Synthetic 9-methylgermacrene B (**1**) separated by GC on a β -cyclodextrin column. (Bottom) Synthetic **1** co-injected with the natural pheromone (*S*)-9-methylgermacrene B [(*S*)-**1**].

- 5 S. Sano and K. Mori, *Eur. J. Org. Chem.*, 1999, 1679–1686; T. Tashiro, M. Bando and K. Mori, *Synthesis*, 2000, 1852–1862.
- 6 J. G. C. Hamilton, A. M. Hooper, H. C. Ibbotson, S. Kurosawa, K. Mori, S.-E. Muto and J. A. Pickett, *Chem. Commun.*, 1999, 2335–2336.
- 7 S.-E. Muto, Y. Nishimura and K. Mori, *Eur. J. Org. Chem.*, 1999, 2159–2165.
- 8 S. Kurosawa and K. Mori, *Eur. J. Org. Chem.*, 2000, 955–962.
- 9 Z. R. Khan, K. Ampong-Nyarko, P. Chiliswa, A. Hassanali, S. Kimani, W. Lwande, W. A. Overholt, J. A. Pickett, L. E. Smart, L. J. Wadhams and C. W. Woodcock, *Nature*, 1997, **388**, 631–632.
- 10 M. A. Birkett and J. A. Pickett, *Phytochemistry*, 2003, **62**, 651–656.
- 11 A. J. Minnaard, J. B. P. A. Wijnberg and A. de Groot, *Tetrahedron*, 1999, **55**, 2115–2146.
- 12 I. Ognjanov, D. Ivanov, V. Herout, M. Horak, J. Pliva and F. Sorm, *Collect. Czech. Chem. Commun.*, 1958, **23**, 2033–2045.
- 13 K. Nozaki, K. Oshima and K. Utimoto, *Tetrahedron Lett.*, 1988, **29**, 6125–6126; K. Nozaki, K. Oshima and K. Utimoto, *Bull. Chem. Soc. Jpn.*, 1990, **63**, 2578–2583; V. T. Perchyonok and C. H. Schiesser, *Tetrahedron Lett.*, 1998, **39**, 5437–5438.
- 14 A. Bianco, P. Passacantilli and G. Righi, *Tetrahedron Lett.*, 1989, **30**, 1405–1408.
- 15 Chiral GC was performed using a β -cyclodextrin GC column, 0.25 mm id \times 30 m \times 25 μ m film thickness, 40 to 180 $^{\circ}$ C at 3 $^{\circ}$ C min $^{-1}$, with the injection port at 180 $^{\circ}$ C.



RSCPublishing

**Fast
Publishing?
Ahead of the field**

To find out more about RSC Journals, visit

www.rsc.org/journals

Green and controlled synthesis of gold and platinum nanomaterials using vitamin B₂: density-assisted self-assembly of nanospheres, wires and rods†

Mallikarjuna N. Nadagouda and Rajender S. Varma*

Received 26th January 2006, Accepted 3rd May 2006

First published as an Advance Article on the web 11th May 2006

DOI: 10.1039/b601271j

For the first time, we report efficient density-assisted self-assembly synthesis of gold and platinum nanospheres, nanowires and nanorods using vitamin B₂ (riboflavin) at room temperature without employing any special capping or dispersing agent; this environmentally benign and general approach affords a facile entry to production of shape-selective Au and Pt noble nanostructures, which can be extended to silver and palladium nanostructures.

The process by which molecular subunits spatially organize into well-defined supramolecular structures in spite of non-covalent interactions, self-assembly is becoming a powerful synthetic approach for creating advanced materials out of nanoparticle building blocks.¹ The preparations of highly structured nanoparticle assemblies, such as wires, rings, and super-lattices are being investigated extensively.² However, controlling the particle size and shape during synthesis is still a major challenge. Nevertheless, some physical and solid state chemical methods have been developed for making semiconductors, metal nanowires, nanobelts, and nanodots.³ Additionally, at present there are various methods for making rods with somewhat controllable aspect ratios using seeding approaches,⁴ pH-dependent assembly of gold nanorods⁵ and streptavidin-linked nanorods.⁶ All these solution-based methods are usually conducted at elevated temperatures and very often afford poor yields of the desired materials with appropriate shape. Thus, the development of bulk solution synthetic methods that offer shape control is of paramount importance if the full potential of these materials is to be realized. Herein, we identify a critical reaction parameter, the density of the reaction medium, which enables the self-assembly of noble metal nanoparticles into spheres, nanowires and nanorods in the presence of vitamin B₂.

There is increased emphasis on the synthesis of nanoparticles using greener methods.⁷ Green chemistry is the design, development, and implementation of chemical products and the process to reduce or eliminate the use and generation of substances hazardous to human health and the environment.⁸ This environmentally benign approach provides a facile entry to producing

multiple shaped noble nanostructures that could find widespread technological and medicinal applications.

The synthesis and self-assembly was carried out by reacting the respective metal salts with vitamin B₂ dissolved in solvents of varying densities, such as ethylene glycol (EG, $\rho = 1.113$), acetic acid ($\rho = 1.049$), *N*-methylpyrrolidinone (NMP, $\rho = 1.03$), water ($\rho = 0.998$), isopropanol (i-PrOH, $\rho = 0.790$), acetone ($\rho = 0.790$), and acetonitrile (MeCN, $\rho = 0.782$) at room temperature (see Supplementary information, S1†).

In the synthesis of metal nanoparticles using the reduction of the corresponding metal ion salt solutions, there are three areas of opportunity to engage green chemistry principles: (i) choice of solvent, (ii) the reducing agent employed, and (iii) the capping agent (or dispersing agent). In this context it would of great interest to identify environmentally friendly materials that are multifunctional. For example, the vitamin B₂ used in this study functions both as a reducing as well as capping agent for Au and Pt metals. In addition to its high water solubility, biodegradability, and low toxicity compared to other reducing agents, such as sodium borohydride (NaBH₄), hydroxylamine hydrochloride, *etc.*, it appears to be an ideal multifunctional agent for deployment in the production of nanomaterials.

Vitamin B₂ is the most frequently encountered organic cofactor in nature, and it can assume three different redox states: fully oxidized, one-electron reduced, and fully reduced⁹ (see Scheme 1). Each of these redox states can exist in a cationic, neutral, or anionic form depending on the pH of the solution, and all can transfer electrons.

The reduction potential of vitamin B₂ is -0.3 V vs. SCE¹⁰ which is sufficient to reduce Au³⁺ to Au⁰, whose reduction potential is 1.50 V vs. SCE, and similarly for Pt (reduction potential 1.20 V), and other noble metals *viz.* Pd (reduction potential 0.915 V) and Ag (reduction potential 0.80 V). The formation of Au and Pt nanoparticles with vitamin B₂ takes place by the following steps:

- complexation with Au and Pt metal salts
- simultaneous reduction of Au and Pt metal salts and formation of capping with oxidized vitamin B₂
- depending on the density of the solvent, self-assembly of nanoparticles to form spheres, nanowires and nanorods

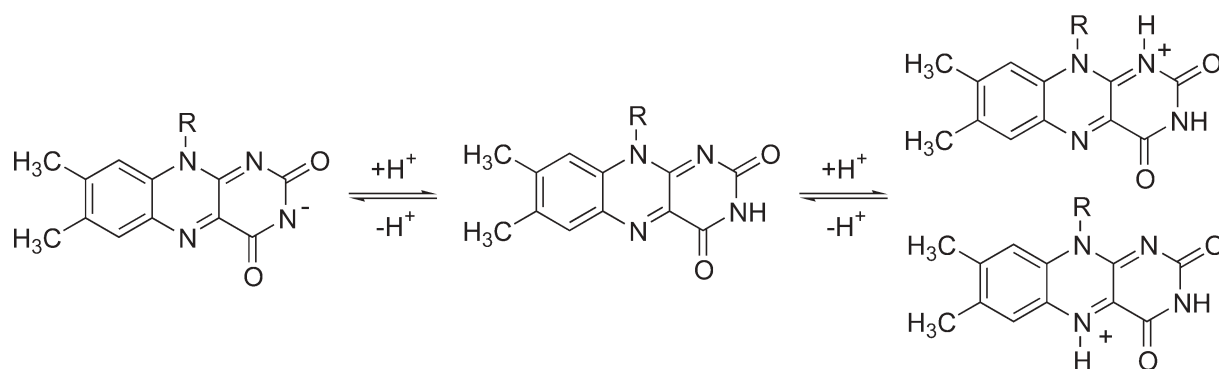
It has been found that the self-assembly of super-lattices of nanoparticles is determined by various factors such as surfactant concentration, ionic strength, pH,^{2f} temperature,^{2e} and slow evaporation of the solvent.^{2d} The spacing between nanoparticles in the solids can be tuned with modification of the capping materials,^{2d} and we have now found that solvent density plays a crucial role in governing controlled growth of different

Sustainable Technology Division, US Environmental Protection Agency, National Risk Management Research Laboratory, 26 W Martin Luther King Drive MS 443, Cincinnati, OH, 45268, USA.

E-mail: varma.rajender@epa.gov; Fax: +1 513-569-7677;

Tel: +1-513-487-2701

† Electronic supplementary information (ESI) available: Synthesis procedure (S1) and UV spectra (Fig. S2). See DOI: 10.1039/b601271j



Scheme 1 Structure of anionic (left), neutral (center) and cationic (right) vitamin B₂ species in the fully oxidized redox state (R = -CH₂(CHOH)₃CH₂OH).

self-assembled structures and shapes. Addition of respective metal salts to the vitamin B₂ in various solvents with varying densities resulted in the reduction of metal salts and concomitant oxidation and capping of vitamin B₂ as confirmed by UV spectroscopy (see Supplementary information, Fig. S2†). The formation of Au and Pt nanostructures with multiple shapes, depending on the density of the solvent used for the preparation, is shown in Fig. 1.

The size of the nanoparticles decreased with increase in density of the solvent used in the preparation (see Fig. 2(a–d)). High density solvents like ethylene glycol yielded nanoparticles in the range 5–12 nm with an average of 8.1 ± 0.1 nm for Au, and 7–11 nm with an average of 9.7 ± 0.1 nm for Pt (see inset of Fig. 2(a,b)). Decreasing the solvent density further, for example using acetic acid, yielded nanoparticles in the range 6–16 nm with an average of 11.54 ± 0.1 nm for Au, and 4–12 nm with average of 8.4 ± 0.1 nm for Pt.

However, in *N*-methylpyrrolidinone media nanoparticles underwent self-assembly to form a wide array of nanorod-type structures (data not shown). Fig. 3 shows the TEM micrographs of Au and Pt nanoparticles self-assembled in water and isopropanol, which have lower densities than ethylene glycol and acetic acid. It was

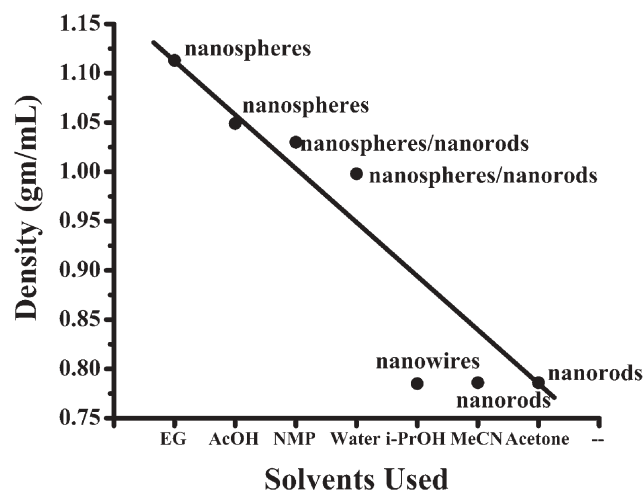


Fig. 1 The formation of Au and Pt nanostructures with multiple shapes depending on the density of the solvent used for the preparation.

observed that at a given instant the driving force (the density of a solvent) was responsible for the self-assembly of Au and Pt nanoparticles. This is due to the mobility of nanoparticles for the considered solvent density. For example, in water, Au and Pt nanoparticles started to self-assemble to form nanorod-like structures (see Fig. 3(a,b) respectively). Further reducing the solvent density, by using isopropanol in the preparation of Au and Pt nanoparticles, yielded nanowire structures with a thickness less than 10 nm (see Fig. 3(c,d) respectively). Interestingly, Pt nanoparticles were self-assembled together to produce preferentially end-to-end-linked Pt nanowires (see Fig. 3(d)).

Additionally, in solvents like acetone and acetonitrile, the Au and Pt nanoparticles self-assembled into a regular pattern, making nanorods with fully embedded nanoparticles (<10 nm particle size) with a thickness ranging from 100 to 200 nm and lengths of few microns (see Fig. 4(a–d)).

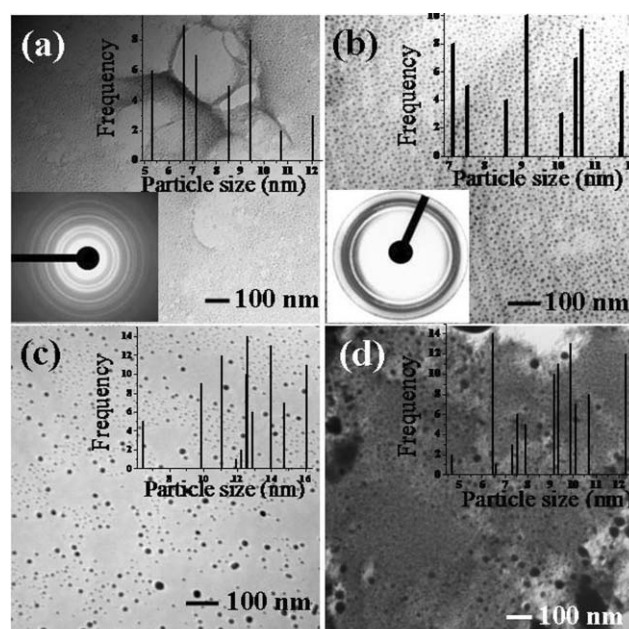


Fig. 2 TEM micrographs of Au and Pt synthesized using (a,b) ethylene glycol and (c,d) acetic acid as solvent media, respectively; the upper insets show the particle size distribution and the lower insets display the corresponding electron diffraction pattern.

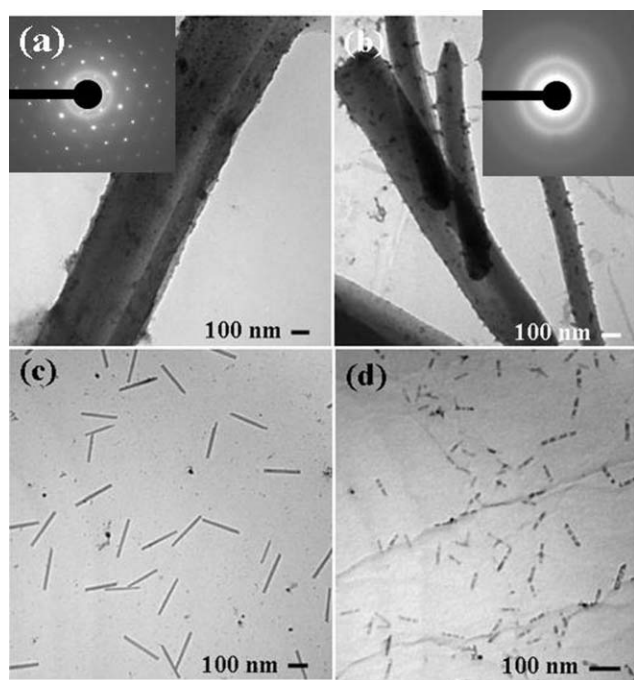


Fig. 3 TEM image of self-assembled Au and Pt nanowires/nanorods synthesized using vitamin B₂ in (a,b) water and (c,d) isopropanol, respectively; the insets show the corresponding electron diffraction patterns.

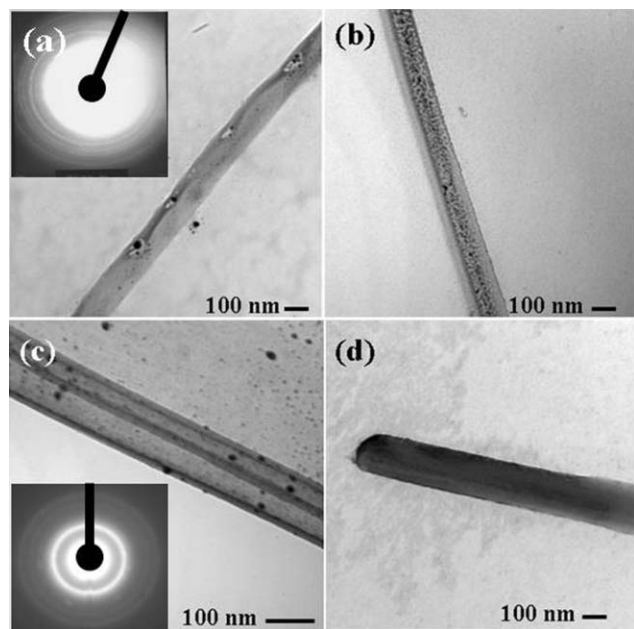


Fig. 4 TEM micrographs of self-assembled Au and Pt nanorods synthesized using vitamin B₂ in (a,b) acetone and (c,d) acetonitrile respectively; the insets show the corresponding electron diffraction patterns.

In all cases, irrespective of the solvent used, Au and Pt crystallized with fcc symmetry. In summary, we report:

i) a high yield, room temperature, density-assisted self-assembly of Au and Pt nanospheres, nanowires and nanorods using vitamin

B₂ in different solvent media, thus opening new opportunities in a myriad of applications, such as catalysis, antibacterial coatings, fuel cell membranes, *etc.*

ii) a method that employs no special capping or dispersing agent, nor any polymer as a coating agent.

iii) the formation of multiple Au and Pt shapes and dependence of their self-assembly on the density of the solvent used. As the density increases, the particles tend to form as individual spheres, and with a decrease in the density, particles will self-assemble to form nanorods and nanowires.

iv) this environmentally benign and general approach may find various medicinal and technological applications, and is extendable to other noble metals, such as Ag and Pd.

Acknowledgements

MNN was supported, in part, by the Postgraduate Research Program at the National Risk Management Research Laboratory administered by the Oak Ridge Institute for Science and Education through an interagency agreement between the U.S. Department of Energy and the U.S. Environmental Protection Agency. We thank Christina Bennett-Stamper, EPA Electron Microscopy Facility, for her help.

References

- (a) B. Zou, B. Ceyhan, U. Simon and C. M. Niemeyer, *Adv. Mater.*, 2005, **17**, 1643; (b) E. Rabani, D. R. Reichman, P. L. Geissler and L. E. Brus, *Nature*, 2003, **426**, 271.
- (a) M. A. El-Sayed, *Acc. Chem. Res.*, 2001, **34**, 257; (b) X.-S. Fang, C.-H. Ye, L.-D. Zhang, Y.-H. Wang and Y.-C. Wu, *Adv. Funct. Mater.*, 2005, **15**, 63; (c) Y. Xia, P. Yang, Y. Sun, Y. Wu, B. Mayers, B. Gates, Y. Yin, F. Kim and H. Yan, *Adv. Mater.*, 2003, **15**, 353; (d) C. Burda, X. Chen, R. Narayanan and M. A. El-Sayed, *Chem. Rev.*, 2005, **105**, 1025; (e) X. S. Fang, C. H. Ye, X. S. Peng, Y. H. Wang, Y. C. Wu and L. D. Zhang, *J. Mater. Chem.*, 2003, **13**, 3040–3043; (f) J. M. Petroski, Z. L. Wang, T. C. Green and M. A. El-Sayed, *J. Phys. Chem. B*, 1998, **102**, 3316; (g) B. Nikoobakht, Z. L. Wang and M. A. El-Sayed, *J. Phys. Chem. B*, 2000, **104**, 8635; (h) L. Zheng and J. Li, *J. Phys. Chem. B*, 2005, **109**, 1108; (i) S. H. Park, R. Barish, H. Li, J. H. Reif, G. Finkelstein, H. Yan and T. H. LaBean, *Nano Lett.*, 2005, **5**, 693; (j) M. M. Maye, I. I. S. Lim, J. Luo, Z. Rab, D. Rabinovich, T. Liu and C. J. Zhong, *J. Am. Chem. Soc.*, 2005, **127**, 1519; (k) I. In, Y. W. Jun, Y. J. Kim and S. Y. Kim, *Chem. Commun.*, 2005, **6**, 800; (l) F. Gao, Q. Lu and S. Komarneni, *Chem. Mater.*, 2005, **17**, 856; (m) N. R. Jana, *Angew. Chem., Int. Ed.*, 2004, **43**, 1536.
- (a) Z. W. Pan, Z. R. Dai and Z. L. Wang, *Science*, 2001, **291**, 1947; (b) J. Hu, T. W. Odom and C. M. Lieber, *Acc. Chem. Res.*, 1999, **32**, 435; (c) C. L. Haynes and R. P. Van Duyne, *J. Phys. Chem. B*, 2001, **105**, 5599.
- N. R. Jana, L. Gearheart and C. J. Murphy, *J. Phys. Chem. B*, 2001, **105**, 4065.
- C. J. Orendorff, P. L. Hankins and C. J. Murphy, *Langmuir*, 2005, **21**, 2022.
- K. K. Caswell, J. N. Wilson, U. H. F. Bunz and C. J. Murphy, *J. Am. Chem. Soc.*, 2003, **125**, 13914.
- (a) B. Ankamwar, C. Damle, A. Ahmad and M. J. Sastry, *J. Nanosci. Nanotechnol.*, 2005, **5**, 1665; (b) S. S. Shankar, A. Ahmad and M. Sastry, *Biotechnol. Prog.*, 2003, **19**, 1627.
- P. Anastas and J. Warner, *Green Chemistry: Theory and Practice*, Oxford University Press, New York, 1998.
- P. V. Jaiswal, V. S. Ijeri and A. K. Srivastava, *Anal. Sci.*, 2001, **17**, 741.
- V. Massey, *Biochem. Soc. Trans.*, 2000, **28**, 283.

An efficient synthesis of 1,5-benzodiazepine derivatives catalyzed by silver nitrate

Rupesh Kumar, Preeti Chaudhary, Surendra Nimesh, Akhilesh K. Verma and Ramesh Chandra*

Received 9th February 2006, Accepted 26th April 2006

First published as an Advance Article on the web 9th May 2006

DOI: 10.1039/b601993e

2,3-Dihydro-1*H*-1,5-benzodiazepines are synthesized by the condensation of *o*-phenylenediamine and various ketones in the presence of silver nitrate under solvent-free conditions.

Benzodiazepines and their polycyclic derivatives are a very important class of bioactive compounds because of their pharmacological properties.^{1,2} They are widely used as anti-convulsant, analgesic, hypnotic, sedative, and antidepressive agents.¹ Benzodiazepines are also used as intermediates for the synthesis of fused ring compounds such as triazolo-,³⁻⁵ oxadiazolo-,⁵ oxazino-,⁴ and furano-benzodiazepines.^{4,6} Due to their wide biological activity, the synthesis of these compounds has received a great deal of attention. Some benzodiazepine derivatives are also used in industry, such as in photography, as dyes for acrylic fibers,⁷ and also as anti-inflammatory agents.⁸ Despite their wide range of pharmacological, industrial and synthetic applications, the synthesis of 1,5-benzodiazepines has received little attention. Benzodiazepines have been synthesized by the condensation of *o*-phenylenediamines with α,β -unsaturated carbonyl compounds, β -haloketones or with ketones. Many reagents have been reported in the literature for this condensation, including BF₃-etherate,⁹ polyphosphoric acid,¹⁰ NaBH₄,¹¹ SiO₂,¹¹ MgO/POCl₃,¹² Yb(OTf)₃,¹³ acetic acid under microwave conditions¹⁴ and in ionic liquids.¹⁵ Many of these processes suffer from one or more limitations, such as long reaction times, occurrence of several side reactions, drastic reaction conditions, low yields, and tedious work-up procedures. Therefore, the search continues for a better catalyst for the synthesis of 1,5-benzodiazepines in terms of mild reaction conditions, operational simplicity, economic viability and selectivity.

In this communication we report a facile method for the synthesis of 2,3-dihydro-1*H*-1,5-benzodiazepines by the condensation of *o*-phenylenediamine with ketones under solvent-free conditions catalyzed by silver nitrate.

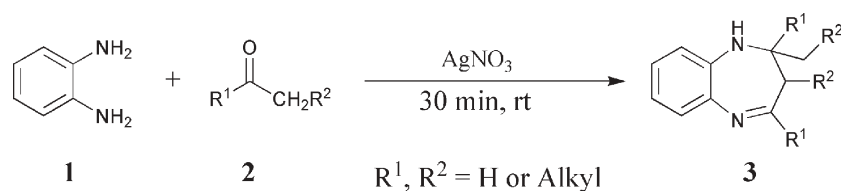
Synthetic Organic Chemistry Research Laboratory, Department of Chemistry, University of Delhi, Delhi, 110007, India.
E-mail: chandra682000@yahoo.co.in; Fax: +91-11-23816312;
Tel: +91-11-9818901344

The reactions were carried out by treating a 1 : 2.5 molar ratio mixture of *o*-phenylenediamine and the ketone with a catalytic amount of silver nitrate in a round-bottomed flask, with stirring at room temperature for an appropriate time (Scheme 1).[†] The reaction proceeds efficiently under the specified conditions in good to excellent yields. This procedure was successfully extended to other 1,5-benzodiazepine derivatives, as summarized in Table 1. As shown in Table 1, acetone in the presence of silver nitrate with *o*-phenylenediamine afforded 2,2,4-trimethyl-2,3-dihydro-1*H*-benzodiazepine (entry 1) in 99% yield. Acetophenone reacted with *o*-phenylenediamine under similar conditions to afford 2-methyl-2,4-diphenyl-2,3-dihydro-1*H*-1,5-benzodiazepine (entry 2) in 95% yield. Reaction of the diamine with other ketones in the presence of silver nitrate gave fused ring 1,5-benzodiazepine derivatives in good yields. It is noteworthy that starting from unsymmetrical ketones such as butanone, the ring closure occurs selectively to give a single product. The progress of the reaction was monitored by TLC; NMR and GC-MS were used for analysis of the products. After completion of the reaction, 10 ml of CH₂Cl₂ was added to the reaction mixture. The organic layer was extracted with water and concentrated *in vacuo*. The product was purified by silica gel chromatography (200–400 mesh), being eluted by ethyl acetate and *n*-hexane.

The scope and generality of this process is illustrated with respect to various cyclic and acyclic ketones, and the results summarized in Table 1.

The mechanism of the condensation reaction probably involves an intramolecular imine–enamine cyclization promoted by AgNO₃, as shown in Scheme 2.¹⁶ The amine of *o*-phenylenediamine attacks the carbonyl group of the ketone, giving the intermediate diimine **1**. A 1,3-shift of the hydrogen attached to the methyl group then occurs to form an isomeric enamine **2**, which cyclizes to afford the seven-membered ring.

In conclusion, we describe a mild and efficient method for the synthesis of 2,3-dihydro-1*H*-1,5-benzodiazepines. The easy work-up, solvent-free conditions, fast reaction rates, mild reaction conditions, good yields, and selectivity of the reaction make the present methodology attractive. This method is also applicable for

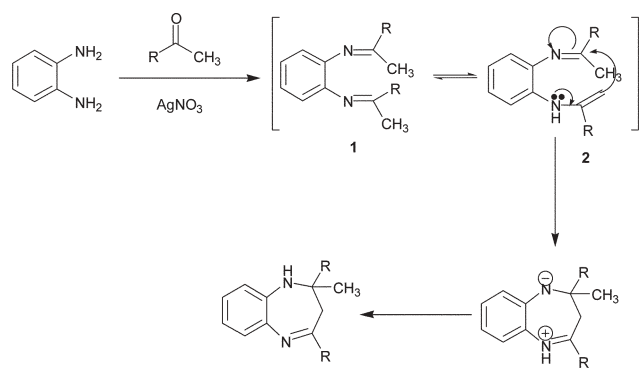


Scheme 1

Table 1 The condensation of *o*-phenylenediamine with ketones in the presence of silver nitrate

Entry	Substrate (1)	Ketone (2)	Product (3)	Yield (%) ^a	Mp/°C (lit.)	Mp/°C
1				99	138–140	137–139
2				95	150–152	151–152
3				92	144–146	144–145
4				89	138–140	138–139
5				95	138–140	138–139
6				84	212–214	NA ^b

^a Isolated yield. ^b Not available.

**Scheme 2**

the preparation of a wide variety of biologically potent 1,5-benzodiazepines under mild reaction conditions.

Notes and references

† General procedure: a mixture of *o*-phenylenediamine (1 mmol) and ketone (2.5 mmol) was stirred at room temperature in the presence of AgNO₃ (catalytic amount). After completion of the reaction (TLC), the reaction mixture was diluted with ethyl acetate, washed with water, dried (Na₂SO₄) and concentrated *in vacuo*. The crude product was purified by silica gel chromatography to afford the pure product. All reactions were

completed within 30 min. All the compounds were characterized by comparison of their mp and ¹H NMR spectra with those of authentic samples.¹⁷ All products gave satisfactory spectral data in agreement with the assigned structures [selected data for comparison: 2,2,4-trimethyl-2,3-dihydro-1*H*-1,5-benzodiazepine (entry 1): Yellow crystals; mp 138–140 °C. ¹H NMR (300 MHz, CDCl₃): δ 7.11 (m, 1H), 6.99–6.96 (m, 2H), 6.74–6.71 (m, 1H), 2.99 (br s, 1H, NH), 2.36 (s, 3H), 2.23 (s, 2H), 1.34 (s, 6H); TOF MS *m/z* 188 (M⁺)].

- (a) H. Schutz, *Benzodiazepines*, Springer, Heidelberg, 1982, vol. 2, p. 240; (b) R. K. Smalley, in *Comprehensive Organic Chemistry*, ed. D. Barton and W. D. Ollis, Pergamon, Oxford, 1979, vol. 4, p. 600; (c) J. K. Landquist, in *Comprehensive Heterocyclic Chemistry*, ed. A. R. Katritzky and C. W. Rees, Pergamon, Oxford, 1984, vol. 1, p. 166, 170.
- L. O. Randall and B. Kappel, in *Benzodiazepines*, ed. S. Garattini, E. Mussini and L. O. Randall, Raven Press, New York, 1973, p. 27 and references cited therein.
- M. Essaber, A. Baouid, A. Hasnaoui, A. Benharref and J.-P. Lavergne, *Synth. Commun.*, 1998, **28**, 4097.
- A. M. El-Sayed, H. Abdel-Ghany and A. M. M. El-Saghier, *Synth. Commun.*, 1999, **29**, 3561.
- J. X. Xu, H. T. Wu and S. Jin, *Chin. J. Chem.*, 1999, **17**, 84; X. Y. Zhang, J. X. Xu and S. Jin, *Chin. J. Chem.*, 1999, **17**, 404.
- K. V. V. Reddy, P. S. Rao and D. Ashok, *Synth. Commun.*, 2000, **30**, 1825.
- R. C. Harris and J. M. Straley, *U. S. Pat.* 1,537,757, 1968 (*Chem. Abstr.*, 1970, **73**, 100054w).
- J. R. De Baun, F. M. Pallos and D. R. Baker, *U. S. Pat.* 3,978,227, 1976 (*Chem. Abstr.*, 1977, **86**, 5498d).

- 9 J. A. L. Herbert and H. Suschitzky, *J. Chem. Soc., Perkin Trans. 1*, 1974, 2657.
- 10 H. R. Morales, A. Bulbarela and R. Contreras, *Heterocycles*, 1986, **24**, 135.
- 11 D. I. Jung, T. W. Choi, Y. Y. Kim, I. S. Kim, Y. M. Park, Y. G. Lee and D. H. Jung, *Synth. Commun.*, 1999, **29**, 1941.
- 12 M. S. Balakrishna and B. Kaboudin, *Tetrahedron Lett.*, 2001, **42**, 1127.
- 13 M. Curini, F. Epifano, M. C. Marcotullio and O. Rosati, *Tetrahedron Lett.*, 2001, **42**, 3193.
- 14 P. Minothora, S. S. Julia and A. T. Constantinos, *Tetrahedron Lett.*, 2002, **43**, 1755.
- 15 D. V. Jarikote, S. A. Siddiqui, R. Rajagopal, D. Thomas, R. J. Lahoti and K. V. Srinivasan, *Tetrahedron Lett.*, 2003, **44**, 1835.
- 16 S. K. De and R. A. Gibbs, *Tetrahedron Lett.*, 2005, **46**, 1811.
- 17 J. S. Yadav, B. V. S. Reddy and P. K. Nagaiah, *Synthesis*, 2005, **3**, 480.

Find a SOLUTION

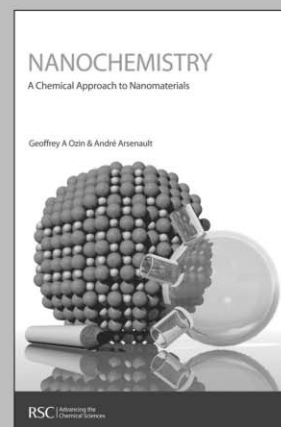
... with books from the RSC

Choose from exciting textbooks, research level books or reference books in a wide range of subject areas, including:

- Biological science
- Food and nutrition
- Materials and nanoscience
- Analytical and environmental sciences
- Organic, inorganic and physical chemistry

Look out for 3 new series coming soon ...

- RSC Nanoscience & Nanotechnology Series
- Issues in Toxicology
- RSC Biomolecular Sciences Series



RSC Publishing

www.rsc.org/books

Water-promoted iodocyclisation of 2-allylphenols

Manolis Fousteris, Carole Chevrin, Jean Le Bras* and Jacques Muzart*

Received 16th February 2006, Accepted 26th April 2006

First published as an Advance Article on the web 11th May 2006

DOI: 10.1039/b602398c

The reaction of a variety of 2-allylphenols with iodine in water produced the corresponding 2-iodomethyl-2,3-dihydrobenzofurans in the absence of any additives or organic solvents.

Iodinated organic molecules are useful intermediates in organic synthesis.¹ The intramolecular co-iodination of alkenes with internal oxygenated nucleophiles allows the preparation of numerous heterocyclic compounds.² The few examples reported for 2-allylphenols used organic media and required the presence of additives such as Envirocat EPZ-10^R or SnCl₄.^{3,4}

Today's environmental and economic concerns lead us to consider the use of water as the solvent.⁵ The fundamental problem in performing reactions in water is that most organic substrates are hydrophobic and sparingly soluble in water. To overcome this problem, a cosolvent⁶ or a micellar system⁷ is often used. In continuation of our research in aqueous media,⁸ in particular the new transformations of allylphenols,⁹ we now disclose that the intramolecular iodocyclisation of 2-allylphenols can be effectively performed with iodine in water, in the absence of any additive.

Results and discussion

Iodocyclisation of 2-allylphenol **1a** with 4 equiv. of iodine in water at 50 °C for 2 h led to **2a** in almost quantitative yield (Table 1, entry 1). This cyclisation occurred through an *exo* process, as generally observed.^{3,4} Lowering the amount of I₂ increased the reaction time and decreased the yield (entry 2); nevertheless, **2a** was obtained in 80% yield using only one equivalent of I₂ (entry 3). The use of a cosolvent or an organic solvent was not beneficial to the process. Indeed, the yield decreased from 94% (entry 1) to 77% in a

mixture of EtOH–H₂O (1 : 1) and excess of I₂ (entry 4), while in EtOH (entry 5), the iodoethoxylation of the double bond was a competing process, leading to small amounts of 2-(2-ethoxy-3-iodopropyl)phenol. The use of MeCN as a solvent led to only 30% of **2a** in 2 h (entry 6).

We further carried out the iodocyclisation of other substituted allylphenols in water (Table 2). Treatment of 2-allyl-6-methylphenol **1b**, 2-allyl-4-methylphenol **1c**, 4-*tert*-butyl-2-allylphenol **1d**, 2-allyl-4-chlorophenol **1e**, 2-allyl-4-methoxyphenol **1f**, 2-allyl-6-methoxyphenol **1g** and 2-allylnaphthalen-1-ol **1h** with 1 or 4 equiv.

Table 2 Oxidation of substituted allylphenols in water^a

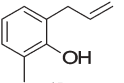
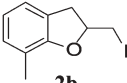
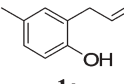
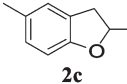
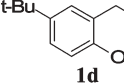
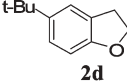
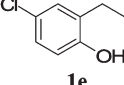
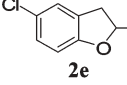
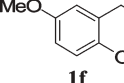
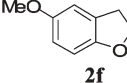
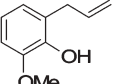
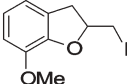
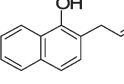
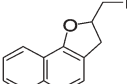
Substrate	I ₂ (equiv.)	Time/h	Product	Yield (%)
	4.0	3		79
	1.0	4		74
	4.0	2.5		94
	1.0	6		77
	4.0	2		76
	1.0	3		70
	4.0	2.25		78
	1.0	7		69
	4.0	3.5		44
	1.0	6		81
	4.0	3.25		— ^b
	1.0	5		68
	4.0	4		Trace
	1.0	2.75		42

Table 1 Effect of solvents on iodocyclisation of allylphenol^a

Entry	I ₂ (equiv.)	Solvent	Time/h	Yield (%)
1	4.0	H ₂ O	2	94
2	1.5	H ₂ O	4	84
3	1.0	H ₂ O	4	80
4	4.0	EtOH–H ₂ O (1 : 1)	2.5	77
5	4.0	EtOH	2	59
6	4.0	CH ₃ CN	2	30

^a Substrate (1 mmol), solvent (2 mL), 50 °C.

Unité Mixte de Recherche "Réactions Sélectives et Applications", Boîte 44, CNRS-Université de Reims Champagne-Ardenne, BP 1039, Reims cedex 2, 51687, France. E-mail: jean.lebras@univ-reims.fr; jacques.muzart@univ-reims.fr; Fax: +33 3 26 91 31 66

^a Substrate (1 mmol), H₂O (2 mL), 50 °C. ^b Mixture of **2g** and over-iodinated compounds.

of I₂ in water gave up to 94% yield of the corresponding 2-iodomethyl-2,3-dihydrobenzofurans. Except for **1f**, **1g** and **1h**, yields were always lower with one equiv. of I₂. From **1f**, an excess of I₂ led to **2f** and 2,3-dihydro-6-iodo-2-(iodomethyl)-5-methoxybenzofuran. Iodination of the aromatic ring has already been observed from electron-rich aromatic molecules in water.¹⁰ Interestingly, the use of one equiv. of I₂ afforded **2f** in 81% yield. 2-Allyl-6-methoxyphenol yielded 68% of **2g** with one equiv. of I₂, while a mixture of **2g** and over-iodinated compounds were obtained with four equiv. of I₂. Finally, 2-allylnaphthalenol **1h** gave the corresponding benzofuran **2h** in 42% yield with one equiv. of I₂ while insoluble materials were obtained with an excess of I₂.

The iodocyclisation probably occurs *via* the iodination of the double bond, leading to an iodonium ion that is opened by the regioselective intramolecular nucleophilic attack of the hydroxy group to afford the iodomethyl-dihydrobenzofuran.¹ The beneficial influence of water on the efficiency of the reaction, which could be attributed to hydrophobic interactions,¹¹ should be emphasised.

In conclusion, 2-allylphenols were converted into 2-iodomethyl-2,3-dihydrobenzofurans with iodine in water. The procedure is easy to set up and allows the transformation of various substituted 2-allylphenols in the absence of any additive.

Experimental

6-Methoxy-2-allylphenol (*o*-eugenol) was purchased from Acros Organics. 2-Allylphenol was purchased from Merck. 4-Methyl- and 6-methylphenol were purchased from Aldrich. 2-Allyl-1-naphthol, 4-*tert*-butyl-2-allylphenol, 4-chloro-2-allylphenol and 4-methoxy-2-allylphenol were prepared according to literature procedures.¹² ¹H and ¹³C NMR spectra were obtained using a Bruker AC 250 spectrometer, with TMS as an internal standard and CDCl₃ as solvent. IR spectra were recorded on a Avatar 320 FT-IR spectrometer as films. Mass spectra were performed using electrospray ionization with a Q-TOF micro from Micromass. Column chromatography was performed using silica gel 60 (E. Merck, 70–230 mesh) and petroleum ether–ethyl acetate mixtures as eluents. TLC was performed on precoated silica gel plates (E. Merck, Kieselgel 60 F₂₅₄).

Typical procedure for the preparation of 2,3-dihydro-2-iodomethyl-7-methylbenzofuran (**2b**).

A mixture of **1b** (148 mg, 1 mmol) and iodine (254 mg, 1 mmol) in water (2 mL) was stirred at 50 °C for 4 h. The reaction mixture was

then diluted with dichloromethane (10 mL) and aqueous saturated Na₂S₂O₃ was added. The phases were separated and the aqueous layer was extracted with dichloromethane (3 × 10 mL). The combined organic phases were dried over MgSO₄ and the solvent was removed under reduced pressure. The crude mixture was purified by silica gel column chromatography to afford **2b** (203 mg, 74% yield). ¹H NMR (CDCl₃): δ 6.95 (m, 2H), 6.75 (t, 1H, *J* = 7.4 Hz), 4.83 (m, 1H), 3.35 (m, 3H), 3.00 (dd, 1H, *J* = 6.4 Hz, *J* = 15.9 Hz), 2.19 (s, 3H). ¹³C NMR (CDCl₃): δ 158.1, 129.9, 125.4, 122.8, 121.2, 120.2, 81.6, 36.8, 15.9, 9.9. IR (film) ν/cm⁻¹: 3023, 2918, 2850, 1597, 1463, 1260, 1185, 762. HRMS: *m/z* calcd for C₁₀H₁₁IONa: 296.9752, found: 296.9757.

Acknowledgements

We are indebted to “Région Champagne-Ardenne” for a PhD studentship to C. C.

Notes and references

- 1 M. Jereb, M. Jupan and S. Stavber, *Green Chem.*, 2005, **7**, 100–104; A. M. Sansaverino, F. M. da Silva, J. Jones, Jr. and M. C. S. de Mattos, *Quim. Nova*, 2001, **24**, 637–645.
- 2 A. D. Bailey, S. M. Cherney, P. W. Anzalone, E. D. Anderson, J. J. Ernati and R. S. Mohan, *Synlett*, 2006, 215–218; F. M. da Silva, J. Junior and M. C. S. de Mattos, *Curr. Org. Synth.*, 2005, **2**, 393–414.
- 3 V. A. Mahajan, P. D. Shinde, A. S. Gajare, M. Karthikeyan and R. D. Wakharkar, *Green Chem.*, 2002, **4**, 325–327.
- 4 K. Orito, T. Hatakeyama, M. Takeo, H. Sugimoto and M. Tokuda, *Synthesis*, 1997, 23–25.
- 5 C.-J. Li and L. Chen, *Chem. Soc. Rev.*, 2006, **35**, 68–82; C.-J. Li, *Chem. Rev.*, 2005, **105**, 3095–3165; U. M. Lindström, *Chem. Rev.*, 2002, **102**, 2751–2772.
- 6 B. Cornils and W. A. Herrmann, *Aqueous-Phase Organometallic Catalysis*, Wiley, New York, 1998.
- 7 T. Dwers, E. Paetzold and G. Oehme, *Angew. Chem., Int. Ed.*, 2005, **44**, 7174–7199.
- 8 J. Le Bras and J. Muzart, *Tetrahedron Lett.*, 2002, **43**, 431–433; J. Le Bras and J. Muzart, *Tetrahedron: Asymmetry*, 2003, **14**, 1911–1915; C. Chevrin, J. Le Bras, F. Hémin and J. Muzart, *Tetrahedron Lett.*, 2003, **44**, 8099–8102; C. Chevrin, J. Le Bras, F. Hémin, J. Muzart, A. Pla-Quintana, A. Roglans and R. Pleixats, *Organometallics*, 2004, **23**, 4796–4799; B. Estrine, S. Bouquillon, F. Hémin and J. Muzart, *Green Chem.*, 2005, **7**, 219–223.
- 9 C. Chevrin, J. Le Bras, F. Hémin and J. Muzart, *Synthesis*, 2005, 2615–2618.
- 10 M. Jereb, M. Zupar and S. Stavber, *Chem. Commun.*, 2004, 2614–2615.
- 11 R. Breslow, *Acc. Chem. Res.*, 1991, **24**, 159–164.
- 12 S. H. Reich, M. Melnick, M. J. Pino, M. A. M. Fuhry, A. J. Trippe, K. Appelt, J. F. Davies, II, B.-W. Wu and L. Musick, *J. Med. Chem.*, 1996, **39**, 2781–2794.

Chemicals from biomass derived products: synthesis of polyoxyethyleneglycol esters from fatty acid methyl esters with solid basic catalysts

M. José Climent,^a A. Corma,^{*a} Sharifah B. A. Hamid,^b S. Iborra^a and M. Mifsud^a

Received 20th December 2005, Accepted 22nd March 2006

First published as an Advance Article on the web 4th April 2006

DOI: 10.1039/b518082a

In the present work, we have studied the possibility of using heterogeneous base catalysts, of various basic strengths, for performing the transesterification between oleic acid methyl ester (MeO) and various polyethyleneglycols of different molecular weights (PEG-600, -400 and -200) to obtain polyoxyethyleneglycol monoesters. Reactions were performed using Brønsted and Lewis solid bases as catalysts: KF/alumina, Li₂O/alumina (Li- γ -Al₂O₃), MgO, Al-Mg (HTc-Al/Mg) and Al-Li (HTc-Al/Li) mixed oxides derived from hydrotalcites, CeO₂, a cesium cation exchanged X faujasite (CsX) and Al/Mg calcined-rehydrated hydrotalcites (HTr). The results showed that the order of activity was: Li- γ -Al₂O₃ > KF/alumina > MgO \geq HTr > HTc-Al/Li > HTc-Al/Mg > CeO₂ > XCs. This is related to differences in the type and strength of the basic sites in these materials. The influence of the chemical composition of the calcined hydrotalcites, the influence of the hydrocarbon chain length of the fatty acid methyl ester on the activity and selectivity to monoester, and the optimization of reaction variables (such as reaction temperature and PEG/MeO molar ratio) have been studied. By combining a solid Brønsted base catalyst with the optimised reaction conditions it is possible to attain conversions higher than 90% with a selectivity to monoester greater than 98%, this being a real alternative to conventional processes using alkaline hydroxide catalysts.

Introduction

Oils and fats of vegetable and animal origin are one of the most important renewable raw materials used in the chemical industry. The benefits of oleochemicals are their biodegradability and non-toxic character, which make them highly desired “green” surfactants, and they are introduced as additives in many industrial and pharmaceutical applications. More specifically, fatty acid monoesters of polyethylene glycols (PEG) are particularly interesting due to their lack of toxicity, absence of antigenicity and immunogenicity, and solubility in water and organic solvents.¹ A wide variety of non-ionic surfactants with different properties may be achieved by varying the length of the hydrophobic fatty acid moiety and changing the degree of polymerization of the hydrophilic PEG part. They have applications as solubilisers, emulsifiers, lubricants, wetting agents and detergents in pharmaceutical, cosmetics and industrial applications.²

Methods for preparing polyoxyethyleneglycol fatty acid monoesters involve ethoxylation, *i.e.* reaction of ethylene oxide with a fatty acid, esterification between fatty acids and polyethylene glycols (PEG), and transesterification between PEG and simple fatty acid esters, such as fatty acid methyl ester (FAME).^{3,4}

Because of the nature of the ethoxylation process, mixtures of compounds with a degree of ethoxylation that usually follow a typical Gaussian distribution curve are obtained. Esterification and transesterification process are preferred because they are safer and the degree of ethoxylation can be more easily controlled. However, in these cases the esterification or transesterification products are normally a mixture of monoester and diester, and a large excess of PEG (between 6–12 times) over fatty acid or fatty acid methyl ester is used in order to minimise diester formation.⁵

Esterification and transesterification are performed in the presence of homogeneous catalysts. Acid catalysts such as sulfuric, *p*-toluenesulfonic, or phosphoric acid⁵ are usually used for the esterification reaction, whereas transesterification requires basic catalysts like hydroxides, methoxides, or alkali metals such as Na.⁶ The main problem associated with these homogeneous catalysts (acids and bases) is the requirement of a final neutralization step with the formation of soaps and large amount of salts.

It is widely accepted that there is a need to develop green and economical processes, where the use of noxious substances and the generation of waste can be avoided. In this sense the replacement of liquid catalysts by solid catalysts will allow separation of the products, avoiding the neutralization and extraction steps while reducing waste formation. Recently the esterification reaction of fatty acids with polyoxyethylenes has been studied in the presence of solid acid catalysts (zeolites, nafion and HPA) giving good selectivities to the monoester.⁷ In addition, the use of heterogeneous base catalysts for the transesterification of glycerol with triglycerides⁸ or with fatty acid methyl esters^{9–12} has been reported. However, as far as we

^aInstituto de Tecnología Química, UPV-CSIC, Universidad Politécnica de Valencia, Avda. de los Naranjos s/n, 46022 Valencia, Spain.

E-mail: acorma@itq.upv.es; Fax: +34 (96)3877809;

Tel: +34 (96)3877800

^bCOMBICAT R&D Centre, Level 2, 3 & 5, Block A, Institute of Postgraduate Studies, University Malaya, 50603 Kuala Lumpur, Malaysia

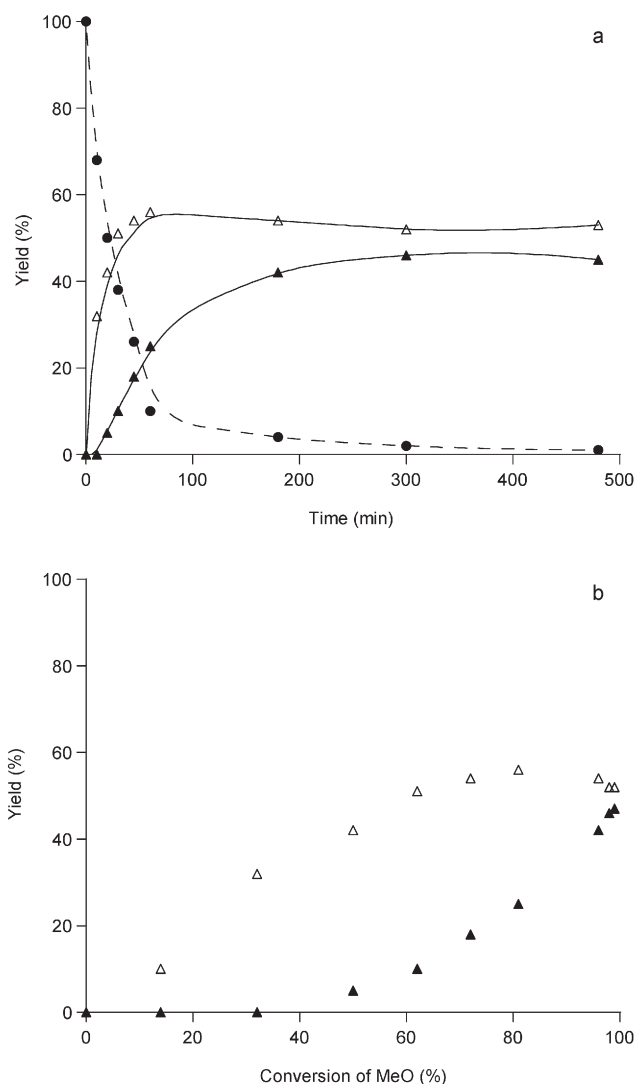


Fig. 1 a) Transesterification reaction between methyl oleate and PEG-600 using MgO as basic catalyst; methyl oleate conversion (●), monoester (△), diester (▲). b) Yields of monoesters and diester *versus* conversion of MeO.

know, there are no reports in the open literature dealing with the transesterification of PEG with fatty acid methyl esters using solid bases as catalysts.

In this paper we have studied the nature of the required basic site, Lewis or Brønsted, as well as the basic strength necessary to selectively carry out the transesterification

Table 1 Transesterification of methyl oleate with PEGs of different molecular weight

PEG	Conversion MeO (%)	Yields ^a (%)		Selectivity to monoester (%)
		Monoester	Diester	
600	81	56	24	69
400	87	51	35	59
200	94	50	43	54

^a After 1 h reaction time, at 493 K, using MgO as catalyst, PEG/MeO molar ratio = 1; reactant/catalyst ratio = 25 g g⁻¹.

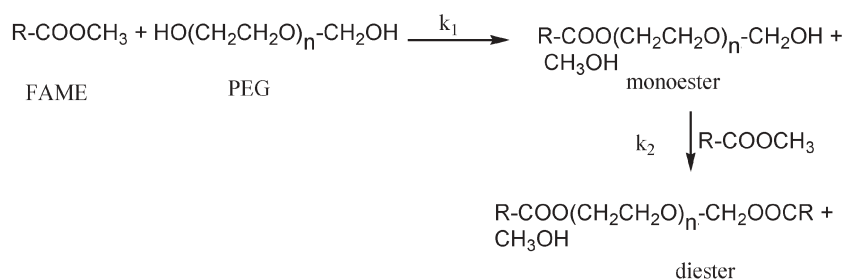
reaction between oleic acid methyl ester (MeO) and various PEGs of different molecular weights, to obtain fatty acid polyoxyethyleneglycol monoesters.

Results and discussion

Transesterification reaction using solid Lewis base catalysts

The transesterification of oleic acid methyl ester (MeO) was carried out using three PEG reactants with different molecular weights (PEG-200, PEG-400 and PEG-600). The reactions were performed in the presence of a high surface area MgO as base catalyst, in absence of solvent, with a PEG/MeO molar ratio of 1, a reaction temperature of 493 K and a reactant to catalyst ratio of 25 g g⁻¹. The kinetic curve obtained using PEG-600 is presented in Fig. 1a. It is possible to infer from Fig. 1b (a plot of the yields of monoesters and diester *versus* conversion of MeO) that oleic acid polyoxyethyleneglycol monoester is formed as a primary product, while the diester is present as a secondary product and can be formed by the consecutive transesterification of the free hydroxyl group of monoester with MeO, or even by interesterification between two monoester molecules (Scheme 1). Conversion from thermal reaction has not been considered, since we have seen that transesterification is a slow reaction in the absence of catalysts, and only 7% conversion was reached after 7 h reaction time.

The results presented in Table 1 show that the molecular size of the PEG influences the level of conversion, the order of reactivity being PEG-200 > PEG-400 > PEG-600. Taking into account that the only difference between the three PEGs is the size of hydrophilic polyether chain, this order in reactivity should probably be related to the miscibility of the MeO with the different PEGs. Therefore, one has to expect that decreasing the hydrophilic character of the reagent, *i.e.* shortening the chain, as in the case of PEG-200, will increase the solubility in the fatty acid methyl ester and both reactants



Scheme 1

will be better mixed, enhancing the rate of transesterification. With PEG-600 the reaction was carried out at different stirring speeds, 500, 700 and 900 rpm, in order to eliminate external diffusion control. It was found that the initial reaction rate increased when the stirring speed was increased from 500 to 600 rpm, and no further increase was observed at 900 rpm. In all the other experiments the stirring speed was 700 rpm. In order to eliminate internal diffusion, three different catalyst (MgO) particle sizes were examined: 0.6–0.8, 0.4–0.6 and 0.2–0.4 mm. We observed that the initial reaction rate did not increase for catalyst particle sizes below 0.4–0.6 mm. Therefore the catalysts in this work were all palletised, crushed and sieved and the 0.2–0.4 mm diameter fraction was selected.

In order to study the activity of different Lewis bases, we selected as catalysts an Al–Mg oxide derived from hydrotalcite (HTc–Al/Mg(0.25)), a Cs exchanged faujasite zeolite (CsX), a rare earth oxide (CeO₂), and KF/alumina. The solids were tested for the transesterification between MeO and PEG-600 using the conditions described in the Experimental section. The yields and selectivities obtained with the different heterogeneous catalysts are presented in Table 2. The order of activity observed is KF/alumina > MgO > HTc–Al/Mg(0.25) > CeO₂ > CsX, which agrees with the order of basicity of these materials. Thus, KF/alumina exhibits the highest basicity, whereas MgO, which possesses a higher concentration of basic sites, although with lower basic strength, performs the transesterification more efficiently than the Al–Mg mixed oxide. Finally, a weak Lewis base catalyst such as CeO₂ shows low activity. The very low conversion observed with CsX zeolite is not surprising taking into account that most of the reaction will occur at the external surface of the zeolite due to the diffusional limitations of the reactants within the pores.

Measures of basicity of solid bases were carried out using one of the recommended test reactions for solid basic catalysts – the condensation between benzaldehyde and ethyl cyanoacetate.¹³ The results given in Fig. 2 show an excellent correlation between the values given by the test and the transesterification reactions.

It is interesting to see that the different catalysts studied have no influence on the selectivity to monoester, this being a function of the conversion level (Fig. 3). In other words, the ratio of k_2 to k_1 (see Scheme 1) is the same for all catalysts and therefore the same active sites are involved in the two consecutive reactions. Similar behaviour has been observed for the glycerolysis of fats and fatty acid methyl esters.^{8,11,12}

Table 2 Transesterification of methyl oleate with PEG-600 using different solid basic catalysts

Catalysts	Conversion MeO (%)	Yields ^a (%)		Selectivity to monoester (%)
		Monoester	Diester	
KF/Al ₂ O ₃	83	54	28	65
MgO	81	56	24	69
HTc–Al/Mg(0.25)	54	48	5	88
CeO ₂	43	42	1	98
CsX	27	27	0	100

^a After 1 h reaction time, at 493 K, PEG/MeO molar ratio = 1, reactant/catalyst ratio = 25 g g⁻¹.

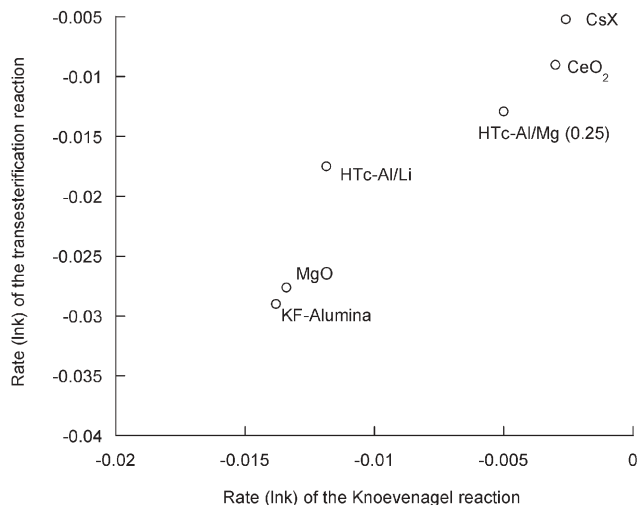


Fig. 2 Rate of Knoevenagel condensation between benzaldehyde and ethyl cyanoacetate *versus* rate of transesterification reaction using different basic catalysts. Conditions of Knoevenagel reaction: benzaldehyde (10 mmol), ethyl cyanoacetate (10 mmol), 5 wt% of catalyst at 333 K.

Overall we can see that by using solid base catalysts it is possible to obtain selectivities to monoester close to 70% for conversions slightly above 80%. Using NaOH as a homogeneous catalyst, 90% conversion with 52% selectivity to monoester was obtained, and consequently the catalytic behaviour of the solid catalysts required further improvement.

Influence of the chemical composition of the calcined hydrotalcite catalysts

Up to now we have seen that KF/Al₂O₃ and MgO followed by Al/Mg mixed oxides are promising catalysts for performing the transesterification reaction between PEG and oleic acid methyl ester. However, as we will discuss later, KF/alumina undergoes

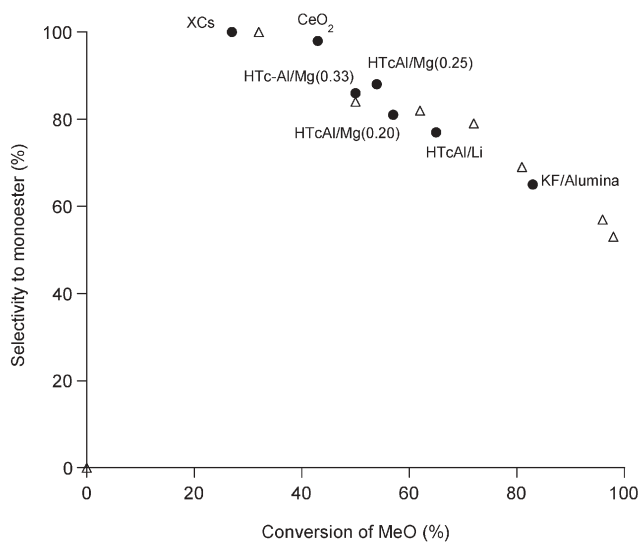


Fig. 3 Results of selectivity of monoester *versus* conversion of methyl oleate obtained in the transesterification of methyl oleate with PEG-600 using MgO (Δ) and other Lewis base catalysts.

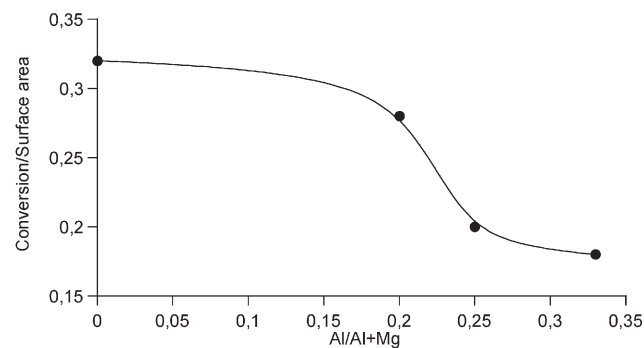
Table 3 Results of the transesterification between methyl oleate and PEG-600 in the presence of HTc-Al/M with different Al/(Al + M) composition

Catalysts	Al/(Al+M)	Conversion MeO ^a (%)	Conversion/surface area (%/m ² g ⁻¹)	Yield (%)		Selectivity to monoester (%)
				Monoester	Diester	
HTc-Al/Mg(0.20)	0.20	57	0.28	46	11	80
HTc-Al/Mg(0.25)	0.25	54	0.20	48	5	88
HTc-Al/Mg(0.33)	0.33	50	0.18	43	7	86
HTc-Al/Li(0.33)	0.33	65	0.27	50	15	76

^a At 1 h reaction time; PEG/MeO molar ratio = 1, reactant/catalyst ratio of 25 g g⁻¹, at 493 K.

a strong deactivation during the reaction, leaching fluoride into the reaction media. On the other hand, while Al/Mg mixed oxides exhibit lower catalytic activity than MgO, they are very stable and mechanically strong catalysts. Therefore, it is of interest to improve the activity of those mixed oxides for the catalytic transesterification of fatty acid methyl esters with PEG. It is known that one way to increase the basic strength of the mixed oxides is by changing their chemical composition. For instance, increasing the aluminium content decreases the basic site density, but the fraction of strong basic sites increases.^{14–16} If this is so, we may expect to find an optimum activity by changing the Al/(Al + Mg) ratio. Three Al/Mg mixed oxide samples with Al/(Al + Mg) ratios of 0.20, 0.25 and 0.33 have been synthesised, and the conversion obtained after 1 h reaction time for the three samples is very similar (Table 3). However, if the specific surface area of the catalyst is considered (Fig. 4), we can see that increasing the aluminium content of the sample decreases the specific activity. From these results, we can conclude that the basic sites present in MgO are already active enough for carrying out the reaction, and the presence of stronger basic sites formed in the hydrotalcite derived oxides does not compensate for the decrease in the total number of basic sites produced in the MgO upon the addition of aluminium.

At this point, in order to test a hydrotalcite-derived catalyst with stronger basicity, we prepared an Al/Li mixed oxide sample with an Al/(Al + Li) molar ratio of 0.33. We can expect that by replacing the Mg²⁺ with Li⁺ the density of negative charge on the oxygen will increase, leading to an increase of the base strength and consequently of the catalytic activity.¹² Following this, the Al/Li mixed oxide was tested in the transesterification reaction of methyl oleate with PEG-600,

**Fig. 4** Influence of the Al/(Al + Mg) of the starting hydrotalcite on the activity for the transesterification reaction between methyl oleate and PEG-600.

and the result obtained is presented in Table 3. As predicted, HTc-Al/Li performs the transesterification reaction more efficiently than Al/Mg mixed oxides, but it gives still lower conversion than MgO and NaOH. Therefore, new catalysts with stronger basicities needed to be synthesised.

It is known that strong basic materials (sometimes in the range of superbases) have been prepared by supporting alkalis on alumina or MgO,^{17–19} potassium amide on alumina,²⁰ or alkaline salts on γ -alumina.^{21,22} The supported neutral salts do not show any strong basicity, but when activated at high temperature (*ca.* 700 K) they decompose, forming strong basic sites with high efficiency in catalytic processes.²² Following this line, we prepared a strong basic material based on LiNO₃ supported on γ -Al₂O₃. Thus, three samples with Li contents of 3, 6, and 9 wt% were prepared by loading LiNO₃ on γ -alumina followed by calcination at 773 K in the presence of CO₂-free air for 6 h, and then stored in closed flasks. These samples, labeled as Li- γ -Al₂O₃(3%), Li- γ -Al₂O₃(6%) and Li- γ -Al₂O₃(9%), were pre-activated before reaction at 723 K for 6 h under N₂ atmosphere, and tested for the transesterification of the methyl oleate with PEG-600 at 493 K in the absence of air, using a PEG/MeO molar ratio of 1. Results from Table 4 clearly show that this was the most active catalyst that we had produced so far, being more active than MgO and much more active than Al/Mg or Al/Li hydrotalcites. With Li- γ -Al₂O₃(6%) it is possible to achieve 95% conversion in 1 h, confirming the presence of very strong basic sites on this catalyst. Concerning the monoester selectivity, results in Fig. 5 show that, as in previous cases, the selectivity to monoester is a function of conversion, but not of basic strength.

From the work presented up to now using Lewis basic catalysts, we can conclude that the number and strength of basic sites play a role in transesterification conversion, but have no influence on the selectivity to monoester.

Table 4 Results of the transesterification between methyl oleate and PEG-600 in the presence of Li- γ -Al₂O₃ catalysts

Catalysts	Time/ min	Conversion MeO ^a (%)	Yields (%)		Selectivity to monoester (%)
			Monoester	Diester	
Li- γ -Al ₂ O ₃ (3%)	15	55	44	11	79
	30	85	55	29	64
	60	90	53	36	59
Li- γ -Al ₂ O ₃ (6%)	15	68	53	15	77
	60	95	55	39	58
Li- γ -Al ₂ O ₃ (9%)	15	73	55	17	75
	60	95	54	40	56

^a PEG/MeO molar ratio = 1, reactant/catalyst ratio of 25 g g⁻¹, at 493 K.

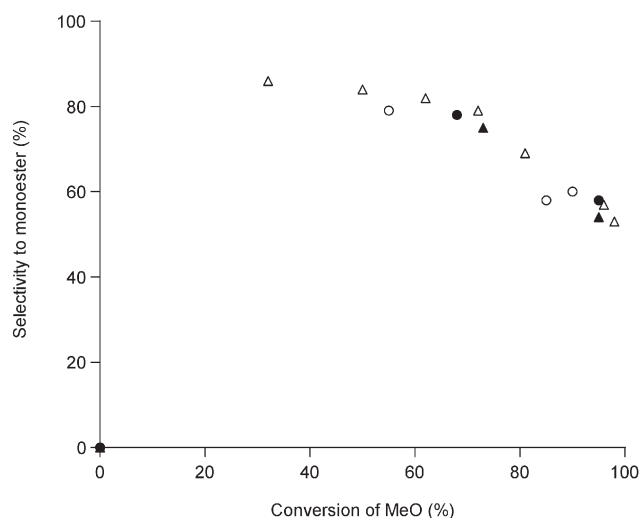


Fig. 5 Results of selectivity of monoester *versus* conversion of methyl oleate obtained in the transesterification of methyl oleate with PEG-600 using MgO (Δ), Li- γ -Al₂O₃(3%) (\circ), Li- γ -Al₂O₃(6%) (\bullet), Li- γ -Al₂O₃(9%) (\blacktriangle) as catalysts.

Catalyst deactivation

In order to study catalyst deactivation, MgO, KF/alumina, HTc-Al/Mg(0.25), HTc-Al/Li, and Li- γ -Al₂O₃(6%), were reused several times under the same reaction conditions. After reaction the catalyst was washed with dichloromethane, dried and used again. As can be observed in Table 5, MgO, HTc-Al/Mg, and HTc-Al/Li maintain their activities at least during the three consecutive cycles studied. On the other hand, with KF/alumina and Li- γ -Al₂O₃(6%), a decrease in catalytic activity is observed, which is attributed to the leaching of F⁻ anions and Li⁺ from the catalysts. Indeed, chemical analysis of the catalysts showed a decrease of 32 and 37% in the content of

Table 5 Results of the reuse of the different catalysts in the transesterification of methyl oleate and PEG-600

Catalyst (cycles)	Conversion ^a MeO (%)	Yields (%)		Selectivity to monoester (%)
		Monoester	Diester	
KF/Al₂O₃				
1st	83	54	28	65
2nd	68	53	15	77
3rd	58	48	10	82
MgO				
1st	81	56	24	69
2nd	80	59	20	73
3rd	82	56	25	68
HTc-Al/Mg(0.25)				
1st	54	48	5	88
2nd	53	49	4	93
3rd	56	50	6	90
HTc-Al/Li				
1st	65	50	15	76
2nd	60	46	14	76
3rd	64	49	15	76
Li-γ-Al₂O₃(6%)^b				
1st	68	53	15	77
2nd	54	46	8	85
3rd	47	42	5	89

^a PEG/MeO molar ratio = 1, reactant/catalyst ratio of 25 g g⁻¹, at 493 K after 1 h reaction time. ^b After 15 min reaction time.

KF and Li in the catalysts, respectively. This certainly leaves MgO, HTc-Al/Mg and HTc-Al/Li as the only Lewis basic sites with practical interest among those studied here.

Transesterification using solid Brønsted basic sites

It is known that the catalytic activity of calcined hydrotalcites can be enhanced by rehydration at room temperature in the absence of CO₂.^{23,24} This treatment results in the restoration of a layered structure where the compensating anions in the interlayer are OH⁻ groups. This material is very active for catalysing different aldol condensations,^{23,25–30} Knoevenagel condensations³¹ and Michael additions.³² This increase in the activity is due to the presence of OH⁻ anions which exhibit Brønsted basicity. Thus, it is clear that rehydrated hydrotalcites have available strong Brønsted basic sites whose activity could be directly compared with that of the homogeneous catalysts usually used for catalysing transesterification reactions.

It has been pointed out that the amount of water on the calcined hydrated catalyst has a strong influence on the catalytic activity, and this parameter must be controlled in order to obtain the optimum activity. In fact, we have shown that for the transesterification of MeO with glycerol,¹² an excess of water on the catalyst surface poisons the stronger basic sites, decreasing the rate of transesterification. Therefore, in order to optimise the water content on the catalysts, a series of rehydrated hydrotalcites were prepared, starting from a calcined hydrotalcite with an Al/(Al + Mg) ratio of 0.25, by flowing N₂ (40 mL min⁻¹), free of CO₂ and saturated with water vapour, over the hydrotalcite for different lengths of time. Samples with water contents of 15, 20, 36, 46 and 60 wt% were labelled as HTr₁₅, HTr₂₀, HTr₃₆, HTr₄₆, HTr₆₀ respectively.

X-Ray diffraction patterns of the hydrotalcites after synthesis, calcination and rehydration are presented in Fig. 6. It can be observed that the layered crystalline structure of hydrotalcite was destroyed during calcination at 723 K, and is restored to a large extent by rehydration, giving a meixnerite-like structure where strong Brønsted OH⁻ sites have replaced the weakly basic carbonate anions. The results obtained for the transesterification reaction with these samples are summarised in Table 6. As can be seen, there was an important increase of activity when the catalyst surface of the mixed oxide was rehydroxylated. Maximum activity is found for a water content in the range 36–46%. The existence of a maximum has also been found for other reactions.^{12,24,27,29,30,33} It should be noted however that while the regenerated hydrotalcite (HTr₄₆) gives much higher activity than the corresponding mixed oxide, the conversion achieved with the former is of the same order as that of the MgO. Nevertheless, if activity per surface area is considered (the BET surface area of the regenerated hydrotalcite HTr₄₆ is 48 m² g⁻¹), the regenerated HTr₄₆ shows a much higher specific activity than MgO.

Taking into account that the number and strength of sites measured by adsorption of CO₂ is lower in the Al/Mg hydrated sample than the mixed oxide,²³ the larger initial activity observed for the Brønsted catalyst can not be related to a higher basicity of the Brønsted sites, but is probably related to

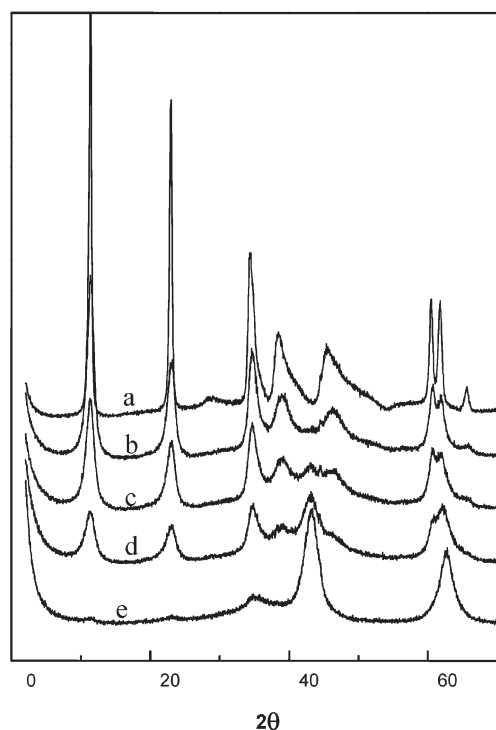


Fig. 6 XRD patterns of Al/Mg hydrotalcites after synthesis, calcination and rehydration: a) fresh hydrotalcite, b) 60 wt% of water, c) 46 wt% of water, d) 36 wt% of water, e) calcined hydrotalcite.

changes in the adsorption and activation of the reactants on these catalysts. Thus, the increased activity of the rehydrated sample compared with the calcined sample can be attributed to the higher hydrophilic character of the former, which improves the adsorption of the highly hydrophilic PEG, thus increasing the conversion.

It should be remarked that regardless of the water content of the sample, the amount of oleic acid detected in the reaction mixture was very low (less than 2%), indicating that under the reaction conditions tested, the hydrolysis of the esters is not a competitive process.

For comparison purposes, another rehydration methodology was used that involves the immersion of HTc–Al/Mg(0.25) in CO₂-free water (100 mL g⁻¹) while stirring under

Table 6 Results of the transesterification between methyl oleate and PEG-600 in the presence of HTc–Al/Mg(0.25) with different water amounts

Water amount (wt%)	Conversion ^a (%)	Yield (%)		Selectivity to monoester (%)
		Monoester	Diester	
0	54	48	5	88
15	66	54	12	82
20	69	56	11	81
36	77	56	20	71
38 ^b	76	58	17	75
46	80	57	22	71
60	74	57	16	77

^a 1 h reaction time, PEG/MeO molar ratio = 1, reactant/catalyst ratio = 25 g g⁻¹ at 493 K. ^b Sample hydrated by immersion in CO₂-free water for 1 h.

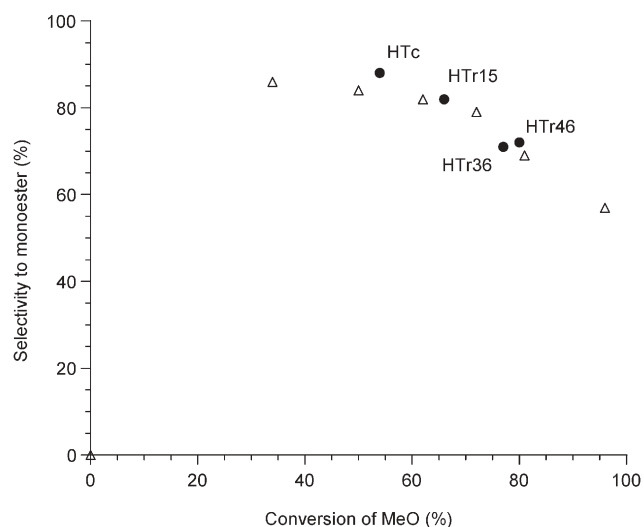


Fig. 7 Results of selectivity of monoester versus conversion of methyl oleate obtained in the transesterification of methyl oleate with PEG-600 using MgO (Δ) and calcined–rehydrated Al/Mg hydrotalcites as catalysts.

an argon atmosphere for 1 h at room temperature. After filtration under inert atmosphere, the solid was washed with ethanol and dried under an argon flow at room temperature. The final water content of the solid was 38 wt%. It can be seen from Table 6 that this sample, and the sample prepared before with 36 wt% water content, gave practically the same conversion and selectivity after 1 h of reaction.

A comparison of monoester selectivity (Fig. 7) shows that MgO and the rehydroxylated samples present similar selectivities, again indicating that the monoester selectivity only depends on the level of conversion, and it is independent of the nature of the basic sites (Brønsted or Lewis).

Finally, in order to study catalyst deactivation, the HTr₄₆ sample was reused three times under the same reaction conditions. As can be seen in Table 7, the Brønsted basic catalyst maintains its activity during the three consecutive reuses. These results indicate that, from the point of view of activity and reusability of the catalyst, rehydrated Al/Mg mixed oxides are excellent candidates to perform this type of reaction.

Influence of the hydrocarbon chain length of the fatty acid methyl ester

To study the influence of the hydrocarbon chain length of the fatty acid methyl ester in the alcoholysis process, we selected

Table 7 Reuse of HTr₄₆ in the transesterification of methyl oleate and PEG-600

Catalyst cycles	Conversion ^a MeO (%)	Yield (%)		Selectivity to monoester (%)
		Monoester	Diester	
1st	80	57	22	71
2nd	78	58	20	74
3rd	79	57	22	72

^a PEG/MeO molar ratio = 1, reactant/catalyst ratio = 25 g g⁻¹, at 493 K after 1 h reaction time.

Table 8 Results of transesterification of PEG-600 with different fatty acid methyl esters in the presence of HTc–Al/Li

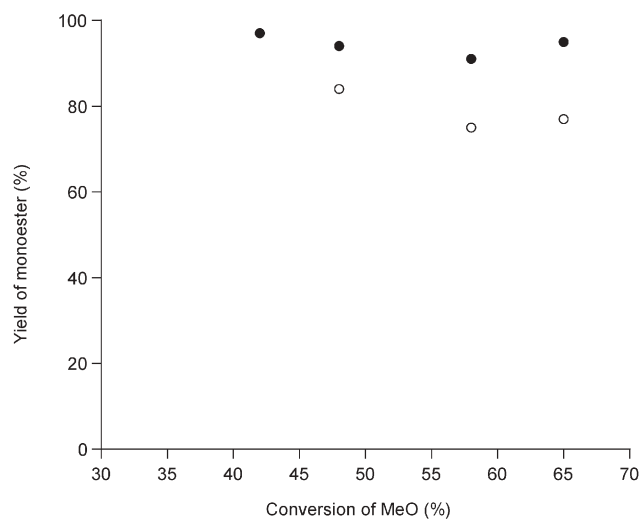
Methyl ester	Conversion of methyl ester ^a (%)	Yield ^a (%)		Selectivity to monoester (%)
		Monoester	Diester	
MeL	81	55	25	68
MeP	72	53	18	73
MeO	65	50	15	76

^a PEG/Fatty acid methyl ester molar ratio = 1, 1 h reaction time, reactant/catalyst ratio = 25 g g⁻¹ at 493 K.

two saturated methyl esters, methyl laureate (MeL) and methyl palmitate (MeP), which have 12 and 16 carbon atoms respectively. The results presented in Table 8 show that the nature of the methyl ester influences the rate of transesterification, the order of reactivity being C₁₂ > C₁₆ > C₁₈. This behaviour has to be related to the different miscibility of the esters with the PEG phase. One can expect that when the number of carbons in the fatty acid methyl ester is decreased, the hydrophobic character of the fatty acid methyl ester will also decrease, giving better solubility of the fatty acid methyl ester in the hydrophilic phase (PEG phase), and therefore enhancing the transesterification conversion.

Influence of the temperature and PEG/MeO molar ratio

The influence of reaction temperature on the transesterification process was studied by carrying out the reaction in the presence of HTc–Al/Li at 453 K with a PEG/MeO 1 : 1 molar ratio. The results in Fig. 8 show that by working at temperatures lower than 493 K it is possible to improve the selectivity. Thus, at 453 K 95% selectivity to monoester for 65% conversion can be achieved after 3 h reaction time. This result can be attributed to the lower solubility of the monoester in MeO when decreasing the temperature. If the solubility of the monoester in MeO is lower, the possibility of subsequent transesterification of the monoester with the MeO to give the

**Fig. 8** Influence of the reaction temperature on the selectivity to monoester in the transesterification of methyl oleate with PEG-600 using HTc–Al/Li as a catalyst: 453 K (●), 493 K (○).**Table 9** Results of transesterification between methyl oleate and PEG-600 using different molar ratios in the presence of HTc–Al/Li

PEG/MeO	Conversion ^a (%)	Selectivity to monoester (%)	Yield of monoester (%)
1 : 1	65	76	50
2 : 1	77	89	69
4 : 1	90	98	88

^a 1 h reaction time, reactant/catalyst ratio of 25 g g⁻¹ at 493 K.

diester will be lower, increasing the selectivity to monoester. These results indicate that an important characteristic of a well defined process is the fast removal of the methanol formed during reaction.

From an economical point of view it is important to optimise the methyl oleate to PEG molar ratio, keeping the conversion and selectivity to monoester at reasonable levels. In order to study this variable the transesterification was carried out using different PEG/MeO molar ratios at 493 K. The results from Table 9 clearly show that an excess of PEG not only allows good conversion to the monoester, but also makes possible a selectivity of 98%.

Experimental

Catalysts

Al–Mg hydrotalcites were prepared from gels produced by mixing two solutions: A and B. Solution A contains (3 – x) mol of Mg(NO₃)₂·6H₂O and x mol of Al(NO₃)₃·9H₂O with an (Al + Mg) concentration of 1.5 mol L⁻¹ for Al/(Al + Mg) ratios of 0.20, 0.25 and 0.33. Solution B is formed by (6 + x) mol of NaOH and 2 mol of Na₂CO₃ dissolved in the same volume as solution A. Both solutions were co-added at a rate of 1 mL min⁻¹ under vigorous mechanical stirring at room temperature. The suspension was left for 12 h at 333 K. The hydrotalcites were filtered and washed until the pH = 7, and the solids were dried at 333 K. The Al/Li layered double-hydroxy carbonate ([Al₂Li(OH)₆]₂CO₃·nH₂O) was prepared according to ref. 34: a hexane solution of aluminium tri(*sec*-butoxide) (17% w/w) was added dropwise to aqueous lithium carbonate (0.55% w/w) with vigorous mechanical stirring at room temperature. The suspension was left for 24 h at 333 K, then the Al/Li hydrotalcite was filtered and washed until the pH = 7, and the solid was dried at 333 K. The hydrotalcites were activated by heating at 723 K in a dry flow of N₂ (99.99%). The temperature was raised at the rate of 2 °C min⁻¹ to reach 723 K and maintained for 8 h. The solid was then cooled to room temperature in N₂. These samples were labelled HTc. Rehydrated Al/Mg calcined hydrotalcites (HTr) were prepared at room temperature under a CO₂-free flow of nitrogen (40 mL min⁻¹) saturated with water vapour, for different times. Analyses of Mg and Al were performed using atomic absorption. The MgO sample was prepared by thermal decomposition of magnesium oxalate at 873 K in vacuum for 6 h.³⁵ CsNaX zeolite was prepared by a repeated exchange of an NaX zeolite (13X) with an aqueous solution of CsCl (0.5 M), at room temperature. The final zeolite contained 23 and 4.4 wt% of Cs and Na respectively, as determined by atomic absorption. 40 wt% KF impregnated on alumina was

Table 10 Main characteristics of the base catalysts

Catalyst	$S_{\text{BET}}/\text{m}^2 \text{ g}^{-1}$	Pore volume/ $\text{cm}^3 \text{ g}^{-1}$	Pore diameter/ \AA
MgO	246	0.615	96
HTc–Al/Mg(0.20) ^a	199	0.604	147
HTc–Al/Mg(0.25) ^a	264	0.461	97
HTc–Al/Mg(0.33) ^a	275	0.558	93
HTc–Al/Li(0.33) ^a	240	0.657	92
KF/Al ₂ O ₃	38	0.138	144
CsX	650	—	7.4
CeO ₂	174	0.195	—
Li– γ -Al ₂ O ₃ (3%)	132	0.259	78
Li– γ -Al ₂ O ₃ (6%)	107	0.217	81
Li– γ -Al ₂ O ₃ (9%)	87	0.198	80

^a Numbers in brackets are the Al/(Al + Mg) or Al/(Al + Li) ratios.

obtained from Aldrich. Samples of lithium oxide loaded on alumina were prepared as follows: a methanolic solution (50 mL) of LiNO₃ containing the corresponding percentage of Li to incorporate (3, 6 and 9 wt%) was added to 3 g of γ -Al₂O₃. The resultant suspension was stirred for 3 h at 323 K. The solvent was removed and the sample dried overnight at 333 K, then the solid was calcined at 723 K for 6 h with a mixture of air and nitrogen. These samples were labelled as Li– γ -Al₂O₃. The main characteristics of the catalysts are summarised in Table 10.

X-Ray diffraction measurements were recorded with a Philips X'PERT (PN 3719) diffractometer (CuK α radiation from a graphite monochromator) equipped with an automatic variable divergence slit and working in the constant irradiated area mode. N₂ and Ar adsorption/desorption isotherms were performed at 77 and 87 K respectively, in an ASAP 2010 apparatus from Micromeritics, after pre-treating the samples under vacuum at 673 K overnight, and the BET surfaces were obtained using the BET methodology.

Reaction procedure

A mixture containing fatty acid methyl ester (1.7 mmol), PEG (1.7 mmol) and with a reactant/catalyst ratio of 25 g g⁻¹ under nitrogen atmosphere were heated in a silicone bath to the required temperature in the absence of solvent with magnetic stirring. A Dean–Stark instrument was attached to the glass batch reactor to remove the methanol formed during the reaction. After the required time, the reaction mixture was dissolved in dichloromethane. The catalyst was filtered and thoroughly washed with dichloromethane. Finally, the organic solvent was evaporated under vacuum and the organic residue was weighed and dissolved in pyridine. An aliquot of the crude was taken and a known amount of internal standard (stearic acid methyl ester) was added and the mixture analyzed by HPLC. HPLC analyses (Waters 1525) were performed using an ELSD detector and a reverse phase C₁₈ column (Symmetry[®] 5 μm \times 4.6 mm \times 159 mm). The analysis was conducted under gradient conditions using an appropriate mixture of acetonitrile and acetone. Each experiment was repeated three times, and the average value was taken.

The fatty methyl ester conversion is the percentage of mmol of MeO which have been converted to the different reaction

products (monoester, diester and fatty acid), and is given by the following equation:

Molar conversion (%) =

$$\frac{A_{\text{mono}}/Fr_{\text{mono}} + 2A_{\text{di}}/Fr_{\text{di}} + A_{\text{FA}}/Fr_{\text{FA}}}{A_{\text{mono}}/Fr_{\text{mono}} + 2A_{\text{di}}/Fr_{\text{di}} + A_{\text{FA}}/Fr_{\text{FA}} + A_{\text{ME}}/Fr_{\text{ME}}} \times 100$$

Where A_{mono} , A_{di} , A_{FA} and A_{ME} are the respective areas of the peaks corresponding to monoester, diester, fatty acid and fatty acid methyl ester, and Fr are their respective response factors.

The yield of monoester is the percentage of mmol of MeO which have been converted to monoester, and is given by the following equation:

Yield of monoester =

$$\frac{A_{\text{mono}}/Fr_{\text{mono}}}{A_{\text{mono}}/Fr_{\text{mono}} + 2A_{\text{di}}/Fr_{\text{di}} + A_{\text{FA}}/Fr_{\text{FA}} + A_{\text{ME}}/Fr_{\text{ME}}} \times 100$$

The yield of diester is the percentage of mmol of MeO which have been converted to diester, and is given by the following equation:

Yield of diester =

$$\frac{2A_{\text{di}}/Fr_{\text{di}}}{A_{\text{mono}}/Fr_{\text{mono}} + 2A_{\text{di}}/Fr_{\text{di}} + A_{\text{FA}}/Fr_{\text{FA}} + A_{\text{ME}}/Fr_{\text{ME}}} \times 100$$

The selectivity to monoester is defined as the percentage of monoester existing in the total mmol of MeO converted, *i.e.* selectivity = (yield_{mono}/conversion) \times 100, and was calculated according to the following equation:

Selectivity to monoester (%) =

$$\frac{A_{\text{mono}}/Fr_{\text{mono}}}{A_{\text{mono}}/Fr_{\text{mono}} + 2A_{\text{di}}/Fr_{\text{di}} + A_{\text{FA}}/Fr_{\text{FA}}} \times 100$$

Conclusions

Solid bases are effective catalysts for the production of polyoxyethyleneglycol esters by transesterification of fatty acid methyl esters with polyethylene glycol.

Both Lewis and Brønsted basic solids are active and selective catalysts, with high surface area MgO and calcined–rehydrated hydrotalcites being the best catalysts.

Selectivity to monoester is not a function of the catalyst but of reaction temperature and ratio of PEG to fatty acid methyl ester.

The polarity of the PEG and fatty methyl esters play an important role in phase miscibility and conversion. The higher the molecular weight of PEG and the higher the number of carbons of the methyl ester the lower the conversion.

Acknowledgements

The authors thank the financial support given by the Generalitat Valenciana (Project GV04B-517), and a research agreement between University of Malaya and UPV.

References

- 1 (a) D. A. Herold, K. Keil and D. E. Bruns, *Biochem. Pharmacol.*, 1989, **38**, 73; (b) A. W. Ritcher and E. Akerblon, *Int. Arch. Allergy Appl. Immunol.*, 1983, **70**, 124.
- 2 F. K. Sagrado, M. Guzmán, M. R. Molpeceres and M. R. Aberturas, *Pharm. Technol. Eur.*, 1994, **6**, 5, 46; F. K. Sagrado, M. Guzmán, M. R. Molpeceres and M. R. Aberturas, *Pharm. Technol. Eur.*, 1994, **6**, 6, 38.
- 3 L. L. Walton, *Am. Perfum. Cosmet.*, 1962, **77**, 41.
- 4 K. Kosswig, in *Nonionic Surfactants, Surfactant Science Series*, ed. N. M. van Os, Marcel Dekker, New York–Basel–Hong Kong, 1998, vol. 72, p. 123 (and references therein).
- 5 J. K. Weil, R. E. Koos, W. M. Linfield and N. Parris, *J. Am. Oil Chem. Soc.*, 1979, **56**, 873.
- 6 H. Pardun, *Cosmet. Toiletries*, 1981, **96**, 69.
- 7 S. B. A. Hamid, F. Z. Abdullah, S. Ariyanchira, M. Mifsud, S. Iborra and A. Corma, *Catal. Today*, 2004, **97**, 271.
- 8 A. Corma, S. Iborra, S. Miquel and J. Primo, *J. Catal.*, 1998, **173**, 315.
- 9 S. Bancquart, C. Vanhove, Y. Pouilloux and J. Barrault, *Appl. Catal., A*, 2001, **218**, 1.
- 10 S. Bancquart, C. Vanhove, Y. Pouilloux and J. Barrault, *OL, Corps Gras, Lipides*, 2001, **8**, 253.
- 11 J. Barrault, Y. Pouilloux, J. M. Clacens, C. Vanhove and S. Bancquart, *Catal. Today*, 2002, **75**, 177.
- 12 S. B. A. Hamid, A. Corma, S. Iborra and A. Velty, *J. Catal.*, 2005, **234**, 340.
- 13 A. Corma, V. Fornes and R. M. Martín-Aranda, *J. Catal.*, 1992, **134**, 58.
- 14 T. Nakatsuka, H. Kawasaki, S. Yamasita and S. Kohijiyi, *Bull. Chem. Soc. Jpn.*, 1979, **52**, 2449.
- 15 D. Tichit, M. H. Lhouty, A. Guida, B. H. Chiche, F. Figueras, A. Auroux, D. Bartalini, D. Tichit and E. Garrone, *J. Catal.*, 1995, **151**, 50.
- 16 M. J. Climent, A. Corma, S. Iborra and J. Primo, *J. Catal.*, 1995, **151**, 60.
- 17 W. O. Haag and H. Pines, *J. Am. Chem. Soc.*, 1960, **82**, 387.
- 18 J. Kijenski and S. Malinowski, *React. Kinet. Catal. Lett.*, 1975, **3**, 343.
- 19 J. Kijenski, P. Radomski and E. Fedorynska, *J. Catal.*, 2001, **203**, 407.
- 20 T. Baba, H. Handa and Y. Ono, *J. Chem. Soc., Faraday Trans.*, 1994, **90**, 187.
- 21 T. Yamaguchi, J. H. Zhu, Y. Wang, M. Komatsu and M. Ookawa, *Chem. Lett.*, 1997, 989.
- 22 J. H. Zhu, Y. Wang, Y. Chun and X. S. Wang, *J. Chem. Soc., Faraday Trans.*, 1998, **94**, 1163.
- 23 K. K. Rao, M. Gravelle, J. Valente and F. Figueras, *J. Catal.*, 1998, **173**, 115.
- 24 S. Abello, F. Medina, D. Tichit, J. Pérez-Ramírez, J. C. Groen, J. E. Sueiras, P. Salangre and Y. Cesteros, *Chem.–Eur. J.*, 2005, **11**, 728.
- 25 R. Teissier, D. Tichit, F. Figueras and J. Kervennal, *Fr. Pat.* 2729137, 1995.
- 26 A. Guida, M. H. Lhouty, D. Tichit, F. Figueras and P. Geneste, *Appl. Catal., A*, 1997, **164**, 251.
- 27 M. J. Climent, A. Corma, S. Iborra and A. Velty, *Catal. Lett.*, 2002, **79**, 157.
- 28 J. A. A. Roelofs, D. J. Lensveld, A. J. van Dillen and K. P. de Jong, *J. Catal.*, 2001, **203**, 184.
- 29 M. J. Climent, A. Corma, S. Iborra and A. Velty, *Green Chem.*, 2002, **4**, 474.
- 30 M. J. Climent, A. Corma, S. Iborra and A. Velty, *J. Catal.*, 2004, **221**, 474.
- 31 M. L. Kantam, B. M. Choudary, C. V. Reddy, K. K. Rao and F. Figueras, *Chem. Commun.*, 1998, 1033.
- 32 B. M. Choudary, M. L. Kantam, C. V. Reddy, K. K. Rao and F. Figueras, *J. Mol. Catal.*, 1999, **146**, 279.
- 33 S. K. Pramod, J. Sanchez-Valente and F. Figueras, *Chem. Commun.*, 1998, 1091.
- 34 C. J. Serna, J. L. Rendon and J. E. Iglesias, *Clays Clay Miner.*, 1982, **30**, 180.
- 35 P. Putanov, E. Kis and G. Boskovic, *Appl. Catal.*, 1991, **73**, 17.

Silicate digestion with fructose under mild conditions

Gang Lu,^a Jonathan E. Grossman,^a Joseph B. Lambert,^{*a} Zhijun Xiao^b and Dan Fu^b

Received 11th January 2006, Accepted 26th April 2006

First published as an Advance Article on the web 19th May 2006

DOI: 10.1039/b600378h

Treatment of silica gel or silicate mineral with an aqueous solution of the weak base triethylenetetraamine and the sugar fructose results in partial dispersion into particles smaller than 450 nm under conditions of ambient pressure and mild heating (60–100 °C) in times less than 1 h. Redeposition occurs at longer times. The final material has 13–31% higher surface area and 17–18% lower D50 (50% of the accumulated weight percentage is smaller than this particle size). Dissolution or decrystallization of some of the aluminosilicate phase is indicated by X-ray diffraction for the Berea sandstone. The proposed mechanism involves deprotonation at the anomeric hydroxyl, followed by attack on the solid silicate centers by fructose to form a pentacoordinate silicon complex. The stereochemistry of fructose then allows a planar diolato ring to form containing C2 and C3 of fructose and a second position on pentacoordinate silicon. The reaction results in displacement of a portion of the silicate matrix. Reformation of Si–O–Si bonds gives rise to redeposition. An equilibrium between dissolution and redeposition results in the final reworked material with reduced particle size.

Introduction

Silicates constitute the largest mineral class in the earth's lithosphere. Because petroleum often is found embedded in silicate formations, the process of petroleum extraction requires dissolution, digestion, pulverization, or otherwise loosening the solid matrix at the bottom of a well to permit flow of the desired material.¹ Current technology involves pumping hydrogen fluoride (HF) to the silicate formations. Production and handling of HF occurs on site, with potential danger both to technicians and to the environment. The development of alternative strategies to dissolve silicate minerals therefore is important to the petroleum industry and for the preservation of the environment.

Dissolution of silicates also is desirable or necessary in several other contexts. (1) The construction industry often is faced with demolition of concrete structures. Removal and transport of a dissolved or slurried silicate would be far easier than of solid concrete blocks.² (2) Solubilized silicate minerals are an important starting material for the silicon and organo-silicon industries when economically viable.³ (3) Rice hulls, containing *ca.* 20% silica, are a potential raw material for silicon industries but again must be solubilized.⁴ In addition, marine organisms such as diatoms, sponges, and radiolarians metabolize silica to construct much of their structure. Silicate minerals thus are an important biosource, although the biochemical mechanisms are not fully understood.

Several groups have reported the dissolution of silica in basic, aqueous media to produce anionic alkoxy and aryloxy silicates.^{5–12} Others have treated aqueous silicic acid with polyols to form penta- and hexacoordinated polyolate

complexes.^{13–16} We recently reported that silicic acid forms stable, hypercoordinated silicates with sugars,¹⁷ and Klüfers *et al.* reported the X-ray structures of complexes between arylsiliconates and sugars.¹⁸

Laine and co-workers^{19–24} found that the reaction of silica gel, fused silica, or sand at high temperatures with ethylene glycol and group 1 metals or group 2 metal oxides produced penta- and hexacoordinated glycolato silicate complexes. In a patent, Bailey *et al.* described the reaction of silica in mixed solvents of simple alcohols (ethanol or propanol) and aromatics (benzene or xylene) with strong base to produce alkoxysilanes.²³ Suzuki and co-workers demonstrated that gaseous dimethyl or diethyl carbonate reacts with alkali-treated silica at very high temperatures to form alkoxysilanes in high yield.²⁴ These routes require strong bases and temperatures usually in excess of 200 °C for a prolonged period of time.

The use of HF or extremely strong bases is not optimal from many points of view. We describe herein a novel and simple procedure for digestion of silicate materials utilizing the weak base triethylenetetraamine (TETA) instead of strong bases. The procedure is carried out at lower temperatures than most previous dissolution procedures. This study was inspired in part by the work of Laine *et al.*²⁰ and the observation of Frye *et al.* that spiro-silicates react with methanol and amines to form pentacoordinated silicates.²⁵ Our work, however, finds that TETA alone is relatively inactive and needs the addition of a chelating agent, which evolved from our previous work with sugar silicates.¹⁷

Results

Digestion experiments were carried out on two silicate materials: silica gel (pore size 60 Å) and Berea sandstone (ground to a fine powder). All experiments were carried out in aqueous solution containing one or more of the following

^aDepartment of Chemistry, Northwestern University, Evanston, IL 60208, USA. E-mail: jlambert@northwestern.edu

^bSchlumberger Corp., Oilfield Chemical Products, 110 Schlumberger Drive, MD-3, Sugar Land, TX 77478, USA

components: TETA to serve as a weak base, EDTA to complex metal cations, and D-fructose to chelate with silicate oxygens. Both temperature and pressure were varied. The weight of the silicate material was measured initially and after treatment. In addition in one set of experiments as indicated, the dissolved silicate levels were measured as a function of time by inductively coupled plasma (ICP).

Silica gel at ambient pressure

Treatment of silica gel in an open round-bottomed flask at 60 °C for 1 h in the presence of TETA, EDTA, and fructose led to a 36% loss of mass. Similar treatment at 80 °C for 48 min led to a 40% loss of mass. Conditions identical to the second experiment but without fructose led to only a 10% loss of mass.

Berea sandstone at ambient pressure

Similar treatment of powdered Berea sandstone with all three components at 60 °C for 4 h led to a 33% loss of mass. An experiment at 80 °C for 48 min led to 32% loss of mass. Three further experiments under the latter conditions were performed without one of the components. When fructose and TETA were present but EDTA was not, loss of mass was 28% after 48 min. When EDTA and TETA were present but fructose was not, there was no loss of mass. When EDTA and fructose were present but TETA was not, there was no loss of mass. Mass loss was measured as a function of time in a series of discrete experiments at ambient pressure and 100 °C (Fig. 1). After 30 min a mass loss of only 5% was obtained. The loss increased to 38% at 48 min and 34% at 1 h. After an hour, secondary precipitation²⁶ of silicate occurred, resulting in little or no net mass loss. At a slightly lower temperature, similar results were obtained (Fig. 2).

Berea sandstone under pressure

Treatment of powdered Berea sandstone in an autoclave permitted use of higher temperature (150 °C) and pressure. With all three components present, loss of mass as a function of time was monitored in a series of discrete experiments, as illustrated in Fig. 3. After only 1 h, a mass loss of 39% was

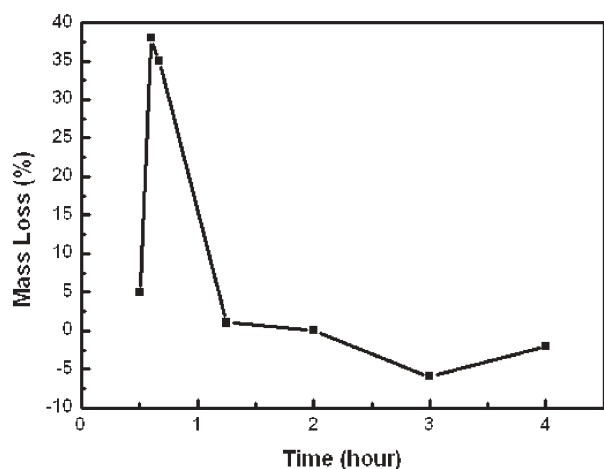


Fig. 1 Dissolution of Berea sandstone at ambient pressure (100 °C).

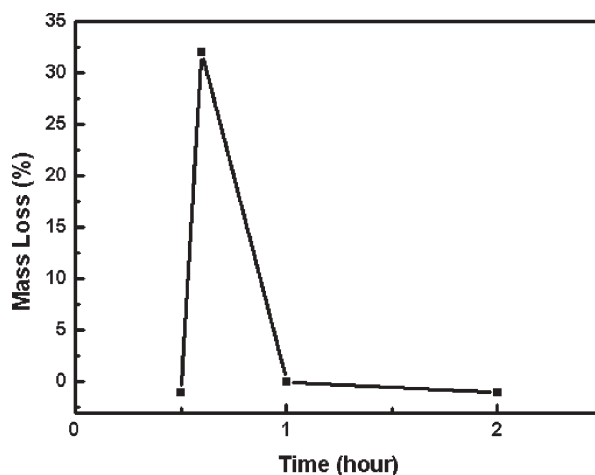


Fig. 2 Dissolution of Berea sandstone at 80 °C and ambient pressure.

achieved. With prolonged heating, however, mass loss decreased drastically, leveling off at about 12% after 7 h. Secondary precipitation of dissolved silicates apparently was occurring.

Effect of pore size on filtration

All the above experiments were carried out with filtration of the aqueous solution through a 0.45 μm (450 nm) filter. The weights reflect the amount of material that failed to penetrate the filter. When a 0.2 μm (200 nm) filter was used, little or no mass loss was observed (and only trace amounts of silicate were detected by ICP analysis of the filtrate).

Powder X-ray diffraction

Untreated samples and samples treated with TETA and fructose for 60 min at 60 °C were examined for their diffraction properties. Silica gel samples showed no diffraction peaks other than those of the sample holder and consequently are amorphous. Untreated Berea sandstone showed strong quartz peaks and minor aluminosilicate phases (clays and feldspars). Sandstone recovered after treatment contained less aluminosilicates than untreated material.

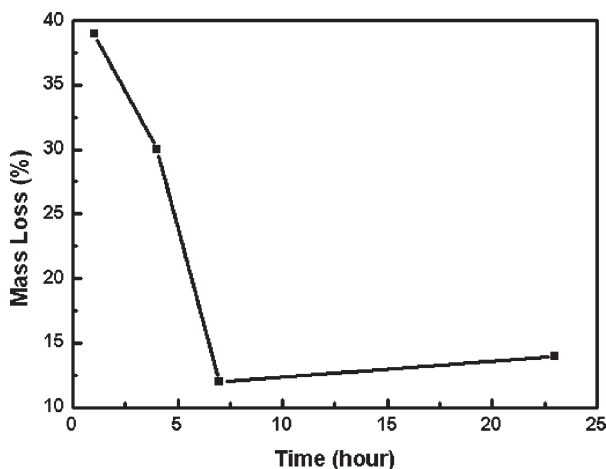


Fig. 3 Dissolution of Berea sandstone in an autoclave at 150 °C.

Particle size distribution

Untreated samples and samples treated as for the X-ray experiments were analyzed for particle size distribution. In a plot of volume% vs. particle size, untreated silica gel exhibited one major peak with a maximum at *ca.* 75 μm and a smaller peak with a maximum at *ca.* 5 μm . The overall specific surface area was $0.182\text{ m}^2\text{ g}^{-1}$. The respective values of D10, D50, and D90 were 37.1, 67.9, and 107.4 μm (10, 50, and 90% of the accumulated weight percentage are smaller than these respective values). The volume weighted mean was 107.4 μm . Following treatment of the silica gel, the two original peaks, now with maxima at *ca.* 8 and *ca.* 63 μm , were joined by a small new peak with a maximum at *ca.* 450 μm . The overall specific surface area had increased to $0.239\text{ m}^2\text{ g}^{-1}$, the respective values of D10, D50, and D90 had decreased to 14.6, 56.4, and 106.8 μm , and the volume weighted mean had decreased to 106.8 μm .

The same plot for untreated Berea sandstone (Fig. 4) showed one major peak with a maximum at *ca.* 160 μm and two broad minor peaks with maxima at *ca.* 6 and *ca.* 20 μm with an overall specific surface area of $0.196\text{ m}^2\text{ g}^{-1}$. The respective values of D10, D50, and D90 were 22.9, 144.9, and 271.0 μm , and the volume weighted mean was 271.0 μm . Following treatment of the Berea sandstone, the peak at lowest particle size had become a shoulder (*ca.* 5–10 μm), the second small peak now with a maximum at *ca.* 25 μm had increased slightly in size, and the large peak had moved only slightly to a maximum at *ca.* 145 μm . The specific surface area had become $0.221\text{ m}^2\text{ g}^{-1}$, D10/D50/D90 were 18.0/119.0/222.0 μm , and the volume weighted mean 122.5 μm .

Discussion

In past work, silicate has been digested under highly basic or acidic conditions.^{22,26} With a weak base such as TETA, very little dissolution or digestion occurs. Silica gel treated at 80 $^{\circ}\text{C}$ and atmospheric pressure for 48 min showed a mass loss of only 10% in the presence of TETA alone. With both TETA and fructose present under the same conditions, the mass loss was 40%. Clearly, fructose plays a critical role in optimizing digestion. At only 60 $^{\circ}\text{C}$ for 60 min, with both TETA and fructose, the mass loss was 35%. EDTA was present in all these experiments, and mass loss was measured by weighing the solid material before and after treatment.

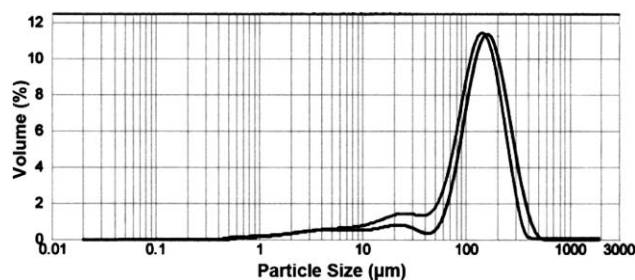


Fig. 4 Particle size distribution as a function of percentage volume for (right curve) untreated Berea sandstone and (left curve) treated Berea sandstone.

Treatment of Berea sandstone with TETA, fructose, and EDTA at 60–80 $^{\circ}\text{C}$ for 48–240 min led to a mass loss of 32–33%. When EDTA was omitted from the experiment, there still was 28% mass loss after 48 min. When either TETA or fructose was omitted, however, the mass loss was zero after 48 min. Thus EDTA plays a minor role, but both the chelating agent fructose and the weak base TETA are necessary for any dissolution to occur. As with silica gel, the mass loss in these experiments with Berea sandstone was measured by measuring the weight of the solid before and after treatment.

At slightly higher temperatures (100 $^{\circ}\text{C}$), mass loss was obtained as a function of time in a series of discrete experiments. Fig. 1 shows that the maximal mass loss occurred at 48–60 min under these conditions. This observation indicates secondary precipitation, which has been observed widely.²⁶ Treatment with TETA and fructose gives optimal results after a relatively short amount of time. Thus apparently negative results (no mass loss) could occur if experiments were allowed to run for longer periods of time. Similar results were obtained at 80 $^{\circ}\text{C}$ (Fig. 2). Although ammonium ions can serve as templates for silicate construction, our basic conditions prohibit the formation of ammonium ions from TETA.

The maximal allowable temperature with ambient pressure is approximately 100 $^{\circ}\text{C}$. Higher temperatures would require higher pressures, which we achieved by the use of an autoclave. With TETA, fructose, and EDTA present at 150 $^{\circ}\text{C}$ for 7 h in an autoclave, mass loss was monitored as a function of time (Fig. 3). After 1 h, mass loss was 39%, comparable to results at lower temperatures and pressures. After 5 h, however, mass loss dropped to about 12% and remained there.

All these experiments involved filtering the solution through a 0.45 μm filter and weighing the mass of the material that failed to pass through the filter. When a 0.2 μm filter was used, in the case of reaction at 80 $^{\circ}\text{C}$ for 4 h, little mass loss was observed. Thus the digestion involves reduction in particle size from macroscopic to nanometer (200–450 nm). A 200 nm sized particle corresponds to an $-(\text{O}-\text{Si})_n-$ length with n equaling approximately 400 in one dimension (each O–Si–O unit requires about 0.25 nm). The dissolution conditions have reduced the silicate minerals from an essentially infinite solid polymer to a highly disperse, low molecular weight material that passes through a 0.45 μm filter but fails to pass through a 0.20 μm filter.

The X-ray experiments indicated that the silica gel samples were amorphous and the Berea sandstone samples were crystalline, even after treatment. No further information could be obtained from the silica gel samples. Diminution of the aluminosilicate peaks in relation to the quartz peaks for the treated Berea sandstone samples indicates preferential digestion of the aluminosilicate phases. Such phases have higher surface area and looser crystal structure than the quartz phase and hence are more susceptible to digestion.

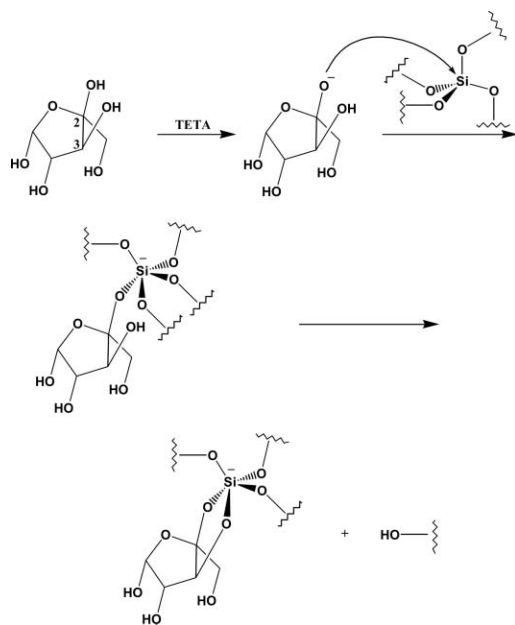
Measurement of particle size distributions revealed that profound changes had occurred following treatment of both materials. The specific surface area of the silica gel had increased by 31%, indicating the more exposed nature of the treated material. Consequently, the volume weighted mean had decreased by 5%. This overall figure, however, is not descriptive of the changes that had occurred within the sample.

Although a small third peak appeared at larger size, the maximum of the major peak moved to a smaller particle size. The net result is a 60% decrease in D10 and a 17% decrease in D50, but only a 0.5% decrease of D90. Treatment of silica gel by TETA and fructose has increased the surface area and decreased the particle size.

Treatment of Berea sandstone does not give rise to the third peak, but similar results are obtained for bulk properties. The plot in Fig. 4 shows that the major peak moves to lower particle size after treatment, and the minor peak at lower particle size increases in intensity. The overall specific surface area increased by 13%, and the volume weighted mean decreased by 20%. Without the new peak at larger size, D10, D50, and D90 all decreased, respectively by 22, 18, and 18%. Once again, treatment by TETA and fructose has increased the surface area and decreased the particle size.

Scheme 1, based on our earlier observations,¹⁷ provides a possible mechanism for the action of fructose on silicate in a weakly basic aqueous solution. In the first step, the weak base TETA removes the most acidic hydrogen, which is found at the anomeric position of fructose. In the second step, the basic, anomeric oxygen attacks a tetracoordinate silicate grouping (the wiggly lines in Scheme 1 indicate further connections to silicon within the solid silicate matrix). The result, following our experiments on the reaction between fructose and silicic acid under highly basic conditions,¹⁷ is formation of penta-coordinate silicon.

It is likely that this charged material would tend to be more soluble in water than the uncharged tetracoordinate silicate. Such a step by itself, however, cannot result in dissolution, as no portion of the silicate matrix has split off. Otherwise, TETA alone should bring about dissolution, which it does not. There must be a special role for fructose, which we envisage to be analogous to its reaction with silicic acid [Si(OH)₄].¹⁷ We observed that fructose, and only certain other furanose (five-membered-ring) sugars, react with silicic acid, because they have an anomeric HO group (at the 2 position in fructose) that



Scheme 1

is *cis* to an adjacent HO group (at the 3 position). Only when this structural grouping (*cis* HO–C–OH) is present can a nearly planar chelate five-membered diolato ring form. When the adjacent HO group is *trans* or when the sugar ring has six members (pyranose), formation of the planar diolato ring is stereochemically impossible.¹⁷

In the present context, the 3-OH in fructose displaces a silicate O–Si bond in the third step of Scheme 1 to form the illustrated, planar diolato chelate product and an extruded silicate fragment (“HO–”). This formal step can occur by either an associative or a dissociative mechanism, and at present we cannot choose between the two possibilities. In the associative mechanism, TETA initially removes the proton from the 3-OH group. The resulting alkoxide ion attacks silicon to form a doubly charged hexacoordinated chelate (the planar diolato ring). Our earlier experiments¹⁷ and those of Kinrade *et al.*^{13–16} have demonstrated that hexacoordinate silicon can occur under these conditions. Loss of siloxide then restores pentacoordination and produces (after reprotonation) the extruded silicate fragment “HO–” depicted as a final product in Scheme 1. In the dissociative mechanism, loss of the siloxide fragment occurs initially from the pentacoordinated species to form tetracoordinate silicon. Attack by the deprotonated 3-OH group of fructose then produces the pentacoordinate product in Scheme 1. By either variant, these final steps begin the process of dissolution. Repetition of the mechanism of Scheme 1 at multiple sites in the solid continues to degrade the silicate matrix. We have found that fructose succeeds in breaking the matrix down in this fashion to particles of the size 200–450 nm.

Redeposition has been discussed thoroughly in the literature.²⁶ In the present context it represents the reversal of the process described in Scheme 1, probably without the involvement of fructose. Redeposition or polysilicate formation takes place by reformation of the stable Si–O–Si bonds. Thus dissolution and redeposition are two aspects of an equilibrium process. The redeposited material of course is not the same as the original. Treatment of silica gel or Berea sandstone with TETA and fructose results in some dissolution of the aluminosilicate phases, some dispersion to colloidal-like particles of size 200–450 nm, overall reduction in particle size, and some production of redeposited solid material. This result, achieved by environmentally benign conditions of weak basicity, would permit flow of petroleum from silicate formations or slurring of concrete residues.

Experimental

Materials

Berea sandstone core (quartz content >85%) was supplied by Schlumberger Corp. and was ground to a fine powder of size <200 mesh ASTM (74 μm) with a mortar and pestle. Silica gel for column chromatography (pore size 60 Å) was purchased from Fisher and used as received.

Procedures

Dissolution of silica gel at ambient pressure. A typical procedure involved heating a mixture of silica gel (1.0 g,

16.7 mmol), D-fructose (1.20 g, 6.7 mmol), TETA (2.2 mL, 7.0 mmol), and ethylenediamine tetraacetic acid (EDTA) tetrasodium salt (3.0 g, 6.7 mmol) in 100 mL of H₂O to 60 °C in a 250 mL, round-bottomed flask for 1 h. The reddish mixture was allowed to cool to room temperature and was filtered with a 0.45 µm filtration membrane (Millipore). The color results from decomposition of sugars in the presence of base and is independent of the presence of silica.²⁷ The residue was washed with deionized H₂O (3 × 50 mL) and dried in an oven (110 °C) overnight. Recovered mass: 0.64 g; mass loss (difference between original and recovered mass): 36.0%.

Dissolution of Berea sandstone at ambient pressure. A typical procedure involved heating a mixture of the powdered rock (1.05 g, 17.3 mmol), D-fructose (1.20 g, 6.7 mmol), TETA (2.2 mL, 7.0 mmol), and EDTA tetrasodium salt (3.0 g, 6.7 mmol) in 100 mL of H₂O to 60 °C in a 250 mL, round-bottomed flask for 4 h. The dark mixture was allowed to cool to room temperature and was filtered with a 0.45 µm filtration membrane (Millipore). The residue was washed with deionized H₂O (3 × 50 mL) and dried in an oven (110 °C) overnight. Recovered mass: 0.70 g; mass loss: 33.3%.

Dissolution of Berea sandstone in an autoclave. A typical procedure involved heating a mixture of the powdered rock (1.04 g, 17.3 mmol), D-fructose (1.20 g, 6.7 mmol), TETA (2.2 mL, 7.0 mmol), and EDTA tetrasodium salt (3.0 g, 6.7 mmol) in 100 mL of H₂O to 150 °C in a 250 mL autoclave for 7 h. The dark mixture was allowed to cool to room temperature and was filtered with a 0.45 µm filtration membrane (Millipore). The solid residue was washed with deionized H₂O (3 × 50 mL) and was dried in an oven (110 °C) overnight. Recovered mass: 0.92 g; mass loss; 11.5%.

Dissolution of Berea sandstone in an orbital shaker. A typical experiment involved heating powdered rock (1.0 g, 17.3 mmol), D-fructose (1.20 g, 6.7 mmol), TETA (2.2 mL, 7.0 mmol), and EDTA (3.0 g, 6.7 mmol) in 100 mL of H₂O at 80 °C at ambient pressure in a 250 mL Erlenmeyer flask on an orbital shaker for 4 h. Two 1 mL aliquots of the liquid portion of the reaction mixture were removed from the vessel every 15 min and were filtered with a disposable Millipore filter (0.45 µm and 0.2 µm, respectively). The aliquots were diluted to 10 mL with deionized water and were subjected to ICP analysis. The ICP results on the liquid portion showed that the concentration of silicon peaked at 1900 mg L⁻¹ at about 1 h for the set using the 0.45 µm filter and became stable after that. For the set using the 0.2 µm filter, the maximum silicon concentration was 20 mg L⁻¹ throughout the experiment. After 4 h, the solid residue was washed with deionized H₂O (3 × 50 mL) and

dried in an oven (110 °C) overnight. Recovered mass: 0.90 g; mass loss: 10%.

Acknowledgements

This work was supported by the National Science Foundation (Grant no. CHE-0349412) and the Schlumberger Corporation.

References

- 1 C. Crowe, J. Masmonteil and R. Thomas, *Oilfield Rev.*, 1992, **4**, 24–40.
- 2 C. Müller, <http://www.b-i-m.de/Public/IBAC/mueller.htm>.
- 3 R. M. Laine, K. Y. Blohowiak, T. R. Robinson, M. L. Hoppe, P. Nardi, J. Kampf and J. Uhm, *Nature*, 1991, **353**, 642–644.
- 4 M. Z. Asunción, I. Hasegawa, J. W. Kampf and R. M. Laine, *J. Mater. Chem.*, 2005, **15**, 2114–2121.
- 5 D. W. Barnum, *Inorg. Chem.*, 1970, **9**, 1942–1943.
- 6 D. W. Barnum, *Inorg. Chem.*, 1972, **11**, 1424–1429.
- 7 F. P. Boer, J. J. Flynn and J. W. Turley, *J. Am. Chem. Soc.*, 1968, **90**, 6973–6977.
- 8 A. Boudin, G. Cerveau, C. Chuit, R. J. P. Corriu and C. Reye, *Angew. Chem., Int. Ed. Engl.*, 1986, **25**, 473–474.
- 9 A. Boudin, G. Cerveau, C. Chuit, R. J. P. Corriu and C. Reye, *Organometallics*, 1988, **7**, 1165–1171.
- 10 J. J. Flynn and F. P. Boer, *J. Am. Chem. Soc.*, 1969, **91**, 5756–5761.
- 11 C. L. Frye, *J. Am. Chem. Soc.*, 1964, **86**, 3170–3171.
- 12 A. Weiss, G. Reiff and A. Weiss, *Z. Anorg. Allg. Chem.*, 1961, **311**, 151–179.
- 13 S. D. Kinrade, J. W. Del Nin, A. S. Schach, T. A. Sloan, K. L. Wilson and C. T. G. Knight, *Science*, 1999, **285**, 1542–1545.
- 14 S. D. Kinrade, E. W. Deguns, A. M. E. Gillson and C. T. G. Knight, *Dalton Trans.*, 2003, 3713–3716.
- 15 S. D. Kinrade, K. J. Maa, A. S. Schach, T. A. Sloan and C. T. B. Knight, *J. Chem. Soc., Dalton Trans.*, 1999, 3149–3150.
- 16 S. D. Kinrade, A. S. Schach, R. J. Hamilton and C. T. G. Knight, *Chem. Commun.*, 2001, 1564–1565.
- 17 J. B. Lambert, G. Lu, S. R. Singer and V. M. Kolb, *J. Am. Chem. Soc.*, 2004, **126**, 9611–9625.
- 18 P. Klüfers, F. Kopp and M. Vogt, *Chem.–Eur. J.*, 2004, **10**, 4538–4545.
- 19 K. Y. Blohowiak, D. R. Treadwell, B. L. Mueller, M. L. Hoppe, S. Jouppi, P. Pansal, K. W. Chew, C. L. S. Scotto, F. Babonneau, J. Kampf and R. M. Laine, *Chem. Mater.*, 1994, **6**, 2177–2192.
- 20 H. Q. Cheng, R. Tamaki, R. M. Laine, F. Babonneau, Y. Chujo and D. R. Treadwell, *J. Am. Chem. Soc.*, 2000, **122**, 10063–10072.
- 21 M. L. Hoppe, R. M. Laine, J. Kampf, M. S. Gordon and L. W. Burggraf, *Angew. Chem., Int. Ed. Engl.*, 1993, **32**, 287–289.
- 22 R. M. Laine, K. Y. Blohowiak, T. R. Robinson, M. L. Hoppe, P. Nardi, J. Kampf and J. Uhm, *Nature*, 1991, **353**, 642–644.
- 23 D. L. Bailey, A. Snyder and F. M. O'Connor, *US Pat.*, 2,881,198, 1959.
- 24 E. Suzuki, M. Akiyama and Y. Ono, *J. Chem. Soc., Chem. Commun.*, 1992, 136–137.
- 25 C. L. Frye, G. A. Vincent and W. A. Finzel, *J. Am. Chem. Soc.*, 1971, **93**, 6805–6811.
- 26 B. B. Williams, J. L. Gidley and R. S. Schechter, *Acidizing Fundamentals*, in *SPE Monograph Vol. 6*, SPE, New York, 1979.
- 27 P. M. Collins and R. J. Ferrier, *Monosaccharides*, Wiley, Chichester, 1995.

Efficient regioselective acylation of 1- β -D-arabinofuranosylcytosine catalyzed by lipase in ionic liquid containing systems

Xiao-Feng Li,^a Wen-Yong Lou,^a Thomas J. Smith,^b Min-Hua Zong,^{*a} Hong Wu^a and Ju-Fang Wang^a

Received 11th January 2006, Accepted 22nd March 2006

First published as an Advance Article on the web 4th April 2006

DOI: 10.1039/b600397d

Seven ionic liquids (ILs) were tested for use in the regioselective acylation of 1- β -D-arabinofuranosylcytosine (ara-C) by vinyl propionate, catalyzed by immobilized *Candida antarctica* lipase B. The results demonstrated that the nature of both the cations and the anions of ILs had a significant effect on the initial rate and the substrate conversion, but little effect on the regioselectivity of the reaction. The lipase displayed enhanced activity toward ara-C when the alkyl chain of $C_n\text{MIm}\cdot\text{BF}_4$ increased in length ($n = 4-8$) and no acylation reaction occurred in $C_4\text{MIm}\cdot\text{Cl}$ or $C_4\text{MIm}\cdot\text{Br}$. To further enhance the initial rate and substrate conversion, co-solvent mixtures of ILs and organic solvents were investigated. Among various IL-containing systems examined, 10% (v/v) $C_4\text{MIm}\cdot\text{PF}_6$ -tetrahydrofuran gave the highest initial rate and substrate conversion. In this reaction medium, the optimal water activity, vinyl propionate/ara-C molar ratio, temperature and shaking rate were 0.07, 15 : 1 (mol/mol), 60 °C and 250 rpm, respectively. Under these conditions, the initial rate, substrate conversion and the regioselectivity were 94.0 mM h⁻¹, 98.5% and 99%, respectively. An additional comparative study demonstrated that the enzymatic acylation proceeded with very similar initial rate, substrate conversion, regioselectivity and activation energy whether the reaction medium was 10% (v/v) $C_4\text{MIm}\cdot\text{PF}_6$ -tetrahydrofuran or 28% (v/v) hexane-pyridine (the best organic solvent mixture for the reaction). However, the lipase exhibited a much higher stability in the IL-containing system, which may also have environmental advantages. The product of the lipase-catalysed reaction was characterized by NMR, FT-IR spectroscopy and was shown to be the 5'-O-monoester of ara-C.

Introduction

Regioselective acylation of nucleosides possessing several hydroxyl groups of similar chemical reactivity is a fundamental challenge to organic chemists.¹ Successful developments in this area may lead to a variety of nucleoside derivatives that could be employed not only as key building blocks in the synthesis of oligonucleotides but also as effective pharmaceuticals for the treatment of viral infections and tumors.^{1,2} Among such compounds, fatty ester derivatives of 1- β -D-arabinofuranosylcytosine (ara-C), which play a crucial role in the therapy of acute leukemia and solid tumors, are particularly interesting.^{2,3} Currently, several strategies for selective acylation of ara-C employing conventional chemical methods have been reported, but their application is somewhat hampered by the relatively low regioselectivity, the lack of easy access to some of the key intermediates, and the environmental concerns of the process.^{4,5} Consequently, more efficient methodologies for the production of these compounds are of considerable industrial significance. Enzymatic acylation of nucleosides in non-aqueous media is a favorable and practicable option for regioselective preparation of the target nucleoside esters under mild conditions. In such a reaction the catalytic specificity of

the enzyme would avoid the need for additional chemical protection/deprotection steps. Some efforts have been made toward enzymatic acylation of nucleosides in organic solvents and it has been found that one of the most troublesome limitations is the poor solubility of the hydrophilic nucleosides in most organic solvents.^{1,6-8} In fact, only polar organic solvents, such as pyridine and DMF, have been commonly used for this purpose.^{9,10} Unfortunately polar organic solvents usually strip essential water from the enzyme molecules and thus inactivate the biocatalyst. Acylation of ara-C has proved to be especially difficult because this compound was found to be unreactive in enzyme-catalysed acylation reactions unless activated by conversion to a modified form such as *N*-butyryl-1- β -D-arabinofuranosylcytosine.¹¹ Recently in our laboratory we have been addressing this problem by developing methods for direct enzyme-catalysed regioselective acylation of unmodified ara-C by using a variety of nonaqueous media.¹² Here we report our investigation of this reaction in media containing ionic liquids (ILs), which was aimed towards effective regioselective catalysis at the same time as minimizing the use of environmentally harmful organic solvents.

Ionic liquids (ILs) have emerged as excellent nonaqueous media for a great variety of biocatalytic reactions, and are becoming more and more attractive in such applications.¹³⁻¹⁵ Their unique properties such as nonvolatility, nonflammability, and excellent chemical and thermal stability have made them an environmentally attractive alternative to conventional organic solvents. Moreover, ILs are capable of dissolving a

^aLab of Applied Biocatalysis, South China University of Technology, Guangzhou 510640, P. R. China. E-mail: btmhzong@scut.edu.cn; Fax: +86 20-22236669; Tel: +86 20-87111452

^bBiomedical Research Centre, Sheffield Hallam University, Howard Street, Sheffield, UK S1 1WB

wide range of substrates, especially those with high polarity such as carbohydrates and nucleosides, which are sparingly soluble in common organic solvents. Another obvious advantage is the possibility of designing a solvent with specific properties (including polarity, hydrophobicity, viscosity and solvent miscibility) by modifying the cation, anion, or attached substituent of the IL.¹⁶ In recent years, a large number of enzymatic reactions have been successfully carried out in IL-containing systems, such as thermolysin-catalyzed synthesis of *Z*-aspartame;¹⁷ alcalase-catalyzed resolution of amino acids;¹⁸ hydroxynitrile lyase-promoted cyanohydrin formation;¹⁹ lipase-catalyzed ammonolysis;²⁰ and enzymatic esterification of carbohydrates.^{21–23} In many cases, enzymes showed a comparable or even higher activity, stability and selectivity in the IL-containing systems than in organic solvents. However, very little work has been done on enzymatic acylation of nucleosides in IL-containing systems.²⁴

Encouraged by our recent achievements in the study of enzymatic reactions in ILs^{20,25,26} and the possibility that some types of ILs could offer both a high solubility of nucleosides and a high stability of a lipase, we tried, for the first time, the enzymatic acylation of ara-C with vinyl propionate (VP) (Scheme 1) by an immobilized lipase in IL-containing systems, in order to develop a novel and efficient route for the preparation of a 5'-*O*-monoester of ara-C.

Results and discussion

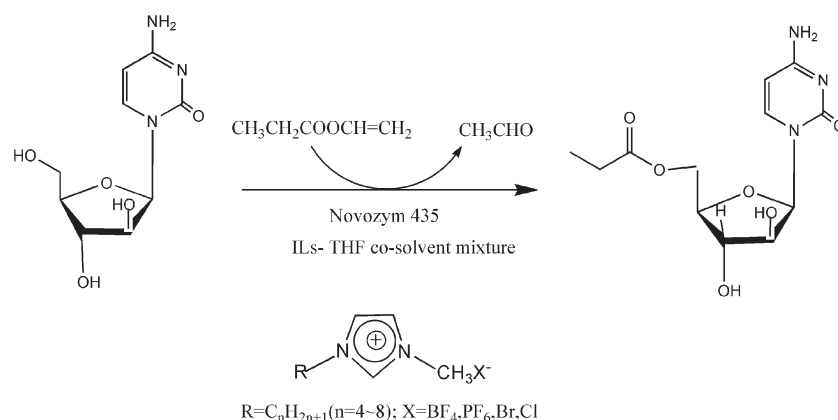
In order to structurally characterize the product of the Novozym 435-catalyzed acylation of ara-C with VP in IL-containing systems, 0.2 mmol of ara-C and 3 mmol VP were reacted in the presence of the enzyme and the product was purified as described in the Experimental section, before characterization by FT-IR and ¹³C NMR analysis.

The FT-IR spectroscopy revealed that characteristic absorptions in common with ara-C still existed in the product spectrum, such as peaks at 3421–3444 cm⁻¹ (–OH and –NH from the sugar and base moieties), 1648 cm⁻¹ (C=C from the base moiety), and 1113/1078 cm⁻¹ (C–O–C, from the sugar). In addition, a new absorbance at 1735 cm⁻¹, corresponding to the carbonyl group of the acyl moiety, appeared in the product spectrum, indicating that ara-C had been acylated. The

structure of the product was further confirmed by ¹³C NMR spectroscopy and it was found that, compared with ara-C, the spectrum of the product exhibited three additional carbon signals at δ 174.2, 27.3 and 9.6, characteristic of a propionyl group. Moreover, the C-5' (δ 61.6) of the sugar moiety shifted downfield by \sim 2.7 ppm and the resonance due to its neighboring carbon atom C-4' (δ 85.5) also showed an upfield shift of \sim 3.2 ppm, which suggested that the acyl group was attached to the –OH at C-5'.²⁷ Thus the product was identified as 5'-*O*-propionyl ara-C.

It has been reported that *Candida antarctica* lipase B (CAL-B), which is the enzyme component of Novozym 435, has a rather narrow and deep channel leading to an open active site.²⁸ The 5'-OH of the sugar moiety of ara-C may have an easier access to the active site of CAL-B to attack the acyl-enzyme intermediate than the other –OH groups at C-3' and C-2', perhaps due to less steric hindrance factors, thus resulting in preferential acylation at the 5'-OH position.

It is well known that the catalytic properties of enzymes in IL-containing systems are dependent on the type of IL used.²⁹ We initially focused on the influence of the cation and the anion of ILs on Novozym 435-mediated regioselective acylation of ara-C (Table 1, entries 1–7). In the case of 1-alkyl-3-methylimidazolium tetrafluoroborate (C_nMIm·BF₄, *n* = 4–8), both the hydrophobicity and the viscosity of ILs increase with increasing length of the alkyl group attached on the cation, while the polarity decreases to some extent.³⁰ The reaction became faster with the elongation of the alkyl chain of the cation (Table 1, entries 1–4). In addition, Novozym 435 showed relatively high activity in C₄MIm·PF₆ as compared to C₄MIm·BF₄ and no activity when C₄MIm·Cl or C₄MIm·Br was the reaction medium. In all IL-containing systems tested, the regioselectivity was effectively constant at 99%. Collectively the results suggested that the anions are more crucial in affecting the initial rate and the substrate conversion than the cations. There were two possible explanations for this difference. Firstly, the enzyme-compatible anions may show lower hydrogen bond basicity, which would minimize interference with the internal hydrogen bonds of the enzyme.^{13,31} The PF₆⁻ anion, for example, spreads its negative charge over six fluorine atoms and thus weakens hydrogen bond basicity of C₄MIm·PF₆. Second, the enzyme-compatible anion PF₆⁻



Scheme 1 Novozym 435-catalyzed acylation of 1- β -D-arabinofuranosylcytosine with vinyl propionate.

Table 1 Effect of various ILs and IL/co-solvent mixtures on Novozym 435-mediated acylation of ara-C by VP^a

Entry	Medium	Solubility of ara-C/mol l ⁻¹ ^b	<i>V</i> ₀ /mMh ⁻¹	<i>C</i> ^c (%)	Regioselectivity (%)
1	C ₄ MIm·BF ₄	0.268	6.3	17.8	99
2	C ₅ MIm·BF ₄	0.101	8.5	29.1	99
3	C ₆ MIm·BF ₄	<0.086	12.0	43.5	99
4	C ₈ MIm·BF ₄	<0.072	17.5	60.5	99
5	C ₄ MIm·PF ₆	<0.064	27.1	65.1	99
6	C ₄ MIm·Cl	0.871	0	0	0
7	C ₄ MIm·Br	0.905	0	0	0
8	20% (v/v) C ₄ MIm·BF ₄ /THF ^{c,d}	<0.198	46.1	95.2	99
9	20% (v/v) C ₅ MIm·BF ₄ /THF ^{c,d}	<0.145	49.0	95.6	99
10	10% (v/v) C ₆ MIm·BF ₄ /THF ^{c,d}	<0.127	50.1	96.0	99
11	15% (v/v) C ₈ MIm·BF ₄ /THF ^{c,d}	<0.075	52.0	97.0	99
12	10% (v/v) C ₄ MIm·PF ₆ /THF ^{c,d}	<0.056	81.5	98.5	99

^a The reaction conditions: 0.04 mmol ara-C; 0.6 mmol VP; 1000 U Novozym 435; 40 °C; 250 rpm; 2 ml of the reaction medium stated in each case and various ILs; *a*_w = 0.07. ^b The solubility of ara-C in each reaction medium was determined by HPLC analysis of saturated solutions at 40 °C. ^c Maximum substrate conversion. ^d Pyridine (20%, v/v) was added to the reaction media for dissolving the substrate.

exhibits lower nucleophilicity than the anions Br⁻ or Cl⁻ and thus may have a lower tendency to change the enzyme's conformation by interacting with positively charged sites on the enzyme.^{32,33}

As can be seen in Table 1, the solubility of the substrate was also greatly improved in all of the ILs tested compared to common organic solvents used in enzymatic reactions, such as THF and hexane, in which the solubility of the substrate was lower than 0.01 mol l⁻¹. However, both the initial rate and the substrate conversion of the lipase-mediated acylation of ara-C with VP in the pure ILs tested were disappointingly low. As an alternative, co-solvent mixtures of IL and organic solvent were investigated. In principle, tetrahydrofuran (THF) can be used as the solvent for enzymatic acylation of nucleosides^{2,6} and it has also been found to be freely miscible with the ILs investigated in all proportions tested. Thus, it was employed as the co-solvent with the ILs tested in this work. The effect of the concentration of ILs on the acylation reaction was then examined to determine the optimal concentration of each IL in the co-solvent mixture. It was found that both the initial rate and substrate conversion were significantly enhanced with increasing concentration of C₄MIm·BF₄, C₅MIm·BF₄, C₆MIm·BF₄, C₈MIm·BF₄, and C₄MIm·PF₆ up to 20%, 20%, 10%, 15% and 10% (v/v), respectively, beyond which further increase in IL content resulted in a substantial decline in both the reaction rate and the substrate conversion. Changes in the concentration of ILs within the examined range, however, showed little effect on the regioselectivity. The results of a comparative study of Novozym 435-catalyzed acylation of ara-C with VP in different co-solvent mixtures containing the optimal concentration of each IL in THF are summarized in Table 1 (entries 8–12). A possible reason that the presence of the ILs at an appropriate concentration can boost the activity of Novozym 435 and the reaction efficiency is that the ILs might interact with charged groups of the enzyme, either in the active site or at its periphery, causing changes in the enzyme's structure³³ and thus making the enzyme's conformation more suitable for the formation of the acyl-enzyme intermediate. On the other hand, a high concentration of IL causes not only a high ionic strength of the reaction medium that might inactivate the enzyme, leading to a lower enzymatic activity,

but also a high viscosity of the reaction mixture, which may limit diffusion of substrates and products to and from the active site of the enzyme, resulting in a drop in both the reaction rate and the substrate conversion.¹³ Of the co-solvent mixtures assayed, 10% (v/v) C₄MIm·PF₆-THF gave the highest initial reaction rate and substrate conversion and thus was selected for subsequent investigations.

To better understand Novozym 435-mediated acylation reaction conducted in the novel system and further optimize the reaction, the initial rate, the substrate conversion and the regioselectivity of the reaction were investigated in the optimal C₄MIm·PF₆-THF co-solvent system as a function of the molar ratio of VP to ara-C, initial water activity, reaction temperature and shaking rate. Fig. 1a depicts the clear *a*_w dependence of the acylation reaction performed in 10% (v/v) C₄MIm·PF₆-THF co-solvent. Both the initial rate and the substrate conversion of the acylation increased markedly with increasing *a*_w up to 0.07. Further increase in *a*_w, however, led to a lower reaction rate and a lower substrate conversion. Although hydrolysis of the substrate could be inhibited when *a*_w was very low, the enzyme was incompletely hydrated and thus showed somewhat lower acylation activity. On the other hand, an *a*_w above the optimum presumably allowed the enzyme to become completely hydrated, but competitive hydrolysis of both the substrate VP and the product 5'-O-monoester limited the acylation. It was also observed that too much water in the co-solvent system caused aggregation of the enzyme, which was clearly related to the decline in the reaction rate and the substrate conversion at high *a*_w. Little influence of *a*_w on the regioselectivity was observed. As a result, a careful regulation of *a*_w to achieve the optimum value of 0.07 was necessary for an efficient lipase-catalyzed acylation of ara-C in the 10% (v/v) C₄MIm·PF₆-THF system. Degradation of the IL by hydrolysis was not detectable over the *a*_w range tested (data not shown).

As shown in Fig. 1b, remarkable enhancement in both the initial rate and the substrate conversion was observed with the increase of the molar ratio of VP to ara-C up to 15, while further increase in this ratio led to only a minor rise in the initial rate and substrate conversion. It is also notable that only a minor change in the regioselectivity of the reaction

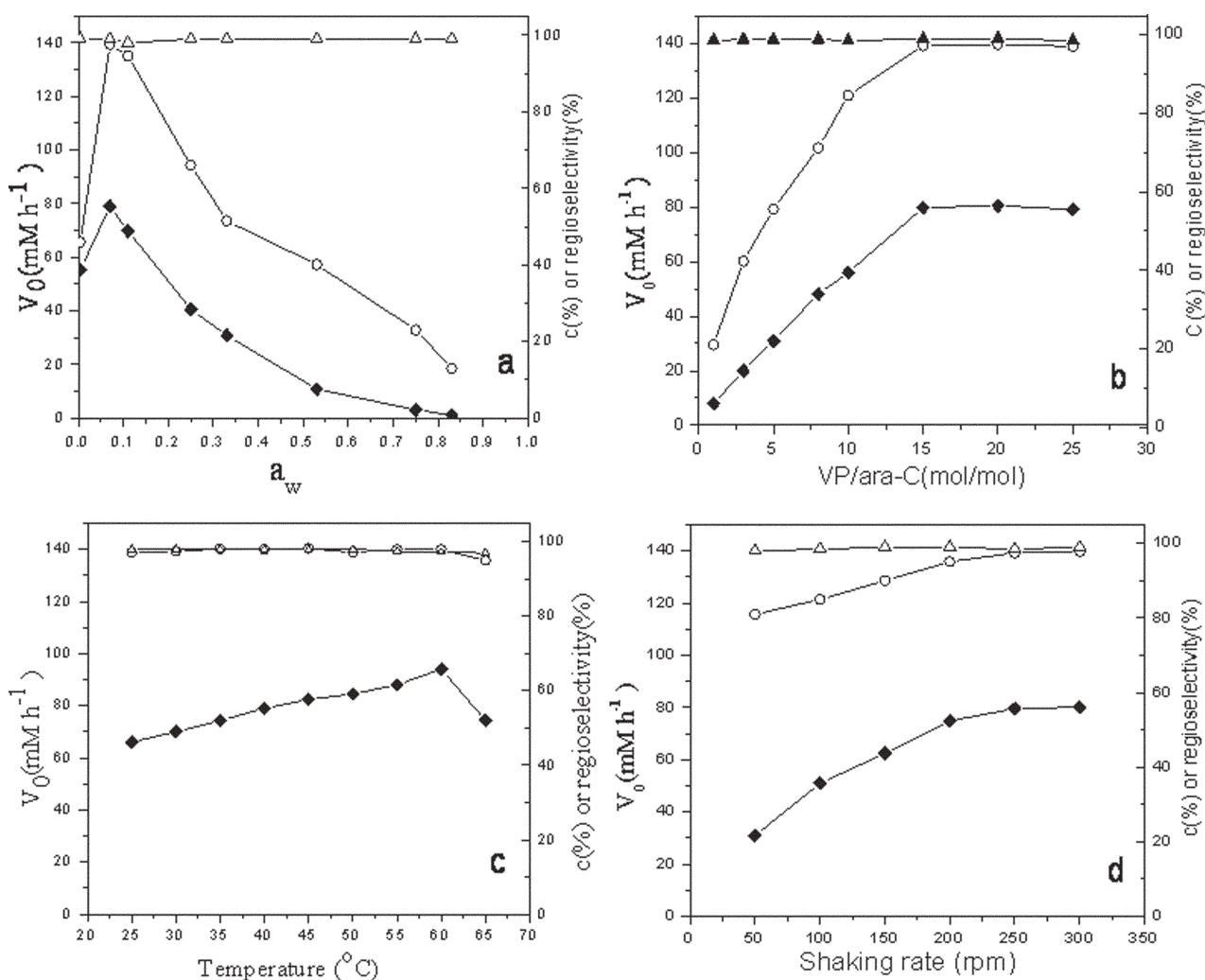


Fig. 1 The regioselective acylation of ara-C with VP mediated by Novozym 435 in the 10% (v/v) C₄MIm·PF₆-THF co-solvent system. (a) Effect of initial water activity (a_w) {0.04 mmol ara-C; 0.6 mmol VP; 1000 U Novozym 435; 40 °C; 250 rpm}. (b) Effect of the molar ratio of VP to ara-C {0.04 mmol ara-C; 1000 U Novozym 435; 40 °C; 250 rpm; $a_w = 0.07$ }. (c) Effect of the reaction temperature {0.04 mmol ara-C; 0.6 mmol VP; 1000 U Novozym 435; 250 rpm; $a_w = 0.07$ }. (d) Effect of the shaking rate {0.04 mmol ara-C; 0.6 mmol VP; 1000 U Novozym 435; 40 °C; $a_w = 0.07$ }. Symbols: (◆) V_0 ; (○) C; (△) regioselectivity. All reactions were performed in 2 ml of reaction medium plus 20% (v/v) pyridine to promote dissolving of the substrate.

occurred with the change in the ratio of the two substrates. It appears that the presence of a substantial excess of VP inhibits the hydrolysis of the product (5'-O-propionyl ara-C) and pushes the reaction equilibrium towards the synthesis of 5'-O-propionyl ara-C. Additionally, the hydrolysis of VP might significantly reduce its concentration, thus reducing the acylation rate and substrate conversion if VP is not initially present in great excess.³⁴

As shown in Fig. 1c, within the range from 25 to 60 °C, higher reaction temperature resulted in both the higher initial reaction rate and the higher substrate conversion in 10% (v/v) C₄MIm·PF₆-THF. However, the reaction rate and the substrate conversion dropped sharply above 60 °C. Temperature showed little effect on the regioselectivity within the range examined.

As can be seen in Fig. 1d, the reaction accelerated rapidly with the increase in shaking rate up to 250 rpm, implying that

mass transfer was the rate-limiting step. Increasing the shaking rate beyond 250 rpm did not significantly change the initial rate observed. The shaking rate showed little effect on the regioselectivity of the reaction.

When the reaction was carried out under the optimum conditions described above, the initial rate, the substrate conversion and the regioselectivity were as high as 94.0 mM h⁻¹, 98.5% and 99%, respectively.

Organic solvent systems containing hexane and pyridine were also found to be effective media for this reaction and so a 28% (v/v) hexane–pyridine system, in which the initial rate, regioselectivity, conversion and activation energy were very similar to the 10% (v/v) C₄MIm·PF₆-THF medium (Table 2), was used to compare the IL-containing system with an organic solvent medium in terms of enzyme stability. Fig. 2 illustrates the deactivation profile of Novozym 435 at various temperatures in 10% (v/v) C₄MIm·PF₆-THF and in 28% (v/v)

Table 2 Enzymatic acylation of ara-C with VP in 10% (v/v) C₄MIm·PF₆-THF or 28% (v/v) hexane-pyridine^a

Medium	V_0 /mM h ⁻¹	C^b (%)	Regioselectivity (%)	E_a^c /kJ mol ⁻¹
10% (v/v) C ₄ MIm·PF ₆ -THF ^d	94.0	98.5	99	7.40
28% (v/v) Hexane-pyridine	91.1	98.0	98	7.47

^a The reactions were conducted under the optimum conditions for each case. ^b The maximum substrate conversion. ^c The apparent activation energy (E_a) of Novozym 435-catalyzed acylation of ara-C with VP was determined according to the linear regression analysis of the Arrhenius plot. ^d Pyridine (20%, v/v) was added to the reaction media for dissolving the substrate.

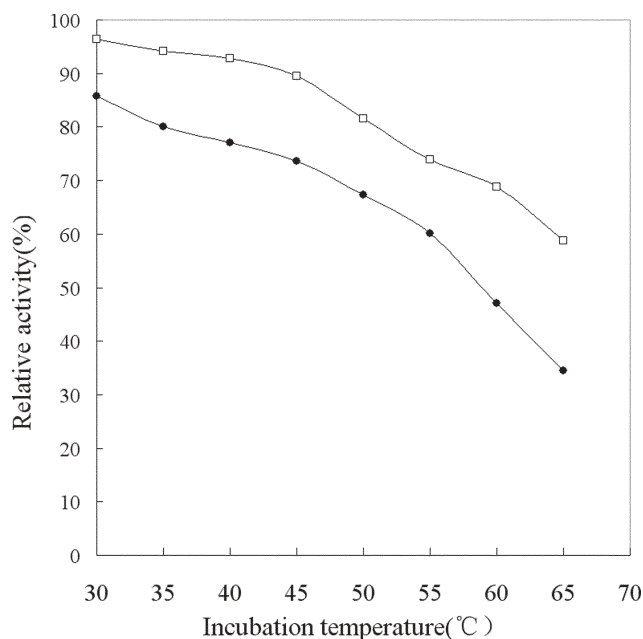


Fig. 2 Thermal stability of Novozym 435 in 10% (v/v) C₄MIm·PF₆-THF (□) and 28% (v/v) hexane-pyridine (●).

hexane-pyridine, assayed on the basis of acylation of ara-C by VP. The much higher enzyme activity after incubation in 10% (v/v) C₄MIm·PF₆-THF than in 28% (v/v) hexane-pyridine under the same conditions demonstrated that the presence of the ionic liquid in the reaction medium markedly increased the thermal stability of Novozym 435, which can greatly improve the re-use times of the enzyme as well as the efficiency of the process. Besides the coating and protection of the essential water surrounding the lipase by the IL, a greatly enhanced interaction of the substrate with the active site of the lipase in the presence of the IL could partly account for this. Furthermore, enzyme-solvent interactions in different media constitute an important factor in maintaining the active conformation of the protein. Hence, the considerably increased stability of Novozym 435 in the C₄MIm·PF₆-THF mixture could be due in part to electrostatic interactions between the IL and protein, leading to a more rigid protein with a higher kinetic barrier against unfolding.

Conclusions

The IL C₄MIm·PF₆ can serve as an excellent co-solvent with tetrahydrofuran in place of traditional organic solvents for Novozym 435-mediated acylation of ara-C with greatly enhanced solubility of the substrate, enzyme's stability and similar enzyme activity. Besides, both the ILs and biocatalyst

are reusable which made the process more environmentally friendly than the traditional chemical procedures. This might become a greener alternative for efficient preparation of the 5'-O-monoester of ara-C. Additionally, the results reported here suggest that enzymatic acylation of nucleosides in IL-containing systems is a promising area that is worthy of further study.

Experimental

Biological and chemical materials

Candida antarctica lipase B (CAL-B) immobilized on a macroporous acrylic support (Novozym 435, 10 000 U g⁻¹) was kindly donated by Novozymes (Denmark). 1-β-D-Arabinofuranosylcytosine (ara-C) and vinyl propionate (VP) were purchased from Aldrich (USA). The ionic liquids 1-butyl-3-methylimidazolium tetrafluoroborate (C₄MIm·BF₄), 1-amyl-3-methylimidazolium tetrafluoroborate (C₅MIm·BF₄), 1-hexyl-3-methylimidazolium tetrafluoroborate (C₆MIm·BF₄), 1-methyl-3-octylimidazolium tetrafluoroborate (C₈MIm·BF₄), 1-butyl-3-methylimidazolium hexafluorophosphate (C₄MIm·PF₆), 1-butyl-3-methylimidazolium chloride (C₄MIm·Cl) and 1-butyl-3-methylimidazolium bromide (C₄MIm·Br) were obtained as gifts from Dr X.-H. Li (Department of Chemical Engineering, South China University of Technology, Guangzhou, China) and were all of over 98% purity. ILs were dried at 200 °C for 48 h prior to use. All other chemicals were obtained from commercial sources and were of analytical grade.

General procedure for enzymatic acylation of ara-C

In a typical experiment, 2 ml of co-solvent mixture of ILs and organic solvents containing 0.04 mmol ara-C, 0.6 mmol VP and 1000 U (100 mg) Novozym 435 were incubated with shaking (250 rpm unless stated otherwise) at a fixed temperature stated for each experiment. Aliquots were withdrawn at specified time intervals from the reaction mixture, and then diluted 100 times with a water-methanol mixture prior to HPLC analysis. In order to structurally characterize the product, the reaction was scaled up (~0.2 mmol ara-C and 3 mmol VP). Upon completion of the reaction, the reaction mixture was filtered to remove the immobilized enzyme and evaporated under vacuum. The residue was extracted three times with ethanol and the collected solution was further evaporated to give the crude product. Then, it was dissolved in *t*-BuOH for crystallization and the product was obtained as a white powder (yield: >91%).

Separate experiments were also conducted in the various media tested with no enzyme added and the results showed

that a chemical acylation reaction did not take place in the absence of the enzyme under the reaction conditions described above.

Control of the initial water activity

The initial water activity of the reaction media, the substrates and the enzyme were controlled by gaseous equilibrium with different saturated salt solutions in separate closed containers at 25 °C. The following salts were used: LiBr ($a_w = 0.07$), LiCl ($a_w = 0.11$), MgCl₂ ($a_w = 0.33$), Mg(NO₃)₂ ($a_w = 0.53$), NaCl ($a_w = 0.75$), and KCl ($a_w = 0.85$).³³ A molecular sieve was used to generate the nearly anhydrous reaction medium ($a_w \sim 0$).

Determination of activation energy

The reactions were performed in various reaction media and different temperatures (varying from 25 to 60 °C). 1000 U (100 mg) enzyme was added to 2 ml of the reaction mixture ($a_w = 0.07$) containing 0.04 mmol ara-C and 0.6 mmol VP. The mixture was then incubated in a water-bath shaker at 250 rpm. The apparent activation energy (E_a) of the Novozym 435-catalyzed acylation of ara-C with VP was calculated according to the linear regression analysis of the Arrhenius plot.

Determination of enzyme thermal stability

In order to assess the thermal stability of the enzyme, 100 mg aliquots of Novozym 435 were added into separate screw-capped vials containing 2 ml of the selected medium {10% (v/v) C₄MIm-PF₆-THF or 28% (v/v) hexane-pyridine} with a fixed initial a_w (0.07) and the reaction mixture was incubated for 6 h at various temperatures from 30 to 65 °C. Then the immobilized enzyme was recovered by filtration from the reaction medium and added to a fresh volume of the same reaction medium containing 0.04 mmol ara-C and 0.6 mmol VP. The assay reaction was then incubated at 250 rpm and 40 °C and enzyme activity was measured by HPLC quantitation of the product ester. The relative activity was expressed as the ratio of the retained activity after incubation to the original activity of the enzyme in the same reaction system.

Analytical methods

The reaction mixture was analyzed by RP-HPLC on a 4.6 × 250 mm (5 μm) Zorbax SB-C18 column (Agilent Technologies Co., Ltd, USA) using an Agilent G1311A pump and a UV detector at 276 nm. The mobile phase was a mixture of ammonium acetate buffer (0.01M, pH 4.27) and methanol (60/40, v/v) at a flow rate of 0.9 ml min⁻¹. The retention times for 1-β-D-arabinofuranosylcytosine and 5'-O-propionyl 1-β-D-arabinofuranosylcytosine were 2.67 and 4.51 min, respectively. Regioselectivity was defined as the ratio of the HPLC peak area corresponding to the indicated product to that of all the products formed.³⁵ The initial rate (V_0) and the substrate conversion (C) were calculated from the HPLC data. The average error for this assay is less than 0.7%. All reported data are averages of experiments performed at least in duplicate.

Structure determination

The position of acylation in enzymatically prepared ester was determined by ¹³C NMR (Bruker AVANCE Digital 400 MHz Nuclear Magnetic Resonance Spectrometer, Bruker Co., Germany) at 100 MHz. DMSO-d₆ was used as a solvent and TMS was used as an internal reference. Chemical shifts were expressed in ppm shift. The FT-IR spectra of both the substrate and the product were recorded on a Nicolet NEXUS™ 470 Fourier-Transform Infrared Spectrometer (Thermo Nicolet Co., USA).

ara-C. ¹³C NMR: $\delta = 61.6$ (C-5'), 74.3(C-2'), 76.7(C-3'), 85.5 (C-4'), 86.5(C-1'), 93.1 (C-5), 144.0 (C-6), 154.3(C-2), 164.9(C-4); FT-IR(KBr): ν (cm⁻¹) = 3357–3442 (OH, NH), 2933(CH), 1648 (C=C), 1110/1071(C–O–C).

5'-O-Propionyl ara-C. ¹³C NMR $\delta = 9.6$ (–CH₃), 27.34 (–CH₂), 64.33 (C-5'), 74.9 (C-2'), 77.3 (C-3'), 82.3 (C-4'), 86.7(C-1'), 93.2 (C-5), 143.5 (C-6), 154.9 (C-2), 165.4(C-4), 174.2 (C=O); FT-IR (KBr): ν (cm⁻¹) = 3421–3444 (OH, NH), 2924 (C–H), 1735 (C=O), 1648 (C=C), 1113/1078(C–O–C).

Acknowledgements

We wish to express our sincere gratitude to Prof. G. J. Peters (VU University Medical Center, Amsterdam, The Netherlands), Prof. F. Myhren and Dr D. L. Swartz (Clavis Pharma, Norway) for their very helpful discussion and Dr X.-H. Li (Department of Chemical Engineering, South China University of Technology, China) for his generous gifts of ionic liquids. The authors are grateful to the National Natural Science Foundation of China (Grant No. 20406006, Grant No.20206010), the Key Project of Chinese Ministry of Education (Grant No.104147), the Research Fund for the Doctoral Program of Chinese Higher Education (Grant No. 20030561017), BBSRC China Partnering Award (Grant No. PA1519), the Natural Science Foundation of Guangdong Province (Grant No. 05006571) and the Natural Science Foundation of South China University of Technology (No. G02-E5051020) for financial support.

References

- 1 M. Ferrero and V. Gotor, *Monatsh. Chem.*, 2000, **131**, 585–616.
- 2 F. Moris and V. Gotor, *J. Org. Chem.*, 1993, **58**, 653–660.
- 3 A. M. Bergman, C. M. Kuiper, D. A. Voorn, E. M. Comijn, F. Myhren, M. L. Sandvold, H. R. Hendriks and G. J. Peters, *Biochem. Pharmacol.*, 2004, **67**, 503–511.
- 4 F. Myhren, B. Børretzen, A. Dalen and K. T. Stokke, *US Pat.*, US 6 335 322 B1, 2002.
- 5 W. J. Wechter, M. A. Johnson, C. M. Hall, D. T. Warner, A. E. Berger, D. T. Gish and G. L. Neil, *J. Med. Chem.*, 1975, **18**, 339–344.
- 6 J. García, S. Fernández, M. Ferrero, Y. S. Sanghvi and V. Gotor, *Tetrahedron Lett.*, 2004, **45**, 1709–1712.
- 7 M. Mahmoudian, J. Eaddy and M. Dawson, *Biotechnol. Appl. Biochem.*, 1999, **29**, 229–233.
- 8 P. Wang and J. S. Dordick, *Macromolecules*, 1998, **31**, 941–943.
- 9 H. Fan, M. Kitagawa, T. Raku and Y. Tokiwa, *Biotechnol. Lett.*, 2004, **26**, 1261–1264.
- 10 C. H. Wong, S. T. Chen, W. J. Hennen, J. A. Bibbs, Y. F. Wang, J. L. C. Liu, M. W. Pantoliano, M. Whitlow and P. N. Bryan, *J. Am. Chem. Soc.*, 1990, **112**, 945–953.

- 11 F. Moris and V. Gotor, *Tetrahedron*, 1993, **49**, 10089–10098.
- 12 X.-F. Li, M.-H. Zong and R.-D. Yang, *J. Mol. Catal. B: Enzym.*, 2006, **38**, 48–53.
- 13 F. van Rantwijk, R. M. Lau and R. A. Sheldon, *Trends Biotechnol.*, 2003, **21**, 131–138.
- 14 R. A. Sheldon, R. M. Lau, M. J. Sorgedragger, F. van Rantwijk and K. R. Seddon, *Green Chem.*, 2002, **4**, 147–151.
- 15 U. Kragl, M. Eckstein and N. Kaftzik, *Curr. Opin. Biotechnol.*, 2002, **13**, 565–571.
- 16 T. Welton, *Chem. Rev.*, 1999, **99**, 2071–2083.
- 17 M. Erbedinger, A. J. Mesiano and A. J. Russell, *Biotechnol. Prog.*, 2000, **16**, 1129–1131.
- 18 H. Zhao and S. V. Malhotra, *Biotechnol. Lett.*, 2002, **24**, 1257–1260.
- 19 R. P. Gaisberger, M. H. Fechter and H. Griengl, *Tetrahedron Asym.*, 2004, **15**, 2959–2963.
- 20 W. Y. Lou, M. H. Zong, H. Wu, R. Xu and J. F. Wang, *Green Chem.*, 2005, **7**, 500–506.
- 21 S. Park and R. J. Kazlauskas, *Curr. Opin. Biotechnol.*, 2003, **14**, 432–437.
- 22 R. P. Swatloski, S. K. Spear, J. D. Holbrey and R. D. Rogers, *J. Am. Chem. Soc.*, 2002, **124**, 4974–4975.
- 23 F. Ganske and U. T. Bornscheuer, *Org. Lett.*, 2005, **7**, 3097–3098.
- 24 A. K. Prasad, V. Kumar, S. Malhotra, V. T. Ravikumar, Y. S. Sanghvi and V. S. Parmar, *Bioorg. Med. Chem.*, 2005, **13**, 4467–4472.
- 25 W. Y. Lou, M. H. Zong and H. Wu, *Biotechnol. Appl. Biochem.*, 2005, **41**, 151–156.
- 26 Y. Y. Liu, W. Y. Lou, M. H. Zong, R. Xu, X. Hong and H. Wu, *Biocatal. Biotransform.*, 2005, **23**, 89–95.
- 27 K. Yoshimoto, Y. Itatani and Y. Tsuda, *Chem. Pharm. Bull.*, 1980, **28**, 2065–2074.
- 28 J. Uppenberg, N. Oehrner, M. Norin, K. Hult, G. J. Kleywegt, S. Patkar, V. Waagen, T. Anthonsen and T. A. Jones, *Biochemistry*, 1995, **34**, 16838–16851.
- 29 S. Park and R. J. Kazlauskas, *J. Org. Chem.*, 2001, **66**, 8395–8401.
- 30 H. Zhao, *Phy. Chem. Liquids*, 2003, **41**, 545–557.
- 31 J. L. Kaar, A. M. Jesionowski, J. A. Berberich, R. Moulton and A. J. Russell, *J. Am. Chem. Soc.*, 2003, **125**, 4125–4131.
- 32 T. De Diego, P. Lozano, S. Gmouh, M. Vaultier and J. L. Iborra, *Biomacromolecules*, 2005, **6**, 1457–1464.
- 33 R. M. Lau, M. J. Sorgedragger, G. Carrea, F. van Rantwijk, F. Secundo and R. A. Sheldon, *Green Chem.*, 2004, **6**, 483–487.
- 34 M. Eckstein, M. Sesing, U. Kragl and P. Adlercreutz, *Biotechnol. Lett.*, 2002, **24**, 867–872.
- 35 M. Therisod and A. M. Klivanov, *J. Am. Chem. Soc.*, 1986, **108**, 5638–5640.

Chemical Science

An exciting news supplement providing a snapshot of the latest developments across the chemical sciences



Free online and in print issues of selected RSC journals!*

Research Highlights – newsworthy articles and significant scientific advances

Essential Elements – latest developments from RSC publications

Free access to the original research paper from every online article

*A separately issued print subscription is also available

RSC Publishing

www.rsc.org/chemicalscience

Efficient biphasic hydroaminomethylation of long chain olefins in ionic liquids†

Ying Yong Wang, Mei Ming Luo,* Qi Lin, Hua Chen and Xian Jun Li

Received 23rd January 2006, Accepted 27th March 2006

First published as an Advance Article on the web 6th April 2006

DOI: 10.1039/b601052k

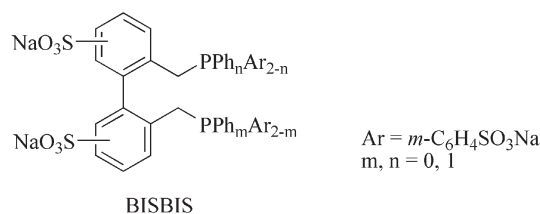
Hydroaminomethylation of long chain olefins with secondary amines was performed efficiently in ionic liquids 1-*n*-alkyl-3-methylimidazolium tosylates [Rmim][*p*-CH₃C₆H₄SO₃] (R = *n*-butyl, octyl, dodecyl, cetyl) with Rh-BISBIS (sulfonated 2,2'-bis(diphenylphosphinomethyl)-1,1'-biphenyl) complex as catalyst. High activity and selectivity for amines were achieved. The ionic liquid containing catalyst can be easily separated from product and re-used several times with only a slight decrease in activity.

Introduction

Hydroaminomethylation, discovered by Reppe¹ in 1949, represents an atom-economic and efficient one-pot process for the synthesis of amines from olefins and primary or secondary amines. This domino reaction consists of initial hydroformylation of an olefin to an aldehyde and subsequent formation of an enamine (or imine) followed by hydrogenation. From both economic and environmental points of view, this direct preparation process of amines from inexpensive feedstock is superior to traditional procedures, which are mostly multi-step and less atom-efficient with a number of by-products.² In the last decade, the reaction has been greatly developed and applied in the synthesis of various amines, such as aminomethyl steroids, diarylalkylamine, azamacroheterocycles and polyamine dendrimers.^{3–6} The classical hydroaminomethylations are generally carried out in a homogeneous catalysis system,^{7–10} where the difficulties of the catalyst recovery and catalyst separation from products constitute major drawbacks. Possible solutions to these problems include 'heterogenizing' a homogeneous catalyst, either by anchoring the catalyst on a support, or by using a liquid–liquid two-phase system. In 1999, Beller and co-workers¹¹ investigated the hydroaminomethylation of lower olefins ($\leq C_5$) in aqueous–organic two-phase catalysis. Recently, Behr and co-workers¹² studied the hydroaminomethylation of 1-octene with morpholine in temperature-dependent solvent systems, which allows a reaction in a single-phase at a higher temperature followed by a phase split at a lower temperature to be carried out. We reported¹³ the hydroaminomethylation of long chain olefins with poor water solubility in an aqueous–organic biphasic system using the water-soluble rhodium complex RhCl(CO)(TPPTS)₂ [TPPTS: P(*m*-C₆H₄SO₃Na)₃] as catalyst in the presence of the cationic surfactant cetyltrimethylammonium bromide (CTAB). Although good activity and selectivity

were achieved and the catalyst could be easily separated through phase separation, the catalyst recycling remained to be improved.

Ionic liquids (IL) have recently attracted considerable attention as efficient and environmental friendly reaction media.¹⁴ The important advantages of ionic liquids include negligible vapour pressure, high thermal stability, compatibility with various organic compounds and organometallic catalysts, ease of separation from products and potential for recycling. From these points of view, many types of reactions such as Diels–Alder reaction,^{15a} Heck reaction,^{15b} dimerization,^{15c} and hydroformylation^{15d} have been utilized in ionic liquids. The commonly used ionic liquids consist of 1,3-dialkylimidazolium cations and halogen containing anions,¹⁶ such as [AlCl₄][−], [PF₆][−], [BF₄][−]. The presence of halogen atoms may cause concerns to some extent,^{17,18} such as the liberation of toxic and corrosive HF and HCl into the environment. Here we report an efficient hydroaminomethylation of long chain olefins in 'greener'¹⁷ ionic liquids [Rmim][*p*-CH₃C₆H₄SO₃] (R = *n*-butyl, octyl, dodecyl, cetyl) catalyzed by Rh-BISBIS complex (Scheme 1). High activity and selectivity for amines were obtained, and recycling of ionic liquid and catalysts was realized.

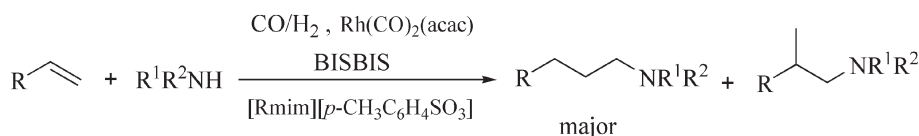


Results and discussion

We firstly investigated the hydroaminomethylation of 1-dodecene with morpholine in ionic liquid [Bmim][BF₄] (Table 1, entry 1). Although good activity and selectivity were obtained, the recovery and recycling of catalyst in ionic liquid were not so good (entries 2 and 3). In view of some serious concerns caused by halogen containing anions,^{17,18} ionic liquid 1-*n*-alkyl-3-methylimidazolium tosylate [Bmim][*p*-CH₃C₆H₄SO₃]

Key Laboratory of Green Chemistry and Technology of Ministry of Education at Sichuan University, College of Chemistry, Sichuan University, Chengdu 610064, P.R. China.
E-mail: Luom2@yahoo.com.cn; Fax: 86-28-85462021;
Tel: 86-28-85462021

† Electronic supplementary information (ESI) available: NMR and mass spectra of the products in Table 3. See DOI: 10.1039/b601052k



Scheme 1

Table 1 Hydroaminomethylation of 1-dodecene and morpholine in ionic liquid and recycling of catalyst^a

Entry	Cycle	Dodecene ^c (%)	Isomerized dodecene ^d (%)	Conversion (%)	Selectivity for amine (%)	L/B (amine)
1	1 ^b	12.5	6.8	90.7	78.8	15.2
2	2 ^b	18.8	8.4	85.0	68.0	10.3
3	3 ^b	22.7	12.4	66.7	47.4	4.4
4	1	13.8	6.5	94.3	78.5	36.0
5	2	15.0	8.4	84.8	72.4	26.9
6	3	22.6	11.9	90.7	62.0	16.6
7	4	22.2	11.9	87.5	61.0	12.7
8	5	22.5	10.0	90.2	64.0	10.1
9	6	20.6	10.6	88.5	64.7	6.4

^a Reaction conditions: 1-dodecene 5 mmol, morpholine 6 mmol, ionic liquid [Bmim][*p*-CH₃C₆H₄SO₃] 1 ml, Rh 0.01 mmol, BISBIS/Rh = 2.5, 130 °C, 3 MPa (CO:H₂ = 1:1), 5 h. ^b Ionic liquid [Bmim][BF₄] 1 ml. ^c Hydrogenation product. ^d By-product generated in the reaction.

was selected as solvent for the Rh–BISBIS-catalyzed hydroaminomethylation of 1-dodecene. It is clear from the data in Table 1 that the catalytic system formed by Rh(CO)₂(acac) and BISBIS in [Bmim][*p*-CH₃C₆H₄SO₃] was more active, giving 94.3% 1-dodecene conversion, 78.4% selectivity for tertiary amine and 97.3% regioselectivity for linear amine (Table 1, entry 4), superior to those obtained with [Bmim][BF₄] under similar reaction conditions (entry 1). At the end of the reaction the products and ionic liquid were easily separated through centrifugation. The rhodium catalyst is nearly completely retained in the ionic liquid phase (0.03% rhodium leaching detected by ICP-AES) and can be recycled several times with only a slight decrease in activity and selectivity for amines (entries 4–9). The decrease of the regioselectivity for linear amines in recycles was mainly due to the partial oxidation of ligand BISBIS during the separation of catalyst.¹⁹

Several kinds of ionic liquid with different alkyl substituents in imidazolium were used as solvents in the hydroaminomethylation. The result, summarized in Table 2, suggested that there was a relationship between the lengths of the olefin chain and alkyl substituents in ionic liquid. The dodecyl-substituted imidazolium ionic liquid showed better activity and selectivity but inferior regioselectivity for linear amines (Table 2, entry 3). Hydrophobic ligand TPP (triphenylphosphine) and BISBI (2,2'-bis(diphenylphosphinomethyl)-1,1'-biphenyl) were also examined, where the catalyst leaching

was obvious (0.5% rhodium leaching detected by ICP-AES) and the recycling experiment was unsatisfactory.

The influences of the reaction temperature and syngas pressure on the catalyst activity and selectivity in ionic liquid [Bmim][*p*-CH₃C₆H₄SO₃] have been investigated and the results are presented in Table 3. The optimum reaction result was obtained at 130 °C and 5 MPa (Table 3, entry 5). Olefins of different chain length also reacted with other amines with good activity and selectivity, giving linear amines as major products (entries 6–10). The hydroaminomethylation of 1-hexene exhibited superior activity but inferior regioselectivity.

In summary, the biphasic hydroaminomethylation of long chain olefins with amines has been efficiently performed in ionic liquid [Rmim][*p*-CH₃C₆H₄SO₃] using Rh–BISBIS complex as catalyst. The catalytic system offers good activity and selectivity for linear amines with a good retention of the catalyst in ionic liquid phase, which is economical and environmentally friendly. The easy separation and recycling of the catalyst make the reaction system promising and attractive.

Experimental

Rhodium complexes Rh(CO)₂(acac),²⁰ water-soluble diphosphine ligand BISBIS²¹ and a series of ionic liquids¹⁸ [Rmim][*p*-CH₃C₆H₄SO₃] (R = *n*-butyl, octyl, dedecyl, cetyl)

Table 2 Hydroaminomethylation of 1-dodecene and morpholine in different ionic liquids^a

Entry	Ionic liquid	Ligand	Dodecene ^c (%)	Isomerized dodecene ^d (%)	Conversion (%)	Selectivity for amine (%)	L/B (amine)
1	[Bmim][<i>p</i> -CH ₃ C ₆ H ₄ SO ₃]	BISBIS	13.8	6.5	94.3	78.5	36.0
2	[Omim][<i>p</i> -CH ₃ C ₆ H ₄ SO ₃]	BISBIS	11.2	4.9	95.5	83.1	10.7
3	[Dmim][<i>p</i> -CH ₃ C ₆ H ₄ SO ₃]	BISBIS	9.5	3.4	95.2	86.4	3.8
4	[Cmim][<i>p</i> -CH ₃ C ₆ H ₄ SO ₃]	BISBIS	13.4	6.7	92.7	78.3	7.3
5	[Dmim][<i>p</i> -CH ₃ C ₆ H ₄ SO ₃]	TPPTS ^b	13.0	6.2	91.1	78.9	1.5
6	[Dmim][<i>p</i> -CH ₃ C ₆ H ₄ SO ₃]	TPP ^b	13.2	6.2	93.9	79.3	2.3
7	[Dmim][<i>p</i> -CH ₃ C ₆ H ₄ SO ₃]	BISBI	11.3	5.5	94.3	82.2	9.6

^a Reaction conditions: 1-dodecene 5 mmol, morpholine 6 mmol, ionic liquid 1 ml, Rh 0.01 mmol, BISBIS/Rh = 2.5, 130 °C, 3 MPa (CO:H₂ = 1:1), 5 h. ^b TPPTS/Rh = 20, TPP/Rh = 20. ^c Hydrogenation product. ^d By-product generated in the reaction.

Table 3 Hydroaminomethylation of different olefins with amines and variation of reaction conditions^a

Entry	Olefins	Amines	Temperature/ °C	Pressure/ MPa	Hydrogenated olefin (%)	Isomerized olefin ^c (%)	Conversion (%)	Selectivity for amine (%)	L/B (amine)
1	1-Dodecene	Morpholine	110	3	9.6	5.2	72.8 ^b	72.0	28.1
2	1-Dodecene	Morpholine	130	3	13.8	6.5	94.3	78.4	36.0
3	1-Dodecene	Morpholine	150	3	16.3	8.6	95.2	73.8	27.1
4	1-Dodecene	Morpholine	130	2	24.1	12.3	92.9	60.8	32.2
5	1-Dodecene	Morpholine	130	5	11.2	5.8	95.6	82.2	41.6
6	1-Hexene	Morpholine	130	3	8.5	4.4	97.0	86.7	11.9
7	1-Octene	Morpholine	130	3	10.2	5.5	96.3	83.7	21.4
8	1-Decene	Morpholine	130	3	12.8	6.0	95.0	80.2	25.3
9	1-Dodecene	Piperidine	130	3	14.7	7.9	90.2	74.9	35.1
10	1-Dodecene	Diethylamine	130	3	14.9	8.1	86.6	73.4	33.5

^a Olefins 5 mmol, amines 6 mmol, ionic liquid [Bmim][p-CH₃C₆H₄SO₃] 1 ml, Rh 0.01 mmol, BISBIS/Rh = 2.5, *t* = 5 h. ^b 5.6% aldehyde was detected. ^c By-product generated in the reaction.

were synthesized according to the literature. 1-Olefin (Fluka) and other reagents (AR) were as commercially supplied and not treated further. Water was doubly distilled. Synthetic gas was obtained by directly mixing carbon monoxide (99.9%) and hydrogen (99.9%) with the ratio of 1 : 1. GC analysis was performed on a gas chromatograph, HP 1890II, equipped with an FID (hydrogen flame ionization detector) and a capillary column SE-30 (30 m × 0.25 mm). NMR spectra were recorded on a Varian INOVA 400 MHz or Bruker AC-E 200 MHz NMR spectrometer. Mass spectra (GC-MS) experiments were conducted on Agilent-6890. The amount of Rh leaching in the organic phase was determined by inductively coupled plasma-atomic emission spectrometry (ICP-AES).

A general procedure for catalytic hydroaminomethylation is as follows: catalyst precursor Rh(CO)₂(acac) (0.01 mmol), phosphine ligand BISBIS (0.025 mmol), ionic liquid [Rmim][p-CH₃C₆H₄SO₃] (1 ml), 1-dodecene (5 mmol) and morpholine (6 mmol) were added successively in a 60 ml stainless steel autoclave equipped with a magnetic stirrer. The autoclave was purged three times with synthetic gas and charged to 3 MPa. After heating for 5 hours at 130 °C, the autoclave was quickly cooled to ambient temperature. The products and ionic liquid were easily separated through centrifugation. The products in the organic phase were analyzed by gas chromatography. The linear and branched amines were purified by column chromatography (silica gel).

4-(2-Methyldodecyl)morpholine²²

4-(2-Methyldodecyl)morpholine (entry 2, Table 3, branched amine) δ_{H} (400 MHz, CDCl₃) 0.75–0.81 (6H, m, 2 × CH₃), 0.93–0.98 (1H, m, CH₂CHCH₂N), 1.25–1.32 (17H, m, br, 8 × CH₂, CH₂CHCH₂N), 1.50–1.55 (1H, m, CH), 1.93–2.07 (2H, m, CHCH₂N), 2.23–2.31 (4H, m, CH₂NCH₂), 3.60 (4H, t, *J* = 4.4 Hz, CH₂OCH₂); δ_{C} (50 MHz, CDCl₃) 67.07, 66.17, 54.12, 35.14, 31.91, 29.96, 29.85, 29.67, 29.34, 26.98, 22.68, 16.26, 14.10; *m/z* (EI) = 267 (M⁺–2, C₁₇H₃₅NO), 210, 196, 182, 154, 140 (100%), 126, 100, 82, 55, 41, 28.

4-Tridecylmorpholine²²

4-Tridecylmorpholine (entry 2, Table 3, linear amine) δ_{H} (400 MHz, CDCl₃) 0.88 (3H, t, *J* = 6.8 Hz, CH₃), 1.25–1.32 (20H, m, br, 10 × CH₂), 1.42–1.52 (2H, m, CH₂CH₂N), 2.32 (2H, t, *J* = 7.6 Hz, CH₂CH₂CH₂N), 2.45 (4H, s, br,

CH₂NCH₂), 3.73 (4H, t, *J* = 4.4 Hz, CH₂OCH₂); δ_{C} (100 MHz, CDCl₃) 67.0, 59.24, 53.81, 31.90, 29.62, 29.59, 29.55, 29.32, 27.51, 26.56, 22.65, 14.07; *m/z* (EI) = 269 (M⁺, C₁₇H₃₅NO), 140, 100 (100%), 87, 70, 55, 43, 28.

4-(2-Methylhexyl)morpholine

4-(2-Methylhexyl)morpholine (entry 6, Table 3, branched amine) δ_{H} (400 MHz, CDCl₃) 0.83–0.91 (6H, m, 2 × CH₃), 1.01–1.09 (1H, m, CH₂CHCH₂N), 1.18–1.43 (5H, m, br, CH₂CHCH₂N, 2 × CH₂), 1.58–1.65 (1H, m, CH), 2.03–2.15 (1H, m, CHCH₂N), 2.15–2.19 (1H, m, CHCH₂N), 2.30–2.43 (4H, m, CH₂NCH₂), 3.70 (4H, t, *J* = 4.4 Hz, CH₂OCH₂); δ_{C} (50 MHz, CDCl₃) 67.01, 66.14, 54.18, 54.07, 34.80, 29.80, 29.20, 22.95, 16.22, 14.09; *m/z* (EI) = 185 (M⁺, C₁₁H₂₃NO), 100 (100%), 70, 56, 42, 28.

4-Heptylmorpholine²³

4-Heptylmorpholine (entry 6, Table 3, linear amine) δ_{H} (400 MHz, CDCl₃) 0.85 (3H, t, *J* = 6.8 Hz, CH₃), 1.19–1.28 (8H, m, br, 4 × CH₂), 1.40–1.51 (2H, m, CH₂CH₂N), 2.27–2.31 (2H, m, CH₂CH₂N), 2.41 (4H, s, br, CH₂NCH₂), 3.70 (4H, t, *J* = 4.4 Hz, CH₂OCH₂); δ_{C} (50 MHz, CDCl₃) 66.91, 59.17, 53.73, 31.72, 29.16, 27.41, 26.50, 22.54, 14.00; *m/z* (EI) = 185 (M⁺, C₁₁H₂₃NO), 100 (100%), 86, 70, 56, 41, 28.

4-(2-Methyloctyl)morpholine²²

4-(2-Methyloctyl)morpholine (entry 7, Table 3, branched amine) δ_{H} (400 MHz, CDCl₃) 0.87–0.95 (6H, m, 2 × CH₃), 1.01–1.08 (1H, m, CH₂CHCH₂N), 1.22–1.42 (9H, m, br, 4 × CH₂, CH₂CHCH₂N), 1.60–1.67 (1H, m, CH), 2.03–2.08 (1H, m, CH₂CH₂N), 2.10–2.18 (1H, m, CH₂CH₂N), 2.30–2.43 (4H, m, br, CH₂NCH₂), 3.70 (4H, t, *J* = 4.4 Hz, CH₂OCH₂); δ_{C} (50 MHz, CDCl₃) 67.02, 66.15, 54.06, 35.11, 31.67, 29.61, 29.59, 26.91, 22.63, 16.22, 14.08; *m/z* (EI) = 213 (M⁺, C₁₃H₂₇NO), 100 (100%), 87, 70, 56, 43, 28.

4-Nonylmorpholine²³

4-Nonylmorpholine (entry 7, Table 3, linear amine) δ_{H} (400 MHz, CDCl₃) 0.81–0.91 (3H, m, CH₃), 1.18–1.32 (12H, m, br, 6 × CH₂), 1.40–1.51 (2H, m, CH₂CH₂N), 2.27–2.32 (2H, m, CH₂CH₂N), 2.41 (4H, s, br, CH₂NCH₂), 3.70 (4H, m, CH₂OCH₂); δ_{C} (50 MHz, CDCl₃) 66.65, 59.14, 53.67, 31.76,

29.47, 29.44, 29.17, 27.42, 26.44, 22.55, 13.96; m/z (EI) = 213 (M^+ , $C_{13}H_{27}NO$), 100 (100%), 70, 56, 43, 28.

4-(2-Methyldecyl)morpholine

4-(2-Methyldecyl)morpholine (entry 8, Table 3, branched amine) δ_H (400 MHz, $CDCl_3$) 0.83–0.89 (6H, m, $2 \times CH_3$), 1.00–1.10 (1H, m, CH_2CHCH_2N), 1.15–1.60 (13H, m, br, CH_2CHCH_2N , $6 \times CH_2$), 1.61–1.70 (1H, m, CH), 2.04–2.18 (2H, m, CH_2CH_2N), 2.38 (4H, s, br, CH_2NCH_2), 3.78 (4H, s, br, CH_2OCH_2); δ_C (50 MHz, $CDCl_3$) 67.02, 66.16, 54.17, 54.07, 35.14, 31.69, 29.94, 29.61, 29.63, 29.32, 26.97, 22.67, 16.26, 14.11; m/z (EI) = 241 (M^+ , $C_{15}H_{31}NO$), 100 (100%), 70, 55, 43, 28.

4-Undecylmorpholine²⁴

4-Undecylmorpholine (entry 8, Table 3, linear amine) δ_H (400 MHz, $CDCl_3$) 0.88 (3H, t, $J = 6.8$ Hz, CH_3), 1.20–1.35 (16H, m, br, $8 \times CH_2$), 1.41–1.55 (2H, m, CH_2CH_2N), 2.30–2.34 (2H, m, CH_2CH_2N), 2.44 (4H, s, br, CH_2NCH_2), 3.72 (4H, t, $J = 4.4$ Hz, CH_2OCH_2); δ_C (50 MHz, $CDCl_3$) 66.95, 59.21, 53.76, 31.67, 29.57, 29.54, 29.30, 27.47, 26.52, 22.64, 14.08; m/z (EI) = 241 (M^+ , $C_{15}H_{31}NO$), 207, 100 (100%), 70, 55, 43, 28.

N, N-Diethyl-2-methyl-1-dodecanamine

N, N-Diethyl-2-methyl-1-dodecanamine (entry 9, Table 3, branched amine) δ_H (400 MHz, $CDCl_3$) 0.80–0.92 (6H, m, $2 \times CH_3$), 0.93–1.10 (6H, m, $N(CH_2CH_3)_2$), 1.18–1.48 (18H, m, br, $9 \times CH_2$), 1.50–1.61 (1H, m, CH), 2.02–2.13 (1H, m, CH_2CH_2N), 2.16–2.25 (1H, m, CH_2CH_2N), 2.42–2.58 (4H, m, br, $N(CH_2CH_3)_2$); δ_C (50 MHz, $CDCl_3$) 60.33, 47.47, 35.30, 31.66, 31.40, 29.96, 29.62, 29.60, 29.30, 27.06, 22.63, 16.47, 14.06, 11.49; m/z (EI) = 255 (M^+ , $C_{17}H_{37}N$), 126, 86 (100%), 58, 41, 28.

N, N-Diethyl-1-tridecanamine²⁵

N, N-Diethyl-1-tridecanamine (entry 9, Table 3, linear amine) δ_H (400 MHz, $CDCl_3$) 0.80–0.90 (3H, m, CH_3), 0.94–1.04 (6H, m, br, $N(CH_2CH_3)_2$), 1.14–1.35 (18H, m, br, $9 \times CH_2$), 1.40 (4H, s, br, $CH_2CH_2CH_2CH_2N$), 2.34–2.41 (2H, m, CH_2CH_2N), 2.44–2.54 (4H, m, $N(CH_2CH_3)_2$); δ_C (50 MHz, $CDCl_3$) 52.66, 46.73, 31.63, 29.55, 29.26, 27.63, 26.78, 22.58, 13.98, 11.46; m/z (EI) = 255 (M^+ , $C_{17}H_{37}N$), 86 (100%), 72, 58, 41, 29.

1-(2-Methyldodecyl)piperidine

1-(2-Methyldodecyl)piperidine (entry 10, Table 3, branched amine) δ_H (400 MHz, $CDCl_3$) 0.81–0.96 (6H, m, $2 \times CH_3$), 0.97–1.08 (1H, m, CH_2CHCH_2N), 1.14–1.50 (19H, m, br, CH_2CHCH_2N , $8 \times CH_2$), 1.51–1.70 (5H, m, CH, $N(CH_2CH_2)_2CH_2$), 1.98–2.06 (1H, m, $CH_2N(CH_2CH_2)_2CH_2$), 2.06–2.34 (1H, m, $CH_2N(CH_2CH_2)_2CH_2$), 2.31 (4H, s, br, $N(CH_2CH_2)_2CH_2$); δ_C (50 MHz, $CDCl_3$) 66.57, 55.01, 35.42, 31.91, 30.24, 29.96, 29.68, 29.35, 27.07, 25.65, 24.52, 22.66, 16.53, 14.11; m/z (EI) = 267 (M^+ , $C_{18}H_{37}N$), 208, 180, 138, 98 (100%), 84, 69, 55, 41, 28.

1-Tridecylpiperidine²⁶

1-Tridecylpiperidine (entry 10, Table 3, linear amine) δ_H (400 MHz, $CDCl_3$) 0.88 (3H, t, $J = 6.8$ Hz, CH_3), 1.20–1.36 (20H, m, br, $10 \times CH_2$), 1.38–1.52 (4H, m, $N(CH_2CH_2)_2CH_2$, CH_2CH_2N), 1.54–1.62 (4H, m, $N(CH_2CH_2)_2CH_2$), 2.22–2.30 (2H, m, $CH_2N(CH_2CH_2)_2CH_2$), 2.37 (4H, m, br, $N(CH_2CH_2)_2CH_2$); δ_C (50 MHz, $CDCl_3$) 59.66, 54.61, 31.70, 29.60, 29.34, 27.76, 26.89, 25.92, 24.47, 22.67, 14.06; m/z (EI) = 267 (M^+ , $C_{18}H_{37}N$), 98 (100%), 84, 69, 55, 41, 29.

References

- 1 W. Reppe and H. Kindler, *Justus Liebigs Ann. Chem.*, 1953, **582**, 148–149.
- 2 T. E. Müller and M. Beller, *Chem. Rev.*, 1998, **98**, 675–703.
- 3 E. Nagy, B. Heil and S. Töhö, *J. Organomet. Chem.*, 1999, **586**, 101–105.
- 4 A. Schmidt, M. Marchetti and P. Eilbracht, *Tetrahedron*, 2004, **60**, 11487–11492.
- 5 G. Angelovski and P. Eilbracht, *Tetrahedron*, 2003, **59**, 8265–8274.
- 6 F. Koç and P. Eilbracht, *Tetrahedron*, 2004, **60**, 8465–8476.
- 7 M. M. Schulte, J. Herwig, R. W. Fischer and C. W. Kohlpaintner, *J. Mol. Catal. A: Chem.*, 1999, **150**, 147–153.
- 8 A. Seayad, M. Ahmed, H. Klein, R. Jackstell, T. Gross and M. Beller, *Science*, 2002, **297**, 1676–1678.
- 9 M. Ahmed, A. M. Seaya, R. Jackstell and M. Beller, *J. Am. Chem. Soc.*, 2003, **125**, 10311–10318.
- 10 A. Seayad, K. Selvakumar, M. Ahmed and M. Beller, *Tetrahedron Lett.*, 2003, **44**, 1679–1683.
- 11 B. Zimmermann, J. Herwig and M. Beller, *Angew. Chem., Int. Ed.*, 1999, **38**, 2372–2375.
- 12 A. Behr and R. Roll, *J. Mol. Catal. A: Chem.*, 2005, **239**, 180–184.
- 13 Y. Y. Wang, M. M. Luo, Y. Z. Li, H. Chen and X. J. Li, *Appl. Catal., A*, 2004, **272**, 151–155.
- 14 (a) T. Welton, *Coord. Chem. Rev.*, 2004, **248**, 2459–2477; (b) C. P. Mehnert, R. A. Cook, N. C. Dispenziere and E. J. Mozeleski, *Polyhedron*, 2004, **23**, 2679–2688; (c) C. M. Gordon, *Appl. Catal., A*, 2001, **222**, 101–117; (d) O. Stenzel, H. G. Raubenheimer and C. Esterhuysen, *J. Chem. Soc., Dalton Trans.*, 2002, 1132–1138.
- 15 (a) I. Meracz and T. Oh, *Tetrahedron Lett.*, 2003, **44**, 6465–6468; (b) A. J. Carmichael, M. J. Earle, J. D. Holbrey, P. B. McCormac and K. R. Seddon, *Org. Lett.*, 1999, **1**, 997–980; (c) B. Ellis, W. Keim and P. Wasserscheid, *Chem. Commun.*, 1999, 337–338; (d) R. P. J. Bronger, S. M. Silva, P. C. J. Kamer and P. W. N. M. van Leeuwen, *Chem. Commun.*, 2002, 3044–3045.
- 16 (a) Y. Chauvin, L. Mussmann and H. Olivier, *Angew. Chem., Int. Ed. Engl.*, 1995, **34**, 2698–2700; (b) J. Dupont, S. M. Silva and R. F. de Souza, *Catal. Lett.*, 2001, **77**, 131–133.
- 17 (a) R. P. Swatloski, J. D. Holbrey and R. D. Rogers, *Green Chem.*, 2003, **5**, 361–363; (b) P. Wasserscheid, R. van Hal and A. Bösmann, *Green Chem.*, 2002, **4**, 400–404.
- 18 N. Karodia, S. Guise, C. Newlands and J. A. Andersen, *Chem. Commun.*, 1998, 2341–2342.
- 19 M. L. Yuan, H. Chen, R. X. Li, Y. Z. Li and X. J. Li, *Appl. Catal., A*, 2003, **251**, 181–185.
- 20 (a) W. L. Niu, L. Chen, J. Y. Hu, H. Chen and X. J. Li, *Chem. Res. Appl.*, 2003, **15**, 414–416; (b) F. Bonati and G. Wilkinsor, *J. Chem. Soc.*, 1964, 3156–3160.
- 21 (a) W. A. Herrmann, C. W. Kohlpaintner, H. Bahrmann and W. Konkol, *J. Mol. Catal.*, 1992, **73**, 191–201; (b) H. Chen, Y. Z. Li, R. X. Li, P. M. Cheng and X. J. Li, *J. Mol. Catal. A: Chem.*, 2003, **198**, 1–7.
- 22 T. Rische and P. Eilbracht, *Synthesis*, 1997, 1331–1337.
- 23 J. Z. Liu, B. Z. Wu, Y. J. Chen, and S. R. Huang, CN Pat. 1031699, 1989.
- 24 J. Beger and E. Meerbote, *J. Prakt. Chem.*, 1984, **326**, 12–22.
- 25 N. G. Kozlov, A. B. Tereshko, L. I. Basalaeva and V. A. Tarasevich, *Russ. J. Gen. Chem.*, 1998, **68**, 1095–1098.
- 26 Y. Emmanuel and C. Georges, *Tetrahedron Lett.*, 1987, **28**, 427–430.

On the active site in heterogeneous palladium selox catalysts†

Adam F. Lee,*^a Simon F. J. Hackett,^a Justin S. J. Hargreaves^b and Karen Wilson^a

Received 9th February 2006, Accepted 27th March 2006

First published as an Advance Article on the web 19th April 2006

DOI: 10.1039/b601984f

The nature of the active site in the Pd-catalysed aerobic selective oxidation of cinnamyl and crotyl alcohols has been directly probed by bulk and surface X-ray techniques. The importance of high metal dispersions and the crucial role of surface palladium oxide have been identified.

Introduction

The direct, aerobic selective oxidation of functionalised hydrocarbons *via* platinum group metal catalysts has been a matter of intense research and debate over the past decade.¹ Such heterogeneously-catalysed routes to valuable fine and agrochemical intermediates and products offer great potential process, safety and environmental benefits over current industrial syntheses employing stoichiometric reagents.² However, full-scale commercialization of these alternative catalytic clean technologies still awaits detailed knowledge of the optimal reaction conditions, activation protocols and deactivation pathways. This information, in turn, requires better insight into both surface reaction mechanisms and nature of the active catalyst site.

Supported monometallic and p-block promoted Pt and Pd catalysts have been the most extensively investigated,^{1,3,4} with particular focus on deactivation pathways. These studies, generally exploring either metal leaching (corrosion), surface 'over-oxidation', or irreversible adsorption of side-products, have provided useful information into optimal start-up/operating conditions, but almost no direct insight into the requisite Pd/Pt species driving the catalytic cycle.

Recent *in-situ* ATR-IR studies by Baiker and co-workers have found some direct evidence for the accumulation of strongly-bound CO at the surface of a 5 wt% Pd–Al₂O₃ catalyst during the oxidative dehydrogenation of 1° alcohols, which may play a role in site-blocking.^{5–7}

Unfortunately the picture regarding the role of oxygen, specifically its interaction and regulation of the active catalytic site, is much less clear. A number of purely kinetic investigations have hypothesised that Pd and Pt surfaces are deactivated by so-called overoxidation.^{8–13} Consequently, several groups have inferred that the requisite active site must comprise reduced metal centres, and claim that 'pre-reduction treatments', paradoxically *under inert atmospheres*, are necessary to generate active sites.¹⁴ A few studies have also turned to electrochemical potential methods to shed further insight into the catalyst oxidation state.^{15–17} However, these indirect measurements, made in the presence of base/acid electrolytes

and Pt foil/wire auxiliary electrodes, introduce a host of possible corrosive/promotional perturbations, and do not mimic simple alcohol oxidation reaction conditions in organic media. Indeed it seems remarkable that the first direct spectroscopic studies of the metal oxidation state, within a working Pd/C catalyst during cinnamyl alcohol oxidation, were only very recently undertaken.^{18,19} Our measurements provided strong support for emerging evidence that palladium oxide may also play an important role in conferring catalytic activity.²⁰ In this paper we set out to test, and validate this hypothesis, by systematically tuning the degree of surface oxidation in a series of Pd/Al₂O₃ catalysts and correlating their resultant performance in the oxidative dehydrogenation of cinnamyl alcohol.

Experimental

Catalyst preparation

A series of γ -alumina (Degussa 180 m² g⁻¹) supported palladium catalysts were prepared from tetraamine palladium(II) nitrate solution (Johnson–Matthey assay 4.16% Pd) by the incipient wetness technique. Dried samples were calcined at 500 °C in static air for 2 h then reduced under H₂ (approximately 10 cm³ min⁻¹) at 400 °C for 2 h. Catalysts were stored in air and not re-activated prior to use. Pd loadings, as determined by ICP-OES, ranged from 0.06 and 8.54 wt% in order to give a broad range of metal dispersions.

Catalyst characterisation

X-ray photoelectron spectra were acquired at normal emission on a Kratos AXIS HiS spectrometer equipped with a charge neutraliser and Mg K α excitation source (1253.6 eV). Binding energy (BE) referencing was employed using the adventitious carbon peak (285 eV) and valence band. Wide scans were recorded for surface elemental analysis (pass energy 160 eV), with high resolution spectra recorded at 40 eV pass energy. Spectral fitting was performed using CasaXPS Version 2.3.5 with a common line shape adopted for all Pd components.

XAS measurements were made on Station 9.3 of the Daresbury SRS facility, using a Si(220) double-crystal monochromator with a beam current/energy of 150 mA/2 GeV. Transmission Pd (24.35 keV) K-edge spectra were acquired using powdered catalysts mounted in stainless steel washers. The lowest loading samples (≤ 1 wt% Pd) were measured in fluorescence mode. Spectra were fitted using the Daresbury

^aDepartment of Chemistry, University of York, York, UK YO10 5DD. E-mail: afl2@york.ac.uk; Fax: 44 1904 432516; Tel: 44 1904 434470

^bDepartment of Chemistry, University of Glasgow, Glasgow, UK G12 8QQ

† Electronic supplementary information (ESI) available: chi data and crotyl alcohol reaction profiles. See DOI: 10.1039/b601984f

EXSPLINE and EXCURV98 packages for background subtraction, and phase shift determination and fitting procedures, respectively. Reference transmission spectra of PdO (>99% Lancaster) and a 10 μm Pd foil standard were also recorded.

A Micromeritics PulseChemisorb 2700 surface area analyser was used to determine both BET surface areas, by N_2 physisorption, and metal dispersions by H_2 chemisorption. Samples were degassed at 100 $^\circ\text{C}$ for 1 h, or reduced at 400 $^\circ\text{C}$ under flowing H_2 for 1 h prior to surface area and dispersion measurements, respectively. Powder XRD measurements were performed using a Siemens D5000 diffractometer with a Cu $\text{K}\alpha$ X-ray source. Data were collected in theta–theta mode over a 2θ range of 10–70 $^\circ$ with a step size of 0.02 $^\circ$.

Reactor measurements

Alcohol oxidation was performed using a Radleys Carousel Reaction Station equipped with 10 ml reactor tubes. Reactors were charged with 8.4 mmol of cinnamyl or crotyl alcohol (Aldrich 99%) in toluene, with mesitylene as an internal standard. Reactions were performed under air at 60 $^\circ\text{C}$ with 50 mg of catalyst. Blank reactions were conducted in parallel under identical conditions in the presence of the bare Al_2O_3 support. Samples were periodically withdrawn for analysis using a Varian CP3800 GC equipped with CP-8400 AutoSampler and DB5 capillary column (film thickness 0.25 μm , id 0.32 mm, length 30 m). Cinnamaldehyde and crotonaldehyde were the principal reaction products (>92%). There were no side-products attributable to toluene oxidation. Reactions were run for up to 24 h with initial rates determined from the linear portion of the reaction profile. Catalyst selectivity and overall mass balances (closure was >98%) were determined using reactant and product response factors with quoted conversions and selectivities ± 2 and $\pm 3\%$, respectively.

Results and discussion

Catalyst characterisation

The bulk and surface structural properties of the Pd– Al_2O_3 series were both extensively characterised in order to identify the key factors influencing their catalytic reactivity. The surface areas of all samples fell only slightly from around 136 to 96 $\text{m}^2 \text{g}^{-1}$ across the series with increasing palladium loading. Surface elemental analysis revealed that the Pd content rose linearly with bulk loading up to ~ 1 wt%, shown in Fig. 1, slowing down at high loadings, corresponding to a maximum surface palladium concentration of only 1.3 wt%. The large discrepancy between bulk and surface concentrations at higher loadings indicates this plateau coincides with the onset of large Pd cluster formation. This observation is supported by dispersion measurements across the series *via* H_2 chemisorption (Table 1), which show the Pd dispersion remains ~ 40 –50% for loadings below 1 wt% total Pd, dropping significantly at higher loadings. These dispersions translate to cluster sizes from 22 \AA to 78 \AA . The principal errors in these size estimates arise from the accuracy of the ICP-OES metal analysis (± 0.01 wt%) and titrated H_2 volumes (± 0.01 μl), and are shown in the table below.

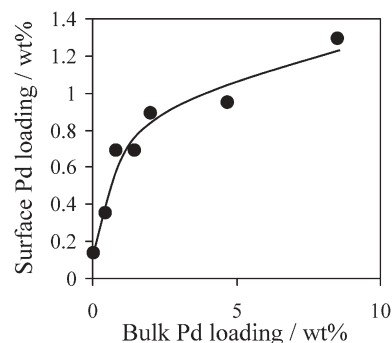


Fig. 1 Surface versus bulk Pd loadings for Pd– Al_2O_3 series.

Table 1 Elemental analysis and physical properties

Bulk Pd loading (wt%)	Surface Pd loading (wt%)	Dispersion (%)	Particle size ^a / \AA
0.06	0.14	40	27 \pm 9
0.44	0.35	40	28 \pm 6
0.84	0.69	51	22 \pm 6
1.48	0.69	31	36 \pm 6
2.02	0.89	24	46 \pm 5
4.72	0.95	26	42 \pm 4
8.54	1.29	14.2	78 \pm 4

^a Sizes calculated according to ref. 21 assuming an equal ratio of (111):(110):(100) facets.

The emergence of large Pd crystallites with metal loading was also followed by XRD. The diffractograms in Fig. 2 do not exhibit any reflections associated with Pd-derived phases for bulk loadings below 1.5 wt%, consistent with the lower particle size detection limit of ~ 30 \AA for powder XRD. Higher loadings result in the emergence of broad features around 40 $^\circ$ and 46 $^\circ$ associated with fcc Pd crystals. Peak-fitting of these reflections yields volume-averaged Pd particle sizes of ~ 60 \AA and 80–100 \AA (each ± 5 \AA factoring in both intrinsic linewidth and step-size) for the 2 wt% and 8.54 wt% samples, respectively, in agreement with Table 1. No ordered palladium oxide phases were observed across the series.

XAS investigations were subsequently undertaken to shed more detailed insight into the local Pd environment,

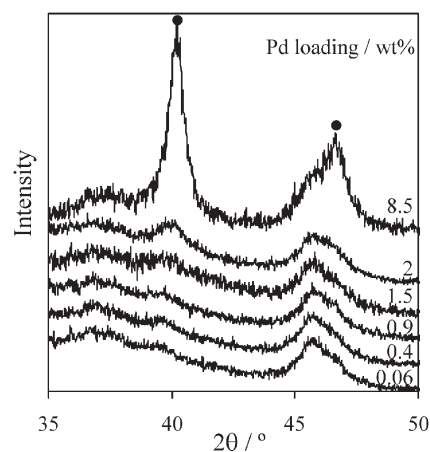


Fig. 2 X-ray diffractograms for Pd– Al_2O_3 as a function of bulk loading.

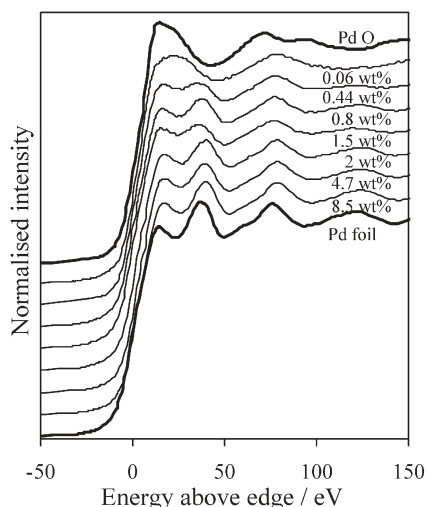


Fig. 3 Normalised Pd K-edge EXAFS spectra for Pd-Al₂O₃ catalysts. Reference PdO and Pd spectra are also shown.

particularly within the smaller clusters. Resultant background-subtracted Pd K-edge spectra for the Pd-Al₂O₃ series are shown in Fig. 3, along with bulk PdO and Pd standards for comparison. All spectra were normalised to give unity edge-jumps 1000 eV above the edge. Visual inspection of the XANES region shows strong similarities between the lowest loading materials and PdO reference, indicating a similar high oxidation state. The low (≤ 0.5 wt% Pd) loading samples also show rapidly damped EXAFS oscillations consistent with low coordination numbers and corresponding short-range order. Representative background subtracted, k^3 -weighted chi data are shown in Fig. 4 for the 0.06, 0.4, 2 and 8.5 wt% Pd-Al₂O₃ samples along with their associated fits. The corresponding radial-distribution functions are shown in Fig. 5 and the fitted parameters given in Table 2.

Spectral fitting confirmed that the high loading samples conformed well to metallic palladium environments with

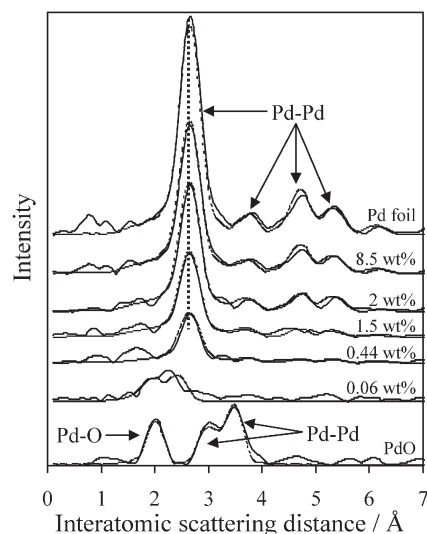


Fig. 5 Radial distribution functions for Pd-Al₂O₃ series.

nearest neighbour coordination numbers and bond lengths in excellent agreement with bulk fcc Pd. Particle size estimates based upon predicted coordination numbers from molecular modelling simulations^{22,23} indicate Pd clusters ranging between 40 and 70 Å diameter for the 2 and 8.5 wt% samples, respectively. These values compare favourably with the analogous XRD and dispersion estimates; however, it is important to note that the sensitivity of EXAFS-derived first shell coordination numbers on particle size decreases sharply for clusters >30 Å, for which H₂ chemisorption provides more accurate estimates. As the Pd loading is decreased below 2 wt%, the lower EXAFS first-shell coordination numbers, and loss of higher coordination shells, indicate the formation of very small, sub-30 Å clusters, which lie below the detection limit of powder diffraction. For the 0.4, 0.8 and 1.5 wt% materials the average local Pd environment remains dominated by Pd-Pd interatomic scattering. Despite their small size, these

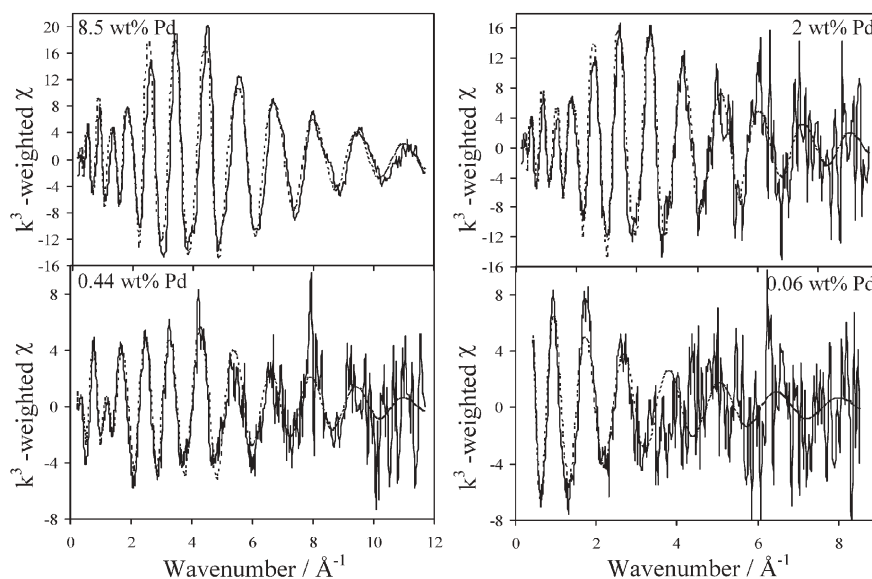


Fig. 4 Raw background-subtracted EXAFS spectra for Pd-Al₂O₃ series.

Table 2 Structural parameters derived from fitted EXAFS of Pd–Al₂O₃ series

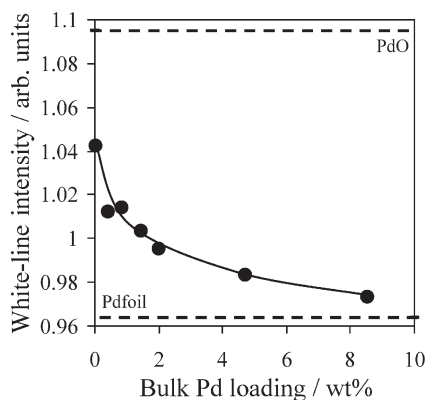
Sample	Parameter												R-Factor
	CN ¹ _{Pd-Pd}	CN ² _{Pd-Pd}	CN ¹ _{Pd-O}	CN ² _{Pd-O}	$r^1_{\text{Pd-Pd}}/\text{\AA}$	$r^2_{\text{Pd-Pd}}/\text{\AA}$	$r^1_{\text{Pd-O}}/\text{\AA}$	$r^2_{\text{Pd-O}}/\text{\AA}$	$\sigma^1_{\text{Pd-Pd}}$	$\sigma^2_{\text{Pd-Pd}}$	$\sigma^1_{\text{Pd-O}}$	$\sigma^2_{\text{Pd-O}}$	
Pd foil	12	6	—	—	2.74	3.87	—	—	0.010	0.018	—	—	22.9
8.54 wt%	12	7	—	—	2.74	3.85	—	—	0.013	0.023	—	—	19.5
4.72 wt%	11.3	7.7	—	—	2.74	3.84	—	—	0.015	0.028	—	—	25.3
2.02 wt%	10.8	7.9	—	—	2.74	3.84	—	—	0.014	0.026	—	—	37.1
1.48 wt%	9.2	8.7	—	—	2.74	3.82	—	—	0.017	0.033	—	—	54.2
0.84 wt%	7.5	8.4	—	—	2.74	3.86	—	—	0.016	0.032	—	—	44.1
0.44 wt%	5.4	4.9	—	—	2.74	3.83	—	—	0.017	0.033	—	—	58.7
0.06 wt%	—	—	4.58	3.79	—	—	2.03	2.49	—	—	0.023	0.007	48.9
PdO	8	2	4	4	3.07	3.45	2.03	—	0.017	0.005	0.007	—	32.3

Pd clusters retain lattice parameters almost identical to the bulk value of 2.74 Å. This observation is consistent with that of Nosova and co-workers,²⁴ who showed that Pd–Pd interatomic distances in supported Pd catalysts were essentially insensitive to either particle size or support effects.

In contrast, the lowest loading 0.06 wt% Pd–Al₂O₃ sample loses almost all characteristic palladium metal features. Indeed the best fit to the EXAFS spectrum was obtained using only Pd–O shells at 2.03 Å and 2.49 Å. The first of these shells is in good agreement with that observed within bulk PdO: however, the second shell cannot be readily assigned to any ordered palladium oxide and may reflect intimate contact with oxygen in the underlying support (*i.e.*, Pd–O–Al coordination), as observed for highly dispersed platinum that adopts 2-dimensional, raft-like morphologies on silica.^{25,26}

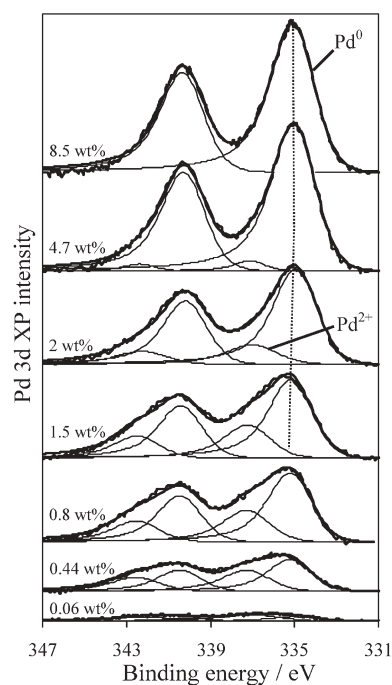
Similar surface structures, closely related to palladium aluminate wherein palladium atoms are localised on vacant octahedral aluminium sites, have been previously postulated from EXAFS measurements of highly dispersed (0.3 wt%) Pd–Al₂O₃ catalysts.²⁷

The average palladium bulk environment thus evolves from bulk-like Pd crystallites to smaller metallic particles with decreasing Pd loading, before eventually forming highly dispersed, oxidic clusters. Associated changes in the overall palladium oxidation state were also examined by tracking the white-line intensity (*i.e.*, maximum in first peak post-edge) across the normalised series (Fig. 6). High palladium oxidation states give rise to a strong peak in the absorption just above the edge-jump (termed the white-line), due to excitation of core

**Fig. 6** White-line intensities from the normalised Pd–Al₂O₃ EXAFS spectra.

electrons into unoccupied (predominantly) 4d states that extend above the Fermi level. This absorbance is attenuated in metallic Pd due to the greater 4d-band occupancy. Fig. 5 shows a general decrease in the white-line intensity (and thus oxidation state) with increasing palladium loading with the limiting value for the 8.5 wt% sample of 0.97 approaching that of the bulk metal. It is interesting to note that while the fitted EXAFS parameters for the 0.06 wt% sample in Table 2 reveal an oxygen-dominated local environment, the corresponding white-line is significantly less than is expected for pure PdO. This may reflect either averaging of multiple Pd^{δ+} environments within the highly dispersed clusters, or the presence of a truncated, PdO-like, phase at the alumina interface with properties intermediate between those of the bulk Pd and PdO. In any event the XAS data show increasing electron density on the Pd clusters as the loading rises, and a corresponding reduction in the formal oxidation state towards Pd⁰.

XPS provides additional insight into the electronic properties of the surface of the Pd clusters. Fig. 7 presents background-subtracted Pd 3d XP spectra which all show the characteristic set of 3d_{3/2,5/2} doublets (ΔBE = 5.25 eV).²⁸

**Fig. 7** Pd 3d XP spectra for Pd–Al₂O₃ series.

The overall spectral intensities rise with Pd loading, as expected from Fig. 1. Of greater interest, however, is the progressive change in peak shape, and shift to lower binding energy, of the peak centroid as the palladium loading increases. In order to better understand these changes, spectra were deconvoluted using two common sets of component doublets with binding energies closely matching those of bulk Pd (335 eV) and PdO (336.9 eV). Peak line shapes and doublet separations were kept constant during fitting throughout the series. All spectra could be accurately fitted using only these two metal and oxide chemical states. Fig. 7 reveals a continuous increase in the proportion of reduced (metallic) surface Pd with increasing loading, in accordance with the X-ray absorption data. The surface electronic properties of the supported clusters essentially revert to those of the bulk metal for loadings above 2 wt% Pd. It is also interesting to note the small decrease in core-level binding energies of both chemical states with loading (~ 0.2 eV); this reflects the well-known cluster \rightarrow bulk transition and associated changes in initial and final-state contributions to core-hole screening.^{29,30}

The switchover from a predominantly oxidised to a reduced palladium surface with falling dispersion (increasing cluster size) is clearly revealed in Fig. 8. This compares the deconvoluted spectra of the 0.06 and 8.5 wt% Pd–Al₂O₃ samples, while the inset quantifies the amount of exposed palladium present as surface oxide over the entire series. The resultant trend is in direct accordance with the corresponding XANES measurements, confirming that both bulk and surface environments evolve simultaneously from oxide to metal with increasing cluster size. It is interesting to note that the Pd XP spectra for the 0.06 wt% sample in Fig. 8 still exhibit a small but significant proportion of reduced palladium. This contrasts with the associated fitted EXAFS, which only indicate Pd–O distances. The discrepancy most likely reflects the

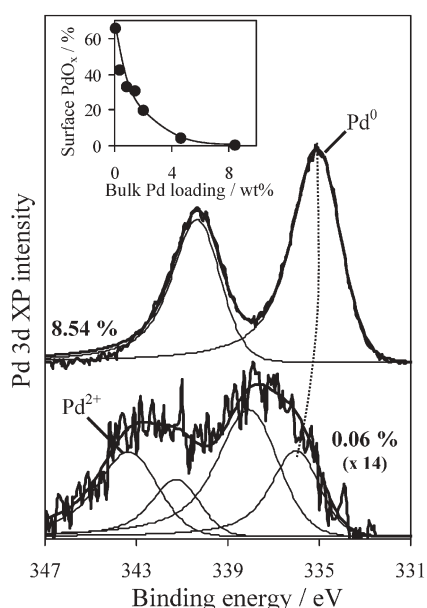


Fig. 8 Comparison of deconvoluted 0.06 and 8.5 wt% Pd–Al₂O₃ Pd 3d XP spectra. Inset shows variation of surface oxide with Pd loading.

averaging nature of the EXAFS technique, which will be insensitive to small amounts of any surface-localised Pd⁰ environments.

Allylic alcohol oxidation

The catalytic performance of the Pd–Al₂O₃ series towards the selective oxidation of cinnamyl and crotyl alcohols was subsequently screened using a parallel reaction station. Reaction profiles for the cinnamyl substrate monitored over 24 hours are shown in Fig. 9.

Oxidation required the presence of Pd–Al₂O₃, with all catalysts exhibiting similar profiles; a fast, initial linear conversion regime during the first 100 min, followed by slower conversion. These reaction profiles are generic to partial oxidation of a host of alcohols/carbohydrates (*e.g.*, refs. 8, 9 and 14 and ref. 31) over various Pd and Pt catalyst formulations. The transition from rapid to slow oxidation was independent of the degree of conversion, eliminating the possibility that this switchover is attributable to mass-transport limitations, and consistent with on-stream catalyst deactivation as widely reported in the literature. Of greater interest is the variation in conversion, and more particularly initial oxidation rates, with Pd loading (into which this paper also represents the first systematic investigation). Considering the former first, the lowest conversion of 16% was unsurprisingly obtained for the 0.06 wt% sample. Conversion rose continuously as the loading increased up to 0.44 and 0.84 wt% Pd (respective conversions of 61 and 99% cinnamyl alcohol). This may be readily rationalised in terms of a simple increase in the number of ‘active’ exposed palladium surface sites. However, this roughly linear increase in performance with palladium content was arrested above 1 wt%. Indeed, additional Pd actually retarded conversion, in line with the larger particle sizes and poorer dispersions. This observation is particularly noteworthy since almost every previous study of alcohol selective oxidation over the past two decades has focused on high (typically 5 wt%) Pt or Pd loading catalysts.

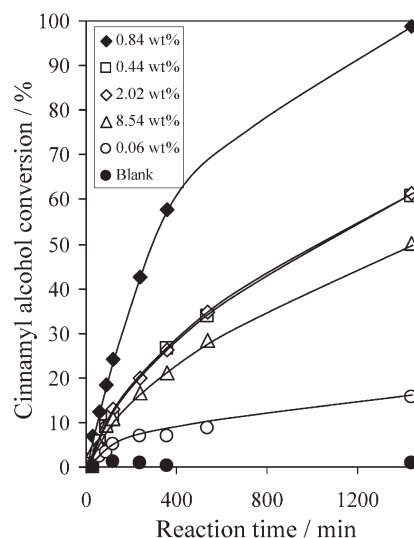


Fig. 9 Reaction profiles for cinnamyl alcohol selective oxidation over Pd–Al₂O₃ catalysts.

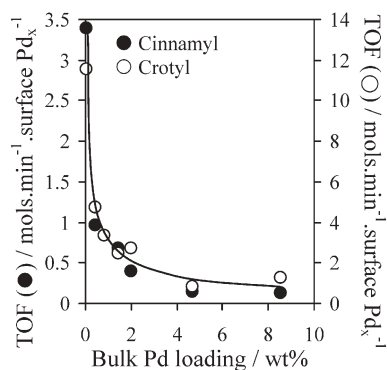


Fig. 10 Loading-dependent TOF in cinnamyl alcohol oxidation over Pd–Al₂O₃ catalysts.

The improved catalytic performance at lower loadings becomes even more striking when turnover frequencies (TOFs) are calculated across the series (Fig. 10). It is immediately apparent from these TOFs that the intrinsic catalytic activity shows an inverse correlation with total Pd loading (and thus particle size). Indeed, each surface site exposed on the highly dispersed, oxidic 0.06 wt% sample is ~26 times as active as those on the larger metallic clusters present in the 8.54 wt% sample. It is important to note that these values are based upon initial rates measured at low conversion *simultaneously under identical reaction conditions*, and thus cannot be attributed to mass-transport differences.

The significance of this trend is reinforced by the analogous results for crotyl alcohol oxidation also shown in Fig. 10 (for simplicity these reaction profiles are presented in the electronic supplementary information†), which confirm that lowering the palladium dispersion dramatically enhances catalyst activity. The higher TOFs towards oxidation of the linear, short-chain crotyl alcohol over its aromatic counterpart may reflect a smaller ensemble requirement, or weaker adsorption of the crotonaldehyde product. We are currently undertaking fast XPS studies of both alcohols over model Pd(111) surfaces to identify their molecular adsorption geometries and associated kinetic parameters. Building upon this data, Fig. 11 now provides the first unequivocal evidence for a direct positive

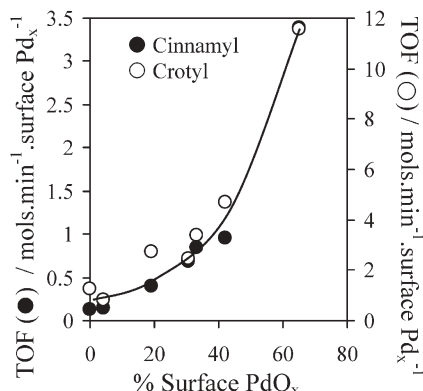


Fig. 11 Correlation between catalyst TOF in cinnamyl alcohol oxidation over Pd–Al₂O₃ catalysts and degree of Pd surface oxidation.

correlation between the presence of palladium oxide surface sites and corresponding reactivity in cinnamyl alcohol selective oxidation over supported Pd catalysts. These results support our recent *in-situ* XAFS measurements which revealed that on-stream reduction of PdO_x to Pd metal suppresses cinnamyl alcohol oxidation, and that catalyst pre-reduction likewise dramatically impairs oxidation.¹⁹

Conclusions

The aerobic selective oxidation of cinnamyl and crotyl alcohols to cinnamaldehyde and crotonaldehyde, respectively, exhibits a strong dependence on metal loading over Pd–Al₂O₃ catalysts. This dependency is directly linked to the Pd dispersion and associated degree of surface oxidation: *catalyst activity scales directly with the proportion of exposed surface palladium oxide*. Conversely, reduced palladium metal sites perform poorly in oxidative dehydrogenation, possibly due to their stronger adsorption of by-products and concomitant rapid self-poisoning.

Acknowledgements

We thank the Royal Society and CCLRC Daresbury Laboratory for financial support and beamtime awards, and Johnson Matthey for the loan of precious metals. S.F.J.H. thanks the EPSRC for a DTA studentship.

References

- 1 T. Mallat and A. Baiker, *Chem. Rev.*, 2004, **104**, 3037–3058.
- 2 R. A. Sheldon, *Pure Appl. Chem.*, 2000, **72**, 1233–1246.
- 3 T. Mallat and A. Baiker, *Catal. Today*, 1994, **19**, 247–284.
- 4 A. F. Lee, J. J. Gee and H. J. Theyers, *Green Chem.*, 2000, **6**, 279–282.
- 5 C. Keresszegi, T. Bürgi, T. Mallat and A. Baiker, *J. Catal.*, 2002, **211**, 244–251.
- 6 C. Keresszegi, D. Ferri, T. Mallat and A. Baiker, *J. Phys. Chem. B*, 2005, **109**, 958–967.
- 7 C. Keresszegi, D. Ferri, T. Mallat and A. Baiker, *J. Catal.*, 2005, **234**, 64–75.
- 8 J. M. Dirkx and H. S. van der Bann, *J. Catal.*, 1981, **67**, 1–13.
- 9 J. M. Dirkx and H. S. van der Bann, *J. Catal.*, 1981, **67**, 14–20.
- 10 P. J. M. Dijkgraaf, M. J. M. Rijk, J. Meuldijk and K. van der Wiele, *J. Catal.*, 1988, **112**, 329–336.
- 11 L. Jemelensky, B. F. M. Kuster and G. B. Marin, *Chem. Eng. Sci.*, 1996, **51**, 1767–1776.
- 12 J. H. Vleeming, B. F. M. Kuster and G. B. Marin, *Ind. Chem. Eng. Res.*, 1997, **36**, 3541–3553.
- 13 J. H. J. Klutymans, A. P. Markusse, B. F. M. Kuster, G. B. Marin and J. C. Schouten, *Catal. Today*, 2000, **57**, 143–155.
- 14 T. Mallat, A. Baiker and L. Botz, *Appl. Catal., A*, 1992, **86**, 147–163.
- 15 Y. Schuurman, B. F. M. Kuster, K. van der Wiele and G. B. Marin, *Appl. Catal., A*, 1992, **89**, 47–68.
- 16 T. Mallat, Z. Bodnar, P. Hug and A. Baiker, *J. Catal.*, 1995, **153**, 131–143.
- 17 T. Mallat and A. Baiker, *Catal. Today*, 1995, **24**, 143–150.
- 18 A. F. Lee, *Abstr. Pap.–Am. Chem. Soc.*, 2001, **221**, 187–COLL.
- 19 A. F. Lee and K. Wilson, *Green Chem.*, 2004, **6**, 37–42.
- 20 T. L. Stuchinskaya and I. V. Kozhevnikov, *Catal. Commun.*, 2003, **4**, 417–422.
- 21 P. Gallezot and G. Bergeret, *Handbook of Heterogeneous Catalysis*, ed. G. Ertl, H. Knözinger and J. Weitkamp, Wiley-VCH, 1997, vol. 2, p. 441.
- 22 B. S. Clausen, L. Grabaek, H. Topsoe, L. B. Hansen, P. Stoltze, J. K. Norskov and O. H. Nielsen, *J. Catal.*, 1993, **141**, 368–379.

- 23 A. Jentys, *Phys. Chem. Chem. Phys.*, 1999, **1**, 4059–4063.
- 24 L. V. Nosova, M. V. Stenin, Y. N. Nogin and Y. A. Ryndin, *Appl. Surf. Sci.*, 1992, **55**, 43–48.
- 25 A. Goguet, M. Aouine, F. J. Cadete Santos Aires, A. De Mallmann, D. Schweich and J. P. Candy, *J. Catal.*, 2002, **209**, 135–144.
- 26 S. D. Jackson, J. Willis, G. D. McLellan, G. Webb, M. B. T. Keegan, R. B. Moyes, S. Simpson, P. B. Wells and R. Whyman, *J. Catal.*, 1993, **139**, 191–206.
- 27 E. Lesage-Rosenberg, G. Vlaic, H. Dexpert, P. Lagarde and E. Freund, *Appl. Catal.*, 1986, **22**, 211–219.
- 28 NIST Standard Reference Database 20, Version 3.4 (Web Version), 2003, <http://srdata.nist.gov/xps/>.
- 29 T. T. P. Cheung, *Surf. Sci.*, 1984, **140**, 151–164.
- 30 G. K. Wertheim and S. B. DiCenzo, *Phys. Rev. B*, 1988, **37**, 844–847.
- 31 C. Keresszegi, J.-D. Grunwaldt, T. Mallat and A. Baiker, *J. Catal.*, 2004, **222**, 268–280.

ReSource

Lighting your way through the publication process

A website designed to provide user-friendly, rapid access to an extensive range of online services for authors and referees.

ReSource enables authors to:

- Submit manuscripts electronically
- Track their manuscript through the peer review and publication process
- Collect their free PDF reprints
- View the history of articles previously submitted

ReSource enables referees to:

- Download and report on articles
- Monitor outcome of articles previously reviewed
- Check and update their research profile

Register today!

RSCPublishing

www.rsc.org/resource

02030508

Innovative direct synthesis of adipic acid by air oxidation of cyclohexane†

Didier Bonnet,^a Tania Ireland,^a Eric Fache^a and Jean-Pierre Simonato^{*ab}

Received 20th January 2006, Accepted 27th March 2006

First published as an Advance Article on the web 7th April 2006

DOI: 10.1039/b600903d

A single-step air oxidation of cyclohexane, based on a new lipophilic catalytic system, leads to the production of adipic acid with excellent results. The catalytic activity outperforms previous reported catalytic systems for this reaction, and provides an environmentally benign alternative to an important industrial reaction.

Introduction

Adipic acid (**1**) is a very important intermediate used for the manufacture of polyamide 6,6 (Nylon-6,6), urethane foams, plasticizers, lubricants *etc.* It is currently produced from benzene, *via* cyclohexane (**2**) or cyclohexene or phenol, in three different multistep processes. These all include, as a final step, a nitric oxidation of a cyclohexanol/cyclohexanone mixture (Scheme 1).¹

This last step dates back to 1893 and was first industrialized by DuPont in the early 1940s.² The main drawback of this reaction is the generation of large amounts of the strong greenhouse gas N₂O. Nevertheless, despite undeniable advances in air oxidation for the conversion of hydrocarbon feedstocks to bulk chemicals,³ the last step of adipic acid synthesis has never been replaced.

Many interesting attempts have been described for the direct synthesis of **1** from **2**, but they generally suffer from low volumetric efficiency, *i.e.* lack of productivity, moderate selectivities or difficult processability, and often require specific oxidizing agents, whereas air is the only acceptable oxidant from an economical point of view.⁴

Our challenge was to build up an economically viable process avoiding N₂O production, and thus use of nitric acid. The most interesting option is the direct conversion of **2** into **1** (in a single step). We report here the results obtained for the development of a new environmentally benign method for the efficient production of **1** by air oxidation of **2** based on an innovative catalytic system.⁵

Results and discussion

We began the study by defining a theoretical process flow chart which would meet the following requirements: a single stage chemical process, an easy recovery of the product, a straightforward recycling of the catalyst, no solvent, no greenhouse gas co-production and a good selectivity for **1** (above 70%). This block diagram is presented in Fig. 1.

It is based on a lipophilic catalyst which would be recycled with the unreacted **2**. Indeed, as with most radical oxidations, one of the main obstacles to the substantial improvement of

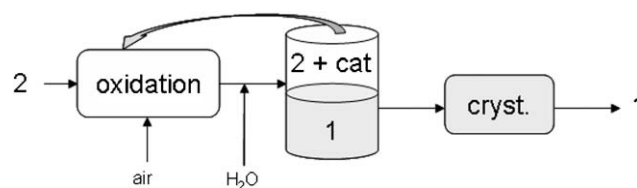
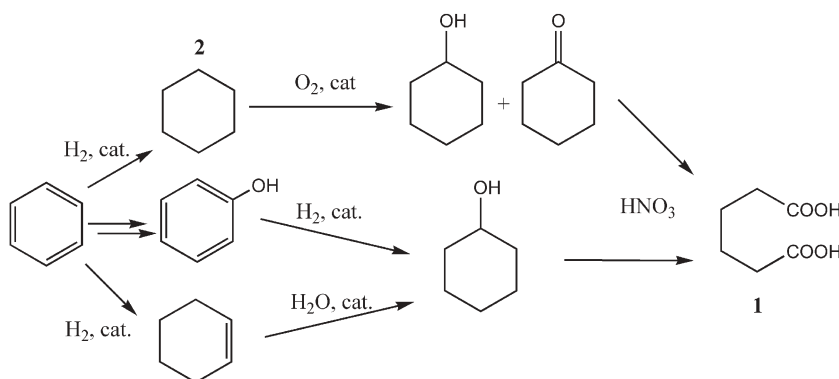


Fig. 1 Schematic flow chart for a one-step adipic acid synthesis from cyclohexane (cat: lipophilic catalyst).



Scheme 1 Current industrial processes for the synthesis of adipic acid.

^aRHODIA Recherches, 85 av. Freres Perret, Saint Fons, France

^bCEA, 17 rue des Martyrs, Grenoble, France.

E-mail: jean-pierre.simonato@cea.fr; Fax: +33 438 785117;

Tel: +33 438 781139

† Electronic supplementary information (ESI) available: Table comparing catalytic systems used in the direct synthesis of adipic acid from cyclohexane. See DOI: 10.1039/b600903d

the selectivity at high alkane conversion is over-oxidation, therefore conversion of **2** will have to be limited and most of **2** will have to be recycled to the oxidation step. Moreover, partially oxidized species like cyclohexanone and cyclohexanol which are highly soluble in **2** will also be recycled directly into the oxidation reactor, allowing further oxidation into **1**. At the end of the reaction, water will be added to solubilize **1**, which will be crystallized later by cooling the aqueous solution, and finally filtered and dried.

Following this concept, drastic specifications were set for the possible lipophilic catalytic system. The catalyst should be very hydrophobic to avoid loss at the extraction step, resistant to oxidizing media, thermally stable, cheap, available at industrial scale, and of course selective for the direct synthesis of **1** from **2**.

In previous studies, it was shown that combinations of manganese and/or cobalt salts with carboxylic acids such as acetic acid were effective for this reaction.^{4a-e,6} Moreover, while studying leaching effects of metal containing zeolites, Fajula *et al.* showed that these metals (cobalt, manganese) could be active at very low concentrations.⁶ Hence, our first experiments were carried out in 25 mL batch reactors to screen potentially active lipophilic carboxylic acids (at 1 mol% to ensure complete solubility), with tiny loadings of Mn^{II} set at 100 wppm (Fig. 2).

These preliminary experiments were conducted with the aim of validating the feasibility of the concept with many carboxylic acids, and not to perform acute data acquisition. As expected, a significant improvement in the conversion of **2** was observed by the addition of various lipophilic carboxylic acids. Acetic acid, which is not hydrophobic, was also tried for comparison since it is often described as a solvent for this reaction. It was 40% less effective when compared to 4-*tert*-butylbenzoic acid (**3**) which gave the best results.

To gain an insight into the catalytic system, the catalytic activity of six catalytic systems were monitored in a 100 mL semi-batch reactor by plotting the initial oxygen consumption rate with respect to the Hammett constant (Fig. 3).

A good correlation was found for four carboxylic acids, indicating that the electronic configuration of the lipophilic acid plays a crucial role on oxidation kinetics: the stronger the

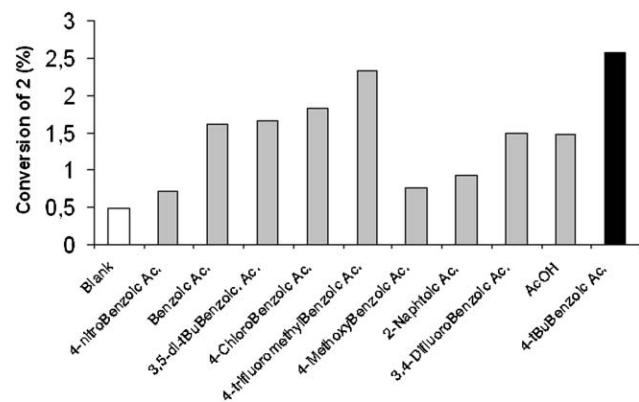


Fig. 2 Screening of lipophilic carboxylic acids (1 mol%) for the oxidation of **2** (4.5 g) at 120 °C, 100 bar air for 3 h in the presence of 100 wppm Mn^{II} and 1 mol% of cyclohexanone (radical initiator)/**2**.

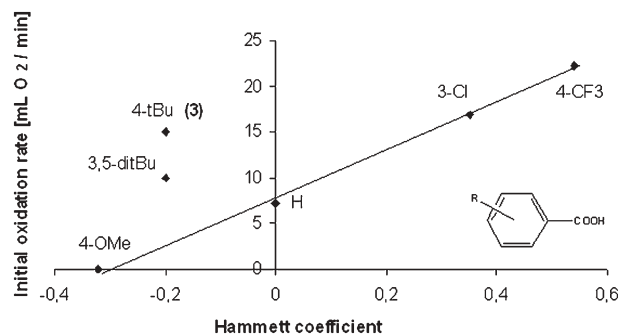


Fig. 3 Initial oxygen consumption rate in a semi-batch reactor *versus* Hammett constant for six lipophilic carboxylic acids. Conditions: 120 °C, 100 wppm Mn^{II}, 5 wt% RCOOH, cyclohexanone 1 mol% (radical initiator)/**2**, 100 bar air.

acid, the faster the oxidation. Interestingly, 3,5-di-*tert*-butylbenzoic acid and **3** were away from the line defined by the other acids. Both compounds showed a reasonable activity and resulted in a good selectivity for adipic acid, whereas stronger acids such as C₈F₁₇CO₂H (not plotted) or 4-trifluoromethylbenzoic acid were also very active but far less selective, leading to side reactions such as the formation of large amounts of formic acid.

Many attempts were carried out to define the catalytically active species and understand the way **2** is transformed into **1**, mainly by relying on published works.^{4a,b,d,7} This appeared to be extremely difficult due to the complexity of the medium, the number of radical intermediates and the coordination chemistry of cobalt and manganese atoms with **3**.⁸ To date, we are not able to explain the remarkable effect of **3** on the multistep (and certainly multipathway) mechanism of this oxidation reaction.

Optimization of reaction conditions was performed with the most promising acid **3** which fulfills all the requirements as defined in the process concept (*vide supra*). Several parameters were studied (Fig. 4) showing an optimum amount of **3** at 10–13 wt% and an optimum temperature of 140 °C. However, regarding both productivity and selectivity, the best conditions appeared to be 10–12 wt% of **3**, a temperature of 130 °C and a target conversion for **2** of nearly 10%.

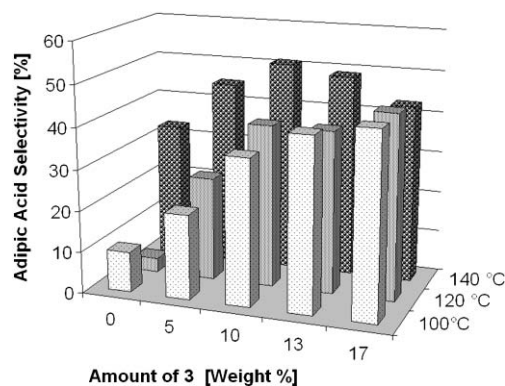


Fig. 4 Optimization of temperature and **3** content for the direct synthesis of **1** from **2**. Conditions: 100 wppm Mn^{II}, cyclohexanone 1 mol% (radical initiator)/**2**, 100 bar air.

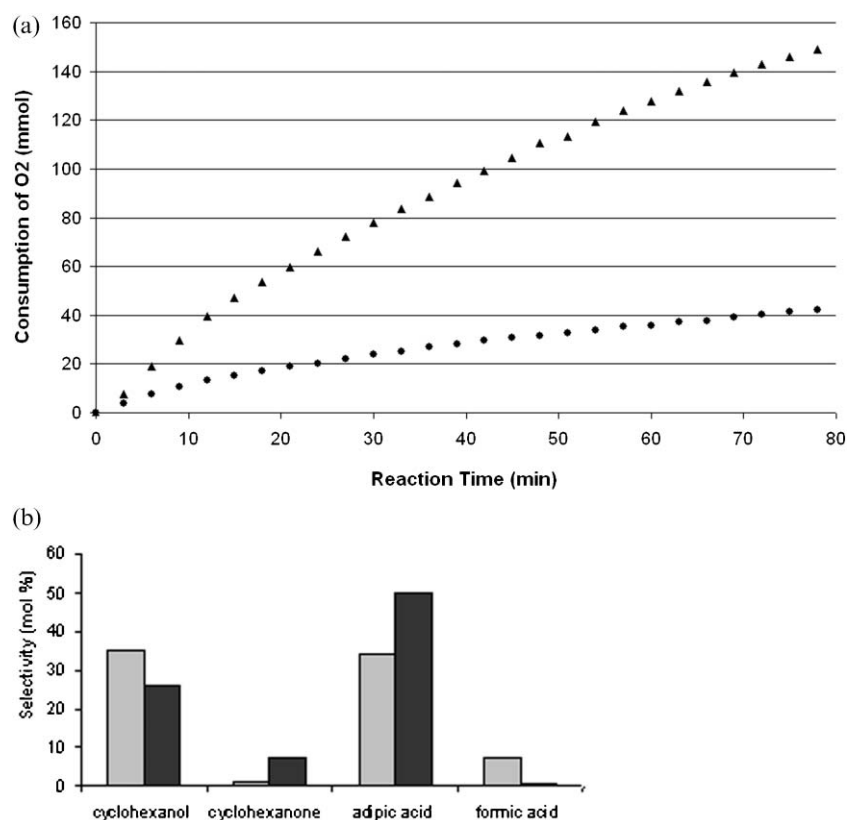


Fig. 5 (a) Comparison of oxygen consumption rates without and with cobalt co-catalyst during air oxidation of cyclohexane. Conditions: 130 °C, 10 wt% of **3**, cyclohexanone 1 mol% (radical initiator)/2, 100 bar air. 100 wppm Mn^{II} (●); 50 wppm Mn^{II} + 20 wppm Co^{II} (▲). (b) Bar chart comparing the product selectivities of the major products without and with cobalt co-catalyst. Conditions: 130 °C, 10 wt% of **3**, cyclohexanone 1 mol% (radical initiator)/2, 100 bar air. 100 wppm Mn^{II} (grey); 50 wppm Mn^{II} + 20 wppm Co^{II} (black).

Although this optimized system already gave acceptable productivity, we looked for co-catalysts in order to improve it. After screening more than thirty metallic precursors as co-catalysts, we found that the best results were obtained with cobalt. By reducing the amount of manganese by a factor of two to 50 wppm and adding 20 wppm of cobalt, a synergistic effect was observed: the productivity was multiplied by more than 3 and the selectivity was strongly improved (Figs. 5a and b). It is of note that no impact of metallic precursors of cobalt and manganese was observed.

It must be stressed that glutaric acid and succinic acid are also produced during the reaction. In the present work, the molar ratio of **1** to the dicarboxylic acids is slightly above 80%. Although they are not desired products, perfectly selective air oxidation of **2** into **1** would be ideal, in reality these two products are always co-produced with **1**. Nevertheless, both glutaric and succinic acids are valuable products and must be considered as such.

Semi-batch experiments were then carried out in a 1 L reactor under 20 bar of air pressure (continuous for gas and batch for liquid phase). During the first run, the selectivity for **1** was 34% for a 10% conversion of **2**. After water extraction of **1**, the organic phase containing **3** was recycled into the reactor and additional **2**, corresponding to the amount consumed in the first run, was added. The selectivity in **1** increased to 44% during the recycling experiment under similar conditions, indicating that partially oxidized species

(cyclohexanol/cyclohexanone) were effectively converted into the desired product. Second and third recycling experiments led to similar results. Since these experiments were conducted by a semi-batch process, we expected a better selectivity for the continuous trials because over-oxidation products of **1**, such as 3-hydroxyadipic acid and formic acid, were observed due to long residence time.

Under entirely continuous conditions, a 56% selectivity into **1** at 10.4% conversion was obtained (value measured after four residence times to ensure representative sampling). After recycling of the organic phase, the selectivity increased to 70.6% (above the initial target) and the measured productivity of **1** exceeded 95 g L⁻¹ h⁻¹.

It was verified that no loss of **3** occurred during the oxidation step, and no degradation by-products of **3** were observed by GC-MS analysis of the final reaction mixture.

Conclusions

In summary, we have demonstrated the potential of a new solventless process for making adipic acid in one step from cyclohexane based on an innovative approach. A new catalytic system was discovered using a very stable lipophilic carboxylic acid and very low loadings of manganese and cobalt salts. The measured catalytic activity outperforms previously reported catalytic systems for this reaction.⁹ Moreover, this new way to produce adipic acid avoids the final nitric oxidation step which

generates a strong greenhouse gas, and thus provides an environmentally benign alternative to an important industrial reaction.

Experimental

Typical procedure for cyclohexane oxidation under continuous conditions.

The experimental setup for the continuous reaction consists of a 1.5 L mechanically stirred titanium autoclave. A typical procedure for the cyclohexane air oxidation was as follows: 546 g of cyclohexane, 62 g of 4-*tert*-butylbenzoic acid, 50 mg of Co(OAc)₂·4H₂O, 140 mg of Mn(OAc)₂·4H₂O and 6 g of cyclohexanone (radical initiator) were added to the reactor. The autoclave was brought to the operating temperature and pressure (under nitrogen), and held at a constant pressure (20 bar) with a flow of 250 L h⁻¹ of air and nitrogen, from 20 : 80 to 100 : 0 in 20 min. An automatic gas oxygen-measuring instrument and gas chromatography apparatus measured online the O₂, CO and CO₂ concentrations of tail gas. At 10% conversion of cyclohexane, the reaction medium was partly removed by a control valve, and a feeding mixture with a composition identical to the initial mixture was introduced to maintain the reaction medium at a constant volume. After four residence times, the reaction was stopped and the mixture was cooled at room temperature. Product analysis was carried out by HPLC and GPC using internal standards.

References

- (a) D. D. Davis and D. R. Kemp, in *Kirk-Othmer Encyclopedia of Chemical Technology*, 4th edn, ed. J. I. Kroschwitz and M. Howe-Grant, Wiley, New York, 1991, vol. 1, p. 446; (b) D. D. Davis, in *Ullman's Encyclopedia of Industrial Chemistry*, 5th edn ed. W. Gerhartz, John Wiley and Sons, New York, 1985, vol. A1, p. 270.
- H. Mager, *Justus Liebigs Ann. Chem.*, 1893, **275**, 362.
- (a) R. A. Sheldon and J. K. Kochi, *Metal-Catalyzed Oxidations of Organic Compounds*, Academic Press, New York, 1981; (b) C. L. Hill, *Activation and Functionalization of Alkanes*, Wiley, New York, 1989; (c) B. Meunier, *Chem. Rev.*, 1992, **92**, 1411; (d) A. E. Shilov and G. B. Shul'pin, *Chem. Rev.*, 1997, **97**, 2879.
- (a) J. G. D. Schulz and A. Onopchenko, *J. Org. Chem.*, 1973, **38**, 3729; (b) K. Tanaka, *Hydrocarbon Process.*, 1974, **53**, 114; (c) T. Iwahama, K. Syojyo, S. Sakaguchi and Y. Ishii, *Org. Process Res. Dev.*, 1998, **2**, 255; (d) D. G. Rao and R. S. Tirukkoyilur, *Ind. Eng. Chem. Prod. Res. Dev.*, 1986, **25**, 299; (e) H.-C. Shen and H.-S. Weng, *Ind. Eng. Chem. Res.*, 1988, **27**, 2254; (f) M. Dugal, G. Sankar, R. Raja and J. M. Thomas, *Angew. Chem., Int. Ed.*, 2000, **39**, 2310; (g) J. M. Thomas, R. Raja, G. Sankar and R. G. Bell, *Acc. Chem. Res.*, 2001, **34**, 191; (h) U. Schuchardt, D. Cardoso, R. Sercheli, R. Pereira, R. S. da Cruz, M. C. Guerreiro, D. Mandelli, E. V. Spinace and E. L. Pires, *Appl. Catal., A*, 2001, **211**, 1; (i) N. Sawatari, T. Yokota, S. Sakaguchi and Y. Ishii, *J. Org. Chem.*, 2001, **66**, 7889; (j) Y. Yuan, H. Ji, Y. Chen, Y. Han, X. Song, Y. She and R. Zhong, *Org. Process Res. Dev.*, 2004, **8**, 418; (k) R. Raja, J. M. Thomas, M. Xu, K. D. Harris, M. Greenhill-Hooper and K. Quill, *Chem. Commun.*, 2006, 448.
- (a) D. Bonnet, E. Fache and J. P. Simonato, *World Pat.* 03014055, 2003 (patent held by Rhodia); (b) D. Amoros, F. Augier, D. Bonnet, M. I. Broglio and J. P. Simonato, *World Pat.* 04041768, 2004 (patent held by Rhodia).
- (a) I. Belkhir, A. Germain, F. Fajula and E. Fache, *J. Chem. Soc., Faraday Trans.*, 1998, **94**, 1761; (b) I. Belkhir, A. Germain, F. Fajula and E. Fache, in *Supported Reagents and Catalysts in Chemistry*, ed. B. K. Hodnett, A. P. Kybett, H. H. Clark and K. Smith, The Royal Society of Chemistry, Cambridge, 1998, pp. 48–53; see also ref. 4j.
- (a) J. Hanotier, P. Camerman, M. Hanotier-Bridoux and P. de Radzitzky, *J. Chem. Soc., Perkin Trans. 2*, 1972, **17**, 2247; (b) J. D. Druliner, *J. Org. Chem.*, 1978, **43**, 2069; (c) L. Saussine, E. Brazi, A. Robine, H. Mimoun, J. Fisher and R. Weiss, *J. Am. Chem. Soc.*, 1985, **107**, 3534; (d) A. Bravo, H.-R. Bjorsvik, F. Fontana, F. Minisci and A. Serri, *J. Org. Chem.*, 1996, **61**, 9409; (e) V. I. Timokhin, M. T. Lisovska and A. P. Pokutsa, *Kinet. Catal.*, 2000, **41**, 179; (f) T. Iwahama, Y. Yoshino, T. Keitoku, S. Sakaguchi and Y. Ishii, *J. Org. Chem.*, 2000, **65**, 6502; (g) F. Minisci, F. Recupero, F. Fontana, H.-R. Bjorsvik and L. Liguori, *Synlett*, 2002, **4**, 610.
- G. Fernandez, M. Corbella, D. Bonnet and J. P. Simonato, unpublished results.
- See supplementary information†.

An assessment of ionic liquid mutagenicity using the Ames Test

Kathryn M. Docherty,* Susanne Z. Hebbeler and Charles F. Kulpa, Jr.

Received 17th February 2006, Accepted 27th March 2006

First published as an Advance Article on the web 18th April 2006

DOI: 10.1039/b602418a

Recent interest in ionic liquids as green replacements for volatile organic solvents has led to an abundance of rapid toxicity testing to provide guidelines for safe designer engineering and synthesis. While toxicity tests have provided a wealth of information, no studies to our knowledge have investigated the mutagenicity of ionic liquids, which should be just as important for design guidelines. Here we present the results of the United States Environmental Protection Agency (US EPA) Ames Test for mutagenicity using *Salmonella typhimurium* strains TA98 and TA100 to ten ionic liquids. These include compounds with imidazolium, pyridinium and quaternary ammonium cations. Tests with these bacteria provide information on the ability of a chemical to cause frameshift and missense mutations, respectively, and can be related to higher organism carcinogenicity. Our test results indicated that none of the ten compounds tested met the US EPA criteria for mutagenicity. Two of the imidazolium cation ionic liquids indicated tendencies toward mutagenicity, but only at the highest doses.

Introduction

In the past several years, there has been a dramatic increase in both academic and industrial interest in novel “green” ionic liquids (ILs). Chemical engineers have been developing ILs to replace conventional volatile organic solvents that contribute to serious air pollution and can result in photochemical smog, ozone layer depletion and global climate change. Ionic liquids are one class of chemicals that have potential as benign industrial alternatives. These organic salts have vanishingly low vapor pressures, are liquid at ambient conditions, and do not evaporate or cause air pollution.¹ Substitution of ILs for traditional solvents could potentially improve environmental health and save industry billions of dollars in environmental mitigation and clean-up.²

Ionic liquids are designed with large organic cations, such as imidazolium, pyridinium, or quaternary ammonium, with alkyl chain substituents that alter the hydrophobicity of the molecule. Common IL anions include hexafluorophosphate (PF₆⁻), tetrafluoroborate (BF₄⁻), chloride (Cl⁻), nitrate (NO₃⁻) and bromide (Br⁻). Designer engineering has made ILs suitable for many applications, including electrolytes in batteries, metal catalysts, solvents in liquid–liquid extractions, and many reactions, including hydrogenations, Diels–Alder reactions, alkylations and others.^{2–6}

While ILs may reduce the costs and environmental mitigation of air pollution, release of water soluble ILs into aquatic environments may lead to water pollution. For example the IL 1-butyl-3-methylimidazolium chloride (bmimCl), was only minimally retained by geologic adsorption in non-interlayer clay systems.⁷ The strength of sorption of ILs to soils and sediments can be related to the substituted alkyl chain length.⁸ Minimal sorption of ILs could result in

unimpeded transport of the chemical through subsurface groundwater, leading to a complex tradeoff between reduced air pollution at the expense of increased water pollution.

Pyridinium, imidazolium and pyrrolidinium ILs have recently been nominated to the United States National Toxicology Program (NTP) for toxicological testing, based upon their widespread interest as possible alternatives to organic solvents, as well as their potential to enter aquatic systems.⁹ The boom of designer solvent synthesis as well as industrial and governmental interest in ILs has sparked a corresponding increase in rapid IL toxicity testing, to determine effective concentrations, or concentrations at which a deleterious effect is observed in a proportion of the test organism population (EC-50). Results of these tests have recently been reviewed.¹⁰ Generally, most tests have indicated that IL toxicity increases with increasing alkyl chain substituent length, regardless of the test organism or cell line.^{11–14} Toxicity was also related mainly to the IL-cation and is independent of the anion. Tests that examined biodegradability of non-branched alkyl substituted imidazolium ILs indicated that they are not readily biodegradable, so that if ILs entered an aquatic system, they would most likely persist as well as be transported.^{15,16}

While research investigating the toxicity of imidazolium, pyridinium and quaternary ammonium ILs has elucidated and addressed many important issues in environmentally friendly IL-design and synthesis, no studies to date have investigated the mutagenicity of these compounds. Incorporation of prior knowledge about IL mutagenicity is just as crucial in green chemical design as information on organismal toxicity. The US-NTP recommendation for testing ILs cites structural similarities of ILs to the herbicide Paraquat, which caused an increased incidence of carcinomas in rat exposure experiments.^{9,17} Preliminary and unpublished genotoxicity results using the Sister Chromatid Exchange (SCE) assay suggest that there may be a trend of increasing genotoxicity with increasing alkyl chain length in imidazolium ILs, as with toxicity.¹⁸ This

University of Notre Dame, Department of Biological Sciences,
PO Box 369, Notre Dame, IN, 46556, USA. E-mail: docherty.3@nd.edu;
Fax: (574) 631-7413; Tel: (574) 631-7187

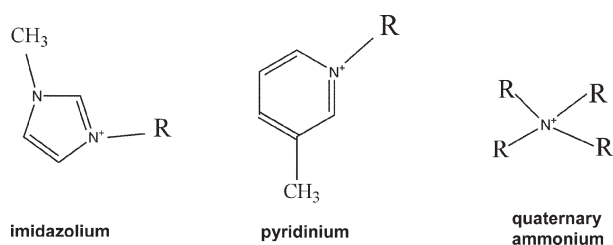


Fig. 1 Chemical structures of imidazolium, pyridinium and quaternary ammonium ionic liquids.

suggests that ILs may also be mutagenic, but, to our knowledge, no studies have been performed to address this question.

Here we present results of the Ames Test for mutagenicity with ten ionic liquids: 1-butyl-3-methylimidazolium bromide (bmimBr), 1-hexyl-3-methylimidazolium bromide (hmimBr), 1-octyl-3-methylimidazolium bromide (omimBr); 1-butyl-3-methylpyridinium bromide (bmpyrBr), 1-hexyl-3-methylpyridinium bromide (hmpyrBr), 1-octyl-3-methylpyridinium bromide (ompyrBr); tetramethylammonium bromide (4M-ammBr), tetraethylammonium bromide (4E-ammBr), tetrabutylammonium bromide (4B-ammBr), tetrahexylammonium bromide (4H-ammBr) (Fig. 1). This assay uses two standard strains of histidine-requiring *Salmonella typhimurium* (TA98 and TA100) bacterial mutants that revert after interaction with

mutants to histidine-independent wild-type state. The rate of reversion indicates the degree of mutagenicity and can be related to the carcinogenicity of the test compound to mammals. The Ames Test for mutagenicity is a standard US EPA protocol for rapid mutagen screening, and an extensive database of results for a broad range of chemicals is readily available.^{19,20}

Results and discussion

Our results indicate that none of the ten ILs tested fit the three USEPA criteria for classification as a mutagenic compound. That is, that none of the ILs tested exhibited (1) a significant relationship between the number of revertant colonies and dose concentration and (2) a two-fold or more increase in the number of revertant colonies over the number of spontaneous revertants seen in the control and (3) a Mutagenicity Index (MI) value greater than 2.0 or a Mutagenicity Activity Ratio (MAR) greater than 2.5. However, some of the compounds we examined did fit one or more of the criteria and may be considered potentially mutagenic, particularly at high doses. We used 2-aminofluorene and sodium azide as positive controls, both of which yielded 20–100 times more revertants than the number of spontaneous revertants, indicating a high level of mutagenicity and confirming proper test strain function.

Table 1 *Salmonella typhimurium* strain TA98 frameshift mutation test results for 3-imidazolium ionic liquids. Statistically significant *p* values are indicated in bold

Dose/mg plate ⁻¹	No S9 RLE added					S9 RLE added				
	No. revertants	MI	MAR	R ²	<i>p</i> value	No. revertants	MI	MAR	R ²	<i>p</i> value
1-Butyl,3-methylimidazolium bromide (bmimBr)										
0.01	15.33 ± 2.08	0.81 ± 0.11	-0.19	0.4932	0.011	25.00 ± 5.57	0.83 ± 0.19	-0.20	0.0021	0.888
1	16.33 ± 3.51	0.86 ± 0.18	-0.14			26.33 ± 6.03	0.88 ± 0.20	-0.15		
5	26.33 ± 5.03	1.39 ± 0.26	0.39			31.00 ± 5.29	1.03 ± 0.18	0.04		
20	28.67 ± 6.66	1.51 ± 0.35	0.51			25.67 ± 4.73	0.86 ± 0.16	-0.17		
Controls										
(10 µg 2-aminofluorene)						3021.33 ± 554.04				
DMSO						28.67 ± 7.09				
H ₂ O						26.00 ± 3.61				
Spontaneous						30.00 ± 6.08				
1-Hexyl,3-methylimidazolium bromide (hmimBr)										
0.01	22.66 ± 2.08	1.19 ± 0.11	0.19	0.0159	0.696	22.00 ± 6.56	0.73 ± 0.22	-0.32	0.0878	0.350
1	19.00 ± 7.00	0.99 ± 0.37	0.00			25.33 ± 2.89	0.84 ± 0.10	-0.19		
5	19.00 ± 2.65	1.00 ± 0.14	0.00			26.66 ± 4.73	0.89 ± 0.16	-0.13		
20	22.00 ± 5.00	1.15 ± 0.26	0.16			27.00 ± 4.58	0.90 ± 0.15	-0.12		
Controls										
(10 µg 2-aminofluorene)						3021.33 ± 554.04				
DMSO						28.67 ± 7.09				
H ₂ O						26.00 ± 3.61				
Spontaneous						30.00 ± 6.08				
1-Octyl,3-methylimidazolium bromide (omimBr)										
0.05	18.67 ± 3.51	0.85 ± 0.16	-0.18	0.5403	0.006	29.33 ± 5.13	0.92 ± 0.16	-0.11	0.0015	0.905
0.10	20.67 ± 5.51	0.94 ± 0.25	-0.07			26.33 ± 8.74	0.82 ± 0.27	-0.23		
0.5	31.33 ± 9.29	1.42 ± 0.42	0.49			37.00 ± 7.55	1.16 ± 0.24	0.20		
1.0	34.00 ± 6.24	1.55 ± 0.28	0.63			27.33 ± 7.77	0.85 ± 0.24	-0.19		
Controls										
(10 µg 2-aminofluorene)						3488.00 ± 640.97				
DMSO						28.00 ± 9.54				
H ₂ O						26.00 ± 4.36				
Spontaneous						32.33 ± 8.08				

Imidazolium compounds

Our test results for bmimBr mutagenicity to TA98 without S9 rat liver enzyme (RLE) added yielded a significant regression ($p = 0.011$) and at very high doses (20 mg plate^{-1}) the average number of revertants (28.67 ± 6.66 , $n = 3$) was near double the number of spontaneous revertants (18.67 ± 3.51 , $n = 3$) (Table 1). Also the MI value at 20 mg plate^{-1} dose was 1.51 ± 0.35 , which is close to the cutoff value of 2.0. However, in the TA98 test with S9 RLE added, none of the criteria for mutagenicity were met, even at high treatment doses (Table 1). This indicates that bmimBr may cause frameshift mutations at high doses, but that the mutagenicity may be diminished within an organism due to enzyme activity. Our tests for bmimBr mutagenicity to TA100 with and without S9 RLE did not fit any of the criteria for missense mutagenicity (Table 2).

None of the test criteria were met in our TA98 or TA100 tests with hmimBr (Tables 1 and 2) even at high doses, indicating that hmimBr is nonmutagenic. Our test results for omimBr mutagenicity to TA98 without S9 RLE added yielded a significant regression ($p = 0.006$, Table 1). At $1.0 \text{ mg plate}^{-1}$ the average number of revertants (34.00 ± 6.24 , $n = 3$) was near double the number of spontaneous revertants in the control (22.00 ± 6.24 , $n = 3$), and the MI value was 1.55 ± 0.28 . We used lower doses (0.05 to $1.0 \text{ mg plate}^{-1}$) of omimBr

than the other two imidazolium compounds because at high doses, omimBr caused a toxic effect to the test bacteria and confounded mutagenicity results. Our TA98 test results with S9 RLE added did not indicate any criteria for mutagenicity, again indicating that omimBr may cause frameshift mutations at doses exceeding 1 mg , but that the mutagenicity will be reduced within an organism. Our tests for omimBr mutagenicity to TA100 without S9 RLE added did not fit any of the criteria for missense mutagenicity (Table 2). In the treatment with S9 RLE, we did obtain a significant regression ($p = 0.015$), however, the number of revertants, even at the highest dose (172.00 ± 15.10 , $n = 3$) was not double the number of spontaneous revertants (152.33 ± 11.15 , $n = 3$) and none of the MI values were near 2.0, indicating that omimBr likely does not cause missense mutations.

Pyridinium compounds

We found that none of the criteria for mutagenicity were met in any of our tests with bmpyrBr, hmpyrBr or ompyrBr, even in the highest dose treatments (Tables 3 and 4). This suggests that pyridinium ionic liquids should not cause frameshift or missense mutations. We used lower doses for ompyrBr because it is more toxic than the lower alkyl chain-length pyridinium compounds and had toxicity effects on the test organisms at doses exceeding $1.0 \text{ mg plate}^{-1}$.

Table 2 *Salmonella typhimurium* strain TA100 missense mutation test results for 3 imidazolium ionic liquids. Statistically significant p values are indicated in bold

Dose/mg plate ⁻¹	No S9 RLE added					S9 RLE added				
	No. revertants	MI	MAR	R ²	p value	No. revertants	MI	MAR	R ²	p value
1-Butyl,3-methylimidazolium bromide (bmimBr)										
0.01	144.33 ± 26.50	1.13 ± 0.21	0.12	0.0134	0.720	163.33 ± 29.14	1.23 ± 0.22	0.20	0.0788	0.377
1	147.00 ± 21.28	1.15 ± 0.17	0.14			117.33 ± 20.53	0.88 ± 0.15	-0.10		
5	171.00 ± 10.44	1.34 ± 0.08	0.31			136.00 ± 21.17	1.02 ± 0.16	0.02		
20	143.00 ± 16.09	1.12 ± 0.13	0.11			124.67 ± 17.01	0.94 ± 0.13	-0.05		
Controls										
Sodium azide	2312.00 ± 835.87									
DMSO	129.00 ± 10.15					131.00 ± 6.08				
H ₂ O	118.00 ± 19.97					145.33 ± 27.39				
Spontaneous	128.00 ± 7.55					133.00 ± 7.00				
1-Hexyl,3-methylimidazolium bromide (hmimBr)										
0.01	129.67 ± 12.66	1.01 ± 0.10	0.01	0.0116	0.739	144.00 ± 16.52	1.08 ± 0.12	0.07	0.1853	0.162
1	117.33 ± 7.02	0.92 ± 0.05	-0.08			161.33 ± 30.09	1.21 ± 0.23	0.18		
5	118.33 ± 37.63	0.92 ± 0.29	-0.07			154.00 ± 6.00	1.16 ± 0.05	0.14		
20	128.00 ± 12.49	1.00 ± 0.10	0.00			129.67 ± 29.14	0.98 ± 0.22	-0.02		
Controls										
Sodium azide	2312.00 ± 835.87									
DMSO	129.00 ± 10.15					131.00 ± 6.08				
H ₂ O	118.00 ± 19.97					145.33 ± 27.39				
Spontaneous	128.00 ± 7.55					133.00 ± 7.00				
1-Octyl,3-methylimidazolium bromide (omimBr)										
0.05	126.67 ± 9.02	1.09 ± 0.08	0.08	0.0833	0.363	153.67 ± 9.71	1.01 ± 0.06	0.01	0.4602	0.015
0.1	161.00 ± 26.29	1.39 ± 0.23	0.33			139.33 ± 14.19	0.92 ± 0.09	-0.08		
0.5	142.67 ± 20.23	1.23 ± 0.17	0.19			160.33 ± 6.66	1.05 ± 0.04	0.05		
1.0	127.00 ± 14.53	1.09 ± 0.13	0.08			172.00 ± 15.10	1.13 ± 0.10	0.13		
Controls										
Sodium azide	2490.67 ± 551.74									
DMSO	126.00 ± 20.66					144.33 ± 20.53				
H ₂ O	119.67 ± 7.57					137.67 ± 16.26				
Spontaneous	116.00 ± 6.93					152.33 ± 11.15				

Table 3 *Salmonella typhimurium* strain TA98 frameshift mutation results for 3 pyridinium ionic liquids. Statistically significant *p* values are indicated in bold

Dose/mg plate ⁻¹	No S9 RLE added					S9 RLE added				
	No. revertants	MI	MAR	R ²	<i>p</i> value	No. revertants	MI	MAR	R ²	<i>p</i> value
1-Butyl,3-methyl pyridinium bromide (bmpyrBr)										
0.01	20.67 ± 2.08	1.03 ± 0.10	0.04	0.0801	0.255	21.33 ± 4.51	0.76 ± 0.16	-0.27	0.0090	0.708
1	21.33 ± 2.08	1.07 ± 0.10	0.07			26.00 ± 3.61	0.93 ± 0.13	-0.08		
5	21.00 ± 9.54	1.05 ± 0.48	0.05			24.33 ± 12.10	0.87 ± 0.43	-0.15		
7.5	19.67 ± 3.06	0.98 ± 0.15	-0.02			25.00 ± 13.08	0.89 ± 0.47	-0.12		
10	22.00 ± 5.29	1.10 ± 0.26	0.11			23.33 ± 11.68	0.83 ± 0.42	-0.19		
20	25.33 ± 8.38	1.27 ± 0.42	0.28			26.00 ± 7.00	0.93 ± 0.25	-0.08		
Controls										
(10 µg 2-aminofluorene)						3291.33 ± 609.08				
DMSO	17.33 ± 4.04					28.67 ± 6.51				
H ₂ O	21.00 ± 5.00					27.33 ± 3.51				
Spontaneous	19.67 ± 5.51					28.00 ± 10.44				
1-Hexyl,3-methyl pyridinium bromide (hmpyrBr)										
0.01	18.00 ± 4.36	0.86 ± 0.21	-0.16	0.2998	0.065	24.00 ± 2.00	1.04 ± 0.09	0.04	0.1822	0.166
1	24.33 ± 7.09	1.16 ± 0.34	0.18			25.00 ± 3.00	1.09 ± 0.13	0.08		
5	23.67 ± 2.31	1.13 ± 0.11	0.14			27.67 ± 3.51	1.20 ± 0.15	0.19		
20	28.00 ± 3.46	1.33 ± 0.16	0.37			27.67 ± 2.52	1.20 ± 0.11	0.19		
Controls										
(10 µg 2-aminofluorene)						3291.33 ± 609.08				
DMSO	17.33 ± 4.04					28.67 ± 6.51				
H ₂ O	21.00 ± 5.00					27.33 ± 3.51				
Spontaneous	19.67 ± 5.51					28.00 ± 10.44				
1-Octyl,3-methyl pyridinium bromide (ompyrBr)										
0.05	27.00 ± 5.57	1.23 ± 0.25	0.26	0.0513	0.479	29.00 ± 8.72	0.91 ± 0.27	-0.12	0.0695	0.408
0.1	19.00 ± 7.94	0.86 ± 0.36	-0.16			26.00 ± 10.44	0.81 ± 0.33	-0.24		
0.5	21.00 ± 8.00	0.95 ± 0.36	-0.05			32.67 ± 11.93	1.02 ± 0.37	0.03		
1.0	28.00 ± 9.17	1.27 ± 0.42	0.32			32.33 ± 3.51	1.01 ± 0.11	0.01		
Controls										
(10 µg 2-aminofluorene)						3488.00 ± 640.97				
DMSO	21.00 ± 4.36					28.00 ± 9.54				
H ₂ O	23.00 ± 3.46					26.00 ± 4.36				
Spontaneous	22.00 ± 6.24					32.33 ± 8.08				

Quaternary ammonium compounds

As with the pyridinium ILs, our tests with the four quaternary ammonium ILs, 4-M ammBr, 4-E ammBr, 4-B ammBr and 4-H ammBr, did not meet any of the criteria for mutagenicity (Tables 5 and 6). This suggests that quaternary ammonium ILs should not cause frameshift or missense mutations. We used lower doses for 4-H ammBr because it had a toxic effect to the test bacteria at doses above 0.05 mg plate⁻¹. Additionally, 4-M ammBr had a toxic effect at 20 mg plate⁻¹, so we removed this dose from our regression calculations.

Conclusion

Our results for the Ames Test for mutagenicity indicated that none of the imidazolium, pyridinium or quaternary ammonium ILs we tested cause frameshift or missense mutations. Some of the imidazolium IL tests (bmimBr and omimBr) indicated trends toward potential mutagenicity at high doses, but did not meet the USEPA criteria for classification as a mutagen. Additionally, the doses we used were often an order of magnitude higher than many other published Ames Test results.¹⁹ Based upon these results, we suggest that designer synthesis and engineering of new green ILs rely more upon the pyridinium and quaternary ammonium cations than the

imidazolium cations, to reduce any potential for mutagenicity. This study represents the first examination, to our knowledge, of IL mutagenicity. However, further studies beyond initial screening with the Ames Test may be necessary to determine whether chronic exposure to ILs may cause an increased incidence of carcinoma. The Ames Test is a short-term test, and it cannot be expected to fully predict carcinogenicity in animals. Because ILs have not been examined in other *in vitro* systems or *in vivo* systems, we are unable to relate the lack of bacterial mutagenicity of these compounds directly with a lack of carcinogenicity. These preliminary tests, however, can play an important role in setting priorities for future testing and as an aid in selecting and designing benign and environmentally friendly green solvents.

Experimental

Imidazolium and pyridinium ILs were synthesized by Dr JaNeille Dixon, University of Notre Dame, Department of Chemical Engineering, according to standard procedures.^{21–23} Quaternary ammonium ILs were purchased from Acros Organics, New Jersey. Mutagenicity of the ten ILs: bmimBr, hmimBr, omimBr, bmpyrBr, hmpyrBr, ompyrBr, 4M-ammBr, 4E-ammBr, 4B-ammBr and 4H-ammBr were tested using the United States Environmental Protection Agency Standard

Table 4 *Salmonella typhimurium* strain TA100 missense mutation test results for 3 pyridinium ionic liquids. Statistically significant *p* values are indicated in bold

Dose/mg plate ⁻¹	No S9 RLE added					S9 RLE added				
	No. revertants	MI	MAR	R ²	<i>p</i> value	No. revertants	MI	MAR	R ²	<i>p</i> value
1-Butyl,3-methyl pyridinium bromide (bmpyrBr)										
0.01	166.67 ± 28.94	1.36 ± 0.24	0.32	0.0182	0.676	154.00 ± 8.00	0.99 ± 0.05	0.00	0.0494	0.488
1	176.67 ± 33.84	1.39 ± 0.30	0.35			206.00 ± 6.00	1.34 ± 0.04	0.34		
5	205.33 ± 6.11	1.67 ± 0.05	0.60			171.00 ± 7.00	1.11 ± 0.05	0.11		
20	182.67 ± 12.70	1.49 ± 0.10	0.43			188.00 ± 13.00	1.22 ± 0.08	0.22		
Controls										
Sodium azide	2312.00 ± 835.88									
DMSO	130.67 ± 10.69					142.33 ± 13.58				
H ₂ O	130.33 ± 11.02					148.33 ± 11.02				
Spontaneous	123.33 ± 10.12					154.00 ± 15.62				
1-Hexyl,3-methyl pyridinium bromide (hmpyrBr)										
0.01	131.00 ± 20.07	1.07 ± 0.16	0.06	0.1290	0.251	174.00 ± 14.00	1.13 ± 0.09	0.13	0.0248	0.625
1	156.67 ± 22.03	1.27 ± 0.18	0.24			167.00 ± 29.00	1.08 ± 0.19	0.08		
5	159.33 ± 41.10	1.30 ± 0.33	0.26			160.00 ± 24.00	1.04 ± 0.16	0.04		
20	166.67 ± 18.58	1.36 ± 0.15	0.32			163.00 ± 9.00	1.06 ± 0.06	0.06		
Controls										
Sodium azide	2312.00 ± 835.88									
DMSO	130.67 ± 10.69					142.33 ± 13.58				
H ₂ O	130.33 ± 11.02					148.33 ± 11.02				
Spontaneous	123.33 ± 10.12					154.00 ± 15.62				
1-Octyl,3-methyl pyridinium bromide (ompyrBr)										
0.05	169.00 ± 24.52	1.46 ± 0.21	0.38	0.0052	0.823	144.67 ± 23.16	0.95 ± 0.15	-0.05	0.0465	0.501
0.1	143.00 ± 8.19	1.23 ± 0.07	0.20			144.67 ± 16.28	0.95 ± 0.11	-0.05		
0.5	109.00 ± 91.54	0.94 ± 0.79	-0.05			152.33 ± 19.03	1.00 ± 0.13	0.00		
1.0	155.33 ± 32.87	1.34 ± 0.28	0.29			135.00 ± 10.00	0.89 ± 0.01	-0.11		
Controls										
Sodium azide	2490.67 ± 551.74									
DMSO	126.00 ± 20.66					144.33 ± 20.53				
H ₂ O	119.67 ± 7.57					137.67 ± 16.26				
Spontaneous	116.00 ± 6.93					152.33 ± 11.15				

Ames Test for mutagenicity.²⁴ We used *His*⁻ *Salmonella typhimurium* strains TA98 for the detection of frameshift mutations (*e.g.*, addition or removal of base pairs) and TA100 for the detection of missense mutations (*e.g.*, replacement of one nucleotide base pair in DNA by another). Cultures were kindly provided by Mary Harrison and Dr George Bennett, Rice University. Strains TA98 and TA100 are daughter strains of *S. typhimurium* strains TA1538 and 1535, respectively, but contain the resistance transfer factor plasmid (R factor) pKM 101, which increases sensitivity to certain mutagens. All test strains were maintained and stored according to USEPA standard protocol, and new master plates were created every 4 weeks. Test strain function (histidine requirement, *rfa* mutation, *uvrB* and R factor) was confirmed each time a new set of master plates was prepared from frozen stock.

We performed mutagenicity tests both with and without metabolic activation with S9 rat liver enzyme (RLE) mix. The S9 Rat Liver Homogenate in KCl was purchased from MP Biomedicals, Ohio; RLE mix was prepared according to USEPA standard protocol. Relevancy of this *in vitro* bacterial test to carcinogenesis is increased by adding rat-liver homogenate to the test system, because it contains enzymes which perform several metabolic conversions similar to those of mammalian organs.²⁴

Preliminary data we obtained from a rapid spot-test screening experiment indicated that the ILs tested were non-mutagenic at quantities below 1 mg plate⁻¹. We performed triplicate Primary Mutagenicity Assays using IL concentrations of 0.01, 1, 5 and 20 mg plate⁻¹. However, for some of the tests we used lower dosages because the IL had a toxic effect to the test bacterium which confounded mutagenicity test results. These chemicals were omimBr, ompyrBr, 4E-ammBr and 4H-ammBr. For the TA98 frameshift mutation test, we used a broader range of dose levels of bmpyrBr because the preliminary testing yielded questionable results with a lower sample size. Briefly, test strains from the master plates were grown overnight (16 h) in Oxoid Nutrient Broth Number 2. Bacterial culture (100 µL), top agar (2 mL) and different doses of IL were mixed and poured onto a minimal agar plate. For tests containing RLE, 500 µL of the S9 mix was added as well. We used 1.5 µg plate⁻¹ of sodium azide dissolved in distilled H₂O as a positive control for tests using TA100 and 10 µg plate⁻¹ 2-aminofluorene in DMSO for TA98. Sterile distilled H₂O and DMSO were used as negative controls. The plates were incubated at 37 °C for 48 h and *His*⁺ revertant colonies were counted and the presence of a background lawn was confirmed. The number of revertants, corrected for the controls, is directly related to the mutagenicity of the test compound. A chemical is considered to be

Table 5 *Salmonella typhimurium* strain TA98 frameshift mutation results for 4 quaternary ammonium ionic liquids

Dose/mg plate ⁻¹	No S9 RLE added					S9 RLE added				
	No. revertants	MI	MAR	R ²	p value	No. revertants	MI	MAR	R ²	p value
Tetramethylammonium bromide (4M-ammBr)										
1	29.33 ± 5.13	1.47 ± 0.26	0.49	0.2300	0.192	25.33 ± 2.08	0.90 ± 0.07	-0.11	0.0020	0.997
5	21.00 ± 6.56	1.05 ± 0.33	0.05			29.67 ± 11.84	1.06 ± 0.42	0.07		
10	21.67 ± 6.43	1.08 ± 0.32	0.09			25.67 ± 4.04	0.92 ± 0.14	-0.09		
Controls						3291.33 ± 609.08				
(10 µg 2-aminofluorene)						28.67 ± 6.51				
DMSO						27.33 ± 3.51				
H ₂ O						28.00 ± 10.44				
Spontaneous										
Tetraethylammonium bromide (4E-ammBr)										
0.01	21.00 ± 1.00	0.91 ± 0.04	-0.11	0.0536	0.469	27.67 ± 4.04	1.20 ± 0.18	0.19	0.1396	0.232
1	30.67 ± 6.43	1.33 ± 0.28	0.40			40.00 ± 6.56	1.74 ± 0.29	0.68		
5	21.67 ± 4.16	0.94 ± 0.18	-0.07			28.67 ± 2.52	1.25 ± 0.11	0.23		
20	29.33 ± 14.01	1.28 ± 0.61	0.33			27.00 ± 4.58	1.17 ± 0.20	0.16		
Controls						3001.33 ± 528.91				
(10 µg 2-aminofluorene)						30.67 ± 4.73				
DMSO						26.00 ± 4.58				
H ₂ O						23.00 ± 8.19				
Spontaneous										
Tetrabutylammonium bromide (4B-ammBr)										
0.01	18.00 ± 4.58	0.78 ± 0.20	-0.26	0.0076	0.787	28.00 ± 2.00	1.22 ± 0.09	0.20	0.0871	0.352
1	24.67 ± 4.73	1.07 ± 0.21	0.09			26.33 ± 8.08	1.14 ± 0.35	0.13		
5	20.33 ± 2.31	0.88 ± 0.10	-0.14			24.00 ± 9.17	1.04 ± 0.40	0.04		
20	20.00 ± 7.00	0.87 ± 0.30	-0.16			23.00 ± 2.65	1.00 ± 0.12	0.00		
Controls						3488.00 ± 640.97				
(10 µg 2-aminofluorene)						28.00 ± 9.54				
DMSO						26.00 ± 4.36				
H ₂ O						32.33 ± 8.08				
Spontaneous										
Tetrahexylammonium bromide (4H-ammBr)										
0.001	18.33 ± 4.04	0.83 ± 0.18	-0.19	0.1980	0.230	23.00 ± 2.00	0.72 ± 0.06	-0.36	0.1730	0.265
0.01	26.67 ± 17.67	1.21 ± 0.80	0.25			22.33 ± 5.86	0.70 ± 0.18	-0.39		
0.05	31.33 ± 6.43	1.42 ± 0.29	0.49			18.00 ± 8.19	0.56 ± 0.26	-0.56		
Controls						3488.00 ± 640.97				
(10 µg 2-aminofluorene)						28.00 ± 9.54				
DMSO						26.00 ± 4.36				
H ₂ O						32.33 ± 8.08				
Spontaneous										

mutagenic if the number of induced revertants is two or more times greater than the number of spontaneous revertants. A two-fold increase in induced revertants coincides with a 90% probability that tumors will be induced by the compounds in laboratory animals.²⁴

Using revertant colony count data, we calculated the Mutagenicity Index (MI) for the 4 test levels of the 10 ILs tested. $MI = R_t/R_c$, where R_t = mean number of revertant colonies with test chemical, and R_c = mean number of spontaneous revertant colonies obtained with a negative control on the day of the test. A significant positive mutagenic effect is determined by a calculated $MI \geq 2$ and a linear relationship between dosage and number of revertant colonies.^{24,25}

We also calculated the Mutagenic Activity Ratio (MAR) for the 4 test levels of the 10 ILs tested. $MAR = (E - c)/c'$, where E = number of revertant colonies, c = number of spontaneous revertants in same test, and c' = historic lab number for spontaneous revertants.

The National Enforcement Investigations Center (NEIC) uses the MAR value as an additional criterion for determining positive mutagenic activity. A MAR of ≥ 2.5 is equivalent to a 95% probability that a substance would produce tumors if administered to laboratory animals, and that it is carcinogenic.²⁴

Acknowledgements

We would like to thank Dr JaNeille K. Dixon and Dr Joan F. Brennecke, University of Notre Dame, Department of Chemical Engineering for providing and synthesizing the ionic liquids; Dr George Bennett and Ms Mary Harrison, Rice University for providing *Salmonella typhimurium* test strains TA98 and TA100; Graduate Assistance in Areas of National Need (GAANN) Fellowship Program, National Science Foundation Graduate Research Fellowship Program, National Oceanographic and Atmospheric Administration, Indiana 21st Century Research and Technology Fund.

Table 6 *Salmonella typhimurium* strain TA100 missense mutation results for 4 quaternary ammonium ionic liquids. Statistically significant *p* values are indicated in bold

Dose/mg plate ⁻¹	No S9 RLE added					S9 RLE added				
	No. revertants	MI	MAR	R ²	<i>p</i> value	No. revertants	MI	MAR	R ²	<i>p</i> value
Tetramethyl ammonium bromide (4M-ammBr)										
0.01	126.67 ± 13.32	1.00 ± 0.10	0.00	0.0040	0.867	184.67 ± 35.50	1.42 ± 0.27	0.35	0.0350	0.630
1	135.67 ± 16.07	1.07 ± 0.13	0.06			150.67 ± 32.72	1.16 ± 0.25	0.13		
5	131.33 ± 11.06	1.03 ± 0.09	0.03			162.33 ± 9.07	1.25 ± 0.07	0.21		
Controls										
Sodium azide	1817.33 ± 5x63.25									
DMSO	112.33 ± 7.23					156.00 ± 6.24				
H ₂ O	135.33 ± 22.03					148.33 ± 9.07				
Spontaneous	127.33 ± 15.50					129.67 ± 1.15				
Tetraethyl ammonium bromide (4E-ammBr)										
0.01	162.00 ± 22.54	1.28 ± 0.18	0.25	0.2921	0.070	156.67 ± 7.02	1.21 ± 0.05	0.17	0.0707	0.403
1	131.67 ± 3.51	1.04 ± 0.03	0.03			164.00 ± 9.54	1.26 ± 0.07	0.22		
5	163.00 ± 22.11	1.28 ± 0.17	0.26			153.67 ± 21.39	1.18 ± 0.16	0.15		
20	179.33 ± 20.03	1.41 ± 0.16	0.38			151.67 ± 12.34	1.17 ± 0.09	0.14		
Controls										
Sodium azide	1817.33 ± 563.25									
DMSO	112.33 ± 7.23					156.00 ± 6.24				
H ₂ O	135.33 ± 22.03					148.33 ± 9.07				
Spontaneous	127.33 ± 15.50					129.67 ± 1.15				
Tetrabutyl ammonium bromide (4B-ammBr)										
0.01	178.00 ± 7.21	1.40 ± 0.06	0.37	0.0394	0.536	151.67 ± 11.24	1.17 ± 0.09	0.14	0.2878	0.072
1	151.00 ± 7.94	1.19 ± 0.06	0.17			154.33 ± 2.08	1.19 ± 0.02	0.16		
5	187.00 ± 38.31	1.47 ± 0.30	0.43			163.33 ± 9.45	1.26 ± 0.07	0.22		
20	157.67 ± 3.79	1.24 ± 0.03	0.22			138.33 ± 14.57	1.06 ± 0.11	0.05		
Controls										
Sodium azide	1817.33 ± 563.25									
DMSO	112.33 ± 7.23					156.00 ± 6.24				
H ₂ O	135.33 ± 22.03					148.33 ± 9.07				
Spontaneous	127.33 ± 15.50					129.67 ± 1.15				
Tetrahexyl ammonium bromide (4H-ammBr)										
0.001	122.67 ± 10.26	1.06 ± 0.09	0.05	0.0860	0.444	138.33 ± 6.66	0.91 ± 0.04	-0.09	0.0160	0.747
0.01	126.00 ± 8.72	1.09 ± 0.08	0.07			125.00 ± 14.11	0.82 ± 0.09	-0.17		
0.05	130.00 ± 14.42	1.12 ± 0.12	0.10			131.00 ± 8.18	0.86 ± 0.05	-0.14		
Controls										
Sodium azide	2490.67 ± 551.74									
DMSO	126.00 ± 20.66					144.33 ± 20.53				
H ₂ O	119.67 ± 7.57					137.67 ± 16.26				
Spontaneous	116.00 ± 6.93					152.33 ± 11.15				

References

- J. F. Brennecke and E. J. Maginn, *Am. Inst. Chem. Eng. J.*, 2001, **47**, 2384.
- D. T. Allen and D. R. Shonnard, *Green Engineering*, Prentice Hall, Upper Saddle River, NJ, 2002.
- K. N. Marsh, A. Deev, A. C. T. Wu, E. Tran and A. Klamt, *Korean J. Chem. Eng.*, 2002, **19**, 357.
- R. A. Sheldon, *Green Chem.*, 2005, **7**, 267.
- J. Dupont, R. F. deSouza and P. A. Z. Suarez, *Chem. Rev.*, 2002, **102**, 3667.
- Q. Liao and L. Hussey, *J. Chem. Eng. Data*, 1996, **41**, 1126.
- D. J. Gorman-Lewis and J. B. Fein, *Environ. Sci. Technol.*, 2004, **38**, 2491.
- P. Stepnowski, *Aust. J. Chem.*, 2005, **58**, 170.
- National Toxicology Program (NTP) and National Institute of Environmental Health Sciences (NIEHS), *Review of Toxicological Literature for Ionic Liquids*, Integrated Laboratory Systems Inc., Research Triangle Park, NC, May 2004.
- P. J. Scammells, J. L. Scott and R. D. Singer, *Aust. J. Chem.*, 2005, **58**, 155.
- J. Pernak, J. Rogoza and I. Mirska, *Eur. J. Med. Chem.*, 2001, **36**, 313.
- J. Ranke, K. Molter, F. Stock, U. Bottin-Weber, J. Poczbott, J. Hoffmann, B. Ondruschka, J. Filser and B. Jastorff, *Ecotoxicol. Environ. Saf.*, 2004, **58**, 396.
- R. J. Bernot, M. A. Brueseke, M. A. Evans-White and G. A. Lamberti, *Environ. Toxicol. Chem.*, 2005, **24**, 87.
- K. M. Docherty and C. F. Kulpa, *Green Chem.*, 2005, **7**, 185.
- N. Gathergood, M. T. Garcia and P. J. Scammells, *Green Chem.*, 2004, **6**, 166.
- N. Gathergood, P. J. Scammells and M. T. Garcia, *Green Chem.*, 2006, **8**, 156.
- U.S. EPA (U.S. Environmental Protection Agency), *Integrated Risk Information System (IRIS): Paraquat (CASRN 1910-42-5)*, 2003, <http://www.epa.gov/iris/subst/0183.htm>.
- B. Jastorff, K. Mölter, P. Behrend, U. Bottin-Weber, J. Filser, A. Heimers, B. Ondruschka, J. Ranke, M. Schaefer, H. Schröder, A. Stark, P. Stepnowski, F. Stock, R. Störmann, S. Stolte, U. Welz-Biermann, S. Ziegert and J. Thöming, *Green Chem.*, 2005, **7**, 362.
- R. E. McMahon, J. C. Cline and C. Z. Thompson, *Cancer Res.*, 1979, **39**, 682.
- U.S. NLM-NIH (National Library of Medicine, National Institutes of Health), *TOXNET Toxicology Data Network, Chemical Carcinogenesis Research Information System*, <http://toxnet.nlm.nih.gov/cgi-bin/sis/htmlgen?CCRIS>.

- 21 L. Cammarata, S. G. Kazarian, P. A. Salter and T. Welton, *Phys. Chem. Chem. Phys.*, 2001, **3**, 5192.
- 22 C. M. Gordon, J. D. Holbrey, A. R. Kennedy and K. R. Seddon, *J. Mater. Chem.*, 1998, **8**, 2627.
- 23 P. Bonhôte, N. Papageorgiou, K. Kalyanaundaram and M. Grätzel, *Inorg. Chem.*, 1996, **35**, 1168.
- 24 W. J. Stang, *NEIC Microbial Bioassay for Toxic and Hazardous Materials (Ames Test for mutagenicity)*, EPA-330/9-80-002, U.S. EPA (U.S. Environmental Protection Agency), August 1980.
- 25 C. Novotny, N. Dias, A. Kapanen, K. Malachova, M. Vandrovicova, M. Itävaara and N. Lima, *Chemosphere*, 2005, DOI: 10.1016/j.chemosphere.2005.10.002.

Chemical Technology

A well-received news supplement showcasing the latest developments in applied and technological aspects of the chemical sciences



Free online and in print issues of selected RSC journals!*

- **Application Highlights** – newsworthy articles and significant technological advances
- **Essential Elements** – latest developments from RSC publications
- **Free access** to the original research paper from every online article

*A separately issued print subscription is also available

RSC Publishing

www.rsc.org/chemicaltechnology

03005020

Synthesis of ozone from air *via* a polymer-electrolyte-membrane cell with a doped tin oxide anode

Yun-Hai Wang, Shaoan Cheng and Kwong-Yu Chan*

Received 29th November 2005, Accepted 26th April 2006

First published as an Advance Article on the web 15th May 2006

DOI: 10.1039/b516927e

The generation of ozone from air using an electrochemical cell consisting of an air cathode, a polymer-electrolyte-membrane (PEM), and a doped tin oxide anode is reported. This synthesis is environmentally friendly compared to the conventional high-voltage corona discharge process since NO_x formation is eliminated; a higher ozone concentration is generated; and lower energy may be required.

Introduction

Ozone is a powerful oxidant in advanced oxidation processes for treating water and solids. Ozone is a green oxidant since it self decomposes in time, leaving no residual effects. It can also oxidize persistent pathogens and contaminants more effectively than chlorine.^{1,2} The conventional route to synthesize ozone is through high voltage corona discharge (CD) in air producing a 2 to 3% concentration of ozone.³ The overall energy consumption of the CD process is high since cooling and drying of air are needed in addition to the electrical energy. This process can produce NO_x as a by-product unless pure oxygen is supplied, which would require additional energy. The energy required to purify air to oxygen is at least two times that of making ozone from oxygen.⁴

The alternative route of ozone generation *via* water electrolysis is attractive since NO_x is not generated and only a low voltage source is needed. If dissolved ozone is the desired product, then the water electrolysis route is more direct and effective. Some losses of ozone to oxygen are expected in the slow dissolution of gaseous ozone generated by the CD process due to self-decomposition. The electrochemical synthesis of ozone has been examined with a number of anode materials.^{5–11} The electrolytic route to generate ozone has been reviewed recently.^{12,13} Until now, only low efficiency has been demonstrated and the most efficient anode material, lead dioxide is environmentally prohibitive for a general usage. A high current efficiency and a high concentration of ozone have only been demonstrated recently by the authors using a doped tin oxide electrode.^{14,15} Some previous reported investigations of water treatment used anodes with undoped tin oxide¹⁶ or tin oxide doped with different elements.^{17,18} The focus of these investigations was direct electro-oxidation, and little ozone was detected. Our previous results of high ozone generation^{14,15} were obtained in a three-electrode test cell containing different acid electrolytes. For corrosion and safety consideration, it would be desirable to have an acid free process, particularly for domestic household applications. Furthermore, hydrogen generated at the cathode during electrolysis creates a safety concern. The water consumed

during electrolysis will need to be replenished regularly to maintain the electrolyte for sustained operation. Here we present, for the first time, the use of the highly efficient nickel–antimony doped tin oxide as the anode in a water filled polymer electrolyte membrane (PEM) cell fitted with an air cathode. Oxygen from the air is consumed in the porous cathode and ozone is produced in pure water and can subsequently evolve into the gas phase for gaseous ozone production. A 15% ozone concentration in the gas phase, 20 mg L⁻¹ dissolved ozone, and a 15% percent current efficiency are observed here. These ozone concentrations reported are much higher than the CD process. In the following sections, we describe the experimental setup, the mechanism of the electrode processes, and the broader implications of the results for general environmental applications.

Experimental

The electrochemical cell

The operation of the electrochemical generator is shown schematically in Fig. 1. Oxygen from air diffuses into the gas diffusion cathode and combines with protons to form water when receiving electrons from the external circuit. Ozone is

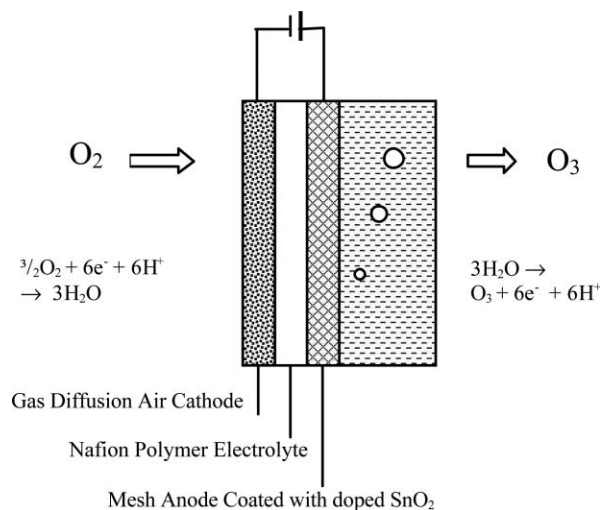


Fig. 1 Illustration of ozone generation in the electrochemical cell.

generated at the anode by oxidation of water with electrons released to the external circuit, protons are simultaneously produced. The protons subsequently diffuse through the proton exchange membrane back to the cathode. The net reaction is the conversion of oxygen to ozone without any consumption of water or protons. With the solid polymer electrolyte providing the protons, the ozone generation occurs in pure water without the need of an acid supporting electrolyte, eliminating the corrosive hazard. The anode was prepared by repeated coating of a titanium mesh with an alcohol solution containing SbCl_3 (BDH, 99.5%), $\text{SnCl}_4 \cdot 5\text{H}_2\text{O}$ (98%, ABCR) and $\text{NiCl}_2 \cdot 6\text{H}_2\text{O}$ (Merck, 98%) precursors followed by pyrolysis at 500 °C. The procedure was similar to that previously described.^{14,15} A 4.0 cm × 6.0 cm titanium mesh (99.5% Goodfellow) with a nominal aperture of 0.19 mm and wire diameter of 0.23 mm was spot-welded with a 1 mm diameter titanium wire (99.5% Goodfellow). The mesh and wire assembly was then treated in 10% boiling oxalic acid for 1 hour, washed with distilled water, and dried before being dip-coated with the precursor solution and pyrolyzed in air. The dip coating and pyrolysis procedure was repeated 7 times and the loading onto the Ti mesh was 61 mg total or 2.55 mg cm⁻² per nominal area, as determined by the weight gained. The cathode was prepared by pasting 55% Pt/C catalyst (De Nora North America, ETEK Division) onto one side of a 4 cm × 6 cm carbon cloth (ETEK, 30% wet proofed). The platinum loading on the cathode was 4.5 mg cm⁻². The membrane-electrolyte-assembly (MEA) was prepared by hot pressing at 140 °C the cathode, a solid electrolyte Nafion 117 membrane (Fuel Cell Scientific) and the anode.

Quantification of ozone production

The amount of ozone generated was determined by a setup as shown in Fig. 2. The water side of the MEA was housed in an acrylic chamber with a gas outlet connected to a 10% potassium iodide bath for idometric measurement. The ozone oxidized iodide to iodine stoichiometrically and the amount of iodine was determined by titration with sodium thiosulfate with a starch end point, as described in the literature.¹⁹ The

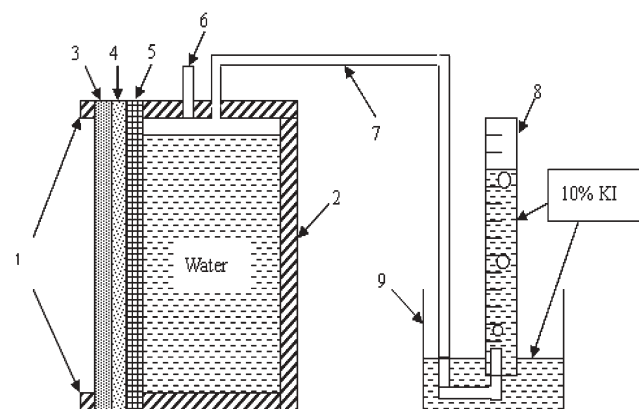


Fig. 2 The schematic drawing of the experimental apparatus. (1) acrylic frame; (2) acrylic chamber; (3) cathode; (4) nafion membrane; (5) anode; (6) hole for extracting water sample; (7) tube for gas transfer; (8) 10 ml cylinder with graduated marks; (9) beaker.

volume of the water chamber was 10 ml. After about 20 min of electrolysis, the ozone concentration in the gas and water phase reached equilibrium. The generated gas was then let out through the tube and absorbed by the KI solution. The unabsorbed residual gas was collected at the top of an inverted graduated cylinder to determine its volume, which was about 7 ml after 30 min. This unabsorbed gas is mainly oxygen generated from the reaction of ozone with KI, or from the electrolysis of water in the PEM. The ozone concentration in the water phase was determined by UV spectrometer (Perkin Elmer Lambda 20). Water samples were extracted with a syringe from an opening fitted with a rubber septum. The ozone concentration in the gas phase was calculated from the amount of ozone absorbed by the KI solution and the residual gas volume at the top of the inverted cylinder.

The electrolysis was performed at constant cell voltage and controlled by a Radiometer Copenhagen/Dynamic-Eis Voltlab PGZ301 potentiostat/galvanostat. The number of coulombs passed during the electrolysis was accurately counted by a built-in integrator. All experiments were carried at room temperature of 20 °C.

Results and discussion

Ozone concentration

Using our experimental setup, we examined the issues of ozone synthesis in terms of ozone concentrations, current efficiency, and energy efficiency. Upon application of a constant voltage across the PEM cell, ozone was generated in water and accumulated until part of the ozone moved from the water phase to the gas phase above. As shown in the aqueous ozone concentration time profiles in Fig. 3, a steady-state was reached after 25 minutes of applied voltage. At this point, ozone was generated steadily in water, then entered into the gas phase, and was eventually absorbed by the KI solution in the absorption chamber. The steady-state dissolved ozone concentration depended on the applied voltage and varied in the range of 5 mg L⁻¹ to 20 mg L⁻¹. This level of dissolved ozone concentration is more than sufficient for most applications and is usually not attained in the conventional CD process.²⁰ Solubility of ozone in water depended on the gas

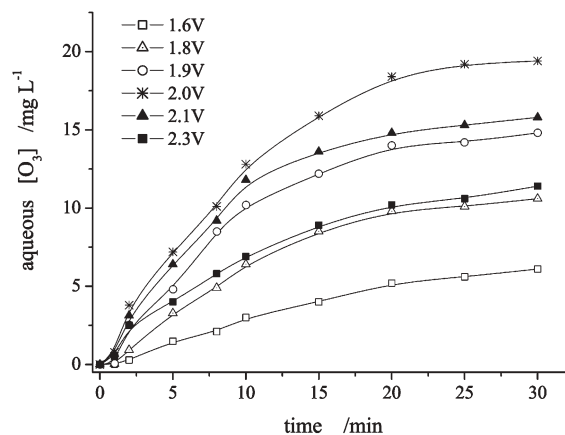


Fig. 3 Ozone concentration in water vs. the electrolysis time at different voltage.

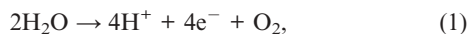
phase ozone concentration, temperature, pH, and the presence of other dissolved species. For a 48.5 mg L^{-1} ozone concentration ($\sim 2\%$) generated in the gas phase, the dissolved ozone concentration was 6.7 mg L^{-1} in a pH 7.1 solution at 25°C .²¹

To avoid disturbance to the titration experiment and the determination of steady-state gas phase ozone concentration, liquid samples were not withdrawn for dissolved ozone measurements after 30 min. The steady-state concentration of ozone in the gas phase correlated to that in the water phase and varied with applied voltage in the same way, as shown in Fig. 4. The highest ozone concentration in gas phase was 15.6% (v/v) equivalent to 334.3 mg L^{-1} (STP), at a voltage of 2.0 V . This concentration was much higher than that achieved by the CD process, which was about 10% (v/v) using a cool, dry, and pure oxygen supply.²²

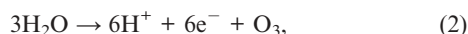
For applications requiring a source of high concentration gaseous ozone,²² the electrochemical process described here provides a convincing and convenient alternative to the CD process. Pure oxygen tank, cooling, and drying are not required in the electrochemical cell. The scalable and modularizable generation is particularly attractive for small and medium scale usage. Previously, a complex procedure was adopted to provide high concentration gaseous ozone for some processes of preparing semi-conductor surfaces.²³

Current efficiency

Fig. 3 and 4 show an optimum cell voltage of 2.0 V for highest ozone concentration. The effect of the cell voltage was partly analysed in light of the parallel electrochemical oxidation of water to form oxygen,



which had an equilibrium potential of 1.23 V (RHE). The oxygen evolution reaction was thermodynamically more favourable than the ozone reaction



which had an equilibrium potential of 1.52 V (RHE).

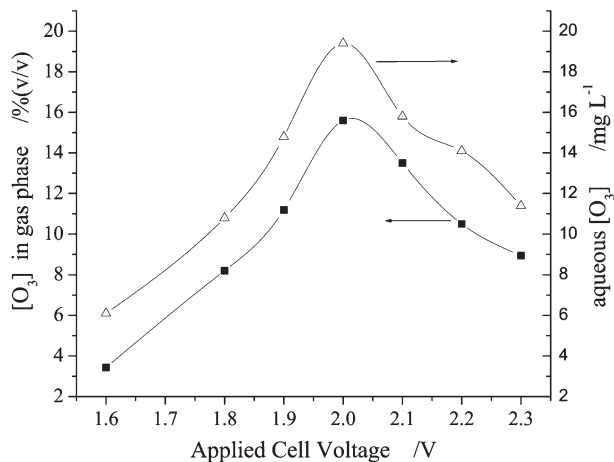


Fig. 4 Applied voltage vs. ozone concentration in gas and water phases.

The presumed role of the doped tin oxide material at the anode was to suppress the kinetics of oxygen evolution reaction and enhance the activation of the ozone generation reaction. Eqn (1) and (2) represent only the overall reactions and the detailed mechanisms may have involved individual steps of precursors and intermediates such as oxygen and hydroxyl free radicals, adsorbed oxygen, and other ions. The specific effect of voltage and materials to individual steps would require more refined experimental works. The electrochemical kinetics of the oxygen evolution reaction and the ozone generation reaction were different. The increase of voltage beyond a certain value may have promoted more oxygen generation than ozone generation. The decrease of ozone concentration beyond the optimum voltage of 2.0 V can be partly explained by this reasoning. It is also possible that the catalytic material or other electrode components were degraded by a high voltage.

While the efficiency of ozone generation falls beyond 2.0 V , the current increased steadily and linearly with applied voltage, as shown in Fig. 5. The effectiveness of using current to produce ozone can be quantified by the current efficiency which is defined according to Faraday's law as

$$\eta = [(\text{moles of ozone generated}) nF/C] \times 100\%, \quad (3)$$

where n is the number of electrons transferred ($n = 6$ in eqn (2)), F is the Faraday's constant, and C is the amount of electric charge passed.

The 15.2% current efficiency observed at 2.0 V is the highest value reported for a MEA cell with a static water electrolyte, whereas a value of $<10\%$ was reported for PbO_2 anode without water flow at room temperature.^{24–27}

The loss of current efficiency was mainly due to production of oxygen either directly at the parallel electrochemical step of eqn (1) or the subsequent decomposition of ozone to oxygen in the water phase and in the gas phase. The half-life of ozone at room temperature is 30 minutes and some losses of ozone to oxygen were expected. It has been demonstrated²⁶ that current efficiency improved by as much as 50% with forced convection of water. We may therefore expect the current efficiency to reach over 20% in our MEA cell with flowing water.

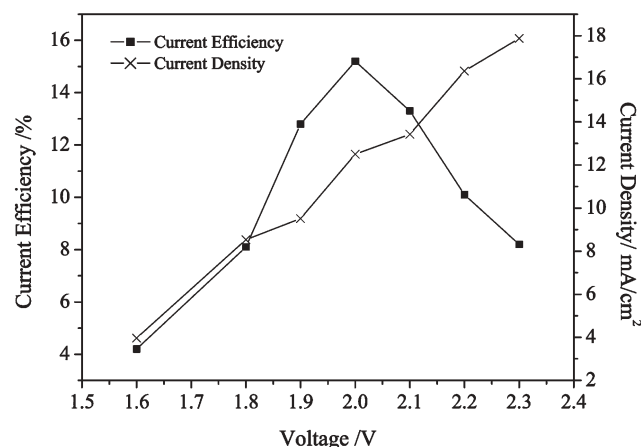


Fig. 5 Applied voltage vs. current density and current efficiency.

A further increase in current efficiency can be envisaged by improving the interfacial contact of the anode and the solid polymer electrolyte. A 36.2% current efficiency was observed in our previous work using a wet acidic electrolyte¹⁵ where the immersed mesh electrode was in more complete contact with protons and water. In the MEA construction, the mesh anode and the solid electrolyte had a planer interfacial contact and the solid-solid interface had limited contact area. Onda *et al.*²⁶ have shown that by using a multi-layer mesh structure in contact with Nafion, interfacial contact was improved and the ozone concentration was increased by 40% compared to a single layer mesh electrode. We may expect a further improvement with a better interfacial construction between the anode and the solid polymer electrolyte.

Energy efficiency

The ozone production rate was the amount of ozone generated in a unit time period, and changed with the applied voltage, as shown in Fig. 6. The ozone was generated on a 4.0 cm × 6.0 cm anode. In principle, the production rate scaled with the electrode area, subject to limitations of uniform current distribution and mass transport. Experience of established electrochemical technologies, such as fuel cells and chloroalkaline production, was helpful to large scale electrochemical generation of ozone. From Fig. 6, the highest steady-state ozone production rate was 12.6 mg h⁻¹ achieved at a cell voltage of 2.0 V over a period of hours. The corresponding energy consumption per unit ozone was also shown in Fig. 6. It varied with voltage in the trend opposite to that of production rate. The energy consumption E_p in kW h kg⁻¹ ozone was determined by:

$$E_p = (VI)/Q, \quad (4)$$

where Q in kg h⁻¹ is the ozone production rate, I in A is the current, and V in volts is the applied cell voltage. From Fig. 6, the lowest energy consumption of 48 kW h kg⁻¹ ozone was achieved at 2.0 V. This energy consumption was lower than the lowest energy consumption reported (65 kW h kg⁻¹) on

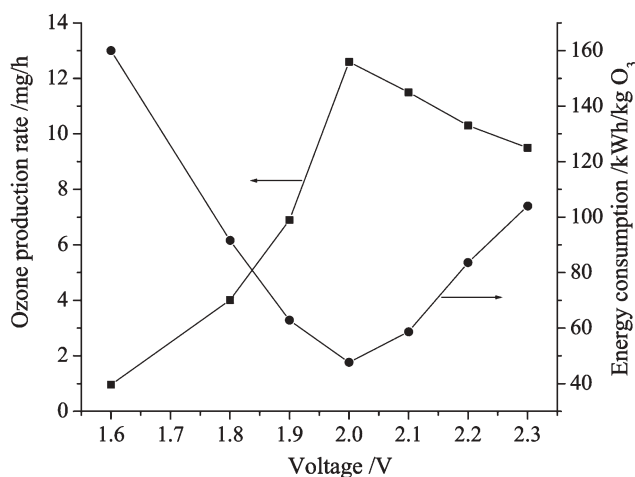
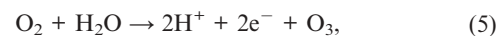


Fig. 6 Applied voltage vs. ozone production rate and energy consumption.

PbO₂.²⁷ It was demonstrated on a PbO₂ electrode that forced convection improved energy consumption by 50%. We would expect a similar improvement when water is circulated through the anode compartment of the PEM cell. The best reported CD energy efficiency was 9.5 kW h kg⁻¹ ozone, assuming that the supplies of cooling water and dry, pure oxygen were available.²⁸ The typical energy requirement was 2–3 times this value when drying, cooling, and oxygen purification were all considered. This would make the energy efficiency of the electrochemical route comparable to the CD process.

The effect of current and voltage on efficiency as given in eqn (4) gave some interesting insight into alternatives in the operation of electrolytic ozone generation. The electrochemical route required a higher free energy barrier since the starting raw material is water, compared to oxygen in the CD process. The possibility of electrooxidation of oxygen to ozone exists with the reaction



which is a 2 electron process with an equilibrium potential of 2.03 V. If oxygen was produced electrochemically *via* eqn (1), then the overall process was still a 6 e transfer and the energy consumption remains the same. If, however, oxygen was supplied to the anode, *e.g.* *via* aeration, and with efficient mass-transfer, then there would have been a substantial gain in energy efficiency. The cell voltage may have increased with reaction (5), but the 1/3 reduction in current per ozone produced lead to an overall decrease in energy consumption, as shown in Eqn (4). The concept of the aerated anode therefore warrants further investigation.

On the other hand, there also exists an alternative route of hydrogen evolution to replace the oxygen reduction reaction at the cathode, given as



which has an equilibrium potential of 0 V. The simultaneous production of hydrogen may be desirable in some applications. In renewable energy applications, hydrogen is produced by electrolysis of water as stored or transportable energy. Oxygen is a byproduct of electrolysis that may be discarded. Co-generating of ozone instead of oxygen in electrolytic hydrogen production can be very desirable. The choice of hydrogen evolution in eqn (6) over oxygen reduction in reverse of eqn (1), however, would require a higher operating cell voltage due to the lower equilibrium potential. In addition, water would be consumed and would need to be replenished steadily to keep the function of the PEM cell. The generation of two useful products: hydrogen and ozone are of interest in environmental applications.

Conclusions

The advantages of the electrochemical route for ozone generation are demonstrated with a polymer–electrolyte–membrane (PEM) cell housed with a novel doped tin oxide anode. Compared to the conventional corona discharge process, the ozone concentrations in gas and dissolved phases

were higher, there were no risks of nitrogen oxide byproducts, and improved energy efficiencies were expected. The electrochemical route offers a modular, scalable production. Further improvements and optimization are expected by forced convection, more thoroughly contacted electrolyte-anode interface, and alternatives in anode and cathode operations. The green synthesis of ozone should widen applications of ozonation for a better environment.

Acknowledgements

This research has been supported by a Seed Funding from CRCG and a University Development Fund for Water Environment Engineering in the University of Hong Kong. Continuation of this project is now partially supported by Clarizon Ltd, U.K.

References

- 1 D. G. Korich, J. R. Mead, M. S. Madore, N. A. Sinclair and C. A. Sterling, *Appl. Environ. Microbiol.*, 1990, **56**, 1423.
- 2 N. P. Cheremisinoff, *Handbook of Water and Wastewater Treatment Technology*, Butterworth-Heinemann, Boston, 2002, pp. 449–465.
- 3 B. Langlais, D. A. Reckhow and D. R. Brink, *Ozone in Water Treatment Application and Engineering*, Lewis, Boca Raton, FL, 1991.
- 4 E. Merz and F. Gaia, *Ozone Sci. Eng.*, 1990, **12**, 401.
- 5 P. C. Foller and C. W. Tobias, *J. Electrochem. Soc.*, 1982, **129**, 506.
- 6 E. R. Kotz and S. Stucki, *J. Electroanal. Chem.*, 1987, **228**, 407.
- 7 T. C. Wen and C. C. Chang, *J. Electrochem. Soc.*, 1993, **140**, 2764.
- 8 J. R. Feng, D. C. Johnson, S. N. Lowery and J. J. Carey, *J. Electrochem. Soc.*, 1994, **141**, 2708.
- 9 A. A. Chernik, V. B. Drozdovich and I. M. Zharskii, *Russ. J. Electrochem.*, 1997, **33**, 259.
- 10 N. Katsuki, E. Takahashi, M. Toyoda, T. Kurosu, M. Iida, S. Wakita, Y. Nishiki and T. Shimamune, *J. Electrochem. Soc.*, 1998, **145**, 2358.
- 11 S. G. Park, G. S. Kim, J. E. Park, Y. Einaga and A. Fujishima, *J. New Mater. Electrochem. Syst.*, 2005, **8**, 65.
- 12 L. M. Dasilva, M. H. P. Santana and J. F. C. Boodts, *Quim. Nova*, 2003, **26**, 880.
- 13 S. D. Han, J. D. Kim, K. C. Singh and R. S. Chaudhary, *Ind. J. Chem.*, 2004, **43A**, 1599.
- 14 S. A. Cheng and K. Y. Chan, *Electrochem. Solid-State Lett.*, 2004, **7**, D4.
- 15 Y. H. Wang, K. Y. Chan, S. A. Cheng and X. Y. Li, *J. Electrochem. Soc.*, 2005, **152**, D197.
- 16 Y. J. Feng and X. Y. Li, *Water Res.*, 2003, **37**, 2399.
- 17 M. A. Quiroz, S. Reyna and J. L. Sanchez, *J. Solid State Electrochem.*, 2003, **7**, 277.
- 18 Y. H. Wang, K. Y. Chan, X. Y. Li and S. K. So, *Chemosphere*, in press.
- 19 K. Rakness, G. Gordan, B. Langlais, W. Masschelein, N. Matsumoto, Y. Richard, C. M. Robson and I. Somya, *Ozone Sci. Eng.*, 1996, **18**, 209.
- 20 J. B. Fernando, *Ozone Reaction Kinetics for Water and Wastewater Systems*, Lewis, Boca Raton, FL, 2004, pp. 78.
- 21 A. K. Bin, *Exp. Therm. Fluid Sci.*, 2004, **28**, 295.
- 22 K. Koike, T. Fukuda, S. Ichimura and A. Kurokawa, *Rev. Sci. Instrum.*, 2000, **71**, 4182.
- 23 E. Coleman, T. Siegrist, D. A. Mixon, P. L. Trevor and D. J. Trevor, *J. Vac. Sci. Technol., A*, 1991, **9**, 2408.
- 24 P. Tatapudi and J. M. Fenton, *J. Electrochem. Soc.*, 1993, **140**, 3527.
- 25 P. Tatapudi and J. M. Fenton, *J. Electrochem. Soc.*, 1994, **141**, 1174.
- 26 K. Onda, T. Ohba, H. Kusunoki, S. Takezawa, D. Sunakawa and T. Araki, *J. Electrochem. Soc.*, 2005, **152**, D177.
- 27 S. Stucki, H. Baumann, H. J. Christen and R. Kotz, *J. Appl. Electrochem.*, 1983, **17**, 773.
- 28 S. Hanft, *Ozone Generation: Technologies, Markets and Players*, B.C.C. Business Opportunity Report, Business Communications Company Inc., Norwalk, CT, U.S.A., 2004, pp. 150.

Surface cleaning under combined microwave and ultrasound irradiation: flash synthesis of 4*H*-pyrano[2,3-*c*]pyrazoles in aqueous media

Yanqing Peng, Gonghua Song* and Ruiling Dou

Received 26th January 2006, Accepted 26th April 2006

First published as an Advance Article on the web 18th May 2006

DOI: 10.1039/b601209d

A clean, rapid and energy-efficient approach to solid–aqueous heterogeneous reactions was developed utilizing the synergistic effect of microwave and ultrasound irradiation. The dramatic acceleration in reaction rates might be explained by the removal of a passivation coating on the substrate particles and the resultant enhancement in mass and heat transfer.

Introduction

To achieve the goal of sustainability, the “greening” of chemical processes has become a major issue in academia and industry. The search for alternative reaction media to replace volatile, flammable and often toxic solvents commonly used in organic synthetic procedures is an important objective of the development of green chemical processes.¹ From both the environmental and economic points of view, using aqueous media to perform organic reactions has attracted intense interest, since water is considered to be the most environmentally acceptable, safe and inexpensive solvent.² In addition, using water as the solvent generally means easier workup because most organic compounds are lipophilic and are easily separated from aqueous media.

However, implementation of many organic reactions in water is not straightforward due to its intrinsic limitation related to the problem of reacting hydrophilic reagents with hydrophobic substrates in heterogeneous systems. In the case of aqueous reactions between hydrophobic organic particles and water-soluble reagents, another unavoidable problem one might encounter is the formation of a capsule-like passivating layer on the surface of substrate particles due to the poor water-solubility of the products. The precipitation on the surface of the substrate may decelerate (or even interrupt) the mass transfer between substrate and reagent in aqueous media, and therefore slow or stop the reaction. This problem could be addressed by using polar water-miscible organic co-solvents.² Unfortunately, this defeats the original intention of reducing the environmental burden of organic contaminants and, furthermore, complicates work-up procedures. In order to circumvent this dilemma, therefore, an alternative, eco-friendly method that would enable efficient execution of these reactions is highly desirable.

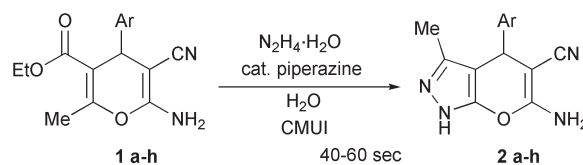
Previous work from our group has demonstrated that combined microwave and ultrasound irradiation (CMUI) gave significant rate enhancements and improved yields in aqueous organic reactions, such as hydrazinolysis of esters,³ Williamson ether synthesis,⁴ Knoevenagel–Doebner reactions⁵

and Mannich reactions.⁶ To overcome the above-mentioned limitation, we considered an alternative approach that takes advantage of the synergy between microwave and ultrasound irradiation. In particular, we thought that the employment of the CMUI technique, if applicable to the model reaction, might solve some of the operational problems associated with the surface passivation in aqueous synthesis.

4*H*-Pyrans constitute the structural unit of a series of natural products,⁷ photoactive materials⁸ and drug candidates.⁹ For example, a 4*H*-pyran derivative, ethyl 2-amino-6-bromo-4-(1-cyano-2-ethoxy-2-oxoethyl)-4*H*-chromene-3-carboxylate (HA14-1), has been found to bind Bcl-2 protein and induce apoptosis of tumor cells.^{9b} Thus, the synthesis of 4*H*-pyrano[2,3-*c*]pyrazoles was chosen as a “proof-of-concept” reaction in our investigation. To identify the generality of the protocol, substrates bearing both electron-donating and -withdrawing substituents on phenyl were employed (Scheme 1). Although this reaction is thermodynamically favored in polar organic solvents,¹⁰ it is slow in water.

Results and discussion

As a starting point for the development of our methodology we chose the transformation of 5-ethoxycarbonyl-2-amino-4-phenyl-3-cyano-6-methyl-4*H*-pyran, **1a-h**, as a model. A mixture of powdered **1a-h** (100–120 mesh), aqueous hydrazine monohydrate and a catalytic amount of piperazine was heated under different conditions and the time–conversion profiles were determined by HPLC. Very recently, Sharpless' group has found that some organic reactions, such as Diels–Alder reactions, ene reactions, Claisen rearrangements, and nucleophilic opening of epoxides, showed unexpected reactivity in aqueous suspensions.¹¹ However, our control experiment failed under aqueous suspension conditions. As illustrated in Fig. 1, when heated by a thermostatted oil bath under vigorous



Scheme 1

Shanghai Key Laboratory of Chemical Biology, Institute of Pesticides & Pharmaceuticals, East China University of Science and Technology, Shanghai, 200237, China. E-mail: ghsong@ecust.edu.cn; Fax: +86-21-64252603; Tel: +86-21-64252945

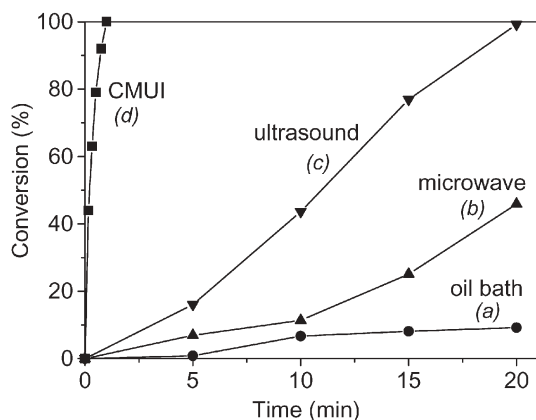


Fig. 1 Time-conversion diagram for the model reaction under various conditions.

magnetic stirring, the model reaction was found to proceed sluggishly, and only 9% conversion of starting material was observed within 20 min [curve (a)]. Interestingly, the trend of the rate-enhancement of different conditions in this reaction is not fully consistent with that observed in our previous investigations.^{3–6} We were surprised that an unexpectedly long reaction time was required to obtain the desired 4*H*-pyrano[2,3-*c*]pyrazole in a reasonably high yield, even with microwave irradiation (power level: 200 W). In contrast, the ultrasound-promoted (power level: 50 W; frequency: 20 KHz) oil bath-heated reaction proceeded much faster than the reaction carried out with microwave irradiation (99% vs. 48% conversion, 20 min). Hence, the rate-limiting step in these reactions might be the mass transfer at the solid-liquid interface. To show the usefulness of CMUI, a control experiment was carried out using the same amount of reactants with the apparatus we described previously (microwave 200 W/2450 MHz + ultrasound 50 W/20 KHz).³ As expected, a dramatic acceleration in reaction rate was observed, with the conversion increasing to 100% within 1 min [curve (d)], indicating the critical role of the sonication for the success of this reaction.

Using the optimized reaction conditions, we next investigated the substrate generality. Various 5-ethoxycarbonyl-2-amino-4-aryl-3-cyano-6-methyl-4*H*-pyrans, **1a–h**, were treated with hydrazine monohydrate in water under CMUI (Table 1). In all cases, reaction times ranged from 40 to 60 seconds and the yields were very high (89–93%). All products are known

compounds and their structures were confirmed by melting point, IR, NMR and MS data.

A likely explanation for this dramatic rate enhancement is as follows. In many heterogeneous reactions, the rate-determining step is the mass transfer process at the interface between two (or more) phases. Since the product, 4*H*-pyrano[2,3-*c*]pyrazole, is insoluble in the aqueous phase, it presumably forms a thin layer on the surface of particles, which decelerates (or even prevents) the mass transfer between the substrate and reagent in aqueous media. It could be predicted that the removal of this inactive surface coating would result in dramatic acceleration of reaction rates. Irradiation of liquids by power ultrasound leads to cavitation phenomena. When a passivation coating is present on the solid surface, the shock waves from cavitation collapse will remove it and provide a cleaner surface. As a result, the mass transfer near the surface will be enhanced.¹² In addition, shock waves exert large forces on small particles, producing high-velocity interparticle collisions. The particles collide with each other in a random manner with large impact forces (the so-called grinding effect).¹³ In this way, product coatings on the surface could be peeled off, and brittle solids may be shock-fragmented to give an increased surface area. As a result, the reactions can be carried out efficiently without any organic co-solvent, despite the poor solubility of substrates in aqueous media.

The development of high-speed synthesis is strongly needed for both laboratory synthesis and industrial production. With faster reactions, a greater quantity of compounds can be produced per unit time. As discussed by Clark and his colleagues,¹⁴ the energy-efficiency is also an important criterion in evaluating the “greenness” (environmental acceptability and economic viability) of a reaction process. Apparently, our flash protocol provides a significant reduction in energy consumption in comparison with other routes.

Conclusion

In summary, we have demonstrated our strategy for aqueous organic reactions using the synergistic effect of microwave and ultrasound irradiation by utilizing “proof-of-concept” models. Importantly, the strategy described above should not be limited to the model reactions but could in principle be applied to other aqueous organic reactions as well. This work will not only lead to a practical synthetic method but also expand the versatility of clean organic reactions in water.

Table 1 Aqueous synthesis of 4*H*-pyrano[2,3-*c*]pyrazole under CMUI

Product	Ar	Time/s	Yield (%) ^a	Mp/°C (obs.)	Mp/°C (lit.)
2a	C ₆ H ₅	50	90	245–246	244–245 ¹⁶
2b	4-CH ₃ O-C ₆ H ₄	55	92	212–213	210 ¹⁷
2c	4-OH-C ₆ H ₄	60	89	223–224	225–226 ¹⁸
2d	4-NO ₂ -C ₆ H ₄	40	92	251–252	251–252 ¹⁶
2e	4-Cl-C ₆ H ₄	40	93	234–235	235 ¹⁷
2f	2-Cl-C ₆ H ₄	40	92	245–246	247–249 ¹⁹
2g	3-CH ₃ O-4-OH-C ₆ H ₃	60	92	233–234	233–235 ¹⁶
2h	3-Br-C ₆ H ₄	45	90	223–224	223–224 ¹⁶

^a Isolated yields.

Experimental

The starting 5-ethoxycarbonyl-2-amino-4-aryl-3-cyano-6-methyl-4*H*-pyrans **1a–h** were readily prepared from aromatic aldehydes, malononitrile and ethyl acetoacetate.¹⁵

Typical procedure under CMUI

Piperazine (0.03 g, 0.4 mmol) and 85% N₂H₄·H₂O (0.30 g, 6.0 mmol) were added to a suspension of powdered **1** (5.0 mmol, particle diameter: 100–120 mesh) in 10 mL of water. The mixture was then treated under combined microwave and ultrasound irradiation for the indicated duration. The crude product was collected by filtration, washed with water and air dried. Recrystallization from ethanol afforded pure 6-amino-3-methyl-5-cyano-4-aryl-1,4-dihydropyran[2,3-*c*]pyrazoles **2**. All products are known and gave ¹H NMR, FT-IR and MS (EI) spectra consistent with the assigned structures.

Selected spectral data: 6-amino-3-methyl-5-cyano-4-(3-bromophenyl)-1,4-dihydropyran[2,3-*c*]pyrazole **2h**: FT-IR (KBr) ν_{\max} 3410, 3370, 3320, 3315, 3180, 2975, 2920, 2195, 1645, 1610, 1605, 1490, 1400, 1160, 1070, 1040, 885, 780, 750, 690 cm⁻¹; ¹H NMR (500 MHz, DMSO-*d*₆) δ_{H} 1.80 (s, 3H, CH₃), 4.62 (s, 1H, 4-H), 6.98 (s, 2H, NH₂), 7.17 (d, 1H, *J* = 7.6 Hz, ArH), 7.28 (t, 1H, *J*₁ = 7.8 Hz, *J*₂ = 7.8 Hz, ArH), 7.34 (s, 1H, ArH), 7.42 (d, 1H, *J* = 8.9 Hz, ArH), 12.16 (s, 1H, NH) ppm; MS (EI) *m/z* 332.0 (M⁺, 5), 264.0 (18), 185.1 (19), 175.1 (100), 128.1 (29), 109.0 (38), 66.0 (19).

Acknowledgements

Financial support from the NSFC (Grant 20376022), the National Key Project for Basic Research (2003 CB 114402, The Ministry of Science and Technology of China) and the Shanghai Educational Commission is gratefully acknowledged.

References

- (a) M. Poliakov, J. M. Fitzpatrick, T. R. Farren and P. T. Anastas, *Science*, 2002, **297**, 807; (b) J. M. DeSimone, *Science*, 2002, **297**, 799.
- For selected reviews, see: (a) C.-J. Li, *Chem. Rev.*, 1993, **93**, 2023; (b) S. Ribe and P. Wipf, *Chem. Commun.*, 2001, 299; (c) U. M. Lindstrom, *Chem. Rev.*, 2002, **102**, 2751; (d) C. C. Tzschucke, C. Markert, W. Bannwarth, S. Roller, A. Hebel and R. Haag, *Angew. Chem., Int. Ed.*, 2002, **41**, 3964.
- Y. Peng and G. Song, *Green Chem.*, 2001, **3**, 302.
- Y. Peng and G. Song, *Green Chem.*, 2002, **4**, 349.
- Y. Peng and G. Song, *Green Chem.*, 2003, **5**, 704.
- Y. Peng, R. Dou, G. Song and J. Jiang, *Synlett*, 2005, 2245.
- S. Hatakeyama, N. Ochi, H. Numata and S. Takano, *J. Chem. Soc., Chem. Commun.*, 1988, 1202.
- D. Arnetso, W. M. Horspool, N. Martin, A. Ramos and C. Seane, *J. Org. Chem.*, 1989, **54**, 3069.
- (a) J. Zamocka, E. Misikova and J. Durinda, *Pharmazie*, 1991, **46**, 610; (b) J. L. Wang, D. Liu, Z. J. Zheng, S. Shan, X. Han, S. M. Srinivasula, C. M. Croce, E. S. Alnemri and Z. Huang, *Proc. Natl. Acad. Sci. U. S. A.*, 2000, **97**, 7124.
- N. M. Abed, N. S. Ibrahim and M. H. Elnagdi, *Z. Naturforsch., B: Anorg. Chem. Org. Chem.*, 1986, **41**, 925.
- S. Narayan, J. Muldoon, M. G. Finn, V. V. Fokin, H. C. Kolb and K. B. Sharpless, *Angew. Chem., Int. Ed.*, 2005, **44**, 3275.
- (a) W. Lauterborn and W. Hentschel, *Ultrasonics*, 1985, **23**, 260; (b) T. J. Mason, *Chem. Soc. Rev.*, 1997, **26**, 443.
- (a) S. J. Doktycz and K. S. Suslick, *Science*, 1990, **247**, 1067; (b) T. Prozorov, R. Prozorov and K. S. Suslick, *J. Am. Chem. Soc.*, 2004, **126**, 13890.
- M. J. Gronnow, R. J. White, J. H. Clark and D. J. Macquarrie, *Org. Process Res. Dev.*, 2005, **9**, 516.
- Y. Peng, G. Song and F. Huang, *Monatsh. Chem.*, 2005, **136**, 727.
- Y. A. Sharanin, L. G. Sharanina and V. V. Puzanova, *J. Org. Chem. USSR (Engl. Transl.)*, 1983, 2291.
- A. A. Harb, A. M. Hesien, S. A. Metwally and M. H. Elnagdi, *Liebigs Ann. Chem.*, 1989, 585.
- A. S. Fahmy, S. M. Sadek, K. U. Elnagdi and M. Hilmy, *Heterocycles*, 1981, **16**, 2177.
- F. F. Abdel-Latif, *Z. Naturforsch., B: Chem. Sci.*, 1990, **45**, 1675.

Continuous esterification or dehydration in supercritical carbon dioxide

Hassan S. Ghaziaskar,^{*a} Ali Daneshfar^a and Lourdes Calvo^b

Received 3rd January 2006, Accepted 27th March 2006

First published as an Advance Article on the web 24th April 2006

DOI: 10.1039/b518463k

This paper describes a study conducted on the catalytic esterification of 2-ethylhexanoic acid with 2-ethyl-1-hexanol in supercritical carbon dioxide (SC-CO₂). The effect of pressure (150–250 bar), temperature (75–140 °C), flow rate of CO₂ (0.36–0.72 g min⁻¹), mole ratio of the alcohol to the acid (0.5–2), and the type of catalyst (Amberlyst[®] 15 as a strong solid-acid catalyst, zirconium oxide as a Lewis acid catalyst, and Novozym 435 as an enzymatic catalyst) has been evaluated. The ester, 2-ethylhexyl 2-ethylhexanoate, was continuously synthesized with 100% selectivity and 40% conversion using zirconium oxide, while the enzymatic catalysis gave no significant conversion (3%) due to acid inactivation. Amberlyst[®] 15 preferentially catalyzed the dehydration of 2-ethyl-1-hexanol to produce 2-ethyl-1-hexene. High temperatures favoured this reaction, so at 140 °C and 150 bar, the conversion to alkene was 99%. This catalyst was stable within the explored pressure interval. An excess of acid resulted in higher ester yield, while increasing the flow rate had no significant impact. Supercritical conditions were compared to liquid phase conditions in n-hexane. The results proved that the conversion to substrates was higher in SC-CO₂, although the selectivity changed. Results were related to the solvating capacity and mass transport properties of the supercritical solvent.

Introduction

In the past decade, supercritical fluids have received extensive attention as green solvents for chemical reactions,^{1–6} and the extraction of organic^{7,8} and inorganic compounds⁹ from different matrices. Supercritical carbon dioxide (SC-CO₂) is an attractive and suitable solvent for chemical reactions because of its low critical temperature (31.3 °C) and moderate critical pressure (73.8 bar), its non-toxicity, high diffusivity, solvent strength variability, and the ease of separating the solvent from the products.

Heterogeneous catalytic chemical reactions in SC-CO₂ are generally performed in the continuous flow mode but they can also be performed in batch reactors.¹⁰ Examples of such processes are dehydration,^{11,12} esterification,¹³ and hydrogenation¹⁴ reactions.

High molecular weight esters can be used as food additives, in cosmetics, for pharmaceutical uses, and as lubricants.¹⁵ The production of these esters is usually carried out under equilibrium conditions and can be shifted towards the products by using an excess of the reactants (alcohol or acid) or by removal of the products (ester or water) from the reaction vessel. In liquid phase esterification using a Dean–Stark apparatus, water-insoluble solvents such as benzene, toluene, or carbon tetrachloride are used to separate out the water, and shift the equilibrium toward the products.¹⁶

The catalytic dehydration of alcohols to the respective alkene is gaining increasing importance as a synthetic

methodology. Since a highly acidic medium is required, the direct dehydration of an alcohol to an alkene is problematic under normal conditions, and side reactions may occur, reducing product quality.¹⁷ As an industrially useful example, isobutene can be synthesized from the dehydration of *t*-butyl alcohol for the production of methyl *t*-butyl ether and other high-octane gasoline components.¹⁸

The aim of this work has been to investigate the synthesis of 2-ethylhexyl 2-ethylhexanoate (2E2E) from the esterification of 2-ethylhexanoic acid with 2-ethyl-1-hexanol in the presence of Amberlyst[®] 15 as a strong solid-acid catalyst, zirconium oxide as a Lewis acid catalyst, and the lipase Novozym 435 as an enzymatic catalyst. As side reactions, the dehydration of 2-ethyl-1-hexanol to produce 2-ethyl-1-hexene (2E1H) and the dehydration of two molecules of the alcohol to produce the symmetrical 2-ethylhexyl ether (2EHE) have been followed. The effect of the reaction temperature, pressure, CO₂ flow rate, the molar ratio of the substrates, and the type of catalyst on the conversion of the substrates has been explored. Since this reaction has not been reported under normal conditions using the catalysts used in this work, the reaction was also performed in n-hexane. The results have been compared to establish the advantages of using a supercritical fluid *versus* the use of an organic solvent.

Knowledge of the phase behaviour is a requirement for designing heterogeneous catalytic reactions under near or supercritical conditions. Therefore, the solubility of the reactants in SC-CO₂ was previously studied.¹⁹ The solubility of 2-ethyl-1-hexanol and 2-ethylhexanoic acid in SC-CO₂ (1 : 1 molar ratio in the equilibrium cell) was found to be similar over the pressure range of 95–180 bar. This finding was related to the existence of intermolecular hydrogen bonding between molecules of 2-ethyl-1-hexanol and 2-ethylhexanoic acid.²⁰

^aDepartment of Chemistry, Isfahan University of Technology, Isfahan, 84156-83111, Iran. E-mail: ghazi@cc.iut.ac.ir; Fax: +98-311-3912350; Tel: +98-311-3913260

^bDepartamento de Ingeniería Química, Facultad de Ciencias Químicas, Universidad Complutense de Madrid, Avda. Complutense s/n, Madrid, 28040, Spain

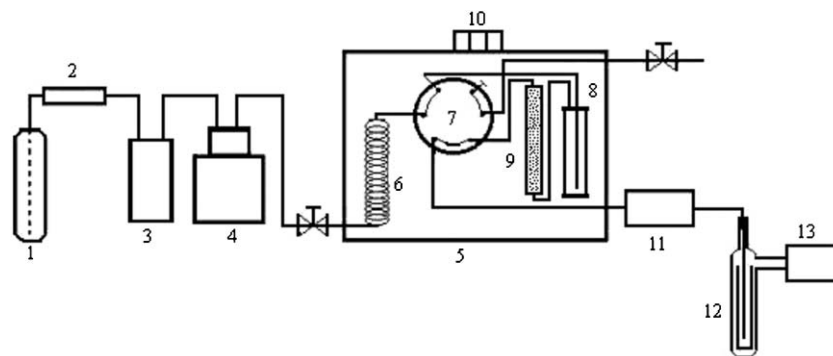


Fig. 1 Scheme of the continuous flow apparatus. 1: CO₂ capsule, 2: purifier, 3: cooling bath, 4: pump, 5: oven, 6: preheating coil, 7: two-position six-port valve, 8: equilibrium cell, 9: catalyst bed, 10: thermocouple and temperature controller, 11: backpressure regulator, 12: collection system, 13: wet gas flow meter.

Experimental

Materials

Carbon dioxide with purity of 99.95% was purchased from ZamZam Co. Ltd (Isfahan, Iran). 2-Ethyl-1-hexanol, 1-hexanol, n-hexane, and Amberlyst[®] 15 were purchased from Merck. The Amberlyst[®] 15 (strongly acidic cation exchanger, macroporous in H⁺ form) was dried to constant weight in an air oven at 90 °C, before use. The catalyst acid capacity was 4.81 meq g⁻¹, measured by titration against standard base.²¹ Zirconium oxide catalyst was prepared from zirconyl(IV) chloride octahydrate (ZrOCl₂·8H₂O, purity >99%, from Merck) as previously reported.¹⁷ 2-Ethylhexanoic acid was purchased from Tat Chemical Co. (purity >99%, Isfahan, Iran). 2-Ethylhexyl 2-ethylhexanoate and 2-ethylhexyl ether were synthesized in toluene using *p*-toluenesulfonic acid (Farzin Chemicals Co., Isfahan, Iran) as catalyst. The achieved purity in both cases was >99%, as verified by GC-FID. Novozym 435, a lipase from *Candida antarctica*, immobilized on a macroporous acrylic resin with a water content of 1–2 wt%, was kindly provided by Novo Nordisk, Denmark.

Apparatus and procedure

The esterification reaction was carried out using the continuous flow apparatus shown in Fig. 1. The major components included a carbon dioxide feeding line, a preheater, an equilibrium cell where CO₂ was saturated by the reactants, a fixed catalyst bed, a pressure control device, and a product collection system. The CO₂ was pumped by a JASCO model PU-980 reciprocating pump. The preheater consisted of 316 ss coiled 1/16" ss tubing. The equilibrium cell had a volume of 8 ml and was filled with glass beads in order to decrease the cell dead volume and increase the contact area between the substrates and the CO₂. The tubular reactor, made of 316 ss, had an internal volume of 15 ml and contained 8–9 g of catalyst. These three elements were placed in an air oven to keep the temperature within ±1 °C using a thermocouple controller device (Alton Ray Co., model TC14, Tehran, Iran). The pressure was controlled by a backpressure regulator (JASCO BP 1580–81) to within ±1 bar. The effluent was quenched in the system shown in Fig. 2, consisting of a condenser and a coil which used an aqueous ethylene glycol

solution as the refrigerant. The liquid product was collected in a two-neck 5 ml flask that was immersed into a 250 ml beaker filled with the same cooling solution. The temperatures of the collection flask and the condenser were maintained at –12 °C and –8 to –10 °C respectively.

At the beginning of each experiment, the carbon dioxide was pressurized and circulated through the preheating coil to reach the operating temperature before entering the equilibrium cell, where the desired amount of 2-ethyl-1-hexanol and 2-ethylhexanoic acid was placed. Then, the SC–CO₂ saturated with the substrates went through the catalytic bed. The SC–CO₂, along with the products and unreacted species, was depressurized through the backpressure regulator, and solutes were gathered in the sample collection system. The same procedure was followed when n-hexane was used as solvent. After each assay, the catalytic bed was washed with n-hexane and dried for the next run.

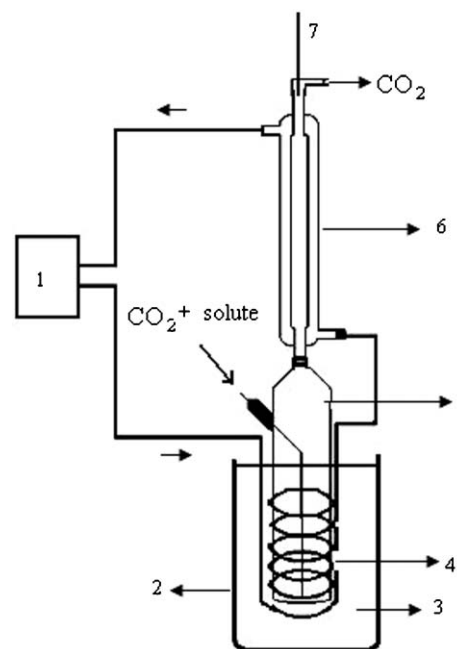


Fig. 2 Scheme of the product collection system. 1: cooling fluid pump, 2: beaker, 3: cooling liquid, 4: coil, 5: collection vial, 6: condenser, 7: thermometer.

Reported yields were affected by the way the components were collected at the exit of the system, so different purge tests were performed with (1) glass beads, (2) n-hexane or (3) glass beads plus n-hexane in the collection flask. The results after a 6 hour run are reported as the trapping efficiency in Table 1. By using the third method of collection, the solute loss due to aerosol formation and entrainment was significantly reduced, being lower than 5% for the alcohol and 4% for the acid and the ester. Therefore, this method was used to conduct all the experimental work, providing a mass balance closure higher than 95%.

Analytical method

After addition of 1 ml of 1-hexanol as an internal standard, the trapped mixture was transferred to a volumetric flask and made up to 5 ml with n-hexane. The samples were analyzed with GC-TCD (Shimadzu Co. model GC-14A) with a packed SE-30 column using the following temperature programming: the GC injection port and the detector temperature were set at 240 °C and 250 °C respectively, the column temperature was programmed from 50 °C to 90 °C at a rate of 6 °C min⁻¹, and from 90 °C to 240 °C at a rate of 40 °C min⁻¹. Peak identification of 2E2E and 2EHE was accomplished by comparison of sample peak retention times with those of standard solutions. Alkene presence was verified by passing the gases exiting from the trap through a dilute solution of bromine in carbon tetrachloride and observing that the solution was decolorized. Moreover, the exit gases were quenched in a 2.5 m long, 1.5 mm i.d. 316 ss tubing immersed in a thermostatted water bath at 5 °C, and analyzed by GC-MS (Trio 1000, Fisons Instruments, model 8060) confirming the presence of the alkene. No other products were detected, so only the ester, the ether and the alkene were used to calculate yield and selectivity. Average uncertainty in reported data was less than 10%.

The molar percentage yield of 2E2E and 2EHE was defined as the amount of each compound produced from the initial quantity of 2-ethyl-1-hexanol. Alkene yield was determined on the basis of mass balance calculations as the difference between the initial moles of 2-ethyl-1-hexanol and the moles of ester and ether produced and the moles of unreacted 2-ethyl-1-hexanol.

Conversion was defined based on alcohol disappearance. In SC-CO₂ experiments with Amberlyst[®] 15, conversion was 100% in all cases since no alcohol was detected on the effluent. Moreover, at the end of each experiment the catalytic bed was

Table 1 Purge tests for 2-ethyl-1-hexanol (2E1He), 2-ethylhexanoic acid (2EHA), and 2-ethylhexyl 2-ethylhexanoate (2E2E)^a

Purge method	Trapping efficiency (%)		
	2E1He	2EHA	2E2E
1 ^b	66.5	72.1	71.4
2 ^c	89.4	94.5	93.6
3 ^d	94.6	96.8	95.7

^a Reaction conditions: CO₂ flow rate = 0.54 g min⁻¹; pressure = 150 bar; temperature = 110 °C; time of purge = 6 h. ^b Recovery on glass beads. ^c Recovery in n-hexane. ^d Recovery on glass beads and n-hexane.

washed with n-hexane and the solution was analyzed by GC-TCD, and no alcohol was detected in the solution.

Results and discussion

In the following sections, the effect of operating conditions, substrate molar ratio and solvent flow rate on the continuous esterification of 2-ethylhexanoic acid with 2-ethyl-1-hexanol in SC-CO₂ is discussed. For these experiments, a strong acid catalyst (Amberlyst[®] 15) was used. Then, other catalysts were explored. Side reactions were also followed, *i.e.* the formation of the ether and the alkene. The use of a supercritical solvent was compared to the use of a typical organic one because the investigation of whether the catalytic activity of the materials changed under supercritical conditions is of crucial importance in scaling-up the process. All experiments were carried out ensuring saturation conditions, so the CO₂ to substrate molar ratio and the substrate flow rate (*F*) were estimated from the solubility values reported elsewhere.¹⁹ The contact time (*W/F*) between the substrates and the catalyst was calculated as (mass of catalyst)/(mass of substrates per min), and is reported in min.

Effect of temperature

Temperature may affect the esterification yield in different ways. On one hand, an increase in temperature would have a positive effect on the kinetic constant, as defined by the transition state theory. However, high temperatures may promote side reactions, such as dehydration, if their activation energy is higher than that of esterification, reducing the ester yield. On the other hand, high temperatures would decrease density and so solubility of reactants, which can reduce the rate of the esterification reaction. Therefore, the effect of temperature is not easy to predict.

The production of 2E2E, 2EHE, and 2E1H from 2-ethyl-1-hexanol and 2-ethylhexanoic acid in SC-CO₂ at different temperatures and 150 bar is shown in Table 2. Raising the temperature from 75 to 110 °C increased the yield of 2E2E and 2EHE. A further increase in temperature from 110 to 140 °C reduced the conversion of the reactants (alcohol and acid) to the ester significantly. This decrease in ester yield could be attributed to the promotion of the dehydration reaction. Due to the high selectivity towards the alkene at these conditions,

Table 2 The formation of 2-ethylhexyl 2-ethylhexanoate (2E2E), 2-ethylhexyl ether (2EHE) and 2-ethyl-1-hexene (2E1H) from 2-ethyl-1-hexanol and 2-ethylhexanoic acid in SC-CO₂ at different temperatures^a

<i>T</i> /°C	CO ₂ /alcohol/acid ^b molar ratio	<i>W/F</i> ^b /min	Yield (%)		
			2E2E	2EHE	2E1H
75	77.2 : 1.2 : 1.0	268	15.2	ND	84.8
110	217.3 : 1.5 : 1.0	667	22.5	2.1	75.4
140	512.7 : 1.8 : 1.0	1402	0.2	0.9	98.9

^a Other reaction conditions: catalyst = Amberlyst[®] 15 (amount = 8.5 g); CO₂ flow rate = 0.36 g min⁻¹; pressure = 150 bar; initial alcohol/acid molar ratio in the equilibrium cell = 1.0. ND: not detected. ^b Estimated by extrapolation of the solubility values reported in ref. 19.

the method could be used for the dehydration of the alcohol to the alkene with high yield (98.8%) in a continuous system.

Effect of pressure

Pressure affects reaction rate in supercritical fluids in two ways. First, the reaction rate constant may change with pressure. Secondly, pressure can vary some physical parameters, such as the partition coefficient, dielectric constant, and fluid Hildebrand solubility parameter. Effectively, by increasing the pressure, the solubility of 2-ethyl-1-hexanol and 2-ethylhexanoic acid in CO₂ is increased.¹⁹ If the solubility is increased, then solvent load is higher, and at equal total flow rate, the amount of reactants passing through the catalyst bed per unit of time is higher. Consequently, residence time of the reactants is also increased as pressure is raised.

The effect of pressure on ester production was investigated between 150 and 250 bar, at a temperature of 110 °C, and is reported in Table 3. The results showed that conversions were approximately constant, *i.e.* independent of the pressure. This behaviour might be due to the fact that at a pressure beyond 130 bar, the solubility of 2-ethyl-1-hexanol and 2-ethylhexanoic acid is nearly constant (*i.e.*, the solubility is in the plateau portion of the solubility–pressure curve).¹⁹ It also means that the change in pressure did not significantly affect solvent properties (*e.g.* solvation capacity or mass transfer properties). In any case, the Amberlyst[®] 15 catalytic activity did not decrease either, indicating that this catalyst was stable at high pressures.

Effect of CO₂ flow rate

The influence of solvent flow rate was investigated within the interval 0.36–0.72 g min⁻¹. Results are reported in Table 4. No significant changes in process yield were observed. This implies that within the interval of explored flow rates, the solvent remained saturated by the alcohol and the acid, and the contact time with the solid catalyst was enough to achieve maximum conversion in all cases. It also means that the external mass transport did not control the process, which in consequence would be controlled by internal diffusion or equilibrium. However, it is expected that mass transport resistance within the pores is minimized due to the high diffusivity of compounds in supercritical fluids, as will be shown later.

Table 3 The formation of 2E2E, 2EHE and 2E1H from 2-ethyl-1-hexanol and 2-ethylhexanoic acid in SC–CO₂ at different pressures^a

P/bar	Yield (%)		
	2E2E	2EHE	2E1H
150	22.5	2.1	75.4
200	21.0	2.0	77.0
250	27.4	2.9	69.7

^a Other reaction conditions: catalyst = Amberlyst[®] 15 (amount = 8.5 g); CO₂ flow rate = 0.36 g min⁻¹; Temperature = 110 °C; Initial alcohol/acid molar ratio in the equilibrium cell = 1.0; CO₂/alcohol/acid molar ratio entering the reactor = 217 : 1.5 : 1.0; W/F = 667 min (assuming that pressure did not significantly affect substrate solubility as indicated in ref.19).

Table 4 The formation of 2E2E, 2EHE and 2E1H from 2-ethyl-1-hexanol and 2-ethylhexanoic acid in SC–CO₂ at different CO₂ flow rates^a

CO ₂ flow rate/g min ⁻¹	W/F ^b /min	Yield (%)		
		2E2E	2EHE	2E1H
0.36	667	15.2	ND	84.8
0.54	444	12.2	ND	87.8
0.72	333	16.0	ND	84.0

^a Other reaction conditions: catalyst = Amberlyst[®] 15 (amount = 8.5 g); temperature = 110 °C; pressure = 150 bar; initial molar ratio of the alcohol to the acid = 1.0; CO₂/alcohol/acid molar ratio^b = 217 : 1.5 : 1.0. ND: not detected. ^b Estimated by extrapolation of the solubility values reported in ref.19.

Effect of molar ratio of reactants

The initial molar ratio (*R*) of 2-ethyl-1-hexanol to 2-ethylhexanoic acid in the equilibrium cell was varied from 0.5–2. It was previously proven that the variation of this ratio also affected the solubility in CO₂.¹⁹ For example, at 60 °C and 138 bar, the solubility of the alcohol increased as *R* was raised. The opposite happened to the acid. Moreover, it was shown that in SC–CO₂ the alcohol to acid molar ratio was closer to the proportion in the equilibrium cell. Consequently, the molar composition of the CO₂–substrate mixture and the proportion between the reactants entering the reactor would be different if *R* is varied. In similar fashion, the contact time with the catalyst would be altered too. Therefore, the impact of this parameter on process yield was investigated. The results are presented in Table 5. When the acid was in excess, the yield of 2E2E and 2EHE was increased. This could be due to the fact that the esterification yield is controlled by protonation of 2-ethylhexanoic acid, so a surplus of this compound would favour the ester production *versus* the dehydration product. In contrast, an excess of alcohol did not exert a significant effect.

Effect of catalyst type

From the results presented up to now, it can be concluded that Amberlyst[®] 15 can not selectively catalyze the esterification reaction under any conditions. In fact, the alcohol dehydration to produce the alkene seemed to be the preferential reaction on this strong acid catalyst. Therefore, to increase the selectivity of the reaction towards ester formation, the reaction was carried out in the presence of a softer acidic catalyst and an enzyme.

Table 5 The formation of 2E2E, 2EHE and 2E1H from 2-ethyl-1-hexanol and 2-ethylhexanoic acid in SC–CO₂ with different initial molar ratios of the alcohol to the acid (*R*)^a

<i>R</i>	Yield (%)		
	2E2E	2EHE	2E1H
0.5	31.9	11.6	56.5
1.0	22.5	2.1	75.4
2.0	24.6	3.4	72.0

^a Other reaction conditions: catalyst = Amberlyst[®] 15 (amount = 8.5 g); CO₂ flow rate = 0.36 g min⁻¹; temperature = 110 °C; pressure = 150 bar.

Table 6 The formation of 2E2E, 2EHE and 2E1H from 2-ethyl-1-hexanol and 2-ethylhexanoic acid in SC-CO₂ using different catalysts^a

Catalyst	Yield (%)		
	2E2E	2EHE	2E1H
Amberlyst [®] 15	22.5	2.1	75.4
Zirconium oxide	40.4	ND	ND
Novozym 435	3.4	ND	ND

^a Other reaction conditions: CO₂ flow rate = 0.36 g min⁻¹; temperature = 110 °C; initial alcohol/acid molar ratio in the equilibrium cell = 1.0; CO₂/alcohol/acid molar ratio entering the reactor = 217 : 1.5 : 1.0; W/F: 667 min (estimated by extrapolation of the solubility values reported in ref.19). ND: not detected.

The comparison of the activity of all the catalysts at 110 °C and 150 bar is shown in Table 6. In the presence of zirconium oxide, the conversion was not complete but it was selective to the ester, since no ether or alkene was detected. Therefore, it seems that this Lewis acid type of catalyst is more suitable for this kind of reaction than Amberlyst[®] 15. This is also in agreement with the reported selectivities in the liquid phase for other esterification reactions.^{22,23}

Novozym 435 has been previously used to synthesize isoamyl acetate from isoamyl alcohol and acetic anhydride in SC-CO₂ with an esterification yield of 100% in continuous operation, proving that is very stable at high pressures.²⁴ It may also maintain its catalytic activity in non-aqueous media at fairly high temperatures. For example, it was able to catalyze the transesterification of octadecanol with palmityl stearate at 130 °C for a considerable time in butylbenzene.²⁵ However, it is very sensitive to acidity of the medium. Thus, its activity decreased by up to three times when the pH was reduced from its optimal value (7.7) to 3.5.²⁶ Moreover, some acids (e.g. acetic acid) may act as potent inhibitors of lipase activity causing dead-end inhibition or acidification of the enzyme microaqueous environment.^{24,27} Another possibility could be the inhibition by the alcohol, but this is unlikely to happen since no indication of isoamyl alcohol inhibition was observed for this same enzyme.^{24,27} In consequence, it seems that the lack of activity detected in this work (only 3% ester yield) could be mainly due to low medium pH and/or enzyme inhibition caused by the acid substrate.

Effect of type of solvent

The use of a supercritical fluid as an alternative to organic solvents for chemical reactions may be beneficial if the process is controlled by the mass transfer, since the diffusion coefficients of the reactants and products in this medium are much higher than in liquid media. However, the density of the supercritical medium is normally lower and so its solvating capacity for reactants and products is reduced. This may alter the selectivity and the process yield. To compare the process in both types of solvents, selected tests were conducted in n-hexane. In these tests, the n-hexane flow rate was 0.36 g min⁻¹, the pressure was 150 bar and the ratio of the alcohol to the acid in the equilibrium cell was 1.0, in the same quantities as in the SC-CO₂ tests. The results are shown in Table 7.

In n-hexane, the catalysts performed differently than in SC-CO₂ – both catalysts seemed to be less active in this medium.

Table 7 The formation of 2E2E, 2EHE, and 2E1H from 2-ethyl-1-hexanol and 2-ethylhexanoic acid in n-hexane using different catalysts^a

Catalyst	Temperature/°C	Yield (%)		
		2E2E	2EHE	2E1H
Amberlyst [®] 15	110	18	ND	ND
	140	43	ND	ND
Zirconium oxide	110	ND	ND	ND

^a Other reaction conditions: n-hexane flow rate = 0.36 g min⁻¹; pressure = 150 bar; initial alcohol/acid molar ratio in the equilibrium cell = 1.0. ND: not detected.

For example, Amberlyst[®] 15 gave a maximum conversion of 43% at 140 °C, while under similar conditions, reactant conversion was 100% in SC-CO₂. In a similar fashion, zirconium oxide, which provided 40% conversion to the ester in supercritical conditions, was not active at all in n-hexane. The selectivity also changed – in supercritical conditions Amberlyst[®] 15 favoured the production of the dehydration product, while in n-hexane the only product was the ester.

It seems that mass transfer was accelerated in supercritical conditions, facilitating the access of the reactants to the active sites of the catalyst, and so providing higher conversions. The change in selectivity can be attributed to different reasons. One possibility is that one of the compounds had a very high molecular size or a bulky structure that retarded its approach to the active centers. Therefore, in supercritical conditions, its diffusion would be easier, favouring one of the routes of reaction. This does not seem to be the case because the molecular size and steric hindrance of the alcohol and the acid are quite similar. Likewise, the ester and the ether are comparable in size and structure, so it is not feasible that one diffused much faster than the other, altering the selectivity of the reaction in such magnitude. The other possibility is that the most acidic sites responsible for dehydration are located in the inner pores of the catalysts, and so at supercritical conditions the alcohol can penetrate into them more easily than in n-hexane – but this is unlikely to happen in both catalysts. What seems to be more probable is that the solubility of the alcohol is higher in SC-CO₂ than in n-hexane. If more alcohol is available in the bulk medium, then the reaction that uses two molecules of alcohol is preferred.

Conclusions

This work demonstrated that selective and continuous production of 2-ethylhexyl 2-ethylhexanoate from the esterification of 2-ethylhexanoic acid with 2-ethyl-1-hexanol could be carried out in supercritical carbon dioxide over a medium acidity catalyst (zirconium oxide) with good yield. If the reaction is performed over a highly acidic catalyst, the reaction is very selective to the dehydration product. Although several methods have been reported which perform the dehydration reaction using strong acids at high temperatures,^{28,29} this method provides a way to do it under milder conditions. Operation at high pressure did not decrease the catalysts' activity, and compared to the liquid organic phase, substrate conversion was higher due to the beneficial mass transfer properties of the supercritical solvent. Consequently, SC-CO₂

can be considered an environmentally benign alternative to conventional organic solvents for the synthesis of both products, the ester and the alkene. Further advantages of using this solvent would be the facilitation of product recovery, since no solvent residues are left in the final product.

Acknowledgements

This work has been partially supported by the Research Council of Iran (# 503495), IUT, and the Centre of Excellency in Chemistry Research of IUT. The critical review of Professor M. Yalpani, and experimental help with the n-hexane assays from M. Rezayat are greatly acknowledged.

References

- 1 E. J. Beckman, *J. Supercrit. Fluids*, 2004, **28**, 121.
- 2 *Green Chemistry Using Liquid and Supercritical Carbon Dioxide*, ed. J. M. Desimone and W. Tumas, Oxford University Press, New York, USA, 2003.
- 3 *Chemical Synthesis Using Supercritical Fluids*, ed. P. G. Jessop and W. Leitner, Wiley-VCH, Weinheim, 1999.
- 4 R. S. Oakes, A. A. Clifford and C. M. Rayner, *J. Chem. Soc., Perkin Trans. 1*, 2001, 917.
- 5 R. P. Unnikrishnan and S. D. Endalkachew, *Chem. Commun.*, 2002, 422.
- 6 M. McCarthy, H. Stemmer and W. Leitner, *Green Chem.*, 2002, **4**, 501.
- 7 C. Simoa, E. Ibanez, F. J. Senorans, C. Barbas, G. Reglero and A. Cifuentes, *J. Agric. Food Chem.*, 2002, **50**, 6648.
- 8 Y. Ikushima, K. Hatakeda, S. Ito, N. Saito, T. Asano and T. Goto, *Ind. Eng. Chem. Res.*, 1998, **27**, 818.
- 9 S. B. Hawthorne and D. J. Miller, *Anal. Chem.*, 1987, **59**, 1706.
- 10 G. P. Foy and G. E. Pacey, *Talanta*, 2000, **51**, 339.
- 11 A. Baiker, *Chem. Rev.*, 1999, **99**, 753.
- 12 W. K. Gary, F. R. Smail, M. G. Hitzler, S. K. Ross and M. Poliakoff, *J. Am. Chem. Soc.*, 1999, **121**, 10711.
- 13 J. S. Brown, H. P. Lesutis, D. R. Lamb, D. Bush, K. Chandler, B. L. West, C. Liotta, C. A. Eckert, D. Schiraldi and J. S. Hurley, *Ind. Eng. Chem. Res.*, 1999, **38**, 3622.
- 14 M. G. Hitzler, F. R. Smail, S. K. Ross and M. Poliakoff, *Org. Process Res. Dev.*, 1998, **2**, 137.
- 15 N. Sánchez, M. Martínez, J. Aracil and A. Corma, *J. Am. Oil Chem. Soc.*, 1992, **69**, 1150.
- 16 *Ullmann's Encyclopedia of Industrial Chemistry*, 6th edn, Wiley-VCH, Weinheim, Germany, 2002, vol. 12, pp. 305–327.
- 17 C. Park and M. A. Keane, *J. Mol. Catal. A: Chem.*, 2001, **166**, 303.
- 18 M. L. Honkela, T. Ouni and A. O. Krause, *Ind. Eng. Chem. Res.*, 2004, **43**, 4060.
- 19 H. S. Ghaziaskar, H. Eskandari and A. Daneshfar, *J. Chem. Eng. Data*, 2003, **45**, 236.
- 20 H. S. Ghaziaskar, A. Daneshfar and M. Rezayat, *Fluid Phase Equilib.*, 2005, **238**, 106.
- 21 S. Fisher and R. Kunin, *Anal. Chem.*, 1995, **27**, 1191.
- 22 G. D. Yadav and N. Kirthivasan, *J. Chem. Soc., Chem. Commun.*, 1995, 203.
- 23 K. Takahashi, M. Shibagaki and H. Matsushita, *Bull. Chem. Soc. Jpn.*, 1989, **62**, 2353.
- 24 M. D. Romero, L. Calvo, C. Alba, M. Habulin, M. Primozic and Z. Knez, *J. Supercrit. Fluids*, 2005, **33**, 77.
- 25 N. A. Turner and E. N. Vulfson, *Enzyme Microb. Technol.*, 2000, **27**, 108.
- 26 M. D. Romero, L. Calvo, C. Alba and A. Daneshfar, *J. Biotechnol.*, 2006 (submitted).
- 27 M. D. Romero, L. Calvo, C. Alba, A. Daneshfar and H. S. Ghaziaskar, *Enzyme Microb. Technol.*, 2005, **37**, 42.
- 28 E. J. Alvarez-Manzaneda, R. Chahboun, E. C. Torres, E. Alvarez, R. Alvarez-Manzaneda, A. Haidour and J. Ramos, *Tetrahedron Lett.*, 2004, **45**, 4453.
- 29 S. Ramayya, A. Brittain, C. DeAlmeida, W. Mok and M. J. Antal, Jr, *Fuel*, 1987, **66**, 1364.

Pharmaceutical Process Chemistry

Optimising strategies for automation, synthesis, scale up and separation to ensure a faster route to highly efficient, robust and green processes

Conference: 12th & 13th September 2006 • Workshops: 11th September 2006 • Café Royal, London

This focussed and practical forum is your guide to overcoming development bottlenecks and maintaining your competitive edge:

- Build effective bridges between discovery and process research to improve technology and knowledge transfer
- Apply and integrate new technology to accelerate process development
- Overcome purification and separation problems in process R&D
- Explore new developments and case studies to optimise route selection
- Assess your options to improve and speed up development by outsourcing process chemistry
- Apply the principles of green chemistry to improve efficiency as well as environmental impact

Interactive pre-conference workshops:
11th September 2006

Book early
and save
up to
£300

A: Developing methods to ensure enantioselective synthesis

Led by: Ian Cunningham, University of Surrey

B: Scaling up separation processes

Led by: Keith Turner, Kappa tau Consulting

Supported by:

TheScientist



Green Chemistry

Process
Development
.net



Your speaker panel includes:

Robert Crook, Senior Team Leader, Chemical Technologies, **Pfizer**

Xiao-jun Wang, Senior Principal Scientist, Chemical Development, **Boehringer Ingelheim**

Eric Stoner, Research Investigator GPRD Process R&D, **Abbott Laboratories**

Alan Harris, Associate Director Business Development, Global Process R&D, **AstraZeneca**

Marco van der Linden, Process Chemist, **NV Organon**

Donna Blackmond, Professor of Chemistry & Chemical Engineering, **Imperial College London**

Jean-Michel Adam, Senior Scientist, Synthesis & Process Research, **F. Hoffmann-La Roche Ltd.**

Bernhard Riss, Lab Head, Process R&D, **Novartis**

Udo Quotschalla, Head of Chemistry, **Schwarz BioSciences**

Jonathan Williams, Professor of Organic Chemistry, **University of Bath**

Ulf Hanefeld, Senior Lecturer, Applied Organic Chemistry and Catalysis, **Delft University of Technology**

David Ripin, Senior Principal Scientist, Chemical R&D, **Pfizer**

Sophie-Dorothee Clas, Distinguished Senior Investigator, Head of the Materials Characterisation Group, **Merck Frosst Canada**

Andras Horvath, Project Leader, Process Research, **Johnson & Johnson PRD**

James Clark, Head of the Green Chemistry Group, **University of York**

Dave Ennis, Senior Team Manager, Process R&D, **AstraZeneca**

Green Chemistry Fellowships

The Home and Personal Care R&D Laboratories of Unilever at Port Sunlight, near Liverpool, UK, has recently been awarded significant support through the EU Marie Curie Transfer of Knowledge Partnerships. This funding will contribute to the development of a significant platform within our research capabilities and scope the future innovation using Green Chemistry approaches. We are seeking senior scientists from Europe to initiate our program and foster relationships with key research centres across the EU.

It is expected that candidates will have a background in one of the areas indicated below with a relevant degree and PhD. Two Fellowships are available for senior scientists with 10+ years' post-graduate research experience (including PhD) and more specifically 3-4+ years' experience of Green Chemistry Techniques. The role of each Fellowship is to review the current state-of-the-art in their field and, through their extensive external networks, develop an implementation plan for research within the Home and Personal Care products markets.

ORGANIC CHEMISTRY FELLOW: Applications are sought from experienced researchers with a background of Green Chemical approaches to Organic Chemistry. Applicants should have an understanding of raw materials from renewable resources and methods for reacting these raw materials using Green processes. Experience of extraction techniques, enzyme catalysed aqueous reactions, fermentation techniques and/or microwave chemistry would be of particular interest.

POLYMER CHEMISTRY FELLOW: Applications are sought from researchers with experience of the extraction/formation of monomer candidates from biomass and their polymerisation to form functional polymeric materials. Applicants should also have an understanding of a range of bio-materials such as polysaccharides, proteins and peptides, and Green methods for their production and modification. Experience of extraction techniques, enzyme catalysed aqueous reactions, fermentation techniques and/or microwave chemistry would be of particular interest.

The Fellowships are for 2 years each with the intention to form strong links to EU centres of excellence. These are challenging roles and therefore salaries range from €65,000 – €70,500 per annum. A mobility allowance will be paid in accordance with EU rules.

Candidates, eligible according to the EU Marie Curie scheme guidelines, (http://europa.eu.int/comm/research/fp6/mariecurie-actions/indexhtm_en.html) should submit a full curriculum vitae and a one-page statement summarising their main research interests, together with the names of two referees. Applications can be sent electronically to recruitment.peoplelinkuk@unilever.com or by surface/airmail to: Unilever UK peoplelink, Walton Court, Station Avenue, Walton-on-Thames, Surrey KT12 1UP. The closing date for applications is 30th June 2006, earliest starting date is 1st August 2006. Please quote reference number 110626 and where you saw this vacancy advertised, on your application.

In applying for the above positions, you agree, unless you notify us when responding to this advert, that we may consider you for other vacancies we have and make your details available to other companies in the Unilever Group for the same purpose. Some Unilever companies are in countries without any data protection laws.

We are committed to diversity in everything we do.

Could it be 
Unilever



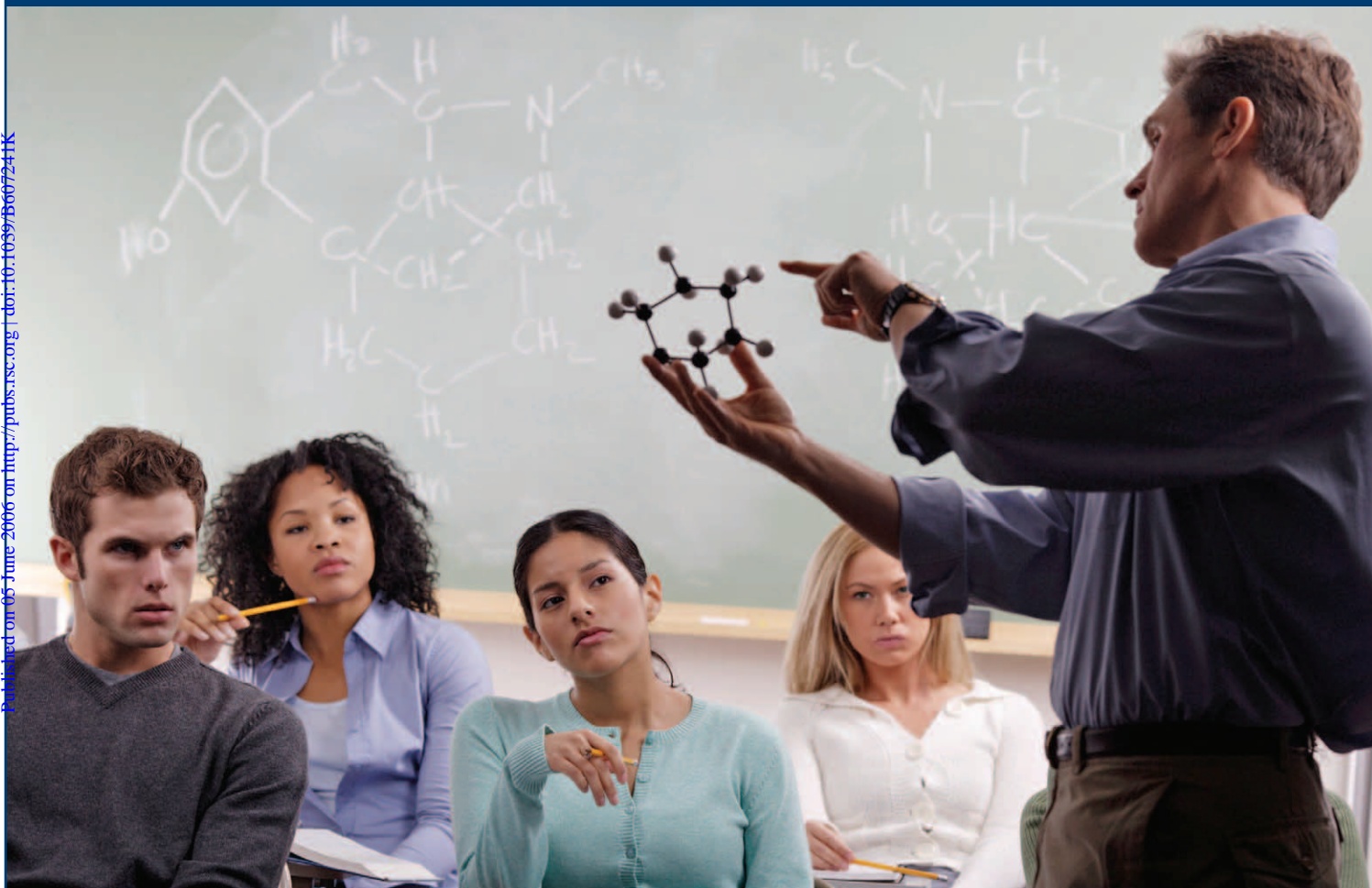







ACS and RSC

Building the Future



The American Chemical Society and the Royal Society of Chemistry are not-for-profit society publishers. We support excellence in education, investing in our future generation of chemists.

Society Publishing: Superior Performance

RSC Registered Charity No. 207890

RSC Publishing

ACS PUBLICATIONS
HIGH QUALITY. HIGH IMPACT

